Dipl.-Ing. Theresa Kainz

Relationship of Structure and Properties of antiferroelectric Lead Zirconate – Lead Titanate

DISSERTATION

Zur Erlangung des akademischen Grades

Doktorin der technischen Wissenschaften

eingereicht an der

Technischen Universität Graz

Betreuer

A.o.Univ.-Prof. Dipl.-Ing. Dr.techn. Klaus Reichmann

Institut für Chemische Technologie von Materialien

Christian Doppler Laboratorium für ferroische Materialien

Graz, Juli 2015

EIDESSTATTLICHE ERKLÄRUNG

Ich erkläre an Eides statt, dass die vorliegende Arbeit selbstständig verfasst, andere als die angegebenen Quellen/Hilfsmittel nicht benutzt, und die den benutzten Quellen wörtlich und inhaltlich entnommenen Stellen als solche kenntlich gemacht habe. Das in TUGRAZonline hochgeladene Textdokument ist mit der vorliegenden Dissertation identisch.

Datum Unterschrift

AFFIDAVIT

I declare that I have authored this thesis independently, that I have not used other than the declared sources/resources, and that I have explicitly indicated all material which has been quoted either literally or by content from the sources used. The text document uploaded to TUGRAZonline is identical to the present doctoral thesis.

Date Signature

All models are wrong, but some are useful.

George E.P. Box

Acknowledgement

At first, I want to thank the supervisor of this work, Prof. Klaus Reichmann, for his advices, help and support throughout all years. His expertise on the field of electroceramics inspired and helped to escape from some dead ends. I would like to say a special thank to Klaus for opening a door and giving me the change to work in the field I really enjoy.

For all the help, input and questions I want to thank my colleagues at the Christian Doppler Laboratory for Advanced Ferroic Oxides. It was a beneficial period.

I want to thank Michael Schossmann for numerous fruitful discussions and the ability to modify the perspective in so many ways.

Moreover, this work would not exist in that extent without the help of the collaborators at EPCOS OHG in sample preparation and measuring.

Prof. Brigitte Bitschnau and Prof. Franz Mautner, Institute of Physical and Theoretical Chemistry, Graz, performed the XRD-measurements and helped very much in characterizing and interpreting the spectra. I would like to thank for their input which deepened the understanding of solid state reactions.

I want to thank Sanja Simic from FELMI-ZFE for bringing the plain truth to light with her wonderful SEM images.

My family I want to thank for the opportunity to study and for all the support and encouragement throughout the years. I also like to thank all my friends and Johannes for being like they are and keeping me down to earth.

This work was supported by EPCOS OHG a Member of TDK-Group. Funding was provided by the Christian Doppler Research Association, Austria, and the Ministry of Science, Research and Economy, Austria.

TABLE OF CONTENT

1 Abstract

In this study the effect of substituents at A- and on B-site of the solid solution Lead Zirconate – Lead Titanate, PZT, on the structural and dielectric properties was examined. The scope of this work was to present a relationship between the structure and the properties of the antiferroelectric compositions of PZT to allow a targeted materials design. The focus was laid on the characterization of the polarization curve and especially on the saturation polarization, the switching fields and the hysteretic losses. All these parameters are used to enhance the energy which can be stored with this material.

Therefore the structural and dielectric variations induced by substitutions of Lead on the A-site with monovalent, divalent and trivalent ions and Zirconium on the B-site with Tin were investigated. By inserting a substituent into a lattice the ionic size, the atomic weight, the valency, the electronegativity, the polarizability and the electronic configurations vary.

Five concepts were chosen to examine these effects on the structure and on the properties: At A-site, substitution with donor ions La^{3+} and Bi^{3+}enables the insight on the influence of the cation vacancies. The substitution with alkaline acceptor ions Li^{+}, Na^{+} and K^{+} in Lanthanum doped PZT shows the impact of charge compensation. When substituting with isovalent earth alkaline ions Ca^{2+}, Sr^{2+} and Ba^{2+} this reveals the dependency of the change in ionic size and atomic weight. At B-site the substitution with isovalent Sn^{4+} demonstrates the effect of a fully occupied d-orbital on the structure and properties. Additionally, combinations of two isovalent substituents permit to enlighten any possible synergy effect.

Solid solutions were prepared by the mixed oxide route and the resulting samples were structurally characterized by X-ray diffraction and scanning electron microscopy. Low signal measurements, relative permittivity measurements over temperature and polarization measurements were performed and the data obtained were put into correlation with the structure.

It was shown that the orthorhombic structure is necessary but not a sufficient requirement to induce antiferroelectric behaviour. Moreover, the close interdependence of ionic size, atomic weight, valency, electronegativity, polarization and electronic configuration of the substituent determines the formability of the orthorhombic structure.

The main result is that by influencing the tolerance factor, the stability of the antiferroelectric phase over field can be controlled over a wide range. This can be used to tailor antiferroelectric materials in order to increase energy storage capacity.

2 Kurzfassung

In dieser Studie wurde der Effekt von Substituenten am A- und am B-Platz von Bleizirkonat – Bleititanat, PZT, auf die strukturellen und dielektrischen Eigenschaften untersucht. Im Rahmen der Arbeit wurde eine Struktur-Eigenschaftsbeziehung von der antiferroelektrischen Zusammensetzung von PZT präsentiert, die ein zielgerichtetes Materialdesign erlaubt. Der Schwerpunkt wurde auf die Charakterisierung der Polarisationskurven gelegt und im Speziellen auf die Sättigungspolarisation, die Schaltfelder und der Hysteresenverlust. All diese Parameter werden zur Steigerung der Energie, die mit diesem Material gespeichert werden kann, benutzt.

Daher wurden die strukturellen und dielektrischen Änderungen untersucht, die durch die Substituierung von Blei auf der A-Stelle mit ein-, zwei und dreiwertigen Ionen und Zirkon auf der B-Stelle mit Zinn hervorgerufen wurden. Durch den Einbau eines Substituenten in die Struktur verändern sich die Ionengröße, das Atomgewicht, die Valenz, die Elektronegativität, die Polarisierbarkeit und die elektronische Konfiguration.

Fünf Konzepte wurden ausgewählt, um diese Effekte auf die Struktur und die Eigenschaften zu untersuchen: Auf der A-Stelle ermöglicht die Substituierung mit den Donor-Ionen La^{3+} und Bi^{3+} den Einblick auf den Einfluss der Leerstellen. Die Subsituierung mit alkalischen Akzeptor-Ionen Li^{+}, Na^{+} und K^{+} in Lanthan dotierten PZT zeigt die Auswirkung der Ladungskompensation. Wenn mit isovalenten Erdalkali-Ionen Ca^{2+}, Sr^{2+} und Ba^{2+} substituiert wird, wird die Abhängigkeit von der Änderung der Ionengröße und des Atomgewichts offen gelegt. Auf der B-Stelle zeigt die Substituierung mit isovalentem Sn^{4+} den Effekt eines voll besetzten d-Orbitals auf die Struktur und die Eigenschaften. Zusätzlich gestattet die Kombination von zwei isovalenten Substituenten einen möglichen Synergieeffekt zu klären.

Feste Phasen wurden mittels Mischmetallroute hergestellt und die daraus resultierenden Proben wurden strukturell mit Röntgenbeugung und Rasterelektronenmikroskopie charakterisiert. Kleinsignalmessungen, Messungen der relativen Permittivität gegen die Temperatur und Polarisationsmessungen wurden durchgeführt und die gewonnenen Daten wurden in Zusammenhang mit der Struktur gebracht.

Es wurde gezeigt, dass die orthorhombische Struktur eine notwendige aber keine ausreichende Vorraussetzung für die Ausbildung von antiferroelektrischem Verhalten ist. Weiters bestimmt die enge gegenseitige Abhängigkeit von Ionengröße, Atomgewicht, Valenz, Elektronegativität, Polarisierbarkeit und elektronische Konfiguration des Substituenten die Formbarkeit der orthorhombischen Struktur.

Das Hauptresultat ist, dass durch die Beeinflussung des Toleranzfaktors die Stabilität der antiferroelektrischen Phase über das elektrische Feld kontrolliert werden kann. Das kann dazu benutzt werden, die antiferroelektrischen Materialien hinsichtlich einer größeren Energiespeicherungskapazität einzustellen.

3 Objectives

This study deals with the structure-property relationship in antiferroelectric Lead Zirconate-Lead Titanate solid solutions (PZT). The perovskite structure of this composition was judiciously modified by the substitution of Lead at the A-site and of Zirconium at the B-site in order to increase the stability range of the antiferroelectric phase. Many effects were claimed to influence the stability of the antiferroelectric phase such as Lead vacancies, valency, ionic size, atomic weight and electronic configurations.

To investigate the effects separately three approaches were applied:

Firstly, donor ions at A-site were chosen to examine the effect of the Lead vacancies on the structural and dielectric properties. Secondly, alkaline acceptor ions at A-site were used to enlighten the impact of charge compensation with La^{3+} on these properties. Thirdly, substitution with isovalent ions focused on the impact of change in effective ionic size and atomic weight on the A- and B-site.

The observed effects on dielectric parameters as relative permittivity, switching fields, hysteretic loss, polarization and the transition temperature were correlated to the ionic radius, the atomic weight, the polarizability and electronegativity of the used substituents.

The results can then be used for tailoring antiferroelectric material in order to increase energy storage capacity. The objective of this work was to provide design tools for increasing charge storage capacity of this material by optimizing switching field and maximum polarization.

4 Introduction

4.1 Lead Zirconate-Lead Titanate solid solution

Solid solutions of orthorhombic Lead Zirconate and tetragonal Lead Titanate, $PbZr_{1-x}Ti_xO_3$, were intensively studied due to their dielectric and piezoelectric properties. It is commonly used due to the excellent properties and the wide application range of these materials[1],

As shown in the phase diagram in Figure 4.1-1, Lead Zirconate and Lead Titanate are completely miscible and their solid solutions exist over the whole compositional range [2],[3],[4].

The ordering of the structure increases from orthorhombic on the Zirconium-rich side of the phase diagram, to rhombohedral to tetragonal structure with increasing Lead Titanate content passing a neally temperature independent phase transition. This morphotropic phase boundary, MPB, at around x~0,52 shows extensive enhancements of electromechanical properties and therefore was and is an interesting topic of scientific questions[5],[6],[7].

Curie Temperature Tc indicates the transition from a structure with lower symmetry and permanent polar axis to the highly ordered cubic structure without orientation polarization[8].

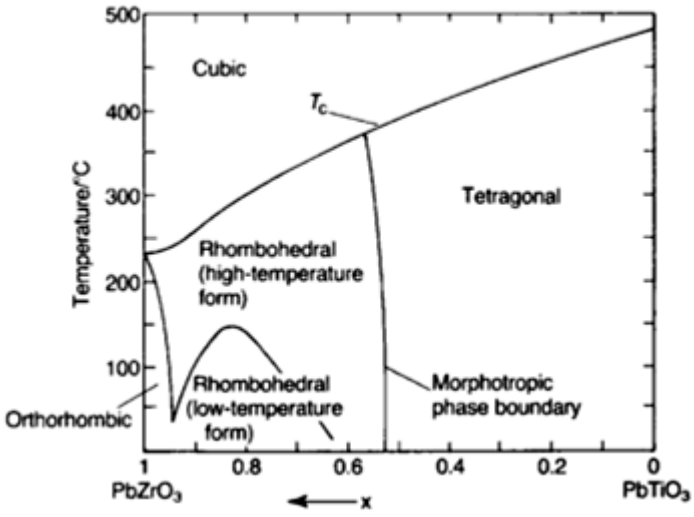

Figure 4.1-1: Phase diagram of Lead Zirconate and Lead Titanate[9].

Bravais lattices describe the lattice by the length of the axes and the angles between those axes. The cubic structure is the parent phase of all others and is defined by having all lattice parameters of the same length which are orthogonally arranged. By increasing one lattice parameter – conventionally attributed to the c-axis – the lattice transforms into the tetragonal structure.

If all lattice parameters differ but all angles between the axes are 90°, the structure is called orthorhombic. The opposite case occurs in the rhombohedral structure, where all lattice parameters are equal, but the angles deviate from the orthogonal arrangement.

The orthorhombic (a_o, b_o c_o) and rhombohedral cell can be converted into a pseudo-cubic cell (a_{pc}) with the following Equation 1 and Equation 2 (see also Figure 4.1-2)[10]:

$$a_{pc} \sim \frac{a_o}{\sqrt{2}} \sim \frac{b_o}{\sqrt{2}} \sim \frac{c_o}{2}$$

Equation 1: Relationship of orthorhombic unit cell (a_o, b_o and c_o) and pseudo-cubic unit cell (a_{pc}).

$$a_f = \frac{\sqrt{2}a_r}{a + cos\alpha_f}$$

$$a_f = acos\left(\frac{1 - 2cos\alpha_r}{2cos\alpha_r - 3}\right)$$

$$a_{pc} \sim \frac{a_f}{2}$$

Equation 2: Relationship of the rhombohedral unit cell (a_r, α_r) to the tilted face centred cubic cell (a_f, α_f) and the pseudo-cubic cell (a_{pc}).

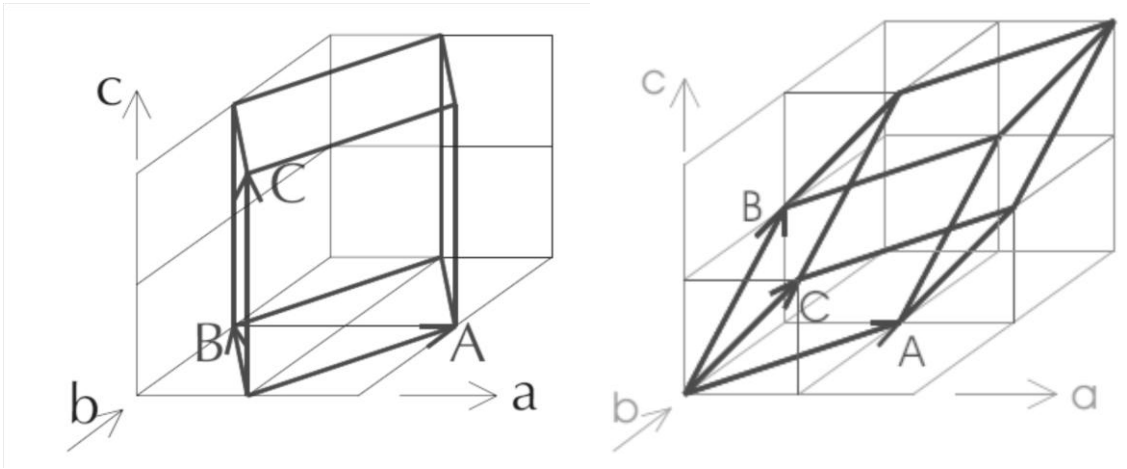

Figure 4.1-2: Left: 3D-scheme of an orthorhombic structure with the lattice parameter A, B and C. Right: 3-D scheme of a rhombohedral structure with the lattice parameters A, B and C. Both crystal systems are plotted in a pseudo-cubic reference system with the lattice parameters a, b and c (after Geller and Balla[11]).

4.2 Phase Transitions

Considering the phase diagram of PZT, over the whole compositional range and in dependence of temperature structural changes occur. Additionally, these structural phase transitions are combined with changes of the dielectric properties of the material. In order to distinguish between various transitions, it is important to identify the changes caused by a phase transition and the sequence of these changes and then classify these transitions according to the literature.

Phase transitions can be divided into first order, second order, order-disorder transitions and are accompanied by significant changes in properties. Near a phase transition the reactivity of many solids is high, which is used in synthesis routes[12].

4.2.1 First order transition

A discontinuous change of the properties with temperature is called a phase transition of first order. Properties which behave like that are lattice constants, dielectric constant, polarization and many more and show a discontinuity of the slope[9]. The reason lies in the sharp intersection of the free energy surfaces of the two phases at the transition temperature[8].

4.2.2 Second order transition

On the other hand, second order transitions show continuous behaviour with the temperature[9]. According to Landau, a structural phase transition occurs due to the decrease of long-range ordering with increasing temperature which equals to zero at the transition temperature. The order parameter extends the concept of free energy and supports the understanding of correlated physical effects[8]. Any temperature-dependent physical property can be identified as order parameter, like polarization in a ferroelectric material or magnetization in a ferromagnetic material. Most striking is the likeliness of the different physical properties approaching a critical temperature. The cooperative interaction of numerous particles leads to large fluctuations near the critical temperature and a change in dimensionality and symmetry of the ordering parameter occurs[8].

Many phase transitions cannot be classified by first or second order but show a mix of these two with features of both. Generally, the symmetry and the disorder of the phase increase with increasing temperature, wherefore a distinction of ordering and disordering passing a phase boundary is very helpful[8].

4.2.3 Order-disorder phase transition

Order-disorder phase transitions can be classified either by a disordering of position, of orientation or of electronics or nuclear spins. Ferromagnetic to paramagnetic transitions belong to this group of transition as well as the ferroelectric to paraelectric transition[8].

4.2.4 Soft modes

Soft modes refer to a collective of totally symmetric optical vibrational modes whose frequency decreases abnormally when approaching the transition temperature[13].

The concept of soft modes gives an explanation of the interdependence between polarizability and lattice dynamics in ferroelectrics and structural transition[13]. It uses the complete set of normal modes of vibrations, the phonons, to describe any dynamic distortion in the lattice. These modes are defined by their displacement eigenvector, frequency and wavelength. The atomic displacements within one cell and the long-distance interplay of the displacements over the whole arrangement of the unit cells are integrated in the soft mode eigenvector. Therefore, if only one such mode becomes unstable, anharmonic interactions in the crystal drive a normal mode to zero frequency and a phase transition occurs[14].

In second order transition, the soft mode has to be zero at the critical temperature leading to a change of phase, whereas in first order, the phase transitions occur, when the soft mode approaches but do not reach zero. The new phase is most commonly a subgroup of the parent phase.

It is worthwhile to stress, that not every phase transition is combined with a soft mode[13].

4.3 Structural changes

A structural change is accompanied by a change in coordination, in electronic structure or bond type resulting in a different atomic arrangement[15]. The new phase generated might be related to the parent phase by simple reconstructive mechanism[15]. First and second order structural transitions can easily be distinguished. In first order transitions no corresponding change in symmetry can be found, whereas in second order transitions the appearance or disappearance of certain symmetry elements can be detected. In that case, these alterations occur discontinuously[13].

4.3.1 Polymorphism

Many materials show polytypic phases, which differ only in the lattice parameter of the unit cell. The structures are arranged by corresponding long-range and short-range order forces and the distinction between the energies of the polytypic phases is demanding[8]. Perovskites of the general formula ABO_3 show tetragonal, rhombohedral, orthorhombic or the more ordered cubic structure. The degree of distortion is mainly influenced by the relative ionic size and the temperature[9].

4.3.2 Displacive transitions

Displacive transitions are most commonly fast and need small activation energies to change the coordination, deform bonds and distort the lattice. Examples of those transitions are the ferroelectric transformation of Barium Titanate or Lead Titanate. In that cases, only the coordination of Titanium is changed caused by the off-centring in the lattice[8]. In contrast to order-disorder structural transitions, where large atomic displacements occur, the displacive transitions only slightly change the atomic arrangements[13].

4.3.3 Ferrodistortive and Antiferrodistortive transitions

With antiferrodistortive transitions the number of formula unit in the unit cell changes, whereas the formula unit remains constant undergoing a ferrodistortive transition. Both transitions can be of displacive or order-disorder type. Comparing the displacive transitions in $BaTiO_3$ and $SrTiO_3$, in the former case the number of the formula unit stays the same. The same behaviour happens in the order-disorder transitions in NH_4Cl, whereas in NH_4Br the transition is associated by a change of occupancy of the unit cell as well as in $SrTiO_3$[13].

4.4 Influencing the phase transition

Structural phase transition can be induced by temperature, where an increase in temperature is associated with an increase of symmetry. A distorted perovskite will form cubic structure at elevated temperature of T_c in the PZT system[16,17,18,19,20].

As also obvious from the phase diagram of Lead Zirconate-Lead Titanate, that a variation in the composition can generate a structural phase transition. With increasing content of Lead Titanate, the structure changes from orthorhombic over rhombohedral to tetragonal symmetry[17,18,19,20,21,22].

By applying pressure, a closer packed cell with a smaller volume is favoured. This means that the more disordered structure is stabilized[13,18,23,24,25,26].

Another way to force a crystal to transform is to apply electric field. In doing so, the lattice parameters reorient and increase the cell volume. This is induced by an increased longitudinal strain – perpendicular to the applied electric field – and by a decreased transversal strain – rectangular to the applied field[17,19,27,28,29,30,31,32].

4.5 Defect chemistry[33,34]

Disturbances in a real crystal lattice lead to defects, which influence transport properties as well as electric properties. In Table 4-1, the Kröger-Vink defect notation is illustrated, which describes the defects according to the ideally occupied lattice and which will be used in the further discussion of defect chemistry. It compares the stoichiometric composition, which corresponds to integer ratios of the component atoms and ions, with the reference structure, from which lattice defects are defined. Defects can be classified by their dimensionality. The 0-dimensional defect or point defect refers to one missing or additional atom in the lattice. The 1-dimensional or line defect is built by dislocations in the lattice, which affect the charge transport in the lattice. The biggest impact on the conductivity have 2-dimensional or planar defects like surfaces or grain boundaries.

The movement of ions within the lattice must obey some conservations rules considering the mass, charge, structure and electronic states. The description and quantification of vacancies have been proved to be important to determine the properties of solids.

Table 4-1: Kröger-Vink notation of ionic point defects and regular lattice sites.

Symbol	
M_M	metal cation M^{x+} on its specific site in the lattice
O_O	oxygen anion O^{2-} on its specific site
V_M^X, V_M', V_M''	cation vacancies on the M-site, with no charge, charge -1 and -2 relative to the metal ion
V_O^X, $V_O^{\circ\circ}$, V_O°	anion vacancies on the oxygen site, with no charge, charge +1 and +2 relative to the oxygen ion
M_i^X, M_i°, $M_i^{\circ\circ}$	neutral metal cation, with charge +1 and +2 at interstices
O_i^X, O_i', O_i''	neutral oxygen anion, with charge -1 and -2 at interstices

Defects can be introduced by doping or non-stoichiometry and are thermodynamically determined equilibrium reactions, which follow the kinetics of the reaction.

Point defects can be distinguished in two main intrinsic ion disorders:

Schottky disorder (1) describes the incorporation of anion and cation vacancies which locate at the crystal surface and expand the lattice.

$$M_M + O_O \leftrightarrow V_M'' + V_O^{\bullet\bullet} + MO \quad (1)$$

Frenkel disorder can be divided in a cation sub-lattice (2) and an anion sub-lattice (3), where ions leave their specific sites and locate on interstices.

$$M_M \leftrightarrow V_M'' + M_i^{\bullet\bullet} \quad (2)$$

$$O_O \leftrightarrow V_O^{\bullet\bullet} + O_i'' \quad (3)$$

Substituting Lead in Lead Zirconate-Lead Titanate with a trivalent ion like Lanthanum, the charge neutrality has to be obeyed in the composition with extrinsic non-stoichiometry. This compensation can occur by the formation of vacancies at different sites which is demonstrated in two different formulations:

$$Pb_{1-3/2a}La^{\bullet}_{a}V_{Pb}''_{a/2}(Zr_{1-x}Ti_x)O_3 \quad (4)$$

$$Pb_{1-a}La^{\bullet}_{a}[(Zr_{1-x}Ti_x)_{1-a/4}V_{Zr/Ti}''''_{a/4}]O_3 \quad (5)$$

Comparing these notations, formula (4) presents a composition lower in content of Lead than that described in formula (5). The latter formula assumes a complete occupancy of A-site and compensates by the creation of (Zr,Ti) vacancies. Both formulations are accepted in literature, where selection between A- site[35],[36],[37] and B-site vacancies [19],[38],[39] in the formula is done regarding the sintering conditions[21].

One way to distinguish between these two formulas is a gravimetrical comparison of the ceramic bodies before and after sintering. Sintering them in a Lead-oxide atmosphere results in an incorporation of Lead-oxide and a weight gain in case (4), whereas in case (5) the material lost weight[21],[40],[41].

Sintering atmosphere has a big impact on the processibility of compositions containing compounds with high vapour pressure as Lead-oxide. Therefore various approaches are provided in literature to prevent weight loss and promote single phase formation[42],[43],[44],[45],[46].

In this study all weighted samples have been calculated with the assumption of the occurrence of Lead vacancies and were sintered in a Lead-oxygen rich atmosphere.

4.6 Lanthanum-substitution of Lead in Lead Zirconate-Lead Titanate, PLZT

The modification of Lanthanum in Lead Zirconate-Lead Titanate PLZT has been in focus of many studies [21],[47],[48],[49]. Modification of PZT with Lanthanum has been widely investigated due to the spe-

cific dielectric characteristics. Lanthanum increases the stability of the orthorhombic, antiferroelectric phase in the Zirconium-rich range of the phase diagram from 5% Titanium in pure Lead Zirconate - Lead Titanate to almost 35% Titanium in Lanthanum modified PZT (Figure 4.6-1)[50].

Lanthanum locates at the A-site substituting Lead [40]. Due to the aliovalency of the trivalent ion, Lead vacancies are formed[41].

In comparison to Lead, Lanthanum only possesses 90% of the ionic radii and therefore the cell volume decreases with increasing content of this substituent. Furthermore Lanthanum contains only two third of the mass of Lead. This is an important fact concerning the soft mode theory of the phase stability.

Comparing Lanthanum and Lead in the point of the electronic configuration, the f-orbital of Lanthanum is empty whereas Lead´s orbital is occupied by 14 electrons. In contrast to Lead, Lanthanum does not have a stereochemically active 6s-orbital, a lone pair, which is claimed to have a great impact on the structure of the PZT and the dielectric properties.

Further explanation about the structure will follow in the next section.

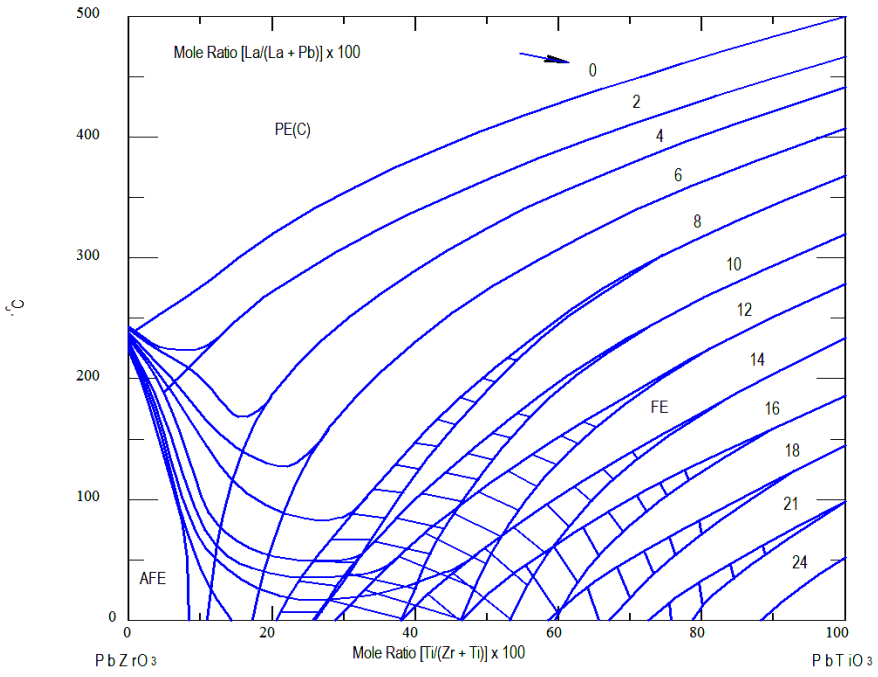

Figure 4.6-1: Phase diagram of Lanthanum doped Lead Zirconate-Lead Titanate[21]. The increasing doping content of Lanthanum shifts the phase transition from paraelectric (PE) to ferroelectric (FE) to lower temperatures and increases the range of the antiferroelectric phase (AFE).

4.7 Structure

4.7.1 The ideal perovskite structure

As Goldschmidt declared in 1926, a crystal structure is determined by the size, the preferred coordination and polarizability of atoms or groups of atoms[51], which can be arranged in a certain ratio. The relationship in Equation 3:

$$t = \frac{(r_A + r_O)}{\sqrt{2}\,(r_B + r_O)}$$

Equation 3: Goldschmidt´s tolerance factor for ABO_3 compounds.

is called tolerance factor or Goldschmidt factor, where r_A, r_B and r_o refer to the ionic radii of the A- and B-cation and the oxygen ion[52], respectively, and describes the formability of the perovskite structure ABO_3[53]. The ideal structure consists of a 3D-network of corner-linked BO_6 octahedra units with the B-atoms situated in the centre of these octahedra and the A-cations filling the space between them. In other words, the structure can be described as a cubic unit cell with a small B-site cation in the centre surrounded by six oxygen ions in octahedral arrangement and with large A-site cations placed at the corners. Thus, A-site cations occupy the 12-fold coordination place, whereas the B-site cations possess 6-fold coordination (Figure 4.7-1).

In a perfect cubic perovskite structure the face diagonal of the unit cell should have the length of the edge multiplied by the square root of two and thus the tolerance factor is unity (Figure 4.7-2). In fact, even the mineral perovskite, which is Calcium Titanate and gave the name for the whole structural group is not cubic, but shows distortion of the lattice[9].

In the case of t<1, the A-O bond is shorter than the ideal face diagonal compared to the B-O bond, which induces a rotation of the BO_6-octahedra to accommodate the mismatch. At a critical value of t a tilting transition occurs[54]. For t>1, rhombohedral structures are found for example in $BaTiO_3$, where in comparison to the A-site cation the B-site cation is too small and tends to displace[55].

Reaney[56] showed a dependency of tilting on the tolerance factor identifying 3 ranges: untilted perovskites with 0.985<t<1.06, perovskites tilted in anti-phase with 0.964<t<0.985 and perovskites which show in-phase and anti-phase tilting with t<0.964 (Figure 4.7-3). Further decrease of the tolerance factor results in a destabilization of the perovskite phase and eventually prevents the formation. According the literature, a stability range of the perovskite structure was determined to be 0.72<t<1.05[9,53,57,46,9,58].

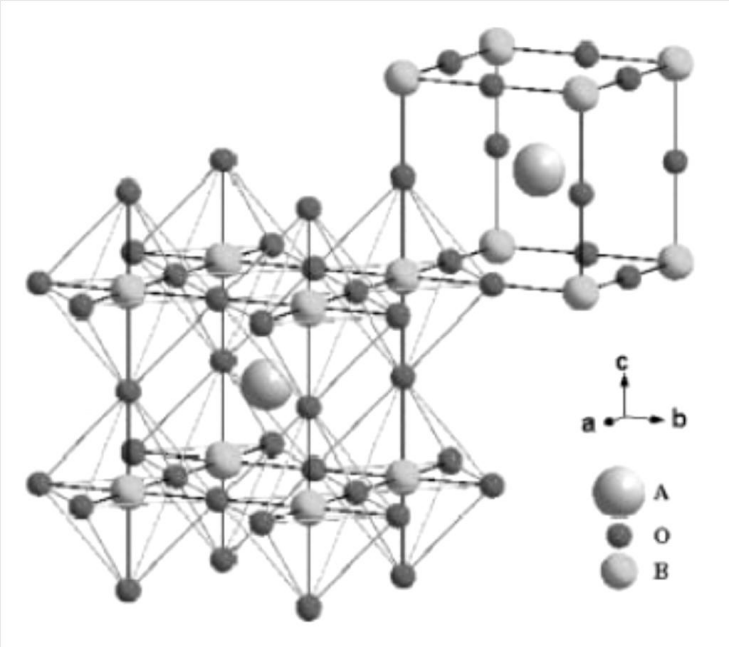

Figure 4.7-1: Schematic drawing of the perovskite structure[59].

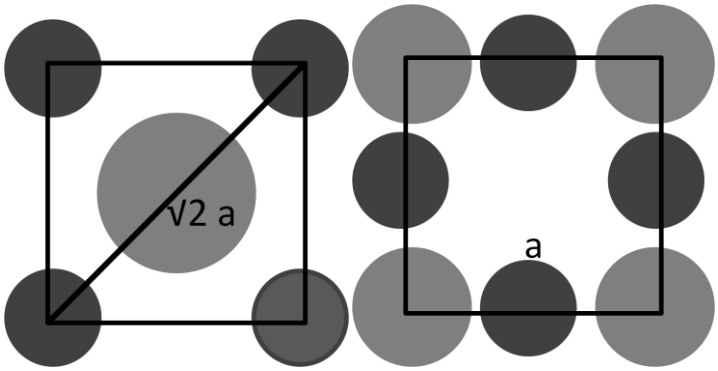

Figure 4.7-2: Geometrical considerations of a cubic perovskite structure leading to the Goldschmidt tolerance factor (after Park[60]).

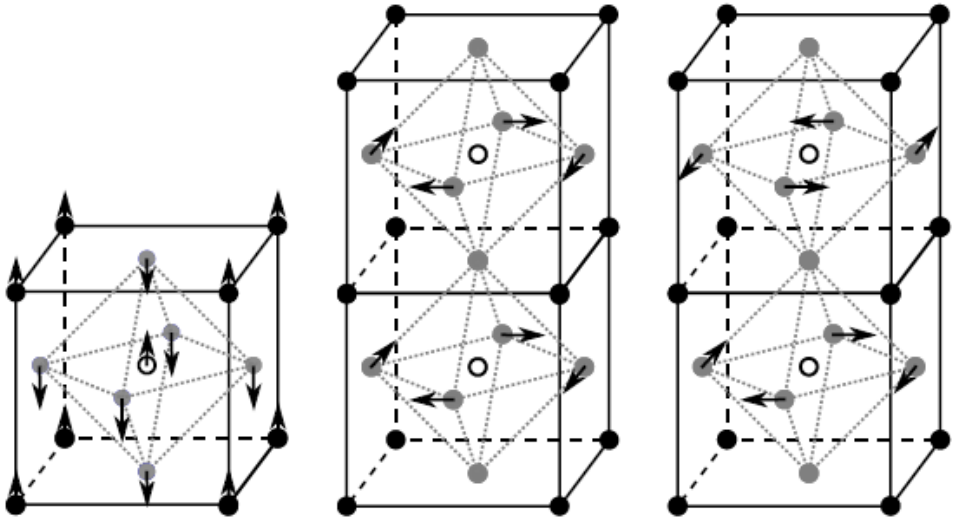

instability in ferroelectric phase - undistorted

antiferroelectric distortion in-phase rotation of the octahedra

antiferroelectric distortion anti-phase rotation of the octahedra

Figure 4.7-3: Atomic displacements corresponding to structural instabilities in perovskites. The unit cell is doubled in the antiferroelectric distortion[61].

4.7.2 Structure-property relationship

The tolerance factor t is assumed to give evidence about the dielectric behaviour of the material[56].

Ranges of t of the perovskite structure exhibiting either ferroelectric or antiferroelectric state have been varied several times. Structures with a tolerance factor around 1 tend to be ferroelectric, and beneath tend to be distorted in-phase or anti-phase causing antiferroelectricity[9],[62],[63]. A decrease in the tolerance factor might stabilize antiferroelectric phase and a value of 0.92 was argued to be the upper limit of antiferroelectric phase to appear [62]. In another study a qualitative relationship of the position of the morphotropic phase boundary and the tolerance factor was established to predict the approximate position of the MPB in $PbTiO_3$-$Bi(Mg_{1/2}Ti_{1/2})O_3$ and $PbTiO_3$-$Bi(Mg_{1/2}Zr_{1/2})O_3$[64].

Presumably, the orthorhombic, the rhombohedral and the cubic structure of the perovskite compete with each other[63]. Thus a comparison of those structures is given in the following.

4.7.3 Orthorhombic structure

In the orthorhombic structure the A-site cation has the coordination of 8 - 4 shorter and 4 longer bonds to the anion are formed. Due to the off-centring of the A-cation, the BO_6 octahedra are tilted or rotated and the tilt angle increases. Therefore a small cation which can easily off-centre and high

A-cation – oxygen covalent bonding favour the orthorhombic structure. Hence, the polyhedral volume of the A-cation is expanded and the anion-anion repulsions are reduced[65]. Overall, the orthorhombic structure shows the lowest energy of all perovskite structures because of the high number of short bonds between A-cation and oxygen ion[63,11].

4.7.4 Rhombohedral structure

By increasing the coordination of the A-cation from 8 to 9, the rhombohedral structure is formed. Six oxygen ions surround the A-cation in an arrangement similar to a twisted trigonal prism, whereas the three closer anions build a perfect trigonal planar coordination perpendicular to the threefold axis of the perovskite lattice. This structure is stabilized by highly charged A-cations and by small tilt angles. Compared to the orthorhombic structure, the ionic interaction between the A-cation and the oxygen ion is increased, whereas the bond between the B-cation and the anion is more covalent to stabilize the structure. The Madelung energy is the energy determining parameter[63].

4.7.5 Cubic structure

The cubic structure is characterized by a perfect 12-fold coordination of the A-cation, which is located in equidistance to all anions in a cubo-octahedral geometry. Therefore no variation of bond lengths and no distortions of the lattice are possible. The ion-ion repulsion is the highest compared to the other structures, which is stabilized by a large A-cations and/or B-O π bondings.

4.7.6 Structure stabilizing effects

Overall, there are different concepts of stabilizing effects of a structure, which can be distinguished in electronic preconditions and structural or geometrical preconditions. The balance of ion-ion repulsion and coherence and the nature of the bonds – the degree of covalency and ionicity – are stabilizing forces. These induce structural arrangements. On the other hand, from the geometrical view, the length of the bonds, the tilting angle, the size and displacement of the ions in the lattice can be summarized as structural conditions[63,66,67,60,68]. In the case of co-substitutions, which lead to different sizes and/or bonding at A-site, the ratio of large-to-small cations is assumed to dictate the most stable tilt system[66].

4.8 Ferroelectric and antiferroelectric phase in Lead Zirconat-Lead Titanate PZT

The ferroelectric phase is considered to be due to displacements of the Titanium ions, which alters the Ti-O bond lengths[69].

Some bonds between Titanium and oxygen break leading to long Ti-O bonds, whereas strong covalency between Titanium and oxygen forms very short Ti-O bonds. Regarding the Zr-O bonds, neither a breaking of bonds between Zirconium and oxygen nor strong covalency occurs. Additionally, an increased hybridization between Ti 3d- and O 2p-orbitals is essential for the ferroelectric state and is enhanced by the ferroelectric distortion[70].

In PZT Pb 6s and O 2p hybridize which is related to the displacement of Titanium[71] and the hybridization of Titanium and oxygen[72]. Furthermore the increased covalency between Lead and oxygen cause short Pb-O bonds. Overall, long-range ordering stabilizes the ferroelectric state, which appears in the rhombohedral structure[70],[58],[72].

In compositions with higher Zirconium content, the antiferroelectric phase can be stabilized. As Zirconium exceeds Titanium in size it tends to push the oxygen ions apart and thus induces large O-O bonds and large distortion. This favours the four-fold coordination of Lead with the oxygen ions which may explain antiparallel cation ordering[73].

This arrangement is accompanied by a rotation of the oxygen octahedra in anti-phase stabilizing orthorhombic structure. Additionally, Lead displacement promotes the octahedral rotations[74].

4.9 Ginzburg-Landau Theory[75]

Ginzburg-Landau Theory describes the interaction of the dipoles in the mean field of all the dipoles by the alteration of the free energy. The free energy is temperature-dependent and symmetric and can be characterized by an order parameter, the polarization, with the following equation:

$$F(P,T) = \frac{1}{2} g_2 P^2 + \frac{1}{4} g_4 P^4 + \frac{1}{6} g_6 P^6$$

Equation 4: The free energy F defined by Ginzburg-Landau theory (P...Polarization, T...Temperature, g_2, g_4, g_6...expansion coefficients).

The minima of the free energy are obtained if the first derivation becomes zero as in Equation 5:

$$\frac{\partial F}{\partial P} = P(g_2 + g_4 P^2 + g_6 P^4) = 0$$

Equation 5: First derivation of the free energy by the polarization.

and identify stable states. Furthermore the second derivation has to be positive and correlates to the inverse of susceptibility χ:

$$\frac{\partial^2 F}{\partial P^2} = g_2 + 3g_4 P + 5g_6 P^6 = \frac{1}{\chi} > 0$$

Equation 6: Second derivation of the free energy by the polarization (χ...susceptibility).

There are some restrictions concerning the temperature-dependent expansion coefficients g_2, g_4 and g_6. If polarization becomes large, the free energy would approach minus infinity, if g_6 would not be larger than zero. g_2 has to be positive in order to obtain stable solutions and shows the highest dependence on temperature. It can be expressed by the distance of the actual temperature from the Curie temperature.

$$g_2 = \frac{1}{C}(T - \Theta)$$

Equation 7: expansion factor g_2 (C…Curie Constant, Θ...Curie temperature).

Combining Equation 6 with Equation 7 the Curie Weiss law is found, which describes the temperature dependence of relative permittivity above ferroelectric/paraelectric phase transition:

$$\chi = \frac{C}{(T-\Theta)} \quad \text{or} \quad \varepsilon_r = \frac{A}{(T-\Theta)}$$

Equation 8: Curie Weiss law (C...Curie Constant, A...constant dependent on the material).

In the case of a second order phase transition the polarization approaches continuously zero and diminishes at the transition temperature T_c. Therefore the expansion coefficient g_4 has to be positive, whereas g_6 has to be close to zero. The Curie temperature equals the transition temperature below which spontaneous polarization is found. Thus, the spontaneous polarization correlates to the deviation of the temperature from the transition temperature:

$$P_s = \sqrt{\frac{T_c - T}{C g_4}}$$

Equation 9: Spontaneous polarization as function of the distance from the transition temperature T_c.

At temperatures above the transition temperature, one minimum is found, which correlates to P_s=0 and refers to the paraelectric state. This minimum expands while approaching the transition temperature. Below the transition temperature, two minima are formed which give the final values of the polarization, $-P_s$ and $+P_s$.

In the case of a first order transition, g_4 has to be negative, whereas g_6 has to be positive in order to find minima. At temperature high above the transition temperature one minimum exists. By approaching the transition temperature two additional minima are created, which do not have zero polarization. This means that the paraelectric state is stable, whereas the coexisting ferroelectric state is metastable. At the transition temperature all minima are equalized. By lowering the temperature, the free energy becomes negative causing a coexisting of stable ferroelectric and metastable paraelectric state. Finally, below the Curie temperature two minima are found, which correspond to the values of spontaneous polarization, $-P_s$ and $+P_s$.

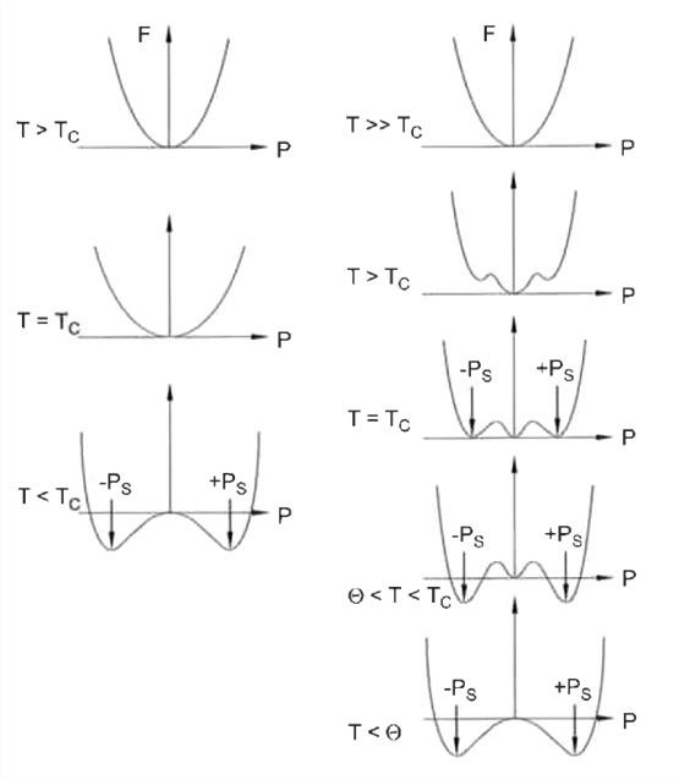

Figure 4.9-1: Free energy of a ferroelectric as function of the second power of the polarization with a second-order phase transition (left) and with a first-order phase transition (right) at different temperatures. T_c is the phase transition temperature and θ is the Curie temperature[75].

4.10 What stabilizes the antiferroelectric phase?

The antiferroelectric phase is correlated to the orthorhombic structure. As the orthorhombic structure is promoted by a decrease in cell volume[50],[62],[76] and a high distortion of the oxygen octahedra[66], the same is true in order to achieve antiferroelectricity. Therefore smaller ions as well as the occurrence of vacancies at A-site might stabilize the antiferroelectric phase.

As the B-site oxygen octahedra network and the long-range ordering were postulated to be responsible of ferroelectricity[77],[78], the disturbance of the coupling of the oxygen octahedra and of the translation invariance decreases the degree of ferroelectricity and thus stabilizes the antiferroelectric phase[47],[48]. Hence, substitution at A-site changing the bonding length of B-O and the tilting angle resulting in a distortion of the oxygen octahedra might destroy the coupling as well as the formation of A-site vacancies.

In the antiferroelectric phase Lead is displaced in the opposed direction which leads to zero polarization at zero field applied which is due to an antiparallel ordering of dipole moments on A-site[79],[80].

The effect of the lone pair of Lead causing a high polarizability[81] depends on the composition: In Lead Titanate it is assumed to favour ferroelectricity[72], whereas in the Lead Zirconate it is the reason for the off-centring of Lead leading to distortion and rotation of the oxygen octahedra[82],[83],[84]. Therefore, the influence of the stereochemically active orbital of Lead is not clarified completely. A-site vacancies provide more free volume which might give an additional basis in stabilizing the off-centring of the A-site.

A decrease in electronegativity[85] of the ions on A- or on B-site leads to a decrease of the hybridization of Pb 6s and O 2p and of Ti 3d and O 2p causing a decrease in ferroelectricity. Therefore Zirconium-substitution of Titanium favours the antiferroelectric phase[71],[86]. Furthermore the lower the bond length of Titanium to oxygen, the lower is the displacement of Titanium claimed to be a reason of ferroelectricity[72]. It was suggested that the displacement of Zirconium is smaller within its octahedron compared to Titanium[73].

The mass might come into play concerning the phase transition of ferroelectric to antiferroelectric phase. This phase transition is known to be a phonon process and therefore might be influenced by substitution with lighter ions[8],[87].

Generally, a symmetric stress on the lattice like hydrostatic pressure tends to stabilize the antiferroelectric phase, whereas an asymmetric stress like electric field stabilizes the ferroelectric phase[88].

Overall, a number of parameters can be summarized which can influence or even stabilize the antiferroelectric phase:

- ionic size
- atomic weight
- number of A-site vacancy
- lone pair effect
- dielectric polarizability
- electronegativity of the ion

4.11 Dielectric Properties[75,34]

To discuss the findings, some dielectric parameters are presented by physical equations.

The displacement of an ion in the lattice results in a development of dipole moment whose strength is dependent on the charge and the degree of the shift in position of the ion (Equation 10). As shown in Equation 11, the sum of all dipole moments in the unit cell leads to a polarization $\vec{\mathrm{P}}$. Consequential a certain relative permittivity ε and capacity C of the device appear.

$$\vec{\mathrm{p}}_{\mathrm{i}} = \mathrm{q}_{\mathrm{i}}\, \delta\vec{\mathrm{x}}$$

Equation 10: dipole moment p_i (q_i…charge, δx…displacement)

$$\sum \vec{p_i} = \vec{P}$$

Equation 11: sum of dipole moments lead to the polarization $\vec{P}$

With the concentration of the dipole moments $c = n/V$, the density of the dipole moment gives the polarization. This parameter is strongly dependent on the material and varies linearly with the concentration of the dipole moments. Introducing the electric susceptibility $\chi = \varepsilon_r - 1$ the electric polarization can be described as a function of the applied field $\vec{\mathrm{E}}$ as in Equation 12:

$$\vec{P} = c\, p_i = \chi\, \varepsilon_0\, \vec{E}$$

Equation 12: polarization P (ε_0… permittivity of the vacuum, χ… electric susceptibility, $\vec{E}$ … electric field)

A further relevant parameter is the relative permittivity which describes the capability of storing energy compared to vacuum with permittivity ε_0. It is related to the polarization $\vec{P}$ and the electric field $\vec{E}$. At high electric field the following Equation 13 is very useful, when relative permittivity cannot be evaluated directly by measuring with an impedance analyzer.

$$\varepsilon_r = 1 + \frac{\vec{P}}{\varepsilon_0 \vec{E}}$$

Equation 13: relative permittivity ε_r (ε_0… permittivity of the vacuum, $\vec{P}$… polarization, $\vec{E}$ … electric field)

The geometric dimensions of the device and the relative permittivity give the capacity of a device (Equation 14). To increase the capacity a high permittivity, a large area of the electrodes and small distances of the electrodes are desirable.

$$C = \varepsilon_o \, \varepsilon_r \frac{A}{d}$$

Equation 14: capacity C (ε_0… permittivity of the vacuum, ε_r… relative permittivity, A…Fläche des Bauteils, d…Höhe des Bauteils)

The loss factor tanδ in Equation 15 describes the specific conductibility of the dielectric and ohmic resistance in a circuit respectively and therefore displays the losses in heat. In other words, the loss factor expresses the ratio of real to imaginary current fraction and the ratio of the ohmic – in phase – to the capacitive – not in phase – current fraction respectively. In the device the phase shift of both current fractions is smaller than 90° and the loss is released as heat.

$$tan\delta = \frac{1}{\omega RC}$$

Equation 15: loss factor (ω…circular frequency, R…ohmic resistance (temperature dependent))

As capacity is frequency and temperature dependent, the measurements of ε(T) and tanδ(T) at various frequencies exerts a distinction of ferroelectric and relaxor materials. Due to the formation of micro domains at certain temperatures the relaxor material shows frequency dependence. The reason lies in the fluctuation of the micro domains which create electric domains. With decreasing temperature the interaction of the dielectric domains and the volume fraction of the micro domains grow. Beneath the critical temperature T_m, the whole volume becomes polar and the behav-

iour of the relaxor assembles that of a ferroelectric material. At this temperature the thermal movements exceed the ferroelectric coupling and remnant polarization vanishes.

By introducing substitutents or dopants the phase transition temperature is influenced. Due to a superposition of several phase transitions, the resulting transition becomes diffuse with a broad maximum of the relative permittivity.

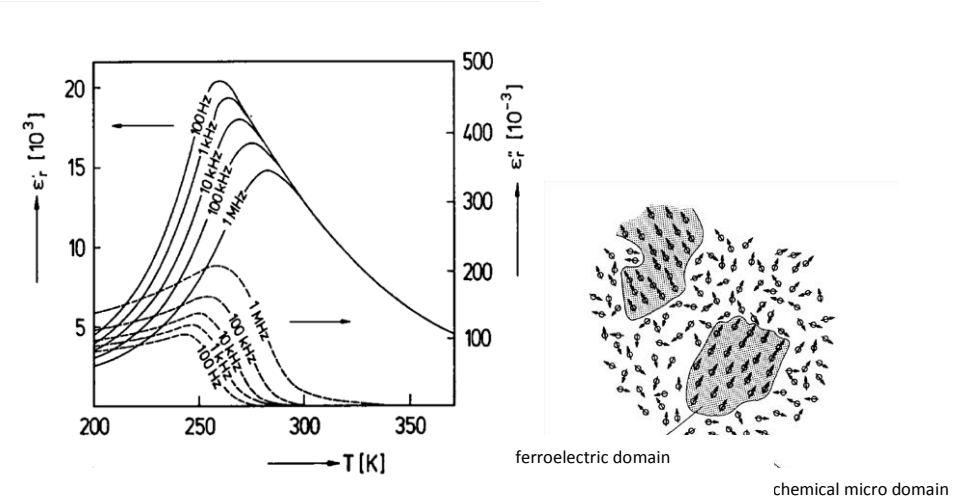

Figure 4.11-1: Left: Temperature and frequency dependence of the relative permittivity (solid line) and the loss factor (dashed line) versus temperature Right: Scheme of chemical micro domains with polarization vector in relaxor materials. The coupling of individual polarization vectors lead to the formation of macroscopic ferroelectric domains (shaded area). The size of these ferroelectric domains is temperature dependent[34].

4.12 Energy storage in dielectric materials

Dielectrics enhance energy density of capacitor due to relative permittivity which supports higher charge per area[75],[89].

4.12.1 Dielectric Materials [34,75,89]

As dielectrics many isolating materials come into play: The three types of dielectrics are paralectrics, ferroelectrics and antiferroelectrics. In the following section the dielectric properties and differences will be laid out.

4.12.1.1 Paraelectrics

Paraelectric materials are linear dielectrics. Linear and non-linear dielectrics distinguish with the respond of the polarization P to an applied electric field E as shown in Figure 4.12-1. Dielectric displacement or in other words the polarization has a linear relationship to the electric field in

paraelectrics. Furthermore the relative permittivity over electric field is constant. As there is no deviation from the linear behavior dielectric losses are very small.

4.12.1.2 Ferroelectrics

In contrast to the paraelectric the ferroelectric enfolds a hysteresis curve, a non-linear relationship of the polarization to the electric field. At zero field applied a spontaneous polarization evolves due to the arrangement of dipoles resulting in a not-zero dipole moment.

In the structure of the ferroelectric material, for example $BaTiO_3$, the Titanium ion is displaced from the central position and forms a dipole moment. While electric field is applied the dipoles align in one direction leading to a maximum in polarization, the so-called saturation polarization. By decreasing the field again the dielectric displacement declines and a remnant polarization remains at zero field. At a certain field no polarization can be displayed which is called the coercive field. This hysteretic behavior in ferroelectrics leads to loss in energy represented as the area in the loop - mostly transferred into heat and acoustic energy.

The alteration of the relative permittivity is shown below the polarization curve in Figure 4.12-1. It starts at a high value and decreases over field reaching a minimum. The following incline of the relative permittivity by decreasing the field again doesn´t lead to the starting point – a lower relative permittivity is achieved.

4.12.1.3 Antiferroelectric

In antiferroelectric materials the alignment of the dipoles is counter-directed resulting in a zero polarization at zero field applied. The linear behavior of the dielectric displacement at low fields only develops low polarization. As the field increases a certain field is reached, called the switching field or forward switching field (sometimes also antiferroelectric to ferroelectric switching field E_{AFE-FE}), where the dipoles are forced to align parallel and convert into the corresponding ferroelectric state. Again by increasing the field all dipoles become ordered in one direction and saturation occurs.

By reducing the field again, a steep decline in polarization is observed due to the rearrangement of the dipole vectors. At a certain field, the so-called backward switching field E_{FE-AFE}, the slope changes and the material returns into the antiferroelectric phase. Polarization decreases further until it reaches zero at zero field applied. The reversal picture is drawn when negative field is applied and the obtained hysteresis curve is known as an antiferroelectric double-hysteresis curve. The enclosed area refers to loss most commonly converted into heat and reduces the dielectric capacity (Figure 4.12-2).

The field-dependence of the relative permittivity shows a constant behavior at low field, followed by a dramatic increase and surpassing of a maximum at the switching field determined with the polarization measurements. In contrast to ferroelectric materials, antiferroelectrics possess capacitance that increase with applied voltage which provides a significantly higher energy-density storage capability.

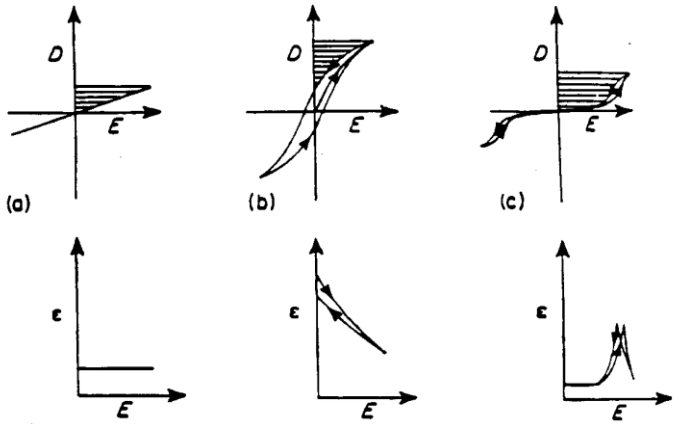

Figure 4.12-1: Distinction of parelectric (left), ferroelectric (middle) and antiferroelectric (right) behaviour by the dielectric displacement D and the relative permittivity versus electric field[90].

4.12.2 Energy storage in dielectrics

Indicated in Figure 4.12-1 by the shaded area the polarization curves of the materials can be used to store energy. The paraelectric material has a linear behavior therefore the area can only be increased by increasing the polarization. In the case of the ferroelectric material much of the originally stored energy is converted into heat and acoustic energy or in other words is lost.

Antiferroelectric material on the other hand has many parameters to tailor the hysteresis curve and increase the stored energy: To enhance the area not only the maximum polarization can be increased, but also the magnitude of the switching field. Additionally the difference of the two switching fields should be kept small to prevent losses. The best result is achieved by a small hysteresis shifted to high electric fields and augmented polarization.

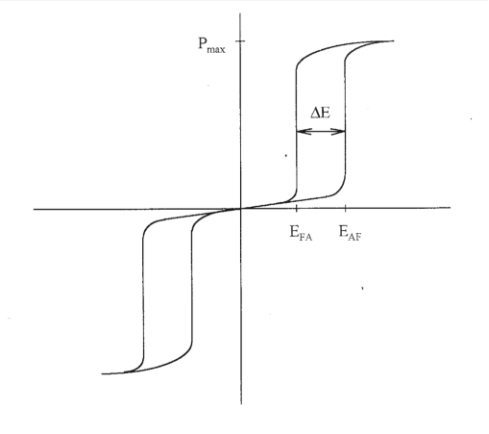

Figure 4.12-2: Idealized antiferrolectric double hysteresis curve. E_{FA} = backward switching field or field of ferroelectric to antiferroelectric phase transition, E_{AF} = forward switching field or field of antiferroelectric to ferroelectric phase transition, ΔE = difference of the switching fields or loss, P_{max} = maximale polarization (after Jaffe[9]).

5 Tasks

In this study substitutions of Lead and Zirconium with various ions in PZT and PLZT are presented with the intention to deepen the understanding of the interplay of structure and dielectric properties.

As starting material compositions in the Zirconium-rich side of the phase diagram have been chosen. The ratio of Zirconium to Titanium varied from 90 to 10, to 85 to 15 and to 80 to 20 and are referred as AA, BB and CC in the following (Figure 4.12-1).

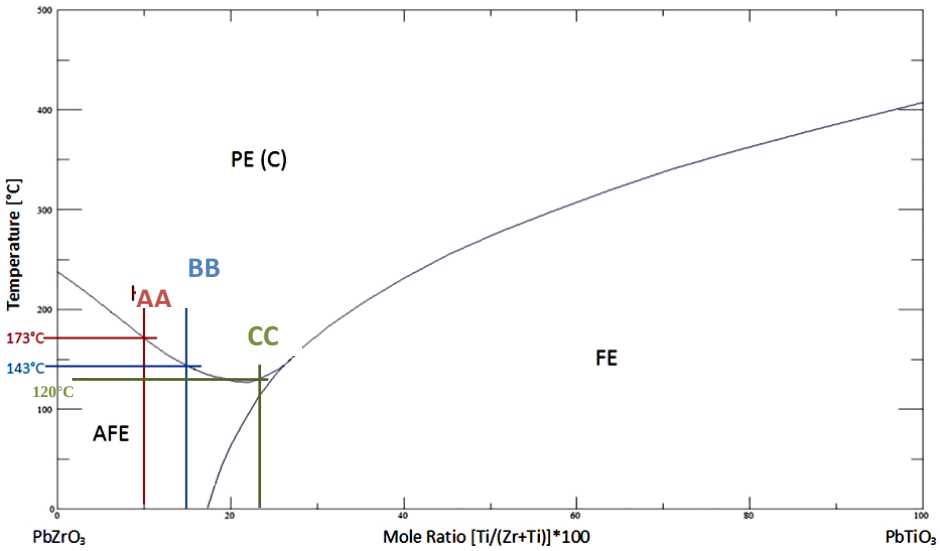

Figure 4.12-1: Phase diagram of Lead Zirconate-Lead Titanate doped with 6mol% of Lanthanum. The references AA, BB and CC were used as starting composition for all following doping experiments

5.1 Doping concepts

5.1.1 Donor ions on A-site

The ions Bi^{3+} and La^{3+} act as donors when substituting Lead in PZT. Lanthanum is known to stabilize the antiferroelectric phase. As Bismuth assembles Lead in many ways, this substituent was chosen to examine the effects of Lead vacancies on the stability range of the antiferroelectric phase with minimal altering the mass, size or electronic configuration[91]. A combination of these two substituents of Lead is also examined.

5.1.2 Monovalent acceptor ions on A-site

Acceptor ions have been introduced into PLZT by substituting Lead by monovalent alkaline ions Lithium, Sodium and Potassium to enlighten the impact of charge compensation, on the structural and dielectric properties. The number of Lead vacancies created by the substitution of Lanthanum has been influenced by inserting acceptor ions. At a certain value the donor-doped changes into an acceptor-doped material with oxygen vacancies which should be obvious in the dielectric behaviour.

5.1.3 Isovalent doping on A-site

In the case of isovalent substitution of Lead with earth alkaline ions Calcium, Strontium and Barium in PLZT, no charge variation at the A-site occurs and therefore any alteration can be assigned to the impact of change in size and mass at the A-site.

5.1.4 B-site substitution:

The tetravalent ion Tin assembles Zirconium, the ion it replaced, except the electronic configuration and mass. In this approach, a d^0-element was substituted by a heavier ion whose electrons occupy the d-orbital completely.

5.2 Complex doping:

5.2.1 Isovalent substitution-pair on A-site

Two isovalent ions were combined in order to examine a possible cancellation effect regarding the structure and the dielectric properties. The substitution pair Barium and Calcium resembles the size of Lead and therefore the effects should be dependent on the mass.

Furthermore, the impact of a self compensation of an acceptor-donor pair - a co-substitution of aliovalent ions Bi^{3+} and Na^{1+} on A-site - on structural and dielectric properties was investigated.

5.2.2 A-and B-site substitution:

Substitutions on A- and B-site were carried out with isovalent ions. Solid solutions with earth alkaline stannates were prepared to see any correlation or interactions of the separate effects of A- and B-site substitution.

Calcium Stannate has a smaller ion at A-site and B-site compared to PZT which might lead to a coupling of the separate effects. Additionally, a different series was prepared. While the same ion at B-site remained, a bigger ion was placed at the A-site. The solid solution of PLZT with Barium Stannate was prepared to make aware a possible detachment or interaction of the individual effects.

All parameters of an ion which might influence the structure and dielectric properties by substitution will be consulted to discuss the changes obtained during the study (ionic size, atomic weight, valency, lone pair, dielectric polarizability and electronegativity of the ion).

I	II	III	II	II	II	II	II	II	II	I	II	III	IV	III	II	I
H 2·20																
Li 0·98	Be 1·57											B 2·04	C 2·55	N 3·04	O 3·44	F 3·98
Na 0·93	Mg 1·31											Al 1·61	Si 1·90	P 2·19	S 2·58	Cl 3·16
K 0·82	Ca 1·00	Sc 1·36	Ti 1·54	V 1·63	Cr 1·66	Mn 1·55	Fe 1·83	Co 1·88	Ni 1·91	Cu 1·90	Zn 1·65	Ga 1·81	Ge 2·01	As 2·18	Se 2·55	Br 2·96
Rb 0·82	Sr 0·95	Y 1·22	Zr 1·33		Mo 2·16			Rh 2·28	Pd 2·20	Ag 1·93	Cd 1·69	In 1·78	Sn 1·96	Sb 2·05	Te	I 2·66
Cs 0·79	Ba 0·89	La 1·10	Hf		W 2·36			Ir 2·20	Pt 2·28	Au 2·54	Hg 2·00	Tl 2·04	Pb 2·33	Bi 2·02		
		Ce 1·12	Pr 1·13	Nd 1·14	Pm	Sm 1·17	Eu	Gd 1·20	Tb	Dy 1·22	Ho 1·23	Er 1·24	Tm 1·25	Yb	Lu 1·27	
					U 1·38	Np 1·36	Pu 1·28									

* The oxidation state is specified at the top of each group.

Figure 5.2-1: Average Electronegativities[85].

Li 1.20	Be 0.19											B 0.05	C	N	O 2.01	F 1.62	Ne
Na 1.80	Mg 1.32											Al 0.79	Si 0.87	P (5+) 1.22	S	Cl	
K 3.83	Ca 3.16	Sc 2.81	Ti (4+) 2.93	V (5+) 2.92	Cr (3+) 1.45	Mn (2+) 2.64	Fe (2+)2.23 (3+)2.29	Co (2+) 1.65	Ni (2+) 1.23	Cu (2+) 2.11	Zn 2.04	Ga 1.50	Ge 1.63	As (5+) 1.72	Se	Br	
Rb 5.29	Sr 4.24	Y 3.81	Zr 3.25	Nb 3.97	Mo	Tc				Ag	Cd 3.40	In 2.62	Sn 2.83	Sb (3+) 4.27	Te (4+) 5.23	I	
Cs 7.43	Ba 6.40	La 6.07	Hf	Ta 4.73	W	Re				Au	Hg	Tl (1+) 7.28	Pb (2+) 6.58	Bi 6.12			

Ce (3+)6.15 (4+)3.94	Pr 5.32	Nd 5.01	Pm	Sm 4.74	Eu (2+)4.83 (3+)4.53	Gd 4.37	Tb 4.25	Dy 4.07	Ho 3.97	Er 3.81	Tm 3.82	Yb 3.58	Lu 3.64
Th 4.92	Pa	U (4+) 4.45											

Figure 5.2-2: Dielectric polarizability of ions in A°³ [81].

6 Experimental:

6.1 Powder preparation

A range of variations of the compositions of PbZr0.90Zr0.10O3 and PbZr0.85Ti0.15O3 were prepared by the conventional solid state synthesis method. Commercially available powders of Pb3O4 (99.99%, Penox GmbH), ZrO2 (Grade 15,MEL Chemicals) and TiO2 (99.8 % purity, Tronox Pigments) were used as starting materials. A list of all starting compounds please find below in Table 6.1-1. All starting materials were dried at 220 °C and stored in a dessicator over silica-gel to avoid moisture. According to the valency of the dopant and the formula, the Lead vacancies at the A-site were considered and the powders were stoichiometrically weighted to obtain the required compounds.

$$Pb_{1-1.5a}La_aV_{Pb}{}''_{0.5a}(Zr_{1-x}Ti_x)O_3 \ (1)$$

According to the formula (1) 1mol% of trivalent Lanthanum at the A-site substitutes 1.5mol% Lead and leads to the formation of 0.5mol% of Lead vacancies for charge compensation.

The formulas for the compositions can be found in the following chapters dealing with them.

Table 6.1-1: List of starting compounds with information of purity.

Powder	Purity	Provider
Pb_3O_4	99.99%	Penox GmbH, Köln, Germany
La_2O_3	min. 99%,	Treibacher, Treibach, Austria
ZrO_2	Grade 15	MEL Chemicals, Manchester, UK
TiO_2	99.8 %	Tronox Pigments, Krefeld, Germany
Li_2CO_3	per analysis	Merck
Na_2CO_3	99.99%	Merck
K_2CO_3	99.9%	Merck
$SrCO_3$	Reagent Grade	Solvay Bario e Derivati, Massa, Italy
$CaCO_3$	High Purity CF 800	Solvay Bario e Derivati, Massa, Italy
$BaCO_3$	Reagent Grade	Solvay Bario e Derivati, Massa, Italy
SnO_2	Pure	Merck
$Bi2O_3$	99.9 %	MCP-HEK GmbH, Lübeck, Germany

To encounter the problem of PbO loss during the high temperature program, 1 mol% of PbO was added in excess. The mixtures were ball milled in ethanol with tungsten carbide-milling balls 5 mm in diameter in stainless steel beakers lined with a tungsten carbide-inlay using a planetary mill (Fritsch, Pulverisette 7). The ballmilling was carried out for 30 min at 300 rpm. After milling ethanol was removed from the suspensions by keeping them in a forced fresh air drying oven (Heraeus LUT

6050) at 120 °C over night. The dry mixtures were then sieved through a 500 µm test sieve, transferred into alumina crucibles, covered with alumina lids and underwent the calcination at 850 °C for 3 h with a heating rate of 5 K/min in a box furnace. The completion of the reaction was checked by X-ray diffraction (XRD) (Bruker AXS D5005 y-y, Cu Kα-emitter, graphite secondary monochromator).

Afterwards the compounds were again milled in ethanol under the same conditions as before, dried at 120 °C and sieved to reduce the agglomerate size less than 180 µm. Before pressing the powder into disc shaped samples, 5 wt% polyethylene-glycol PEG 20000 (per analysis, Merck) as a binding agent were added to ensure sufficient mechanical strength for handling. The samples were pressed with 150 MPa for 5 min into discs of 13 mm diameter and a height about 1 mm. To remove the binder before sintering, the samples were heated up to 500 °C in open alumina crucibles to promote the decomposition of PEG to H_2O and CO_2. Pellets were arranged in a coin roll set-up separated by ZrO_2-powder. Additionally atmospheric powder, a 1:1 mixture of Pb_3O_4 and ZrO_2, was put close to the set-up to provide a PbO and oxygen rich atmosphere according to the equation $Pb_3O_4 \rightarrow 3\ PbO + ½\ O_2$. All was covered with two alumina crucibles. Sintering was performed at 1250 °C for 3 h with a heating rate of 5 K/min in a box furnace.

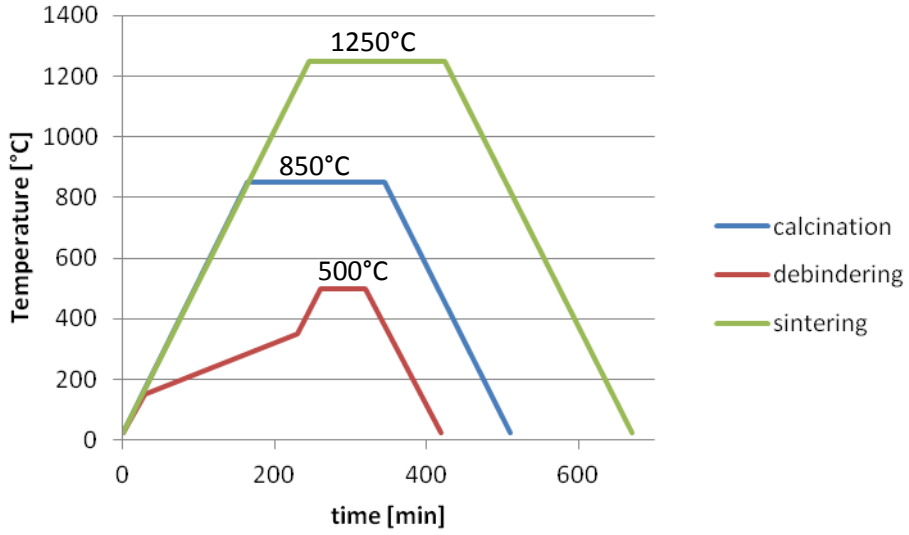

Figure 6.1-1: Scheme of the temperature programs calcination, debindering and sintering.

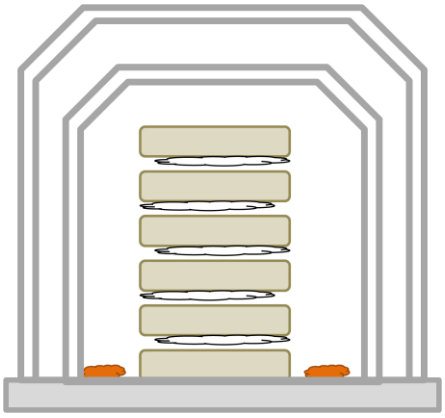

Figure 6.1-2: Scheme of the sintering set-up. Stacked pellets (beige) with Zirconium dioxide powder in between, surrounded by atmospheric powder (orange) and covered with two alumina crucibles.

6.2 Density Measurements

The apparent density was measured using Archimedes method (Mettler Toledo SX204 DeltaRange). For determination of the theoretical density, the sintered samples were ground in an agate mortar to a fine powder and analyzed by XRD leading to the lattice parameters. The geometrical density was calculated using the thickness and the diameter obtained with a calliper rule (Mitutoyo CD-15DCX) and the weight of the discs. From the apparent density and the theoretical density, the relative density was calculated.

6.3 Dielectric Measurements

All samples were polished and coated with silver paste to measure the permittivity ε and loss factor tanδ (HP 4192A LF Analyzer) at 1 kHz with 1 V at room temperature. The geometrical dimensions were measured with a caliper rule (Mitutoyo CD-15DCX). Furthermore temperature and frequency dependency of permittivity ε and loss factor tanδ were determined. Therefore measurements from minus 50 °C up to 300 °C with a ramp of 2 K/min at 0.1 kHz, 1 kHz, 10 kHz, 100 kHz and 1 MHz were carried out (Novocontrol, alpha, beta analyzer). Polarization curves of samples were recorded with an aixACCT aicPES system. The electric field was applied with a frequency of 0.1 Hz (triangular shape) and was varied to reveal saturation in polarization if possible. Some compositions had a break through voltage below saturation and therefore it was tried to increase breakdown voltage and to achieve saturation by lapping the samples to 300 µm, ground to a circular shape of 10.0 mm and sputtered with a 0.3 µm Cr-Ni-Ag layer.

6.4 Microstructural Characterization

Microstructure and elemental analysis were evaluated with scanning electron microscopy combined with energy dispersive X-ray spectroscopy SEM/EDS (Zeiss Ultra 55). For sample preparation the discs were broken, embedded in epoxy resin, polished with silica gel and sputtered with carbon. This procedure was necessary to perform channeling contrast imaging to reveal the microstructure.

7 Results and Discussion

7.1 Donor Doping at A-site

7.1.1 PZT modified with Lanthanum

Lanthanum modified Lead Zirconate-Lead Titanate has been widely examined in the literature[21],[47],[48],[92],[93],[87]. This chapter deals with the comparison and the reproducibility of the data from literature and the data obtained in this study.

The composition $Pb_{1-1.5a}La_aV_{Pb}''_{0.5a}Zr_{0.9}Ti_{0.1}O_3$ is referred to A-aLa where `a' is the molar percentage at A-site added to PZT. Every mol of Lanthanum replaces 1.5 mol of Lead. Due to the maintenance of the electric neutrality the substitution of one mol of trivalent ion creates 0.5 mol Lead vacancies.

7.1.1.1 XRD Characterization:

In Table 7.1-1 the characteristics of the ions used are listed. Lanthanum is a lighter and smaller ion to substitute Lead. The mass of Lanthanum is only around two third and the ionic radius is around 90% of that of Lead.

The XRD of the calcined $Pb_{1-1,5a}La_aV_{Pb}''_{0,5a}Zr_{0,9}Ti_{0,1}O_3$ series (a=0,01-0,08) is shown below. After calcination next to the main reflection pattern of the perovskite structure a secondary phase was detected which could be identified as Zirconium dioxide. This may be caused by the sequence of the insertion of the compounds in the solid state reaction[94],[95],[96]. This assumption is supported by the increasing intensity of the secondary phase with increasing amount of Lanthanum. But after sintering only the perovskite phase could be detected (see Figure 7.1-1 and Figure 7.1-2).

Table 7.1-1: Comparison in charge, atomic weight and radius of the ions used to build the perovskite structure.

	Pb	La	Zr	Ti
Charge	+2	+3	+4	+4
Atomic weight	207.2	138.9	91.22	47.87
Radius [XII]	1.49	1.36		
Radius [VI]			0.72	0.605

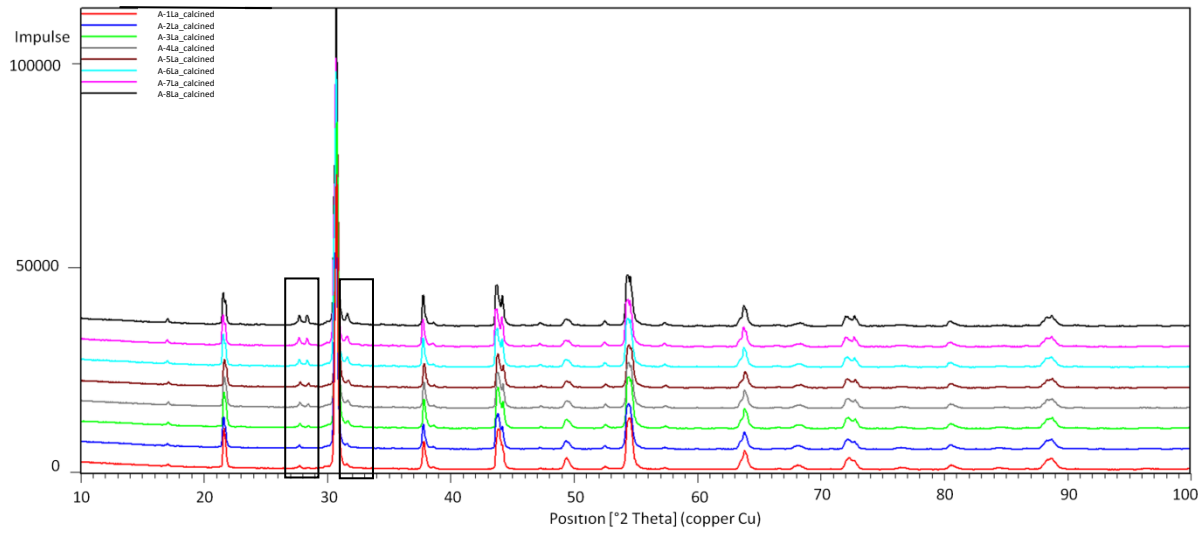

Figure 7.1-1: XRD of calcined powders of Lanthanum-substitution in PZT $PbZr_{0.9}Ti_{0.1}O_3$ (reflection patterns of the secondary phases are highlighted by rectangles).

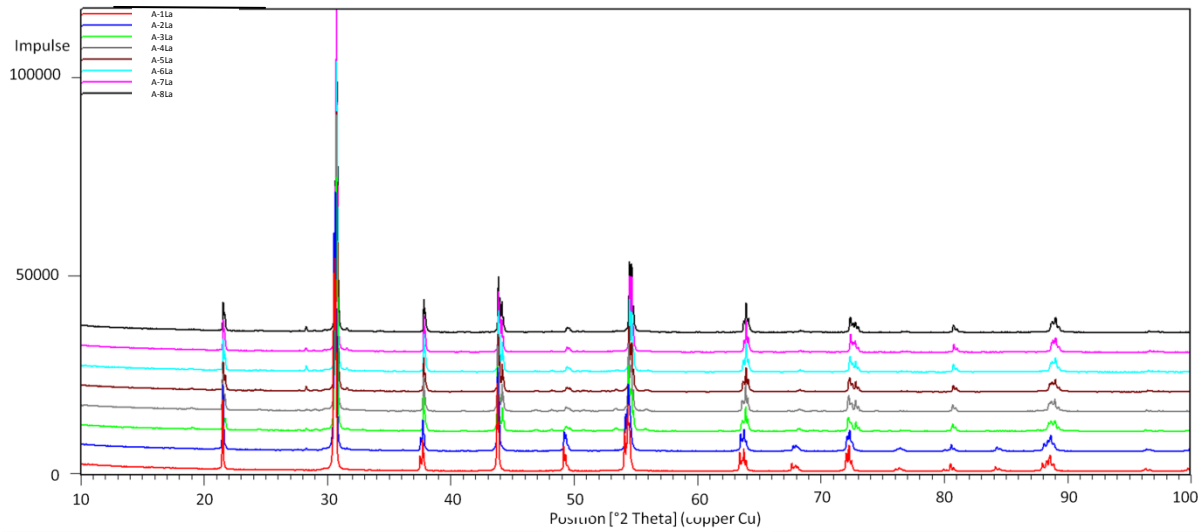

Figure 7.1-2: XRD of sintered powders of Lanthanum-substitution in PZT $PbZr_{0.9}Ti_{0.1}O_3$.

With increasing content of Lanthanum one has to face a phase transition from rhombohedral to orthorhombic structure. This can be identified by the splitting and shifting of the reflection patterns. A detailed view of three reflexion groups is shown below. The phase transition occurred at the substitution of 3mol% of Lanthanum. This is in good accordance to the literature[19, 21].

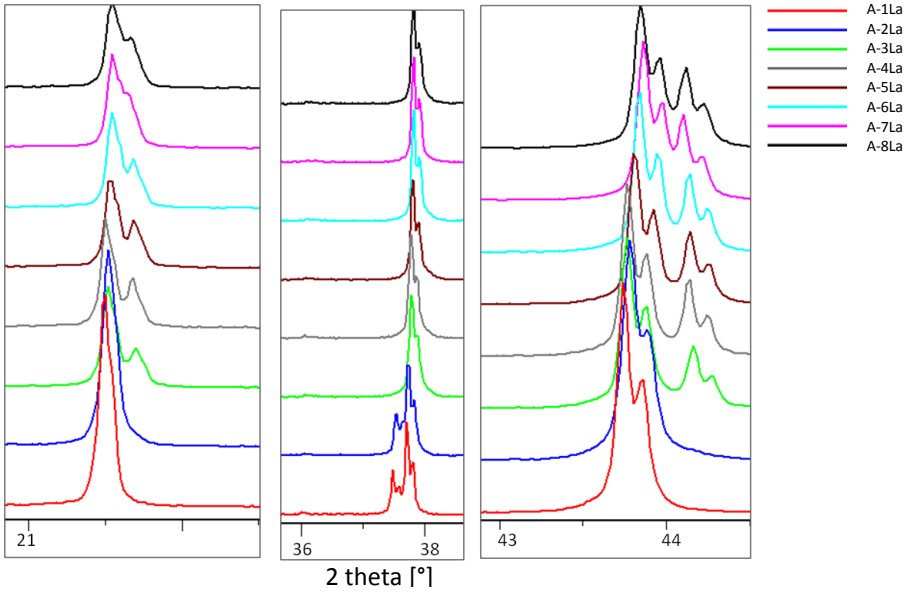

Figure 7.1-3: Details of the splitting and shifting of the XRD reflections of Lanthanum-substitution in PZT $PbZr_{0.9}Ti_{0.1}O_3$: with the substitution of 3%La the reflections split and shift due to the structural transformation from rhombohedral to orthorhombic.

In accordance to the smaller ionic radius of Lanthanum compared to Lead, the substitution reduced the cell volume and this might also lead to the structural change from rhombohedral to orthorhombic. In the reflection pattern of the examined composition some reflections referring to the orthorhombic structure Pbam were missing. This might be due to the occurrence of vacancies in the composition. Therefore a reference pattern of orthorhombic structure Amm2 of $PbZrO_3$ was used for Rietveld refinement.

In Table 7.1-2 the lattice parameters, the cell volume and the density are summarised. From these data it is obvious that lattice parameters and therefore also the cell volume decreased with increasing Lanthanum-substitution. Following the increase of the Lanthanum content a decrease of the theoretical density as well as of the Archimedes´ density was recorded. All samples exhibited a relative density above 95%.

Table 7.1-2: List of the cell parameters, the cell volume and the densities of Lanthanum substitution in PZT $PbZr_{0.9}Ti_{0.1}O_3$.

sample	c [Å]	b [Å]	a [Å]	c/a	cell volume [Å³]	theoretical density [g/cm³]	Archimedes´ density [g/cm³]	relative density [%]
A_1La	14.4007	5.8401	5.8401	2.4658	425.3578	7.97	7.75	97.25
A_2La	14.3851	5.8391	5.8391	2.4636	424.7520	7.94	7.62	95.92
A_3La	5.8556	5.8504	4.1037	1.4269	140.5839	7.96	7.71	96.90
A_4La	5.8520	5.8476	4.1038	1.4260	140.4334	7.93	7.67	96.80
A_5La	5.8481	5.8451	4.1045	1.4248	140.3022	7.89	7.61	96.45
A_6La	5.8443	5.8421	4.1049	1.4237	140.1541	7.93	7.59	95.73
A_7La	5.8387	5.8363	4.1063	1.4219	139.9253	7.83	7.55	96.37
A_8La	5.8416	5.8394	4.1057	1.4228	140.0506	7.79	7.57	97.23

7.1.1.2 Microstructure:

SEM images revealed a homogeneous composition for all samples. Pores could be detected in the ceramics which inhibited a higher relative density (Figure 7.1-4 and Figure 7.1-5).

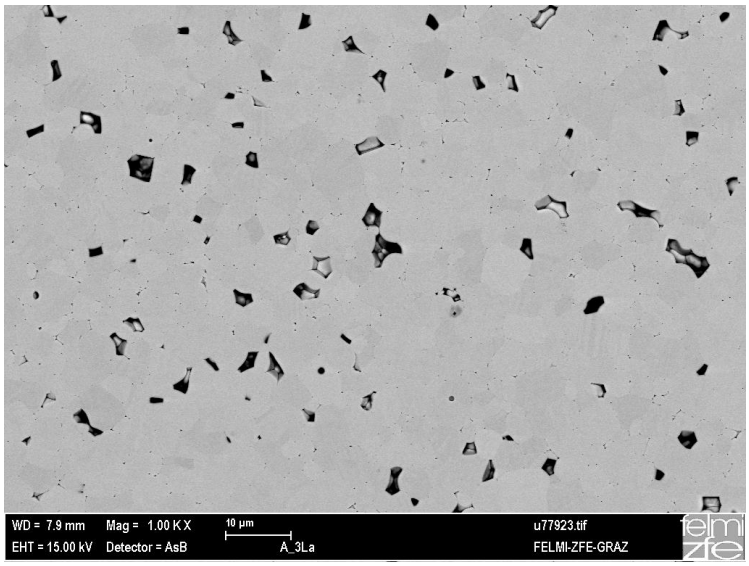

Figure 7.1-4: SEM backscattered electron image of A-3La: No secondary phases could be detected.

An inhomogeneous grain growth was illustrated by the channelling contrast mode: Smaller grains are next to bigger grains. 180° and 90°-domains can be observed in all samples.

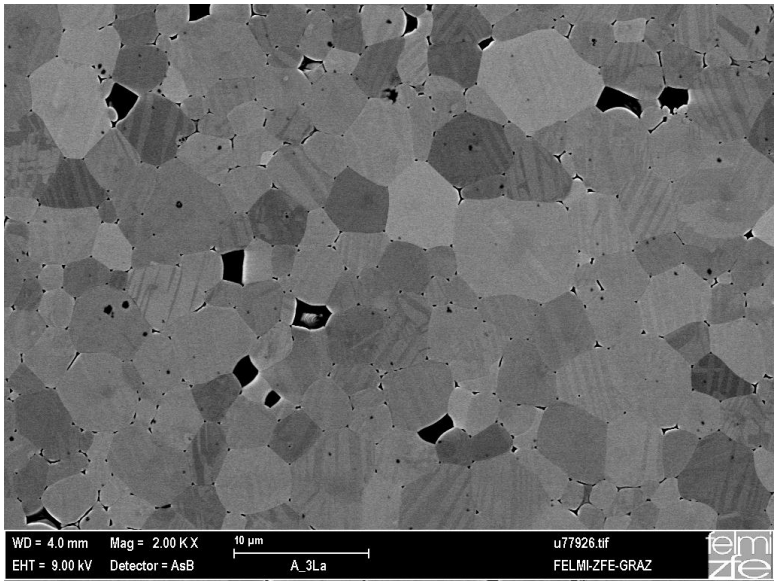

Figure 7.1-5: SEM in the channelling contrast mode of sample A-3La.

7.1.1.3 Dielectric and Piezoelectric Characterization:

In Table 7.1-3 the results of the low signal dielectric and piezoelectric measurements are illustrated. A decrease in loss factor tanδ and piezoelectric constant d_{33} and an increase in capacitance and

thus in relative permittivity ε can be recognized. By increasing the molar content of Lanthanum from 1 to 8 mol% the capacitance doubled nearly from 380 to 700 pF, whereas relative permittivity increased over the same compositional range from ~305 to ~600. The loss factor decreased from 0.06 with increasing content of Lanthanum. Interestingly, with the substitution with 3 mol% of Lanthanum capacitance changed from 360 pF to 780 pF. The maximum in capacitance of 830 pF was reached with the insertion of 4 mol%. Though, the loss factor decreased with increasing fraction of the substituent. With the substitution of 4 mol% a value of 0.01 was obtained and that remained constant for the following compositional range.

Considering the piezoelectric constant, the samples A-1La and A-2La had values of d_{33} of 66 and 83 respectively. Then with further increase of Lanthanum the piezoelectric constant dropped beneath 1. This might be associated with a phase transition.

Table 7.1-3: Results of low signal dielectric measurements of Lanthanum substitution in PZT $PbZr_{0.9}Ti_{0.1}O_3$.

Sample / 0.1 kHz	capacitance [nF]	loss factor []	relative permittivity []	piezoelectric constant d33 [pC/N]
A_1La	0.38	0.06	307	66.00
A_2La	0.42	0.02	368	83.00
A_3La	0.78	0.02	661	0.30
A_4La	0.83	0.01	720	0.09
A_5La	0.73	0.01	642	0.01
A_6La	0.71	0.01	624	0.02
A_7La	0.70	0.01	600	0.04
A_8La	0.65	0.01	581	0.04

By measuring the temperature dependency of relative permittivity and loss factor, peaks evolved which address phase transitions (see Figure 7.1-6 and Table 7.1-4), which coincide with phase transition in the phase diagram[21].

In the case of the samples A-1La and A-2La the peaks indicate a conversion from ferroelectric to paraelectric state and for the other samples from antiferroelectric to paraelectric state which are both accompanied by a structural change to pseudo-cubic[21]. With low content of dopant the peak height was enhanced and had a narrow shape. But with further increase a decline occurred and the peaks appeared to flatten. This broadening implies a more diffuse phase transition by inserting Lanthanum. Overall the value of maximum permittivity was forced to drop from 9500 to 900 with increasing the fraction of Lanthanum from 1 mol% to 8 mol%.

With increasing content of Lanthanum the temperature of maximum permittivity T_m is shifted to lower temperature. A deviation from 213 to 173 °C was observed, but the effect on T_m became

smaller at the point of 4 mol%. Due to a broadening of the peak, some peak values could not be determined exactly.

A special behaviour was detected at the composition A-3La: An additional step was observed at around 100 °C. This caused a more detailed examination of this composition with respect to the polarization at higher temperature.

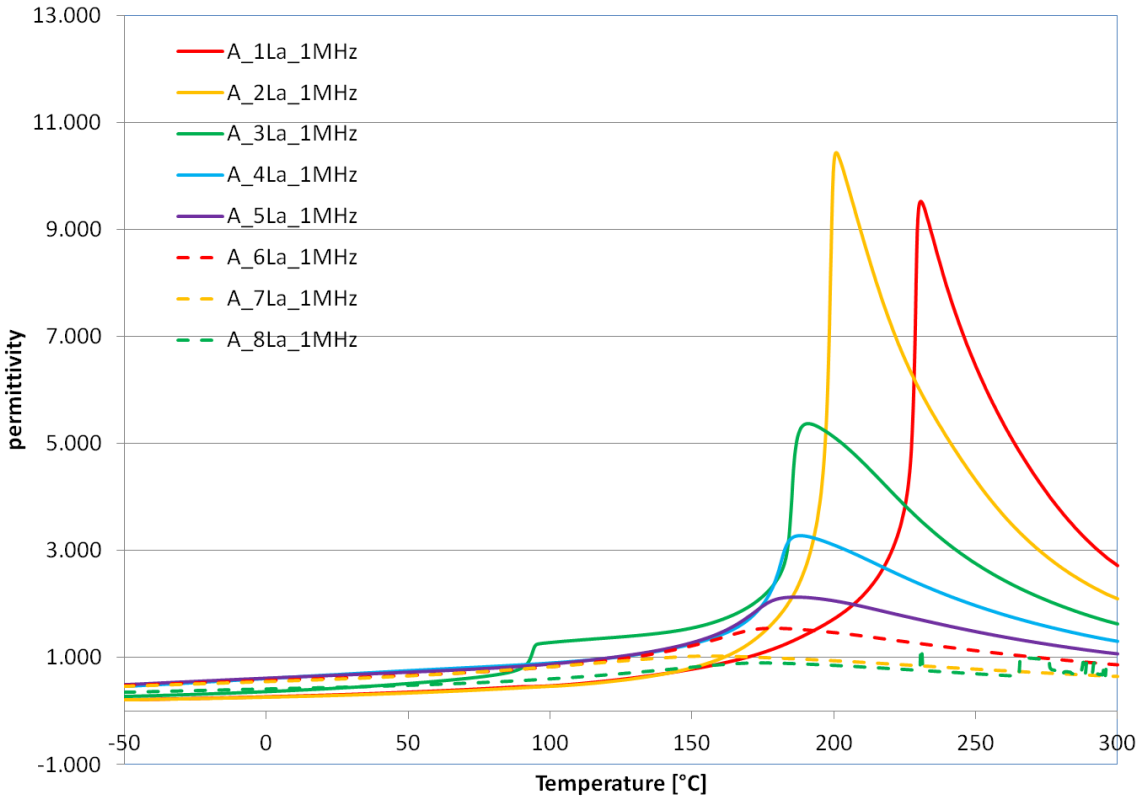

Figure 7.1-6: Permittivity measurements versus temperature of Lanthanum-substitution in PZT $PbZr_{0.9}Ti_{0.1}O_3$ at 1 MHz.

Table 7.1-4: Results of the relative permittivity versus temperature curves of Lanthanum substitution in PZT $PbZr_{0.9}Ti_{0.1}O_3$.

sample	maximum relative permittivity	Temperature Tm [°C]	Temperature maximum in tanδ[°C] (above 100 °C) [1MHz]
A_1La	9469	213	227 (184)
A_2La	10350	202	198 (174)
A_3La	5369	193	190
A_4La	3275	188	185
A_5La	2138	186	180
A_6La	1552	179	175
A_7La	1022	157	
A_8La	899	173	

Figure 7.1-7 demonstrates the frequency dependence of selected samples. The position of the peak did not alter with varied frequency, excluding any relaxor behaviour, only the height suppressed with higher frequency. Regarding the curves of sample A-3La, the anomaly is visible in all curves at the same temperature and did not change the position. Therefore it is also frequency independent.

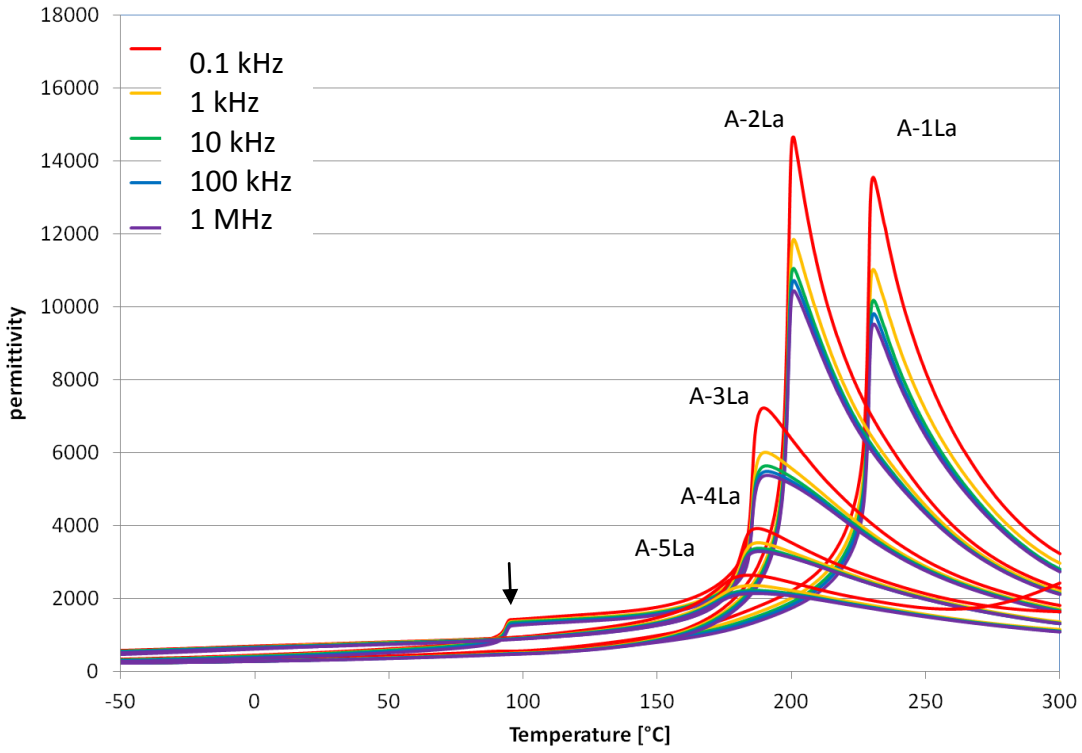

Figure 7.1-7: Frequency dependent measurements of the relative permittivity of Lanthanum-substitution in PZT PbZr0.9Ti0.1O3 (measured at 0,1 kHz, 1 kHz, 10 kHz, 100 kHz and 1 MHz). Anomaly in the curve of sample A-3La indicated by an arrow.

The dielectric responses, relative permittivity and loss factor, showed similar peak positions. As an example the curves of the samples A-3La are plotted in Figure 7.1-8. At around 100 °C a sharp decline in the loss factor curves was detectable, whereas a step in relative permittivity curves occurred. The decrease in loss factor might signify a transition from ferroelectric to antiferroelectric behaviour. The next alteration happened at ~150 °C, where both the relative permittivity curves and those of the loss factor correlated with each other. An abrupt slope appeared which ended in a peak at around 200 °C followed by a steep decline.

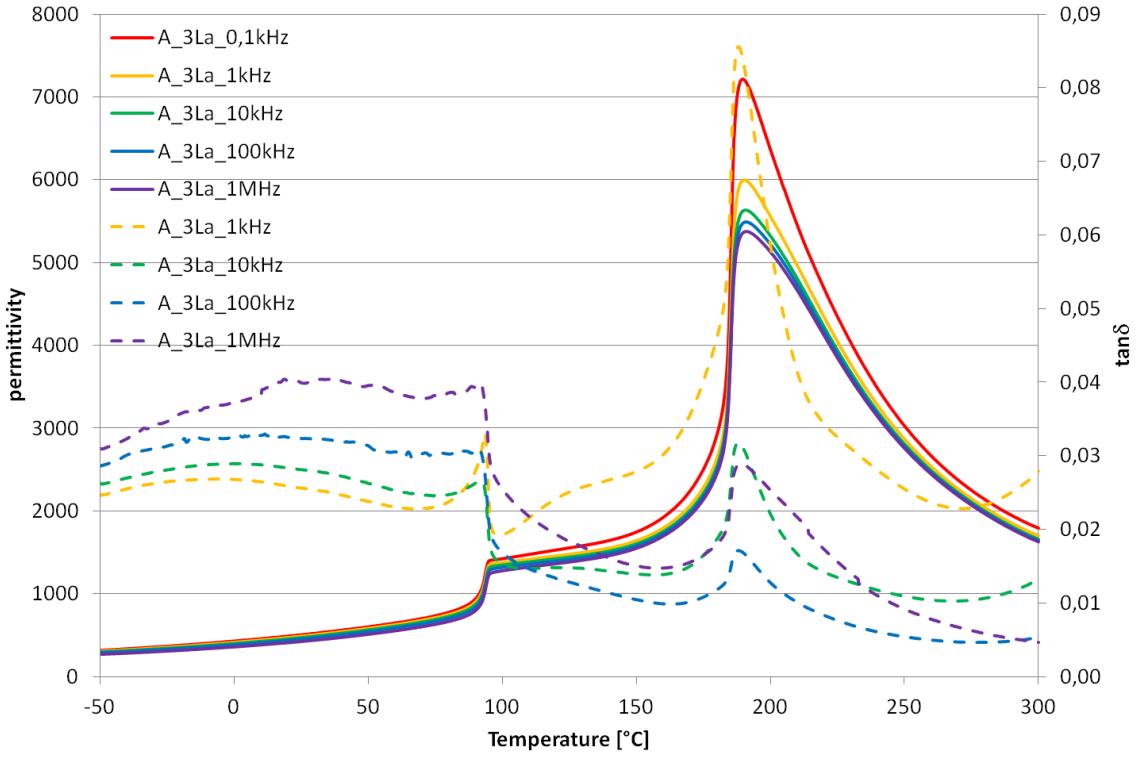

Figure 7.1-8: Frequency dependent measurements of the relative permittivity (solid line) and loss factor (dashed line) of the sample A-3La (measured at 0,1 kHz, 1 kHz, 10 kHz, 100 kHz and 1 MHz).

Figure 7.1-9 shows the polarization curves of the varying Lanthanum content. With small fractions of Lanthanum ferroelectric hystereses are obtained.

At a certain point a transformation from ferroelectric at low content of Lanthanum to antiferroelectric behaviour at higher content was observed. This transition lies between 3 and 4 mol% substitution of Lanthanum: The remnant polarization dropped and approached nearly zero and the saturation polarization decreased as well as the coercive field. Characteristic antiferroelectric double hysteresis loops developed.

In Table 7.1-5 the parameters determined from the polarization curves are presented. A decrease of saturation polarization P_s from almost 40 µC/cm² to nearly 20 µC/cm² was achieved by increasing the content of Lanthanum from 1 mol% to 5 mol%. The coercive field E_c also decreased, while the remnant polarization P_r dropped dramatically with the insertion of 4 mol% Lanthanum.

A big problem is the break down voltage at which the sample cracks. If this voltage is lower than the voltage needed to saturate the polarization, no comment can be made about the characteristics. Therefore the data of A-6La, A-7La and A-8La are missing in the table.

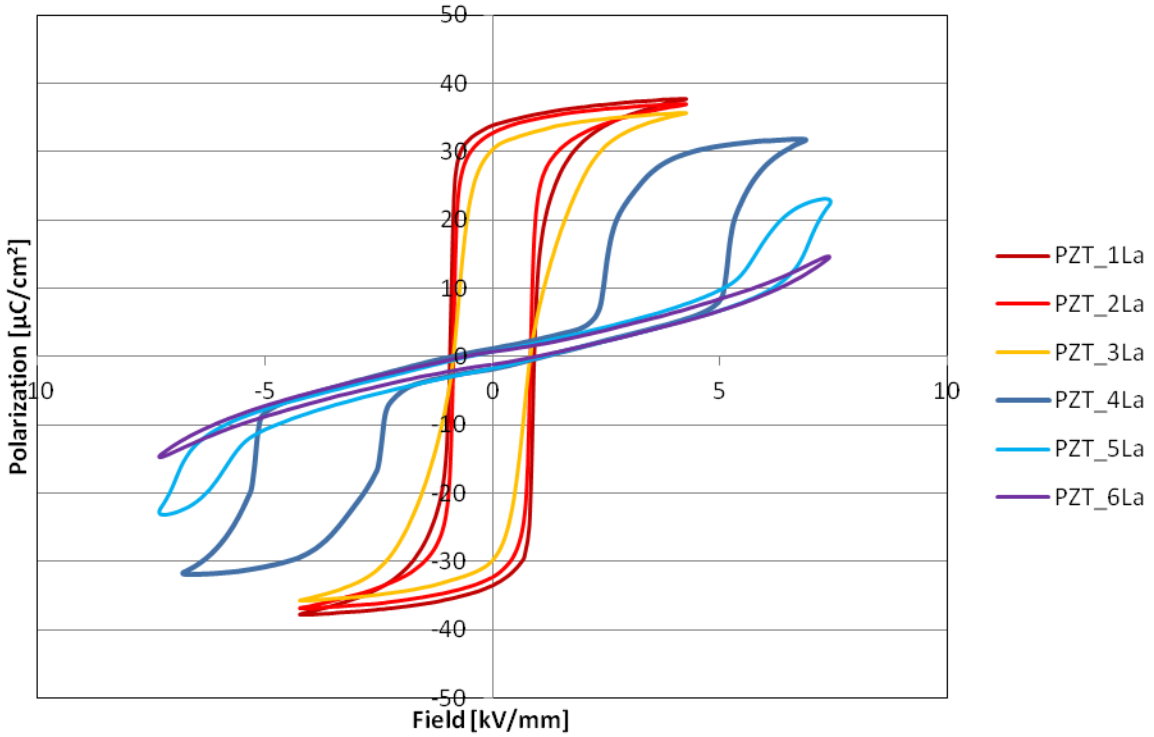

Figure 7.1-9: Polarization curves of Lanthanum-substitution in PZT $PbZr_{0.9}Ti_{0.1}O_3$.

Table 7.1-5: Results of polarization measurements of Lanthanum-substitution in PZT $PbZr_{0.9}Ti_{0.1}O_3$.

sample	Ps	Pr	Ec [kV/mm]
A_1La	38	35	3.25
A_2La	37	34	3.23
A_3La	36	33	3.08
A_4La	32	1	2.08
A_5La	23	1	2.20

As the measurements of relative permittivity versus temperature showed some peculiarity at around 100 °C, a detailed examination of the sample A-3La was pursued. The step found in the relative permittivity versus temperature curve was analyzed by heating the sample to 120 °C and measuring the polarization over field. At this temperature the ferroelectric transformed into an antiferroelectric behaviour and a double hysteresis loop appeared (see Figure 7.1-10). This behaviour was reversible and reproducible. This is in good accordance to the phase diagram of Härtling[21], where the curvature of the phase boundary between antiferroelectric and ferroelectric phase changed as the Lanthanum content is increased from 2 to 4 mol%.

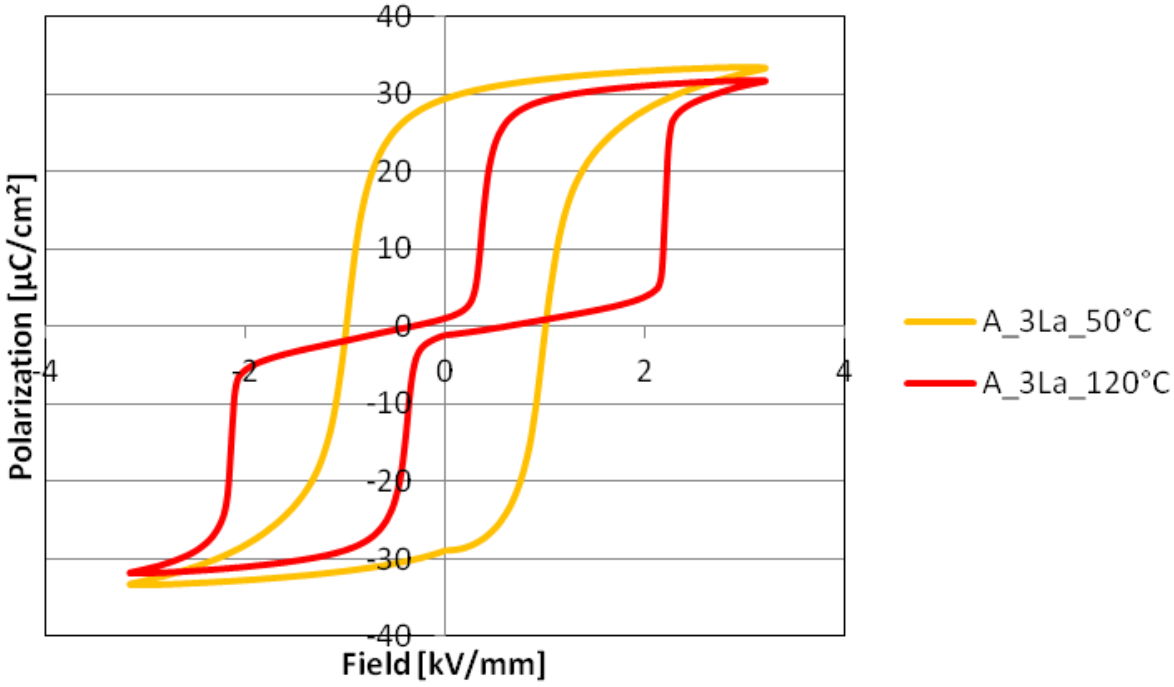

Figure 7.1-10: Polarization curves of A-3La at 50 °C and 120 °C.

7.1.2 PZT modified with Bismuth:

Bismuth was chosen as substituent of Lead due to the similarity in ionic radius, electronic structure and atomic weight. The polarizability of Bismuth due to the stereochemically active $6s^2$ orbital, a lone pair, is comparable to that of Lead. This should off-centre the cation and thus should promote a distortion of the cell. Distortion might induce structural changes and could favour orthorhombic phase[30],[63],[97].

Regarding the perovskite structure $Bi(Mg_{0.5}Ti_{0.5})O_3$, Bismuth ions are assumed to be displaced like Lead ions in the antiferroelectric Lead Zirconate. Additionally, the octahedra are tilted in anti-phase resulting in an orthorhombic structure[98].

Hence, by the substitution of Lead with Bismuth in PZT an antiferroelectric phase could be stabilized

The ionic radius of Bismuth is pretty close to Lead but is still smaller (r_{Bi}= 1,45 Å, r_{Pb}=1,49 Å) and should lead to a smaller cell volume additionally favouring a structural change. The value for Bismuth was linearly extrapolated from literature data[52]. The mass of Bismuth is 208.98 g/cm³ which is close to the mass of Lead, 207.2 g/cm³. This might come into play at the field dependent phase transition of ferroelectric to antiferroelectric behaviour which is assumed to be a phonon process.

The valency of Bi^{3+} ions creates Lead vacancies in the same amount as at the substitution with Lanthanum:

$$Pb_{1-1.5a}Bi_aV_{Pb}''_{0.5a}Zr_{1-x}Ti_xO_3.$$

This should interfere with the coupling of the oxygen octahedra and reduce the translation invariance. The comparison of this series with the Lanthanum substituted PZT should reveal the relevant factors stabilizing antiferroelectric behaviour amongst ionic radius, atomic mass, electronic structure and lattice vacancies.

In the following chapters the composition is labelled as A-aBi where `a´ refers to the molar percentage of Bismuth. All results are compared to those of the substitution with Lanthanum.

7.1.2.1 XRD Characterization

After calcination secondary phases emerged which remain and even grew in intensity after sintering. The precipitations were identified as Zirconium dioxide and Pb-Bi-O-compounds and the amount increased with further substitution of Bismuth (see Figure 7.1-11). This might be due to the fact that a solubility limit at 4 mol% of Bismuth occurred. Bismuth precipitated associated with Lead. According to the phase diagram of PbO and Bi_2O_3 and the Inorganic Crystal Structure Database, ICSD, the precipitations were most probably $Pb_5Bi_8O_{17}$, $Pb_5Bi_8O_{21}$, $Pb_2Bi_6O_{11}$ and $PbBi_{12}O_{20}$. As Zirconium oxide is the last compound in the formation sequence of PZT, whose reaction agents are no longer provided, it remained as secondary phase. This shifted the main composition to the Titanium-rich side of the phase diagram.

That resulted in a reduction of the lattice parameters and the cell volume due to the lower cell volume of Lead Titanate in comparison to Lead Zirconate. Up to the substitution with 2 mol% Bismuth the densification increased, but then the Archimedes´ density as well as the relative density deteriorated (see Table 7.1-6). Overall the theoretical density decreased with increasing content of Bismuth.

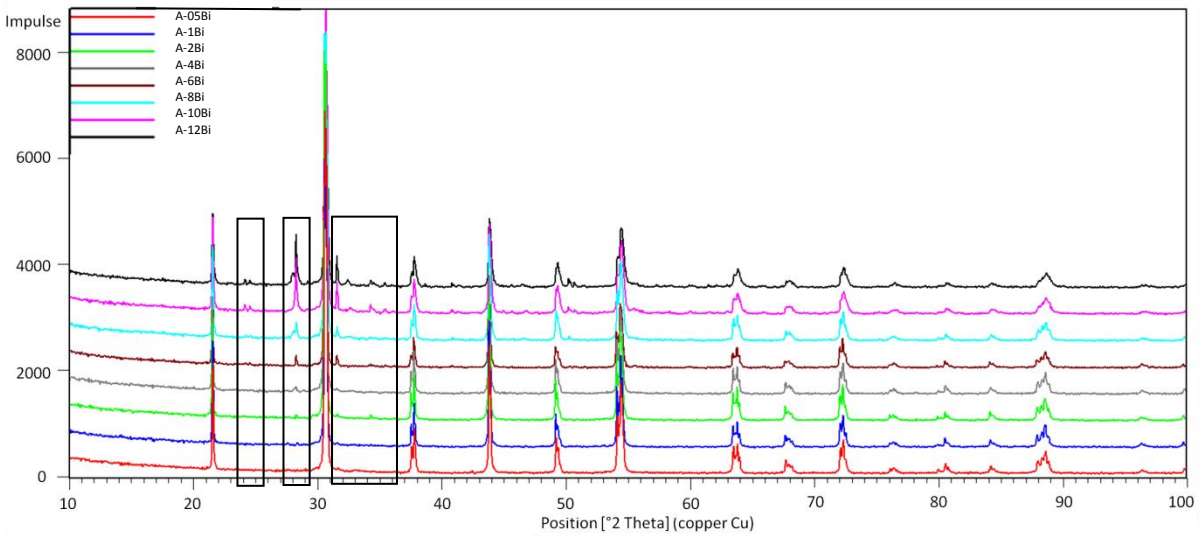

Figure 7.1-11: XRD of sintered powders of Bismuth substitution in PZT $PbZr_{0.9}Ti_{0.1}O_3$ (reflection patterns of the secondary phases are highlighted by rectangles).

Table 7.1-6: List of the cell parameters, the cell volume and the densities of Bismuth substitution in PZT $PbZr_{0.9}Ti_{0.1}O_3$.

sample	c [Å]	a [Å]	c/a	cell volume [Å ³]	theoretical density [g/cm³]	Archimedes´ density [g/cm³]	relative density [%]
A_05Bi	14.4079	5.8418	2.4664	425.8132	7.91	7.46	94.31
A_1Bi	14.4138	5.8423	2.4671	426.0711	7.98	7.65	95.86
A_2Bi	14.4095	5.8411	2.4669	425.757	7.96	7.64	95.98
A_4Bi	14.4036	5.8404	2.4662	425.4903	7.87	7.50	95.30
A_6Bi	14.4148	5.8417	2.4676	426.0088	8.18	7.56	92.42
A_8Bi	14.3979	5.8381	2.4662	424.9899	7.83	7.25	92.59
A_10Bi	14.3859	5.8338	2.4659	424.0035	7.80	7.33	93.97
A_12Bi	14.3820	5.8335	2.4654	423.8403	7.75	7.22	93.16

7.1.2.2 Microstructure

InFigure 7.1-12 to Figure 7.1-14 backscattered images demonstrate the increase in the formation of secondary phases with increasing fraction of Bismuth. With lower fraction of Bismuth Zirconium dioxide precipitated, but with higher content additionally Pb-Bi-O-compounds were visible.

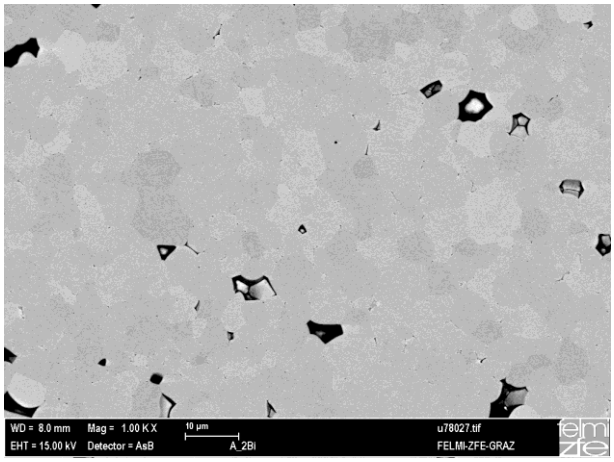

Figure 7.1-12: SEM backscattered electron image of A-2Bi: No secondary phases could be detected.

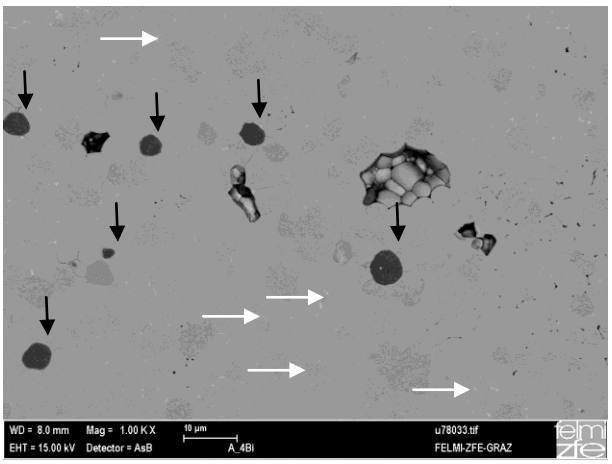

Figure 7.1-13: SEM backscattered electron image of A-4Bi: ZrO2 secondary phases marked by a black arrow, Bi-Pb-precipitations are highlighted by white arrows.

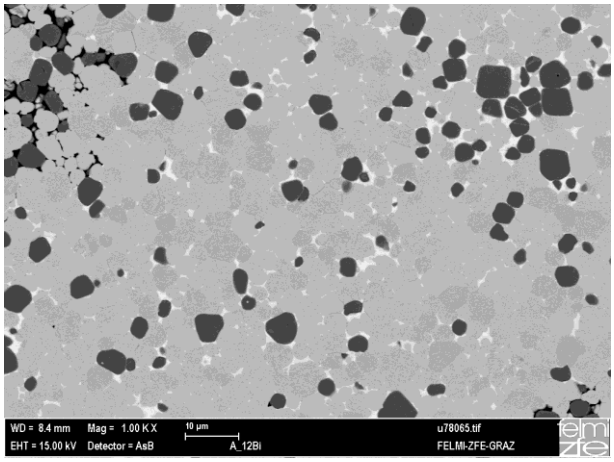

Figure 7.1-14: SEM backscattered electron image of A-12Bi. Precipitations of ZrO2 (dark) and Bi-Pb-O-compounds (light) are visible. The amount of secondary phases has been increased by further substitution of Bismuth.

7.1.2.3 Dielectric Characterization:

In Table 7.1-7 all measured low signal dielectric parameters are summarized. Relative permittivity and loss factor varied with the modification, but no clear trend could be observed due to the formation of secondary phases. Secondary phases can interfere with the dielectric properties and lead to deviated value of the examined parameters. Capacitance, loss factor and relative permittivity increased slightly with increasing the molar content of Bismuth. The values of capacitance varied from 190 to 270 pF and relative permittivity from ~220 to ~335. In reverse, the piezoelectric constant decreased from 69.3 to 15.8 pC/N. The value of the sample A-1Bi of 3.0 pC/N is an outlier, which cannot be explained by now.

Table 7.1-7: Results of low signal dielectric measurements of Bismuth substitution in PZT $PbZr_{0.9}Ti_{0.1}O_3$.

Sample / 0.1 kHz	capacitance [nF]	loss factor []	relative permittivity []	piezoelectric constant d33 [pC/N]
A_05Bi	0.19	0.02	219	69.3
A_1Bi	0.20	0.03	236	3.0
A_2Bi	0.25	0.03	280	50.5
A_4Bi	0.23	0.06	284	60.5
A_6Bi	0.27	0.12	335	54
A_8Bi	0.22	0.09	291	31
A_10Bi	0.26	0.14	324	33.6
A_12Bi	0.22		292	15.8

Relative permittivity measurements versus temperature at 1 MHz revealed the temperature of maximum permittivity. This peak refers to a phase transition - in this case from ferroelectric to paraelectric phase. A shift to lower temperature is visible as well as a decrease in relative permittivity by increasing the Bismuth fraction. Moreover, the peak flattens with higher content of Bismuth referring to a more diffuse phase transition. This is in good accordance to the literature[99], [100], [101], [102].

Further substitution from 1 mol% to 8 mol% forced the value of relative permittivity to drop from 12300 to 4200 (see Figure 7.1-15andTable 7.1-8). In addition to that, the transition temperature decreased only slightly from ~250 to ~230 °C.

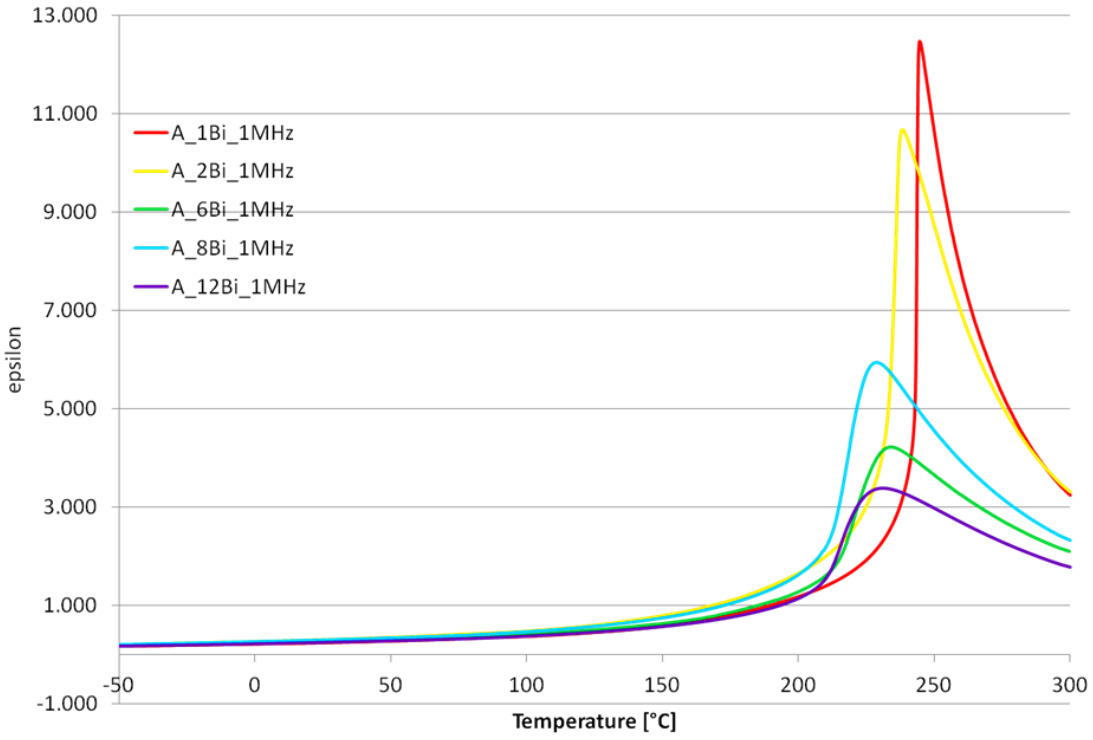

Figure 7.1-15: Permittivity measurements versus temperature of Bismuth-substitution in PZT $PbZr_{0.9}Ti_{0.1}O_3$ at 1 MHz.

Table 7.1-8: Results of the relative permittivity versus temperature curves of Bismuth substitution in PZT $PbZr_{0.9}Ti_{0.1}O_3$.

sample	maximum relative permittivity	Temperatur Tm [°C]
A_05Bi	12299	252
A_1Bi	12459	245
A_2Bi	10292	237
A_4Bi	9645	235
A_6Bi	4202	233
A_8Bi	5900	231
A_10Bi	2585	231
A_12Bi	3366	233

The dielectric response under various frequencies is plotted in Figure 7.1-16. No frequency dependence could be proven for any sample. By increasing the frequency the peak temperatures stayed the same, but the height of the peaks declined. The shape of the curves resembled those of the Lanthanum substituted Lead Zirconate-Lead Titanate samples. Therefore, relaxor behaviour of that material can be excluded.

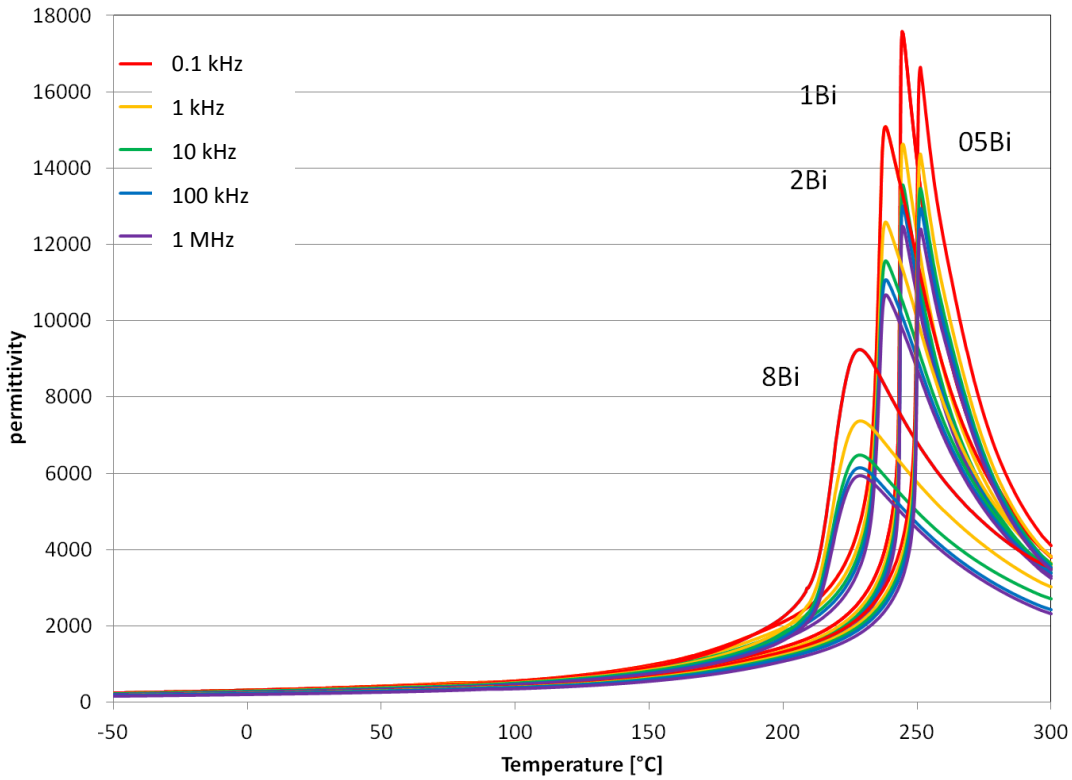

Figure 7.1-16: Frequency dependent measurements of the relative permittivity of selected Bismuth-substitution in PZT $PbZr_{0.9}Ti_{0.1}O_3$ (measured at 0,1 kHz, 1 kHz, 10 kHz, 100 kHz and 1 MHz).

All polarization curves of the Bismuth-substitution in PZT-samples revealed ferroelectric behaviour. As demonstrated in Figure 7.1-17 and Table 7.1-9, all parameters - saturation polarization P_S, remnant polarization P_r and the coercive field E_c - decreased with increasing fraction of Bismuth. No phase transition from ferroelectric to antiferroelectric behaviour could be observed. This might be an effect of the secondary phases which occurred with the insertion of 4 mol% of Bismuth, where the hysteresis loop appeared very lossy. This curve exceeded all others in remnant polarization. No comment on the influences of the substitution of Lead with Bismuth could have been done due to the occurrence of secondary phases.

Table 7.1-9: Results of polarization measurements of Bismuth-substitution in PZT $PbZr_{0.9}Ti_{0.1}O_3$.

sample	Ps [µC/cm²]	Pr [µC/cm²]	Ec [kV/mm]
A_1Bi	32	30	1.16
A_2Bi	25	21	1.09
A_4Bi	37	41	1.23
A_6Bi	31	27	1.19
A_8Bi	27	23	1.24
A_10Bi	30	25	1.45
A_12Bi	21	17	1.25

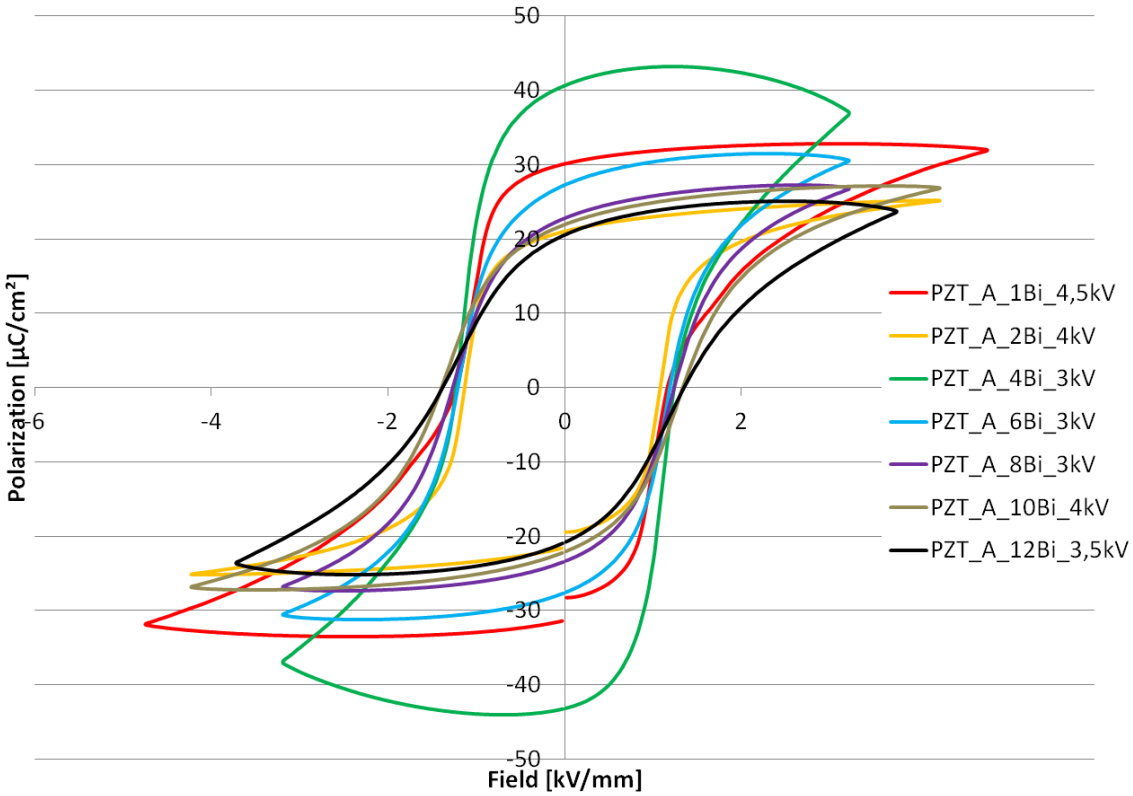

Figure 7.1-17: Polarization curves of Bismuth-substitution in PZT $PbZr_{0.9}Ti_{0.1}O_3$.

A detailed view of the curve of A-05Bi showed a peculiarity at around 100 °C (see Figure 7.1-18). This slight increase was not that dominant, but it is also displayed in the loss factor curves. For further investigations, this sample was heated up and polarization curves were recorded. No evidence of a ferroelectric to antiferroelectric phase transition at elevated temperature could be observed. The shape of the hysteresis curves slimmed and the values of polarization enhanced with increasing temperature. In Figure 7.1-19 the reduction of the area of the curves by increasing the temperature is obvious.

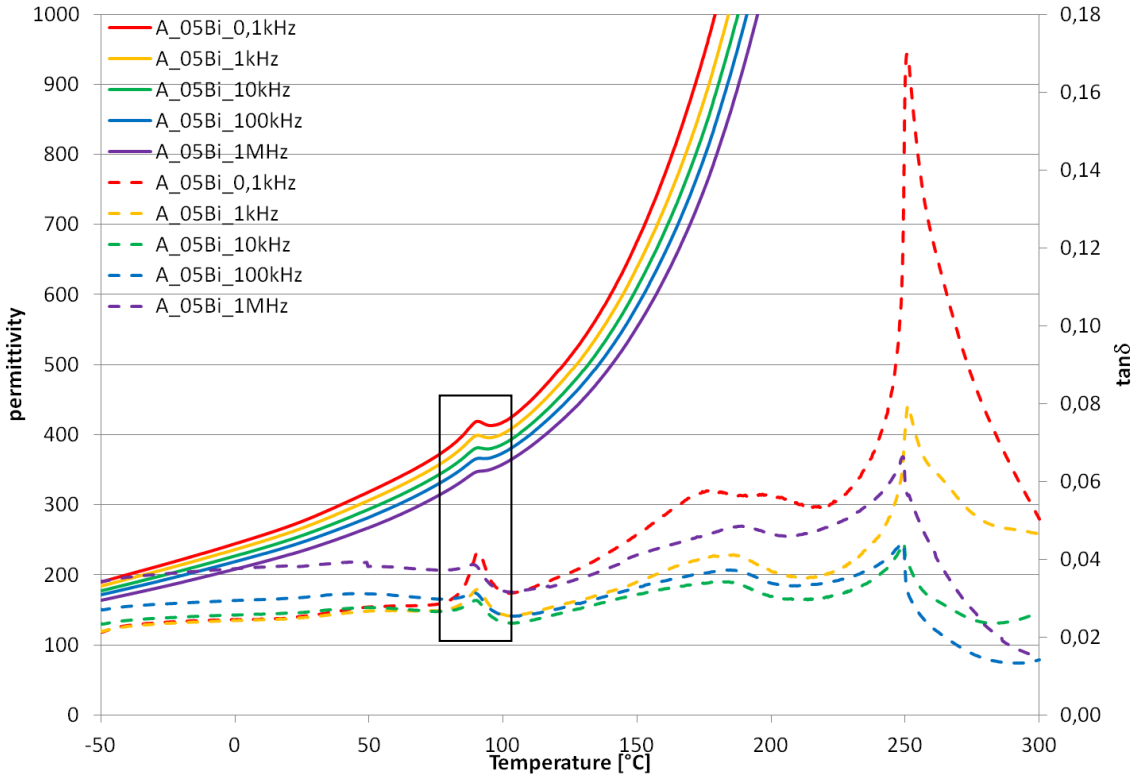

Figure 7.1-18: Frequency dependent measurements of the relative permittivity and loss factor of A-05Bi sample. The rectangle emphasizes the anomaly of around 90°C.

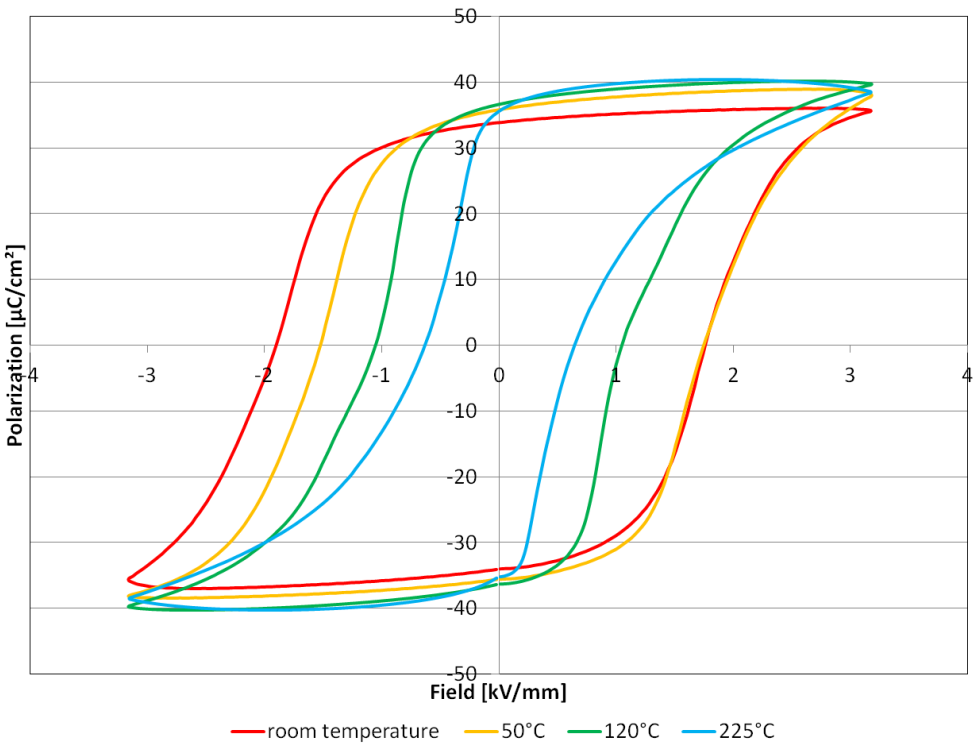

Figure 7.1-19: Polarization curves of sample A-05Bi at elevated temperatures.

7.1.3 PZT modified with Lanthanum and Bismuth

By introducing Bismuth into the system a donor takes the place at A-site which assembles Lead in weight, ionic radii and polarizability, but has a higher valency. In the previous section the substitution of Lead only with Bismuth in PZT was examined. This sections deals with the interaction with Lanthanum.

Substitution of Lead with the trivalent Bismuth in the PLZT system increases the Lead vacancies according to the equation

$$Pb_{1-1.5a-1.5b}La^{\circ}_{a}Bi^{\circ}_{b}V_{Pb}''_{0.5a+0.5b}Zr_{1-x}Ti_{x}O_{3}$$

As the content of Lanthanum is kept constant at 6 mol% for every composition, the increase of the Lead vacancies is only dependent on the amount of Bismuth. In this study the compositions with two ratios of Zirconium to Titanium were investigated. In the following, the composition with 90 to 10 will be labeled as AA and the composition with 85 to 15 will be labeled BB.

According to the literature, the combination of these two trivalent substituents deteriorates the homogeneity of the material[100]. Furthermore, the substitution-pair induces an increase in disorder resulting in a more diffuse phase transition demonstrating a broadening of the relative permittivity peak[99],[101]. Relative permittivity should increase with increasing content of the substitution-pair[100] and the transition temperature should be shifted to higher temperature[101].

7.1.3.1 XRD Characterization

As shown in Figure 7.1-20, Figure 7.1-21, the XRD spectra of the sintered samples demonstrate next to the main reflections of the perovskite phase several additional peaks. These enhanced with further increase of the content of substituents. This might most probably be Zirconium dioxide and additionally reflections of Bismuth-Titanate compounds.

In comparison to the samples $PbZr_{0.9}Ti_{0.1}O_3$, where Lead was substituted with Bismuth and, all samples had rhombohedral structure, this time all reflection patterns were refined by the Rietveld method using an orthorhombic reference of Pba2 symmetry. As mentioned above, the ionic size of the substituents is smaller than that of Lead and therefore the reduction in cell volume did not surprise. Additionally the occurrence of secondary phases shifted the composition to a higher Titanium content causing a decrease in the cell volume. That confirmed the low solubility of Bismuth in the Lead Zirconate-Lead Titanate system.

Comparing Table 7.1-10 and Table 7.1-11, the substitution of Lead with Bismuth in the AA system resulted in a higher reduction of the cell volume as in the BB system. The cell volume of the Zirconium-richer composition is influenced by the substitution in a higher extent as the Titanium-richer composition. The explanation might lie in a better incorporation of Bismuth in the BB composition and therefore less and lower reflections of secondary phases were obvious. Therefore no comments on the influence of the molar ratio of the substituents on the dielectric properties can be done, but a comparison of the data obtained is given.

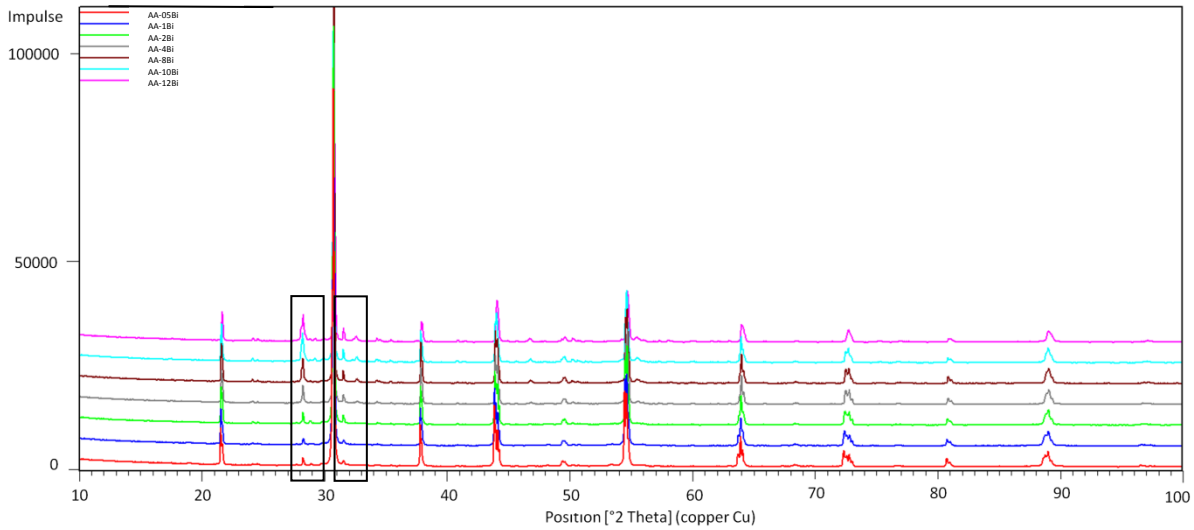

Figure 7.1-20: XRD of sintered powders of Bismuth-substitution in PLZT (AA = $Pb_{0.91}La_{0.06}Zr_{0.9}Ti_{0.1}O_3$).

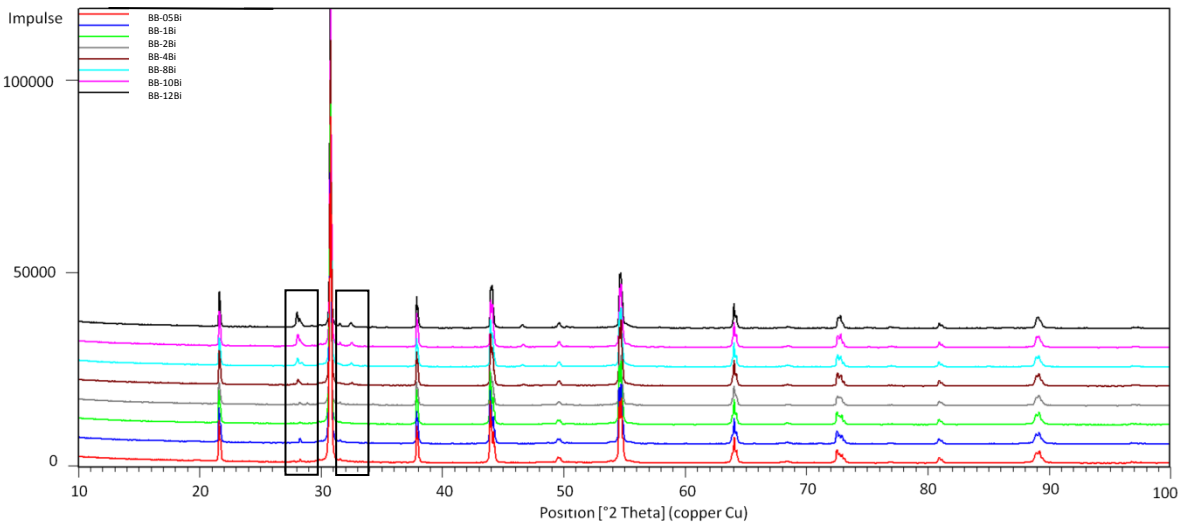

Figure 7.1-21: XRD of sintered powders of Bismuth-substitution in PLZT (BB = $Pb_{0.91}La_{0.06}Zr_{0.85}Ti_{0.15}O_3$).

Inserting Bismuth in the system AA led to an increase in theoretical density, while the Archimedes´ densities decreased with following the substitution. Therefore the relative densities dropped from ~94 to ~89% in this series (Table 7.1-10).

Table 7.1-10: List of the cell parameters, the cell volume and the densities of Bismuth substitution in PLZT AA.

sample	c [Å]	b [Å]	a [Å]	c/a	cell volume [Å³]	theoretical density [g/cm³]	Archimedes´ density [g/cm³]	relative density [%]
AA_1Bi	8.2118	11.6900	5.8400	1.4061	560.6206	7.86	7.42	94.33
AA_2Bi	8.2136	11.6870	5.8367	1.4072	560.2706	7.87	7.86	99.92
AA_4Bi	8.2141	11.6804	5.8318	1.4085	559.5237	7.88	7.67	97.41
AA_6Bi	8.2143	11.6742	5.8293	1.4091	559.0109	7.89	7.47	94.72
AA_8Bi	8.2149	11.6687	5.8269	1.4098	558.5475	7.89	7.32	92.67
AA_10Bi	8.2199	11.6672	5.8242	1.4113	558.5660	7.89	7.27	92.04
AA_12Bi	8.2216	11.6574	5.8198	1.4127	557.7806	7.91	7.05	89.12

In the case of the Titanium-richer composition, the theoretical density was almost not affected by Bismuth. Archimedes´ density on the other hand decreased from 7.41 to 7.24 g/cm³, which led to a drop in relative density of 2.5%. Overall, all samples of both series revealed relative densities below 95% and therefore a poor densification (Table 7.1-11).

Table 7.1-11: List of the cell parameters, the cell volume and the densities of Bismuth substitution in PLZT BB.

sample	c [Å]	b [Å]	a [Å]	c/a	cell volume [Å³]	theoretical density [g/cm³]	Archimedes´ density [g/cm³]	relative density [%]
BB_05Bi	8.2001	11.6696	5.8286	1.4069	557.7444	7.85	7.41	94.39
BB_1Bi	8.2012	11.6691	5.8284	1.4071	557.7773	7.85	7.45	94.94
BB_2Bi	8.2021	11.6668	5.8276	1.4075	557.6538	7.85	7.54	96.07
BB_4Bi	8.2046	11.6621	5.8241	1.4087	557.2641	7.86	7.51	95.52
BB_6Bi	8.2072	11.6624	5.8256	1.4088	557.5942	7.86	7.40	94.24
BB_8Bi	8.2100	11.6646	5.8275	1.4088	558.0750	7.85	7.48	95.27
BB_10Bi	8.2114	11.6584	5.8242	1.4099	557.5619	7.86	7.31	93.02
BB_12Bi	8.2140	11.6519	5.8196	1.4114	556.9857	7.87	7.24	92.06

7.1.3.2 Dielectric Characterization:

Low signal values of capacitance, relative permittivity and loss factor of all samples are listed in the following tables (Table 7.1-12 and Table 7.1-13).

Inserting Bismuth in the system AA, capacitance and relative permittivity decreased, while the loss factor increased. With increasing the content of the ion capacitance dropped from ~750 to ~440 pF and relative permittivity from ~655 to ~400, while the loss factor tripled from 0.0090 to 0.0274.

In the case of the Titanium-richer system a similar behaviour can be observed: Capacitance and relative permittivity lowered and the loss factor increased with increasing substitution of Lead with Bismuth. The values dropped from ~810 to ~620 pF and from ~1040 to 790 in relative permittivity, while the loss factor duplicated from 0.0224 to 0.0420.

Table 7.1-12: Results of low signal dielectric measurements of Bismuth-substitution in PLZT AA.

sample	capacitance [nF]	loss factor []	relative permittivity []
AA_05Bi	0.7518	0.0090	654
AA_1Bi	0.7252	0.0089	633
AA_2Bi	0.7152	0.0091	644
AA_4Bi	0.6213	0.0205	536
AA_6Bi	0.6600	0.0269	590
AA_8Bi	0.5559	0.0511	499
AA_10Bi	0.4977	0.0251	446
AA_12Bi	0.4392	0.0274	401

Table 7.1-13: Results of low signal dielectric measurements of Bismuth-substitution in PLZT BB.

sample	capacitance [nF]	loss factor []	relative permittivity []
BB_05Bi	0.8137	0.0224	1043
BB_1Bi	0.8249	0.0232	1056
BB_2Bi	0.9171	0.0215	1176
BB_4Bi	0.9142	0.0443	1164
BB_6Bi	0.8578	0.0305	1714
BB_8Bi	0.8354	0.0462	1071
BB_10Bi	0.6316	0.0407	787
BB_12Bi	0.6205	0.0420	786

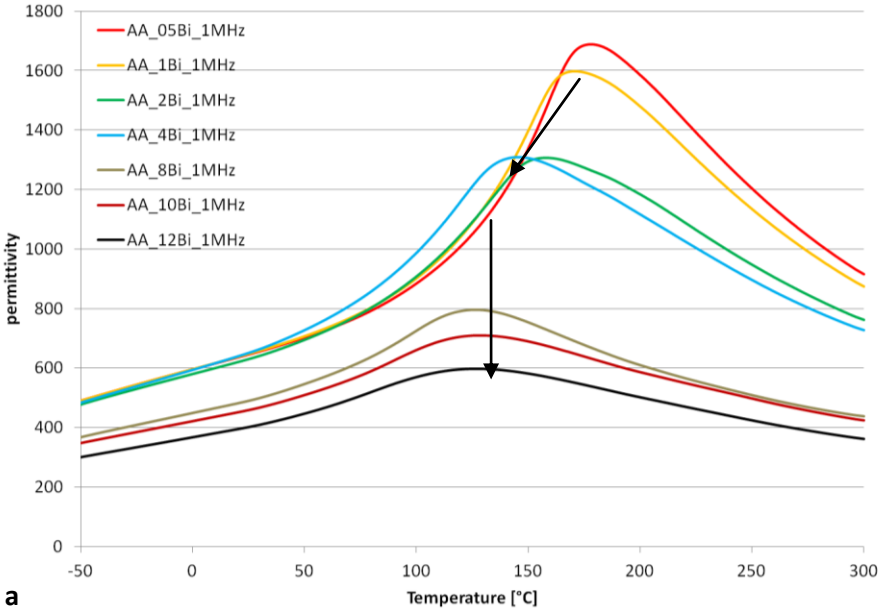

a

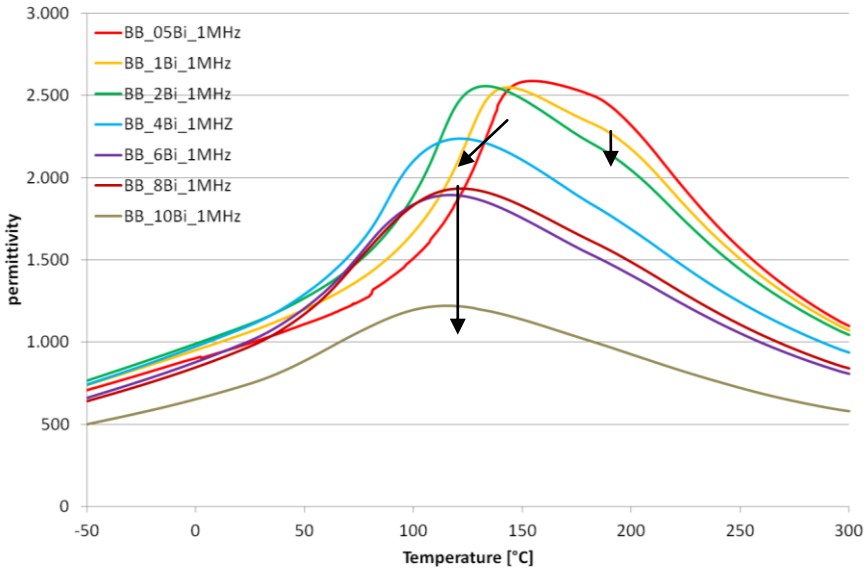

b

Figure 7.1-22: Relative permittivity curves versus temperature at 1 MHz (arrows indicate the maximum in relative permittivity and demonstrate the alteration with increasing concentration of substituents (AA = $Pb_{0.91}La_{0.06}Zr_{0.9}Ti_{0.1}O_3$, BB= $Pb_{0.91}La_{0.06}Zr_{0.85}Ti_{0.15}O_3$).

In Figure 7.1-22a and b the progressively addition of Bismuth into the composition AA and BB is demonstrated. In both cases a decrease in height of the curve with increasing insertion of the substituent occurred. Furthermore the curve flattened and the peak broadened. This addressed a more diffuse phase transition by substituting with Bismuth. Additionally, the peak position was shifted to the left in the graph. Hence, the transition temperature was shifted to lower temperatures. In the samples called AA-05Bi, AA-1Bi and AA-2Bi an additional step was evident at higher temperatures. This shoulder was not shifted in the small compositional range but stayed at around 200 °C. With increasing the addition of Bismuth this step disappeared.

The results of the measurements are presented in Table 7.1-14. Comparing these two series AA and BB, over the whole range, the relative permittivity is approximately divided by 2.8 and 2.2, respectively. The values in the AA system are far beyond those of the BB system. To quantify these figures, a decrease from ~1680 to ~600 in relative permittivity in the former case and from ~2600 to ~1150 in relative permittivity in the latter one appeared.

Regarding the temperature shift by inserting the substituents, the reduction of the temperature in the AA series was higher than in the BB series. Over the whole range the temperature was lowered by 50 °C from ~180 to ~130 °C in the AA system, while in the BB system the temperature of the peak in the curve of the sample with the highest content of Bismuth deviated by ~35°C from 155 °C, which was the starting point. Having a closer look, the continuously decrease in temperature stopped at a certain amount of substituents, where only a scattering around a value occurred. In the case of AA this happened with the sample AA-6Bi. Once this level of addition was passed, the transition temperature oscillated around 130 °C. Likewise, by proceeding the insertion into the composition BB the temperature did only marginally change and could be set at around 120 °C after exceeding 4 mol% addition of Bismuth.

Comparing these results with the values of the starting composition AA and BB, temperature shifted to lower degrees as well as the drop in relative permittivity was induced by increasing content of Bismuth. Interestingly, with low concentration of Bismuth in AA relative permittivity exceeded slightly that of the starting composition, which was 1550.

Table 7.1-14: Results of the relative permittivity versus temperature curves of Bismuth-substitution in PLZT AA and BB.

sample	maximum in relative permittivity	Temperature Tm [°C]	sample	maximum in relative permittivity	Temperature Tm [°C]
AA_05Bi	1689	178	BB_05Bi	2591	155
AA_1Bi	1597	171	BB_1Bi	2550	144
AA_2Bi	1306	158	BB_2Bi	2556	134
AA_4Bi	1309	146	BB_4Bi	2237	122
AA_6Bi	1163	135	BB_6Bi	1897	117
AA_8Bi	795	127	BB_8Bi	1934	122
AA_10Bi	709	129	BB_10Bi	1222	116
AA_12Bi	597	127	BB_12Bi	1146	120

In Figure 7.1-23a and b curves of the measurement of relative permittivity and the loss factor versus temperature at various frequencies of sample AA-1Bi and BB-1Bi are plotted. The peaks of the relative permittivity curves did not show any frequency dependence and correlated well with the

peaks of the loss factor curves. In the case of the sample BB-1Bi one additional peak was detected at higher temperature. It decreased but did not vanish with increasing frequency.

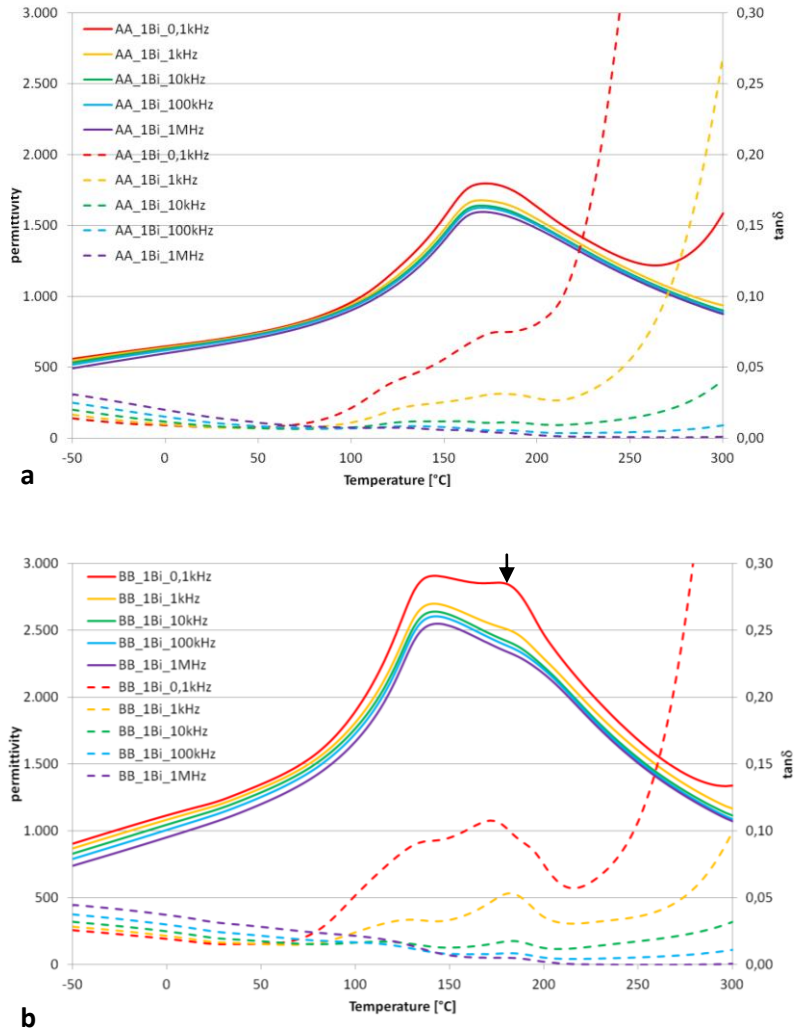

Figure 7.1-23: Frequency dependent measurements of the relative permittivity (solid line) and loss factor (dashed line) of Bismuth in PLZT (measured at 0,1 kHz, 1 kHz, 10 kHz, 100 kHz and 1 MHz). Anomalies are accentuated by an arrow (AA = $Pb_{0.91}La_{0.06}Zr_{0.9}Ti_{0.1}O_3$, BB= $Pb_{0.91}La_{0.06}Zr_{0.85}Ti_{0.15}O_3$)

The polarization curves of the AA compositions could not reach saturation at all and therefore they were left out in this chapter. Thus only the polarization curves of the BB system are shown below. In Figure 7.1-24 the hysteresis curves of samples of the BB system with the Bismuth-substitution are depicted. With increasing the content of Bismuth in the structure the shape of the loops varied. Only with low content of Bismuth saturation in polarization could be achieved. Therefore only these curves were considered to discuss the influence of Bismuth on the polarization over field. At low content, the maximum of the curves did not change. But with increasing Bismuth content the switching fields were shifted to higher fields and the area of the curves was reduced.

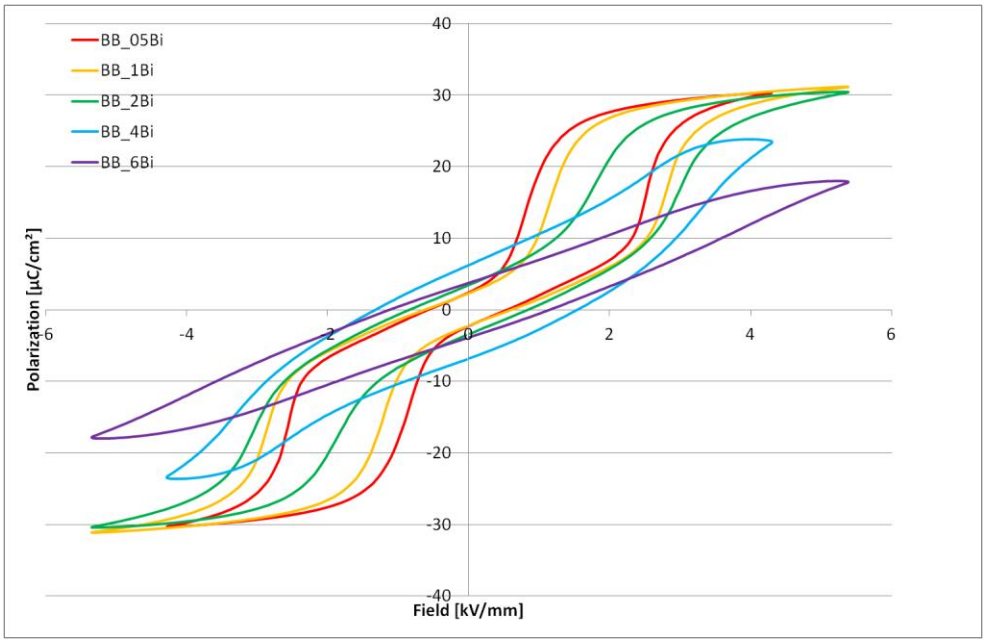

Figure 7.1-24: Polarization curves of Bismuth substitution in PLZT BB.

The substitution of Lead with Bismuth in Lead Zirconate-Lead Titanate did not reveal antiferroelectric polarization curves. All hysteresis loops showed ferroelectric behaviour. In Figure 7.1-25 a comparison of the polarization curves of PZT-samples containing either Bismuth or Lanthanum or both are shown. By replacing 6 mol% of Lead with Lanthanum a double hysteresis curve was recorded. In the case of Bismuth-substitution, a single loop could be detected, which became gradually lossy with increasing content of the substituent, most probably due to a solubility limit where secondary phases appeared. For that reason it could not have been demonstrated if higher content of Bismuth would induce a double hysteresis curve. Combining both substituents in one composition, a slim double hysteresis curve could be recorded. The remnant polarization and the forward switching field were lower than in the case of substitution with Lanthanum and the backward switching field was higher. The resulting curve demonstrated reduced losses and nearly no change in the saturation polarization compared to the sample containing Lanthanum. This superior behaviour of the combination of both substituents was not expected and could not be explained by a coinciding of the separate effects of the substituents. On the other hand, again with increasing Bismuth content in the samples, a solubility limit occurred and no saturation in polarization could be obtained. Therefore no comment on the effect of the following substitution of Bismuth in the system on the dielectric behaviour could be made.

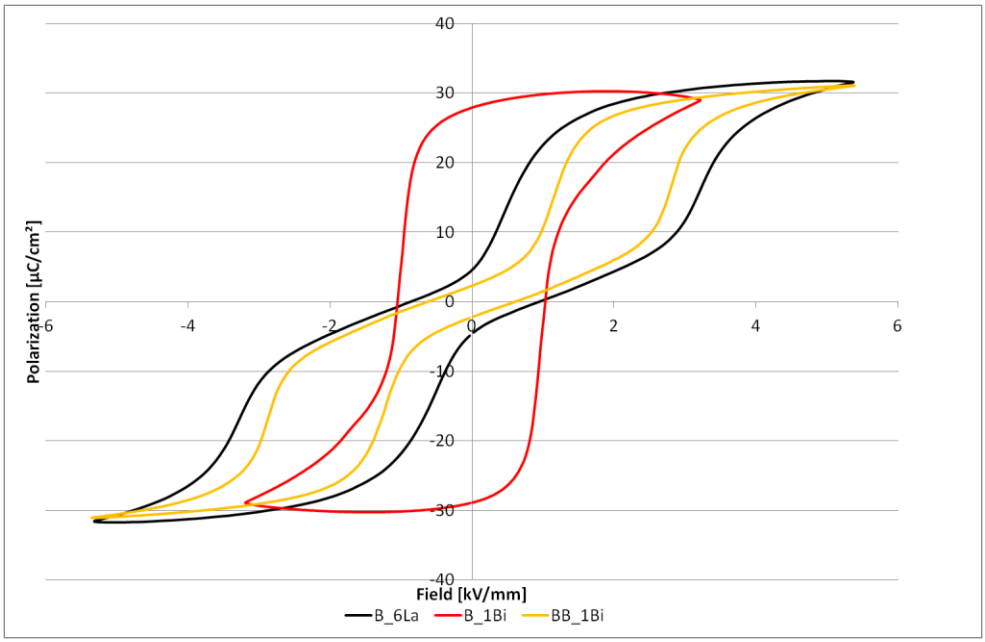

Figure 7.1-25: Comparison of the polarization curves of Lanthanum- and Bismuth-substitution in PZT with co-substitution of Bismuth-Lanthanum in PZT $PbZr_{0.85}Ti_{0.15}O_3$ (samples contain either no or 6 mol% of Lanthanum (B_6La and BB-1Bi), and no or 1 mol% of Bismuth (B-1Bi and BB-1Bi)).

7.1.3.3 Summary

In this chapter Lanthanum and Bismuth, two trivalent substituents of Lead in PZT were examined. In contrast to Lanthanum a solubility limit arose at 4 mol% of substitution of Bismuth. At higher contents precipitations of Zirconia, Pb-Bi-O compounds and Bismuth Titanates occurred. In the combination of Lanthanum and Bismuth, the solubility increased and less intense reflections of secondary phases were detected.

The properties of Bismuth are similar to that of Lead: It has also a stereochemically active $6s^2$-lone pair and approximately the same mass. Lanthanum on the other hand does not develop stereochemically active orbitals and possesses a higher degree of covalency in the cation-oxide bonding and a lower mass. The mass might come into play as the ferroelectric to antiferroelectric transition under field is a phonon process. As the electronic configuration has a high impact on the structure, the Bismuth should interact with the surrounding oxygen ions similar to Lead. The high polarizability should displace the cations and lead to a bigger distortion in the unit cell which should be released in a structural change to a less ordered system such as the orthorhombic structure. However, this transformation was not detected within the solubility range.

In the case of Lanthanum the orthorhombic structure can be identified with the substitution of 3 mol% of Lead, which is obviously an effect of the reduction in cell volume. Although small signal values indicated no polarization, the high signal measurements could not exhibit a double hystere-

sis loop at room temperature. Interestingly, Härtling[21] recognized a change in the slope of the ferroelectric-antiferroelectric phase boundary between 2 mol% and 4 mol% of Lanthanum substitution in PZT. However, by now no explanation was found, why temperature supports the enfolding of a double loop of an already orthorhombic material.

The difference in ionic radius between Bismuth and Lead is much smaller compared to the difference between Lanthanum and Lead. Together with the limited incorporation of Bismuth into the perovskite it seems that the reduction in cell volume by Bismuth substitution is not sufficient to cause a ferroelectric to antiferroelectric phase transition.

Interestingly, the combination of both substitutents revealed an orthorhombic structure. This leads to the assumption that the Lanthanum substituted PZT tries to preserve the orthorhombic structure even in association with another substituent which could not stabilize this structure.

Regarding the permittivity measurements, all values decreased with increasing substitution content and a more and more diffuse phase transition occurred which was shifted to lower temperature.

In comparison to Lanthanum, which stabilizes the antiferroelectric phase In Lead Zirconate-Lead Titanate at a certain amount of substitution of Lead, Bismuth did not induce a ferroelectric to antiferroelectric transition. Although Bismuth has the same valency as Lanthanum and therefore creates the same amount of Lead vacancies in PZT no antiferroelectric behaviour could be observed. By introducing both trivalent ions increasing the number of Lead vacancies again double hysteresis loops were recorded. This suggests that Lead vacancies play a minor role in the stabilization of the antiferroelectric phase.

Overall, the appearance of double hysteresis loops does not depend on the amount of vacancies, but on the structural change to orthorhombic symmetry. It might be possible to induce these correlating phase transitions with higher content of Bismuth, but this is hindered by the solubility limit of Bismuth at the A-site.

In the following chapters the influence of co-doping of Lanthanum and another substituent in PZT on the properties will be investigated.

7.2 Monovalent acceptor ions at A-site

In this chapter the effect of dopant-pairs at the A-site on structural, electric and related properties is examined by the co-substitution of Lanthanum with either Sodium, Lithium or Potassium. The substitution with a donor-acceptor–pair at A-site should create more structural disorder in the PZT system, a more diffuse phase transition[103],[104].

Concerning the relative permittivity, in literature no homogeneous picture is drawn and the trend deviates according to the consulted paper. The same is true regarding the transition temperature. In the case of Sodium it is said to increase[105],[106], whereas in the case of Potassium decrease[104] and in Lithium both might happen[107], [108]. Interestingly, a tripe point was detected with substitution of Lanthanum and Lithium in PZT. At that temperature antiferroelectric phase, ferroelectric phase and paraelectric phase coexist and as the energy barrier is not high can convert into each other easily[109].

As alkaline ions possess a valency of one, the substitution of Lead with alkaline ions in PLZT compensates the same amount of the substituent Lanthanum reducing the number of Lead vacancies. According to the equation,

$$Pb_{1-1.5a-0,5b}La^{\circ}_{a}M'_{b}V_{Pb}''_{0,5a-0,5b}(Zr_{1-x}Ti_{x})O_{3}\ .$$

two alkaline ions M´ eliminate one Lead vacancy.

For this study, three ratios of Zirconium to Titanium were investigated, which were 90 to 10, 85 to 15 and 80 to 20. In the following chapter these compositions are labeled to AA for the Zr:Ti 90:10, BB for Zr:Ti 85:15 and CC for Zr:Ti 80:20.

The concentration of Lanthanum for all samples remained at 6 mol% and only the content of alkaline ions varied. Therefore, at a certain value the Lead vacancies erased - namely at 6 mol% substitution with alkaline ions. At higher concentration of the alkaline ions, the material becomes acceptor doped and oxygen vacancies occur to maintain charge neutrality.

7.2.1 XRD-Characterization

As the XRD-patterns in Figure 7.2-1 and Figure 7.2-2 display, the alkaline ions incorporated well into the perovskite structure. Shifts in the reflection patterns only occurred due to the deviation in atomic weight and in size of the substituent. According to the literature[50],[62], a substituent of Lead with a bigger ionic radius increases the cell volume and vice versa. The valency, the atomic weight and the ionic radii of all ions participating in the structure can be found summarized in Table 7.2-1.

All alkaline ions are lighter than Lead. Additionally, Lithium and Sodium are smaller than Lead, whereas Potassium possesses a higher ionic radius. Therefore the cell volume should decrease in the former two cases and increase in the latter, which was confirmed regarding the data in Table 7.2-2 to Table 7.2-8 and Figure 7.2-8.

A closer look at the ionic radii revealed a peculiar image: Lithium has two possibilities of site occupancy. In the twelve-fold coordination Lithium can incorporate at the A-site and due to the ionic radius should reduce the cell volume. On the other hand in the six-fold coordination it occupies the B-site and should enlarge the cell volume. At low content of Lithium the cell volume increased slightly, but over the whole compositional range it decreased. At first the bigger ionic radius of Lithium in the six-fold coordination comparing to Zirconium or Titanium enlarged the cell volume, but then with higher content of Lithium, the cell volume dropped. This might be due to precipitations of Zirconium dioxide, which shifted the compositions to a higher Titanium-level and thus a reduction in the cell volume could be noticed. In Figure 7.2-3, to guide the eye, the secondary phase in AA-xLi was marked with rectangles next to the main reflection of the perovskite structure. In the Titanium-richer composition BB, this secondary phase could not be detected (compare Figure 7.2-3 with Figure 7.2-4). With further increasing the Titanium content, again additional peaks of ZrO_2 could be found (Figure 7.2-5). As the composition of the matrix deviated from the weighted composition the insertion of Lithium is difficult to discuss. Therefore all data obtained from these samples were treated with caution.

All samples of the series AA and BB were refined with the reference pattern of the orthorhombic structure Pba2. The compositions with the ratio Zirconium to Titanium 80 to 20 were refined with the rhombohedral structure R3cH. The most striking result was that the substitution with Sodium induced a structural change from rhombohedral to orthorhombic phase with the substitution of 8 mol% of Lead with Sodium. That can obviously be seen by the splitting of the reflection patterns (Figure 7.2-6 and Figure 7.2-7). The reason might lie in the smaller size of Sodium compared to Lead which changed the B-O distances favouring distortion and resulting in a structural transition[30]
As the phase transition from rhombohedral to orthorhombic structure occurred, the lattice parameter changed. The c-axis decreased, while the a-axis increased (Table 7.2-8). Thus in this series the cell volumes cannot be compared directly with each other (Table 7.2-9).

Table 7.2-1: Comparison in charge, atomic weight and radius of the alkaline ions used to build the perovskite structure.

	Pb	La	Li	Na	K	Zr	Ti
Charge	+2	+3	+1	+1	+1	+4	+4
Atomic weight	207.2	138.9	6.94	22.99	39.098	91.22	47.87
Radius [XII]	1.49	1.36	1.25	1.39	1.64		
Radius [VI]			0.76			0.72	0.605

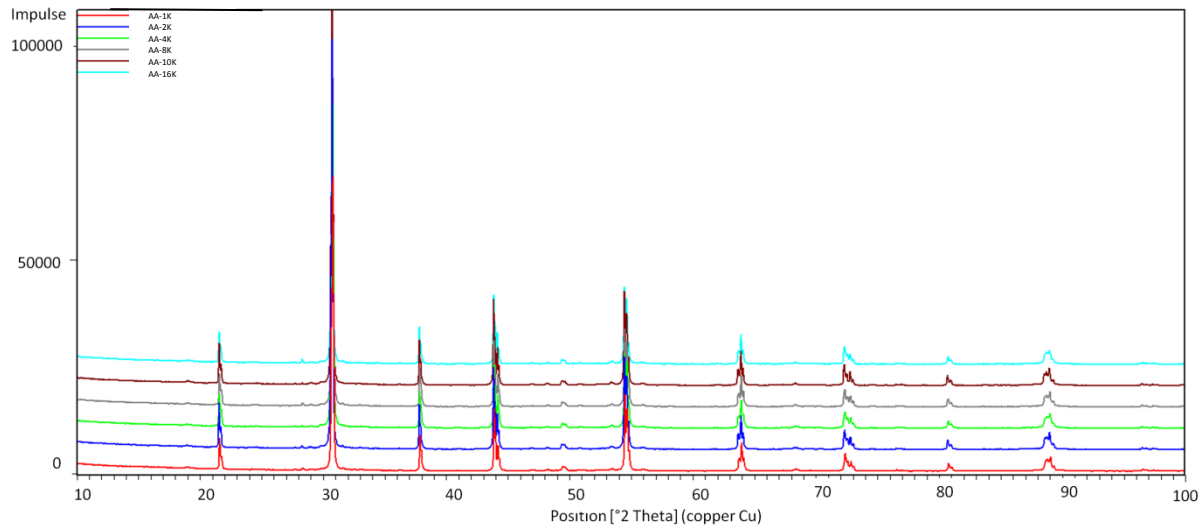

Figure 7.2-1: XRD of sintered powders of Potassium-substitution in PLZT (AA=$Pb_{0,91}La_{0,06}Zr_{0,9}Ti_{0,1}O_3$).

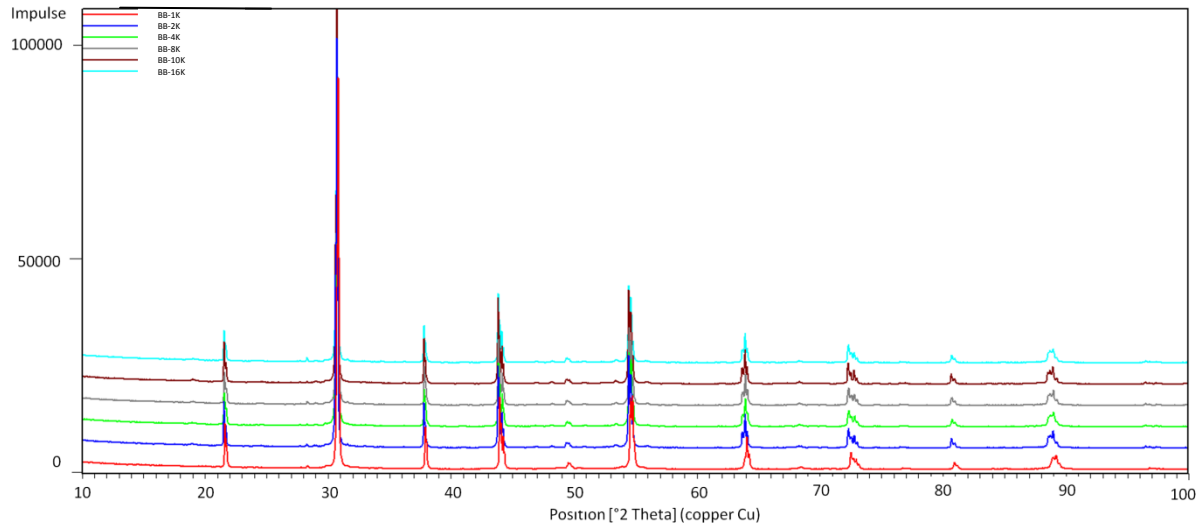

Figure 7.2-2: XRD of sintered powders of Potassium-substitution in PLZT (BB=$Pb_{0,91}La_{0,06}Zr_{0,85}Ti_{0,15}O_3$).

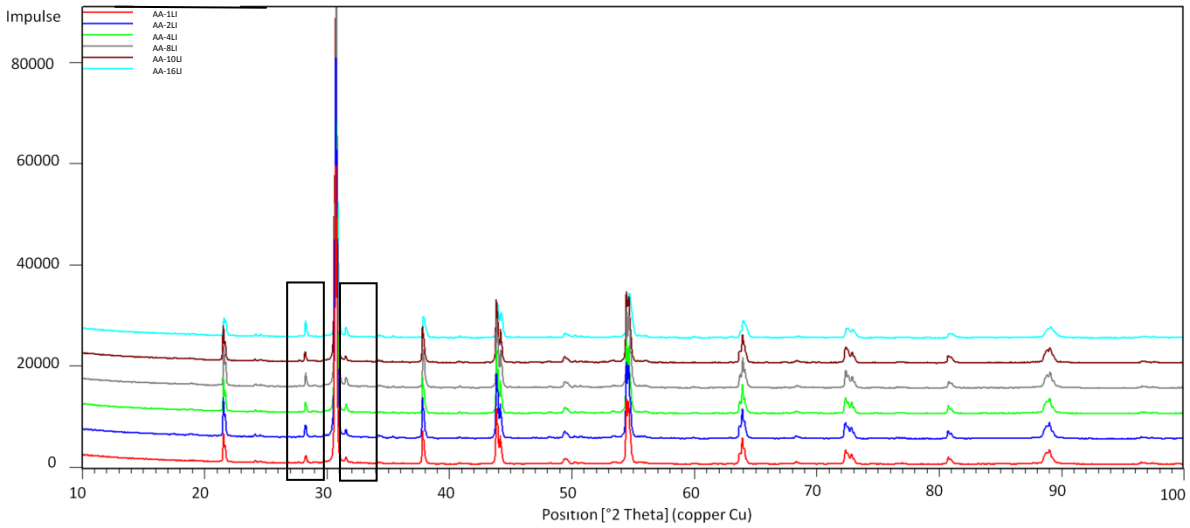

Figure 7.2-3: XRD of sintered powders of Lithium-substitution in PLZT (AA=$Pb_{0,91}La_{0,06}Zr_{0,9}Ti_{0,1}O_3$). Secondary phases are highlighted by rectangles.

Comparing the substitution with alkaline ions in the AA system, the highest relative densities could be achieved with the substitution with Potassium (Table 7.2-2 to Table 7.2-4). By inserting Lithium the relative density was about 95% and only varied little within the samples. In the case of the substitution with Sodium it decreased from ~97.5 to 95 %. With the substitution with Potassium at first the values increased to ~99% but then declined to ~95%. The lowest densification with 92.25% was observed in the sample AA-10K.

Table 7.2-2: List of the cell parameters, the cell volumes and the densities of Lithium-substitution in PLZT (AA).

sample	c [Å]	b [Å]	a [Å]	c/a	cell volume [Å³]	theoretical density [g/cm³]	Archimedes´ density [g/cm³]	relative density [%]
AA_1Li	8.1986	11.6741	5.8289	1.4066	557.8864	7.93	7.46	94.08
AA_2Li	8.1986	11.6754	5.8296	1.4064	558.0182	7.90	7.39	93.50
AA_4Li	8.1977	11.6767	5.8308	1.4059	558.1366	7.85	7.42	94.53
AA_8Li	8.1954	11.6750	5.8293	1.4059	557.7507	7.77	7.34	94.44
AA_10Li	8.1959	11.6759	5.8296	1.4059	557.8642	7.72	7.38	95.57
AA_16Li	8.1942	11.6762	5.8289	1.4058	557.6969	7.58	7.16	94.39

Table 7.2-3: List of the cell parameters, the cell volumes and the densities of Sodium-substitution in PLZT (AA).

sample	c [Å]	b [Å]	a [Å]	c/a	cell volume [Å³]	theoretical density [g/cm³]	Archimedes´ density [g/cm³]	relative density [%]
AA_1Na	8.2089	11.6961	5.8430	1.4049	560.9965	7.89	7.69	97.56
AA_2Na	8.2077	11.6946	5.8427	1.4048	560.8120	7.87	7.65	97.23
AA_4Na	8.2053	11.6841	5.8450	1.4038	560.3705	7.84	7.61	97.08
AA_8Na	8.1961	11.6879	5.8240	1.4073	557.9062	7.80	7.37	94.50
AA_10Na	8.1893	11.6777	5.8174	1.4077	556.3237	7.78	7.50	96.45
AA_16Na	8.1933	11.6757	5.8290	1.4056	557.6092	7.65	7.26	94.93

Table 7.2-4: List of the cell parameters, the cell volumes and the densities of Potassium-substitution in PLZT (AA).

sample	c [Å]	b [Å]	a [Å]	c/a	cell volume [Å³]	theoretical density [g/cm³]	Archimedes´ density [g/cm³]	relative density [%]
AA_1K	8.2117	11.6939	5.8418	1.4057	560.9676	7.79	7.68	98.62
AA_2K	8.2110	11.6940	5.8421	1.4055	560.9587	7.78	7.70	99.01
AA_4K	8.2123	11.6961	5.8423	1.4057	561.1695	7.74	7.69	99.29
AA_8K	8.2152	11.7002	5.8453	1.4054	561.8419	7.67	7.19	93.73
AA_10K	8.2142	11.6890	5.8455	1.4052	561.7824	7.64	7.05	92.25
AA_16K	8.2148	11.6966	5.8428	1.4060	561.4051	7.56	7.15	94.65

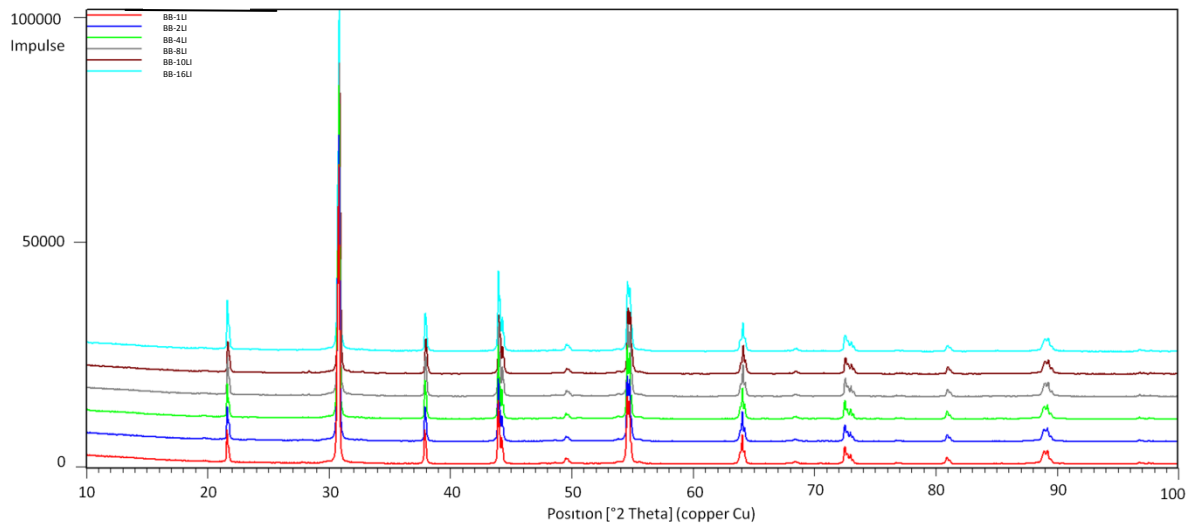

Figure 7.2-4: XRD of sintered powders of Lithium-substitution in PLZT (BB=$Pb_{0,91}La_{0,06}Zr_{0,85}Ti_{0,15}O_3$).

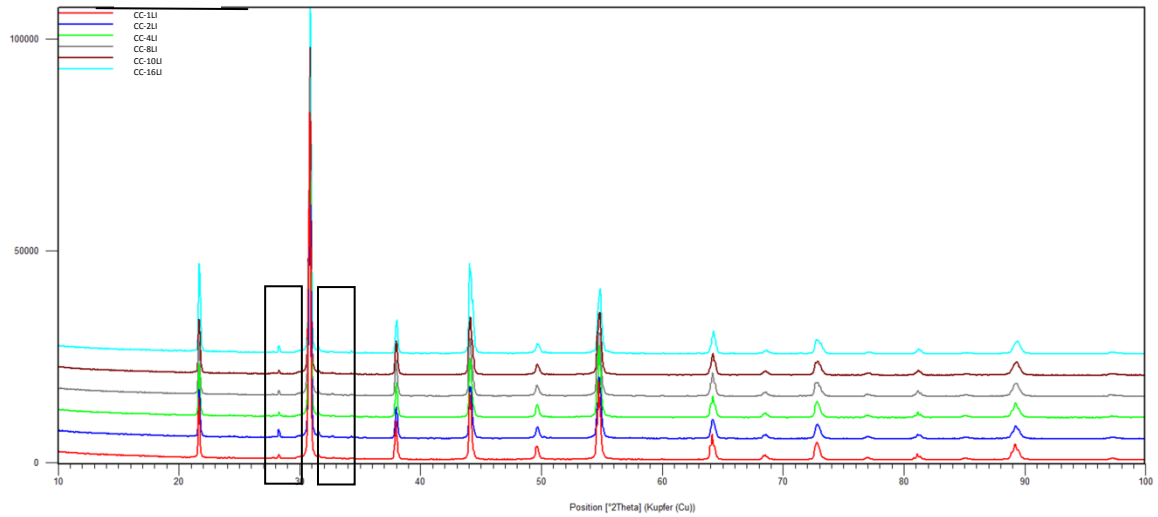

Figure 7.2-5: XRD of sintered powders of Lithium-substitution in PLZT (CC=$Pb_{0,91}La_{0,06}Zr_{0,80}Ti_{0,20}O_3$). Secondary phases are highlighted by rectangles.

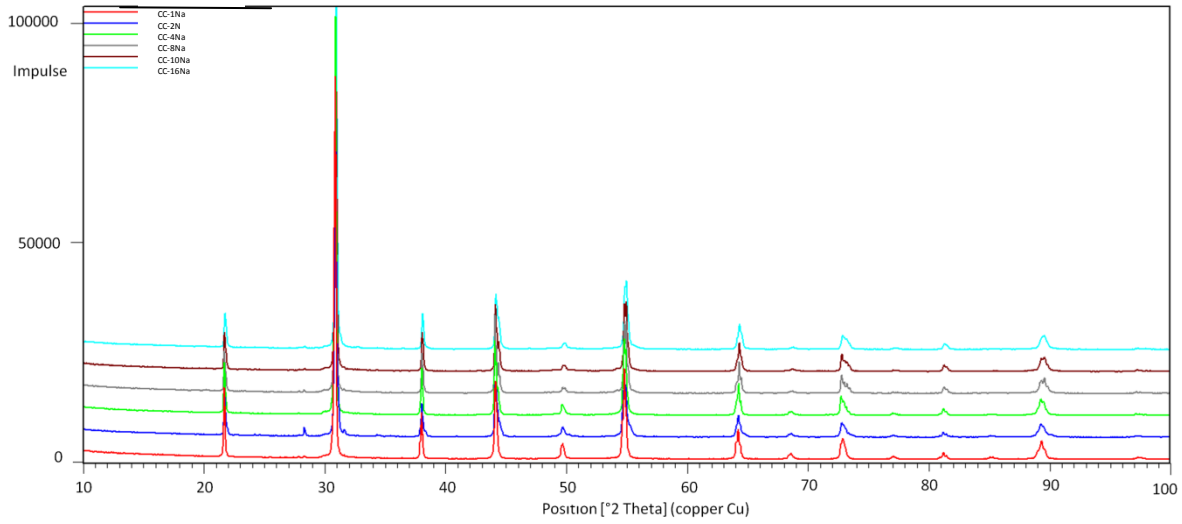

Figure 7.2-6: XRD of sintered powders of Sodium-substitution in PLZT (CC=$Pb_{0,91}La_{0,06}Zr_{0,80}Ti_{0,20}O_3$).

The relative densities in the system BB, where Lead was substituted with alkaline ions, were all about 90 % except the sample BB-1Na which only achieved a densification of ~89% (Table 7.2-5 to Table 7.2-7). In the case of Lithium the relative densities increased with further increase of the concentration. This implies a higher densification with increasing insertion of Lithium. With the substitution with Sodium the values fluctuated around 95%. At low content of Potassium the relative density reached ~99%, but dropped then to 97%.

Table 7.2-5: List of the cell parameters, the cell volumes and the densities of Lithium-substitution in PLZT (BB).

sample	c [Å]	b [Å]	a [Å]	c/a	cell volume [Å ³]	theoretical density [g/cm³]	Archimedes´ density [g/cm³]	relative density [%]
BB_1Li	8.1987	11.6742	5.8288	1.4066	557.8869	7.93	7.49	94.51
BB_2Li	8.1986	11.6753	5.8296	1.4064	558.0112	7.90	7.62	96.43
BB_4Li	8.1977	11.6768	5.8307	1.4060	558.1328	7.85	7.66	97.47
BB_8Li	8.1954	11.6752	5.8292	1.4059	557.7518	7.77	7.57	97.40
BB_10Li	8.1960	11.6760	5.8296	1.4059	557.8696	7.72	7.47	96.79
BB_16Li	8.1943	11.6763	5.8288	1.4058	557.6956	7.58	7.36	97.06

Table 7.2-6: List of the cell parameters, the cell volumes and the densities of Sodium-substitution in PLZT (BB).

sample	c [Å]	b [Å]	a [Å]	c/a	cell volume [Å³]	theoretical density [g/cm³]	Archimedes´ density [g/cm³]	relative density [%]
BB_1Na	8.1961	11.6636	5.8228	1.4076	556.6312	7.90	7.01	88.79
BB_2Na	8.1939	11.6626	5.8218	1.4075	556.3369	7.88	7.58	96.19
BB_4Na	8.1914	11.6615	5.8268	1.4058	556.6001	7.84	7.39	94.26
BB_8Na	8.1718	11.6524	5.8067	1.4073	552.9205	7.81	7.35	94.03
BB_10Na	8.1810	11.6529	5.8194	1.4058	554.7805	7.75	7.40	95.53
BB_16Na	8.1817	11.6485	5.8139	1.4073	554.0835	7.64	7.34	95.98

Table 7.2-7: List of the cell parameters, the cell volumes and the densities of Potassium-substitution in PLZT (BB).

sample	c [Å]	b [Å]	a [Å]	c/a	cell volume [Å ³]	theoretical density [g/cm³]	Archimedes´ density [g/cm³]	relative density [%]
BB_1K	8.2010	11.6732	5.8289	2.4613	558.0150	7.88	7.66	97.13
BB_2K	8.2024	11.6754	5.8305	2.4612	558.3632	7.86	7.78	98.92
BB_4K	8.2038	11.6772	5.8298	2.4611	558.4800	7.83	7.66	97.81
BB_8K	8.2035	11.6798	5.8323	2.4615	558.8214	7.76	7.60	97.82
BB_10K	8.2038	11.6798	5.8318	2.4621	558.7964	7.73	7.39	95.54
BB_16K	8.2100	11.6761	5.8312	2.4575	558.9824	7.64	7.41	96.93

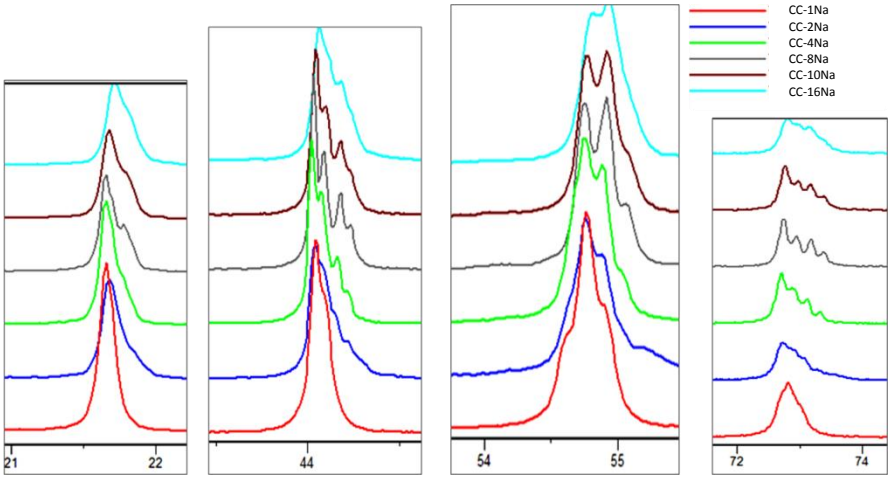

Figure 7.2-7: Detailed view of the shifting and splitting of the reflection patterns by increasing the Sodium content in the composition CC ($Pb_{0,91}La_{0,06}Zr_{0,80}Ti_{0,20}O_3$).

In the series CC with the highest content of Titanium the relative densities were the highest in comparison to the other, Zirconium-richer compositions (Table 7.2-8 and Table 7.2-9). Nearly all relative densities were above 95%. While the insertion of Lithium reached a densification of about 95%, the substitution with Sodium achieved values of around 97% and above.

Table 7.2-8: List of the cell parameters, the cell volumes and the densities of Lithium-substitution in PLZT (CC).

sample	c [Å]	b [Å]	a [Å]	c/a	cell volume [Å³]	theoretical density [g/cm³]	Archimedes´ density [g/cm³]	relative density [%]
CC_1Li	14.2667	5.8076	5.8076	2.4566	416.7270	7.86	7.71	98.21
CC_2Li	14.2636	5.8058	5.8058	2.4568	416.3785	7.84	7.44	94.96
CC_4Li	14.2682	5.8071	5.8071	2.4570	416.6326	7.79	7.37	94.62
CC_8Li	14.2668	5.8055	5.8055	2.4575	416.4219	7.70	7.37	95.69
CC_10Li	14.2633	5.8058	5.8058	2.4567	416.3673	7.65	7.33	95.80
CC_16Li	14.2618	5.8014	5.8014	2.4583	415.6960	7.53	7.24	96.25

Table 7.2-9: List of the cell parameters, the cell volumes and the densities of Sodium-substitution in PLZT (CC).

sample	c [Å]	b [Å]	a [Å]	c/a	cell volume [Å³]	theoretical density [g/cm³]	Archimedes´ density [g/cm³]	relative density [%]
CC_1Na	14.2630	5.8044	5.8044	2.4573	416.1526	7.87	7.76	98.60
CC_2Na	14.2499	5.8078	5.8078	2.4536	416.2525	7.85	7.54	96.09
CC_4Na	14.2771	5.8051	5.8051	2.4594	416.6663	7.80	7.58	97.10
CC_8Na	8.1728	11.6380	5.8110	1.4064	552.7151	7.76	7.58	97.57
CC_10Na	8.1751	11.6370	5.8096	1.4072	552.6836	7.73	7.50	97.12
CC_16Na	8.1783	11.6376	5.8082	1.4081	552.7950	7.61	7.36	96.75

In Figure 7.2-8 the cell volume of the orthorhombic samples was plotted versus the concentration of the alkaline ion. It is obvious that the values fluctuate and did not show any trend except the addition of Potassium. In that case the cell volume increased slightly.

A big problem with the insertion of alkaline ions is the determination of the chemical composition of the sintered bodies. Next to the change in occupancy in the case of Lithium, which resulted in secondary phases, the high vapour pressure and resulting evaporation of the alkaline ions cause deviation of the weighted composition. Chemical analysis with EDS does not give data with the necessary accuracy to calculate the stoichiometry of the matrix or of the secondary phase.

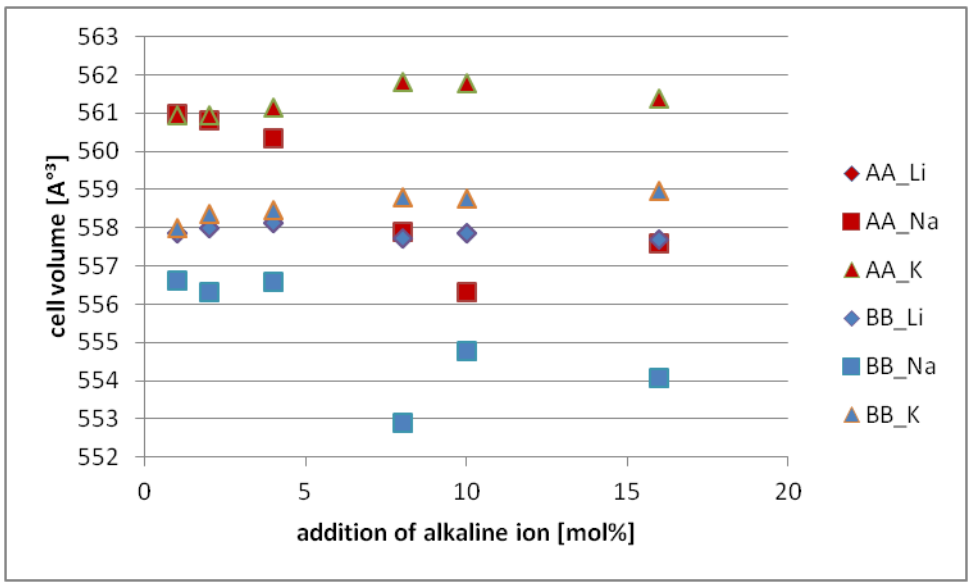

Figure 7.2-8: Cell volume versus addition of alkaline ions.

7.2.2 Microstructure

In Figure 7.2-9 the backscattered SEM image of the sample AA-4Li is shown. It demonstrates the emerging of secondary phase. According to the EDS-measurements, Zirconium-dioxide with incorporation of Lanthanum precipitated. Thus the matrix composition deviated from the formal composition and no comments on the concentration of Lithium in the samples can be made.

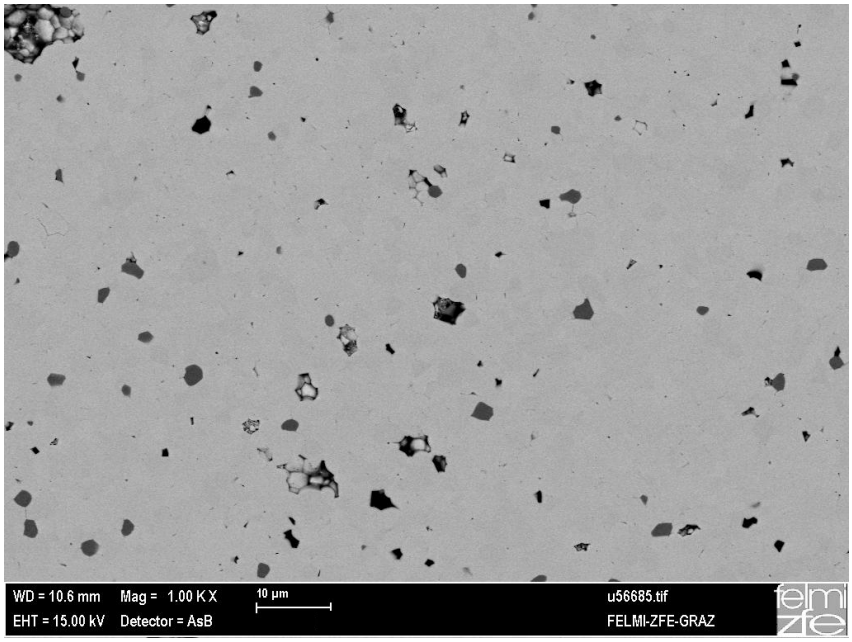

Figure 7.2-9: Backscattered SEM image of the sample AA-4Li: the dark grey inclusions refer to Zirconium-Lanthanum-Oxide-precipitates.

Channelling contrast mode uncovered the microstructure and the domain structure of the samples. As an example, AA-1Na-sample is shown in Figure 7.2-10. Grains of approximately 2µm with curved boundaries are next to smaller grains. This indicates a homogeneous grain growth during sintering. Domains are visible in different orientations.

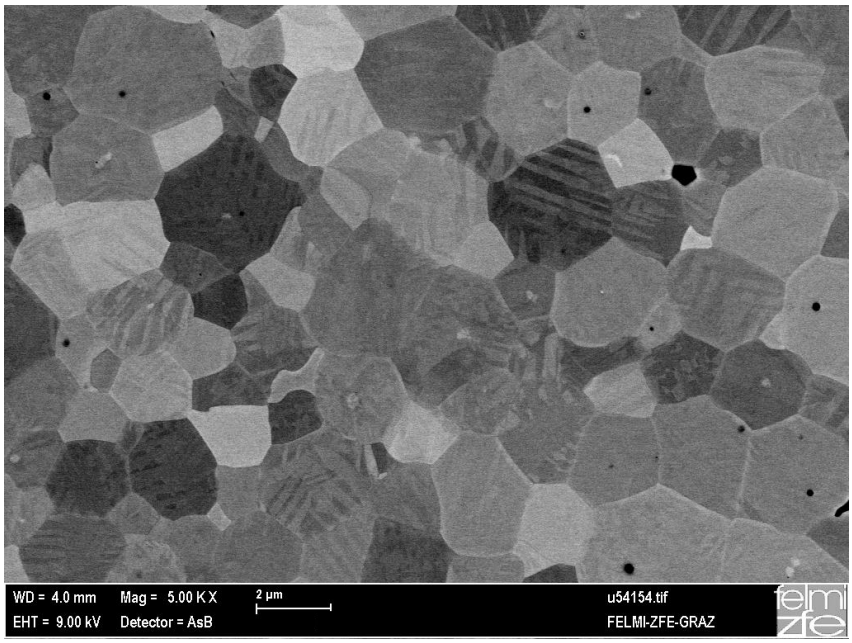

Figure 7.2-10: Backscattered SEM image of AA-1Na sample. The channelling contrast mode revealed the grain size and the domain structure of the sample.

7.2.3 Dielectric Characterization

Low signal properties are summarized in Table 7.2-10 to Table 7.2-17.

The dielectric properties in the AA system varied slightly with the substitution of Lead with alkaline ions. Capacitance did only fluctuate by substitution with Lithium around 335 pF and with Potassium around 430 pF. The mean value of relative permittivity of the samples with the insertion of Lithium is 500 which is only a bit lower than 624, which was obtained by substitution with Potassium. The increasing content of Sodium reduced the capacitance from ~330 to 190 pF and the relative permittivity from 478 to 304. The loss factor decreased slightly in all cases with increasing alkali content. Samples with Lithium and Sodium as substituents exhibit loss factors well below 0.01, loss factors of samples containing potassium are found between 0.008 and 0.029.

Table 7.2-10: Results of low signal dielectric measurements of Lithium-substitution in PLZT AA.

sample	capacitance [nF]	loss factor []	relative permittivity []
AA_1Li	0.3308	0.0082	498
AA_2Li	0.3136	0.0061	473
AA_4Li	0.3386	0.0057	498
AA_8Li	0.3495	0.0054	514
AA_10Li	0.3414	0.0048	510
AA_16Li	0.3373	0.0053	514

Table 7.2-11. Results of low signal dielectric measurements of Sodium-substitution in PLZT AA.

sample	capacitance [nF]	loss factor []	relative permittivity []
AA_1Na	0.3267	0.0055	478
AA_2Na	0.3158	0.0038	462
AA_4Na	0.2950	0.0034	438
AA_8Na	0.2714	0.0028	399
AA_10Na	0.2604	0.0034	397
AA_16Na	0.1893	0.1046	304

Table 7.2-12: Results of low signal dielectric measurements of Potassium-substitution in PLZT AA.

sample	capacitance [nF]	loss factor []	relative permittivity []
AA_1K	0.4522	0.0104	577
AA_2K	0.4590	0.0094	611
AA_4K	0.4737	0.0107	617
AA_8K	0.4196	0.0119	870
AA_10K	0.3407	0.0084	551
AA_16K	0.4193	0.0289	516

In the composition BB with the substitution of Lead with alkaline ions, a similar picture is drawn. The values of capacitance and relative permittivity respectively fluctuated by the incorporation of Lithium and Potassium. Compositions containing Lithium revealed a mean value of capacitance of about 630 pF, whereas those with Potassium achieved a bit higher value of 875 pF. The corresponding relative permittivity values were ~990 and 1167. In the case of Sodium, the values decreased from ~690 to ~380 pF in capacitance and ~1020 to ~545 in relative permittivity by increasing the molar ratio from 1 mol% to 10 mol% Sodium. The substitution of Lead with 16 mol% Sodium increased the capacitance again to ~535 pF and the relative permittivity to ~825.

The values of the loss factors fluctuated with the substituents Lithium or Potassium and decreased with Sodium. An exceptionally high value was obtained by a substitution with 16 mol% Sodium, which was 0.3032.

Table 7.2-13: Results of low signal dielectric measurements of Lithium-substitution in PLZT BB.

sample	capacitance [nF]	loss factor []	relative permittivity []
BB_1Li	0.6194	0.0161	963
BB_2Li	0.7122	0.0177	1080
BB_4Li	0.6810	0.0552	1038
BB_8Li	0.5727	0.0175	949
BB_10Li	0.6345	0.0182	985
BB_16Li	0.5621	0.0247	907

Table 7.2-14: Results of low signal dielectric measurements of Sodium-substitution in PLZT BB.

sample	capacitance [nF]	loss factor []	relative permittivity []
BB_1Na	0.6891	0.0161	1019
BB_2Na	0.6492	0.0150	1019
BB_4Na	0.5297	0.0098	775
BB_8Na	0.4567	0.0067	639
BB_10Na	0.3819	0.0088	546
BB_16Na	0.5359	0.3032	827

Table 7.2-15: Results of low signal dielectric measurements of Potassium-substitution in PLZT BB.

sample	capacitance [nF]	loss factor []	relative permittivity []
BB_1K	0.8180	0.0228	1065
BB_2K	0.9096	0.0189	1193
BB_4K	0.7433	0.0248	983
BB_8K	0.9132	0.0266	1209
BB_10K	0.8819	0.0230	1189
BB_16K	0.9813	0.0170	1362

The incorporation of the substituents Lithium and Sodium in the system PLZT with a ratio of Zirconium to Titanium 80 to 20 revealed a decrease in capacitance and relative permittivity. In samples containing Lithium, the values of the relative permittivity decreased from ~1100 to ~900. A similar behaviour could be detected with the addition of Sodium in PLZT.

Overall, in the case of Sodium, capacitance C and thus also relative permittivity ε decreased, while the loss factor tanδ increased. A bigger ion on the other side, as Potassium is, showed contrary behaviour. A peculiar occurrence happened by the substitution with Lithium: In the Zirconium-rich composition, Lithium insertion enhanced capacitance and relative permittivity and declined loss factor. This might be due to the incorporation of Lithium ion at A- and B-site resulting in secondary phases and a change in composition. Therefore no comments can be done about the influence of Lithium-substitution in PLZT.

Table 7.2-16: Results of low signal dielectric measurements of Lithium-substitution in PLZT CC.

sample	capacitance [nF]	relative permittivity []
CC_1Li	0.8842	1087
CC_2Li	0.8145	1017
CC_8Li	0.9563	1158
CC_10Li	0.7988	1037
CC_16Li	0.7323	888

Table 7.2-17: Results of low signal dielectric measurements of Sodium-substitution in PLZT CC.

sample	capacitance [nF]	relative permittivity []
CC_1Na	0.7930	1044
CC_2Na	0.9454	1147
CC_4Na	0.9686	1170
CC_8Na	0.9388	1154
CC_10Na	0.8183	1094
CC_16Na	0.6993	890

In Figure 7.2-13a-g the relative permittivity measurements versus temperature from minus 50 °C to 300 °C for 1 MHz are presented for all compositions. As already mentioned, the maximum of each curve refers to a phase transition.

The increasing alkaline ion content in PLZT-system in AA plotted in Figure 7.2-13a to c induced a broadening and flattening of the relative permittivity curves.

A closer look at Figure 7.2-13f revealed a second step in the curves of BB-1K. A shoulder near the peak could be recognized which vanished with further increasing of the concentration of Potassium.

Consulting the phase diagram of Ishchuk[109] in Figure 7.2-11 for alkaline ion substitution in PLZT a triple point of antiferroelectric, ferroelectric and paraelectric phases occurs. At this point, the values of the free energy of all orderings are very close to each other. Additionally a compositional range of a mixed phase was observed. In this area an antiferroelectric phase is stable unless electric field is applied, which transforms to a ferroelectric state. This ferroelectric state exhibits a temperature dependent phase transition to antiferroelectric phase.

Considering this, the composition of BB-1K might be close to this triple point. Due to that, the broadening of the curve indicates an increase of the diffuseness of the phase transition. Hence, the first peak most probably refers to the phase transition of the mixed phase to antiferroelectric phase. Following the curve to higher temperature, the next hump refers to a transition to paraelectric phase. By increasing the content of Potassium the composition changes and only one peak was observed which might represent the phase transition from antiferroelectric to ferroelectric state. For AA and BB-compositions only an antiferroelectric to paraelectric transition observed.

In the case of CC-compositions plotted in Figure 7.2-13fg and h again two peaks were detected. Taking into account the above mentioned phase diagram, the compositional range might be close to the triple point and therefore revealed two phase transitions. For nearly all samples, where Lead was substituted by Lithium, this behaviour was evident, except for the highest alkaline ion content of 16 mol%. Also this feature can be explained by the deviation in the composition away from this triple point to the range of antiferroelectric phase.

Regarding the curves of the samples with the substitution of Lead with Sodium this transformation from two peaks to one happened at lower concentrations – to be precise at 4 mol%.

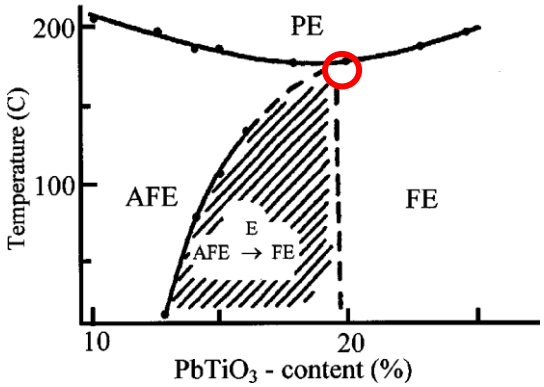

Figure 7.2-11: Phase diagram of PZT containing 10 mol% of Lithium and Lanthanum. The triple point ferro-electric-antiferroelectric-paraelectric is highlighted by a red circle. The shaded area represents the mixed phase, where antiferroelectric phase can be transformed to a ferroelectric one by applying electric field[109].

For comparison, the data of the starting compositions AA, BB and CC were inserted in Figure 7.2-13. By increasing the Titanium content, the maximum relative permittivity increased from 1552, to 2964 and finally to 4312, whereas the peak temperature decreased from 180 °C, to 156 °C and to 136 °C. Table 7.2-18, Table 7.2-19 and Table 7.2-20 and Figure 7.2-12 summarize the results of the relative permittivity measurements of all alkaline substitution in PLZT samples. No interpretation about the height of the permittivity curves can be done due to the uncertain composition of the samples. In the case of the temperature shift no significant alteration was observed.

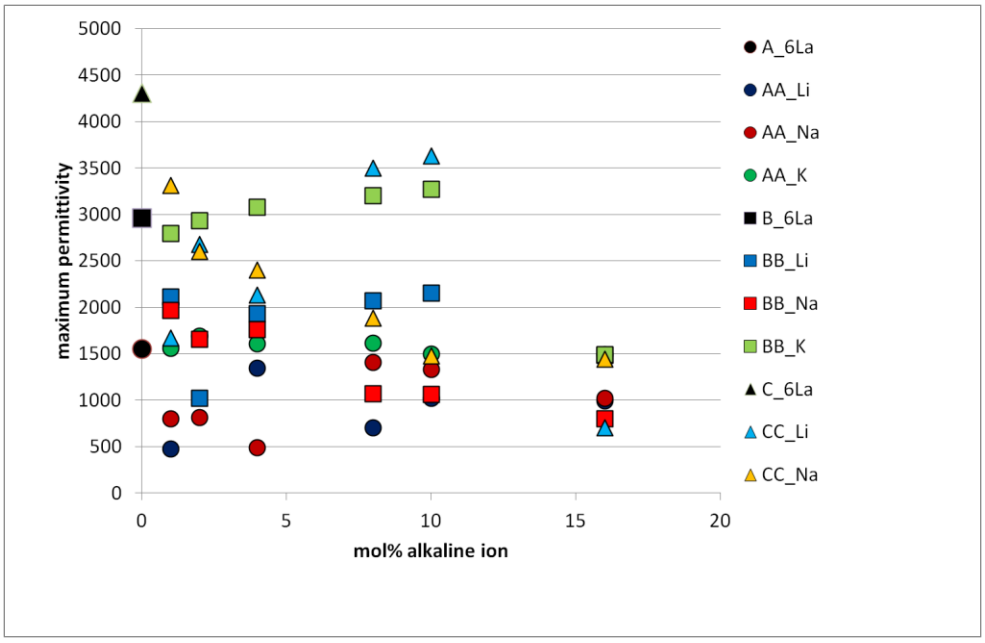

Figure 7.2-12: maximum permittivity versus content of alkaline ions in PLZT samples AA, BB and CC.

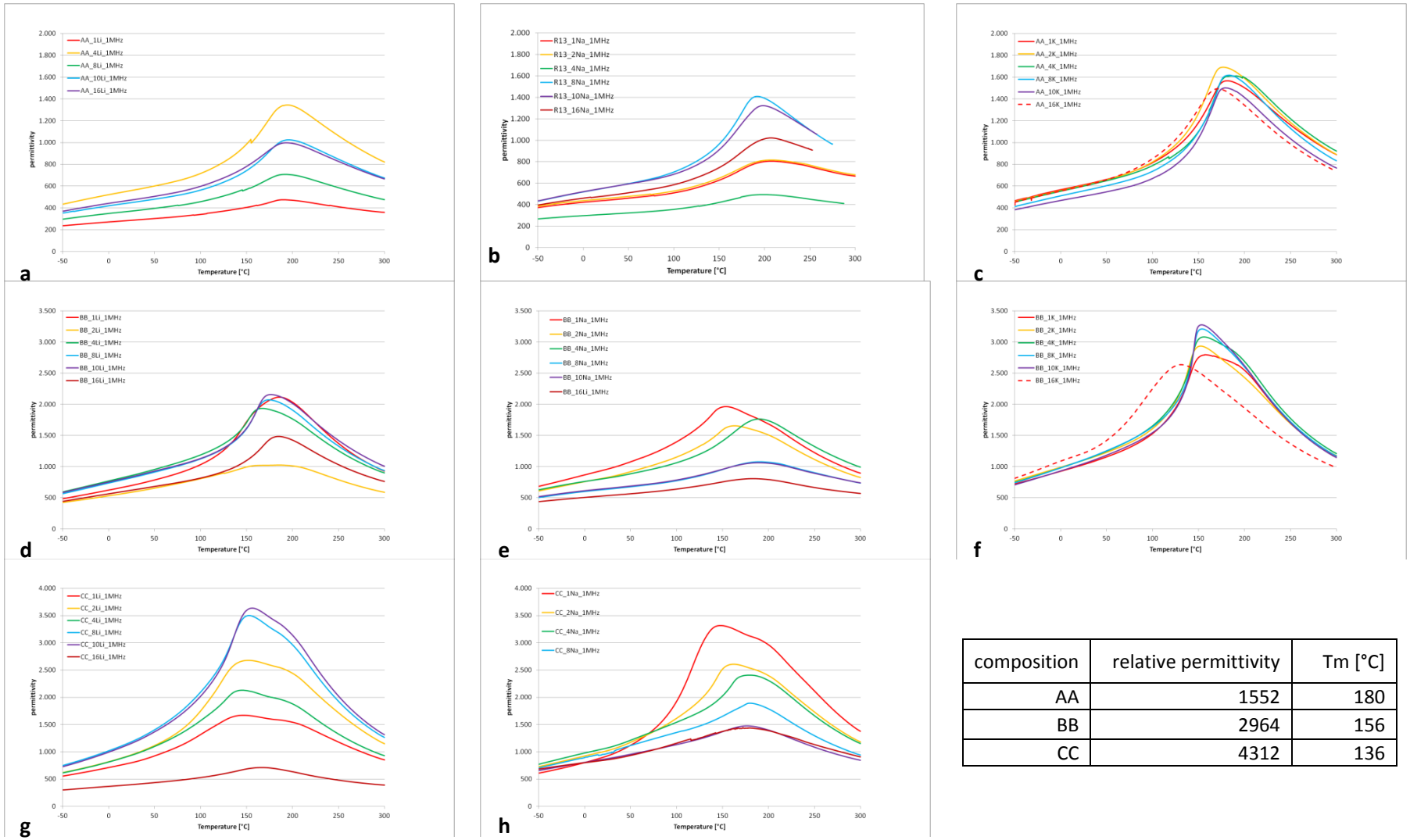

composition	relative permittivity	Tm [°C]
AA	1552	180
BB	2964	156
CC	4312	136

Figure 7.2-13: Relative permittivity curves versus temperature at 1 MHz (arrows indicate the maximum in relative permittivity and demonstrate the alteration with increasing concentration of substituents (AA= $Pb_{0,91}La_{0,06}Zr_{0,9}Ti_{0,1}O_3$, BB= $Pb_{0,91}La_{0,06}Zr_{0,85}Ti_{0,15}O_3$, CC= $Pb_{0,91}La_{0,06}Zr_{0,80}Ti_{0,}$).

Consulting Table 7.2-18, the values of the compositions AA where Lead was substituted with Lithium, Sodium and Potassium are presented. The transition temperature scattered around 190 °C for samples containing Lithium, around 200 °C for samples with Sodium and around 180 °C for Potassium substitution. A closer look revealed a slight decrease of 15 °C with incorporation of the Potassium ion. Potassium with its larger size occupies more space in the lattice as Lead would do. Therefore, by inserting a bigger ion the system has to cope with stress and distortion, which can be released by a structural change. This might be the reason for the shift of the phase transition to lower temperatures.

A range from ~480 to ~1345 in maximum of relative permittivity was achieved by varying the content of Lithium. An exceptionally high value of 1345 was achieved with the sample AA-4Li. Excluding this sample from the data, an increase from ~480 to ~1000 with increasing Lithium content was obtained.

With the incorporation of Sodium, the maximum in relative permittivity increased from ~800 to ~1410 with 8 mol% of Sodium and decreased with further increase of the concentration to ~1020.

Regarding the influence of Potassium on the dielectric response, the values of relative permittivity extended over the small interval of 1494 to1691. Excluding the value 1690, a fluctuation of the values of relative permittivity around 1560 can be observed. Overall, inserting Potassium in the system relative permittivity increased only slightly and the highest relative permittivity was achieved by the substitution of 2 mol% of Lead with Potassium.

In the system BB the substitution of Lead with Lithium showed a different behaviour: At first, with increasing amount of Lithium the transition temperature decreased from 186 °C to 168 °C and then increased again to 185 °C. With assumed 4 mol% of Lithium in the system, the lowest temperature of the phase transition could be obtained. Overall the maximum of relative permittivity varied with the concentration of Lithium and a decrease from ~2115 to ~1490 could be discovered. This decline of the values was around one third.

Replacing Lead with Sodium in the system, a bigger shift of transition temperature appeared. By increasing the content from 1 mol% to 10 mol% of Sodium the temperature increased by 35 °C. Considering also the composition with 16 mol% the increase in temperature was only 30 °C. Like with the substitution of Lead with Lithium, the relative permittivity decreased with substituting Lead with Sodium. But in this series the value of relative permittivity was divided by two. To be precise a decrease from ~1965 to 805 could be observed.

As remarked before, substitution of Lead with Potassium did not seem to have any impact on the transition temperature of the system. In the case of the system BB the degrees scattered around

155 °C. The only exception was the sample BB-16K which demonstrated a phase transition at about ~172 °C. By increasing the content of Potassium from 1 mol% to 10 mol% the relative permittivity increased from ~2800 to ~3275. Then with further substitution of Lead with Potassium a decrease to ~1494 was determined (see Table 7.2-19).

Proceeding from the Zirconium-richer to the Titanium-richer composition, a decrease in the peak temperature and an increase in the height of the curves were observed. Additionally, the curves of the compositions with the ratio of Zirconium to Titanium 80 to 20 showed a shoulder at higher temperature. Inserting Lithium in this system shifted the transition to higher temperature. By increasing insertion of Lithium an increase of 20 °C occurred. A big jump in the maximum of relative permittivity could be determined. The values were more than doubled from ~1670 to ~3635. But then a drop to ~710 could be recorded. Due to the precipitation of Zirconium dioxide, these data cannot be correlated to a concentration of Lithium in the composition.

The opposed behaviour was observed by the substitution with Sodium: The transition temperature altered by ~30 °C and shifted from ~150 °C to 180 °C by increasing the content from 1 mol% to 8 mol%. With the same amount of substituent, the relative permittivity dropped from ~3315 to ~1890. Then with further increasing the Sodium content, a shift in the phase transition temperature to ~172 °C and a decline to ~1445 was achieved (compare in Table 7.2-20).

Comparing the dielectric response of the samples substitution in with alkaline ions with those of the composition AA, BB and CC, different effects occurred. In the case of Lithium and Sodium lower values were obtained, while with the substitution of Lead with Potassium higher values could be achieved. Although the substitution of Lead with Lithium could increase the height of the peak, the same value as of the starting composition was not reached.

Overall the influence of the alkaline ions on the relative permittivity might lie in the size: If an ion with bigger ionic radius substitutes another ion in the lattice, the relative permittivity is shifted to higher values and vice versa. This might be independent on the site where the ion is located. As Lithium can either take place at the A-site and reduces the mean volume of the A-site or enhances the needed space at B-site both effects might be visible. In the system AA and CC Lithium might be placed at B-site and in the system BB at the A-site. The flipping of the arrows indicates the reversal of the influences (see first column in Figure 7.2-13). Additionally the mass might have an effect on the magnitude of the change. If the ion size is smaller and therefore a decrease in relative permittivity occurs, then the extent of this decline might be enhanced with the heavier one (compare second row in Figure 7.2-13).

Regarding the influence of the substituents on the temperature shifts, Sodium demonstrated the biggest impact. Following the substitution of that alkaline ion an increase in the transition temperature occurred. Having a closer look at the effect of the substitution with Lithium to the various systems revealed different behaviours. Overall an increase was observed. Substitution with Potassium on the other side did not alter the transition temperature.

Table 7.2-18: Results of the relative permittivity versus temperature curves of Lithium, Sodium and Potassium substitution in PLZT AA.

sample	maximum in relative permittivity	Temperature Tm [°C]	sample	maximum in relative permittivity	Temperature Tm [°C]	sample	maximum in relative permittivity	Temperature Tm [°C]
AA_1Li	476	190	AA-1Na	805	208	AA_1K	1565	187
AA_2Li			AA-2Na	816	208	AA_2K	1691	177
AA_4Li	1345	195	AA-Na	493	199	AA_4K	1613	187
AA_8Li	707	192	AA-8Na	1410	193	AA_8K	1619	183
AA_10Li	1023	197	AA-10Na	1335	199	AA_10K	1502	180
AA_16Li	997	193	AA-16Na	1023	208	AA_16K	1494	172

Table 7.2-19: Results of the relative permittivity versus temperature curves of Lithium, Sodium and Potassium substitution in PLZT BB.

sample	maximum in relative permittivity	Temperature Tm [°C]	sample	maximum in relative permittivity	Temperature Tm [°C]	sample	maximum in relative permittivity	Temperature Tm [°C]
BB_1Li	2113	186	BB_1Na	1966	154	BB_1K	2795	159
BB_2Li	1027	185	BB_2Na	1657	163	BB_2K	2936	153
BB_4Li	1933	168	BB_4Na	1763	190	BB_4K	3080	156
BB_8Li	2070	175	BB_8Na	1075	191	BB_8K	3207	154
BB_10Li	2156	176	BB_10Na	1064	190	BB_10K	3276	155
BB_16Li	1487	185	BB_16Na	805	184	BB_16K	1494	172

Table 7.2-20: Results of the relative permittivity versus temperature curves of Lithium and Sodium substitution in PLZT CC.

sample	maximum in relative permittivity	Temperature Tm [°C]	sample	maximum in relative permittivity	Temperature Tm [°C]
CC_1Li	1670	147	C_1Na	3314	148
CC_2Li	2679	152	C_2Na	2607	162
CC_4Li	2132	146	C_4Na	2405	180
CC_8Li	3501	153	C_8Na	1889	181
CC_10Li	3633	157	C_10Na	1476	177
CC_16Li	709	167	C_16Na	1443	173

Recording relative permittivity versus temperature at various frequencies can show relaxor behaviour if existing. With changing the frequency, the fluctuations of nanopolar domains would promote a shift of the peaks in the curves. For all compositions with alkaline ions such a shift with frequency was not observed. In Figure 7.2-14a to c the permittivity at various frequencies for a selection of one composition of each alkaline ion is presented. No relaxor-like dielectric response could be observed within this series.

Figure 7.2-14a plots the relative permittivity and loss factor-curves of BB-1Li at various frequencies. It is obvious that the transition temperature is independent of the applied frequencies and does not alter. Only the value of the relative permittivity decreased with increasing frequency. Furthermore, the correlation of the peak in the curves of the loss factor with the peak in the relative permittivity curves can easily be recognized.

In Figure 7.2-14b the curves of the sample BB-1Na are demonstrated. Measuring the relative permittivity at 0.1 kHz a broad peak was detected, which might cover an additionally step next to the peak. But with increasing frequency the peak narrowed again. As remarked above, only the height of the curves decreased by enhancing the frequency.

Adding 1 mol% Potassium revealed a second step at higher temperatures shown in Figure 7.2-14c. This shoulder in the curves remained even with increasing frequency. Again the height of the peaks decreased with increasing frequency, but the position of both transition temperatures did not change.

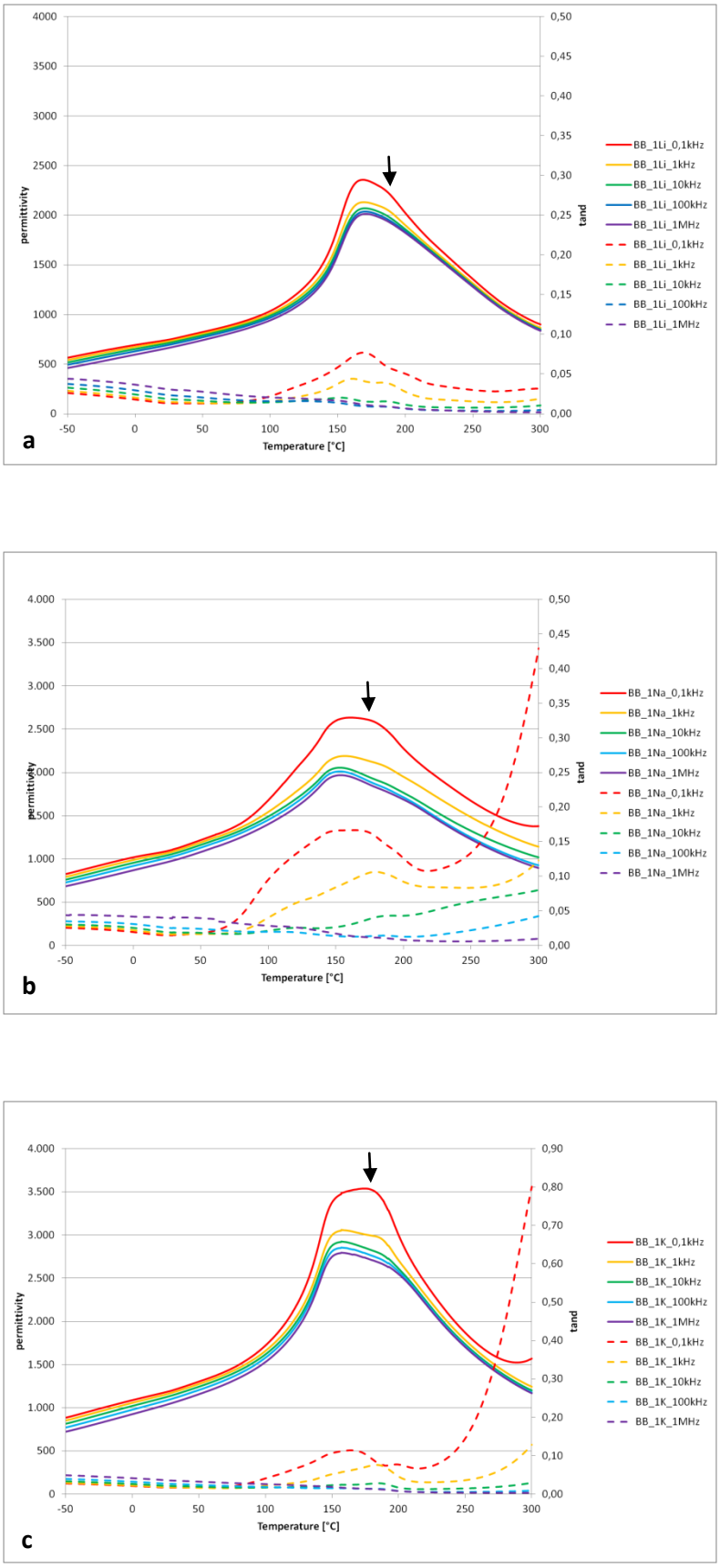

Figure 7.2-14: Frequency dependent measurements of the relative permittivity (solid line) and loss factor (dashed line) versus temperature of BB-1Li, BB-1Na and BB-1K (measured at 0.1 kHz, 1 kHz, 10 kHz, 100 kHz and 1 MHz). Anomalies are accentuated by arrows.

Measuring polarization curves can reveal antiferroelectric behaviour by evolving double hysteresis loops under field. As it can be seen in Figure 7.2-15, the Titanium concentration in the solid solution PLZT influences the shape of the hysteresis curves. Only the composition with the lowest amount of Zirconium exhibits a ferroelectric hysteresis curve. The other two demonstrate antiferroelectric double hysteresis curves. With increasing the amount of Zirconium the saturation polarization and the area of the hysteresis decreases. Keeping this in mind the following polarization curves can be discussed concerning the effects of the alkaline ions.

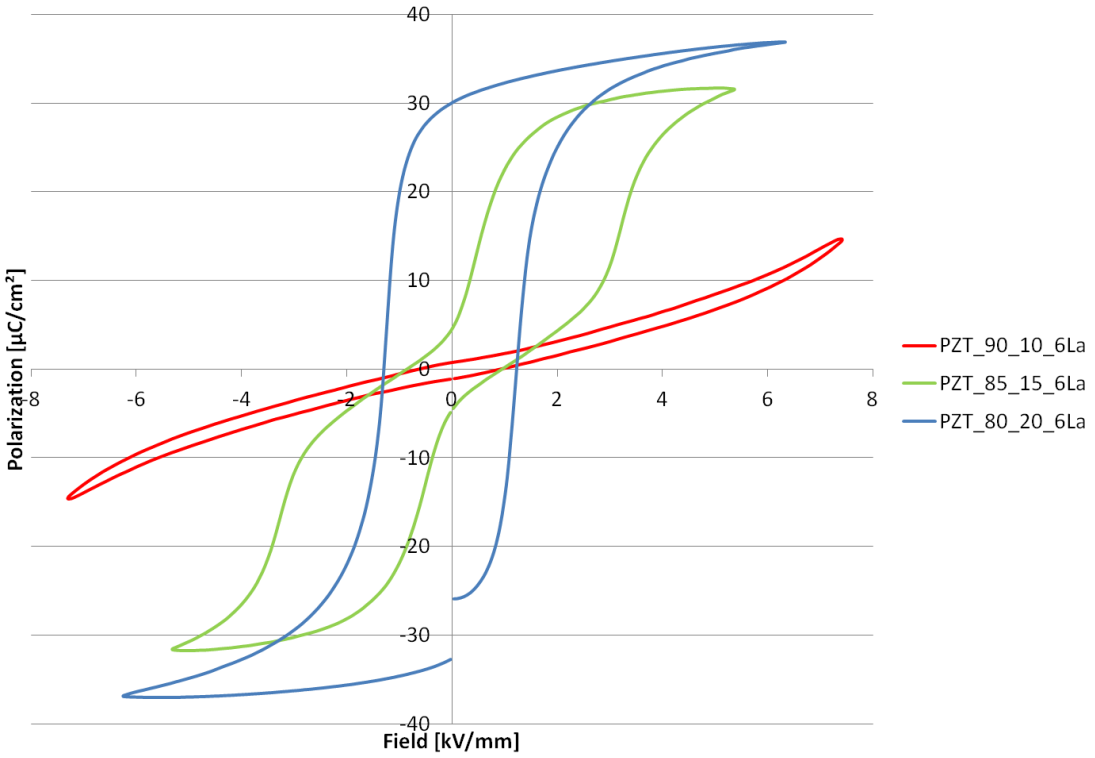

Figure 7.2-15: Influence of the Zirconium to Titanium ratio on the shape of the hysteresis curve (all three examples were with 6 mol% substitution of Lead with Lanthanum and refer to blank AA, BB and CC).

In Figure 7.2-16a to f the hysteretic behaviour of the alkaline-substitution in samples AA and BB with Lithium and Potassium and composition CC with Lithium and Sodium are shown.

In Figure 7.2-16a and b the dielectric behaviour of the composition AA, where Lead was replaced with alkaline ions, can be seen - on the left the samples containing Lithium and on the right side the substitution with Potassium. Double hysteresis loop evolved with both alkaline ions.

Keeping in mind that the observed changes were not correlated to an incorporation of Lithium replacing Lead, a decrease of the maximum in polarization and an increase of the switching fields could be remarked. Furthermore the difference of the switching fields increased, whereas the slope of the hysteresis curves declined and flattened. Not all curves reached saturation.

On the right side, the dependence of the shape of the loops on Potassium content is demonstrated. The substitution of Lead with Potassium decreased saturated polarization and the switching fields but increased the area of the hysteresis. The red curve of the composition with the highest molar ratio shows a double hysteresis curve with the highest remnant polarization and coercive field.

In Figure 7.2-16c and d, double hysteresis loops can also be observed. Unfortunately, in the case of Lithium the saturation in polarization could not be achieved for all samples and therefore the characteristic parameters could not be determined. Only 1 mol% and 2 mol% substitution can be compared. The composition with the higher content of Lithium exceeded the other in maximum in polarization and obtained higher switching fields. No change in the amount of the area of the hysteresis loop could be detected.

On the other hand, all samples where Lead was substituted with Potassium could gain saturation, which only decreased slightly with the content of the substituent. Besides, the switching field shifted to higher fields. At first the hysteresis curves slightly broadened with increasing Potassium content but then with the substitution with 16 mol% of Potassium slimmed remarkably.

Comparing the Lithium and the Potassium-substitution in the samples, the ones with Lithium possessed a lower breakdown voltage which inhibited full saturation in most cases. Also the shape of the curves deviated. At the switching fields the slope of the curves to saturation of the samples with Potassium-substitution was steeper and almost went parallel to the y-axis.

The incorporation of Sodium leads to similar polarization curves as of Potassium.

In Figure 7.2-16e and f, the polarization loops of the compositions with the highest Titanium content are plotted. On the left side, all curves show ferroelectric behaviour. The insertion of Lithium decreased the maximum in polarization and the area of the hysteresis due to smaller values of coercive field and remnant polarization. All these samples contain secondary phases and therefore the shape of the polarization curve did not discover a picture of the influence of Lithium-substitution.

On the right side, a different appearance can be seen. In this case, the maximum in polarization also decreased with adding the substituent, but not in that extent. Nearly no change in the coercive field was observed. Interestingly, a peculiarity occurred by substituting 8 mol% of Lead with Sodium. The maximum in polarization reached again a higher value and remnant polarization decreased resulting in an antiferroelectric polarization curve or at least a pinched one. This correlated with the structural change from rhombohedral to orthorhombic.

Substitution with alkaline ions decreased the maximum in polarization and in the case of the two compositions with higher Zirconium content shifted the transition from antiferroelectric to ferroelectric state to higher fields. Comparing the curves in Figure 7.2-15 with those of Figure 7.2-16a to f, a deviation of the switching field to higher field occurred. Furthermore the breakdown voltage decreased with the addition of Lithium. In the case of the composition with the ratio Zirconium to Titanium 80 to 20, the double hysteresis could be induced by the substitution of 8 mol% of Lead with Sodium.

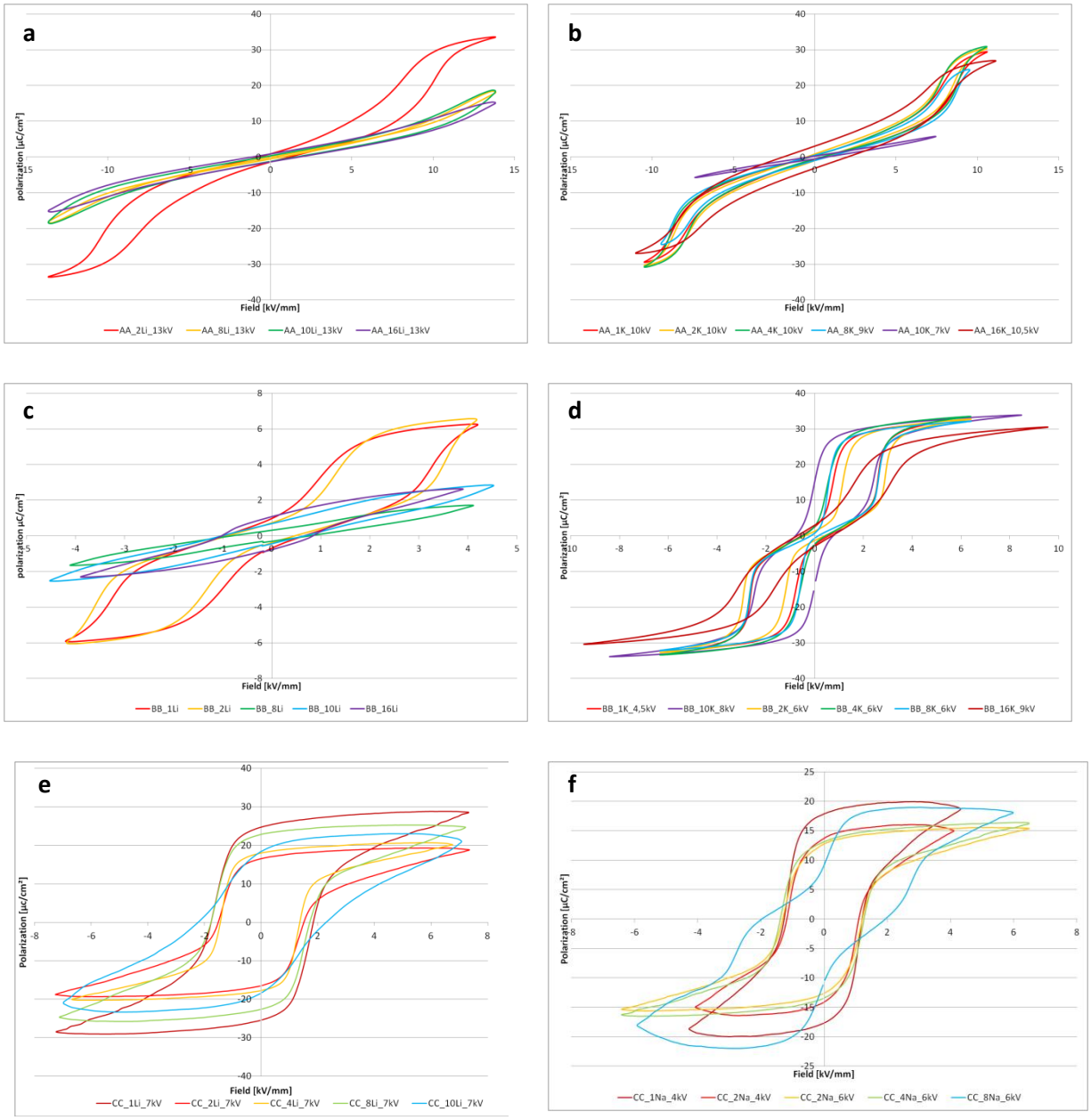

Figure 7.2-16: Polarization curves of PLZT samples with various content of Titanium and alkaline substituents (AA= $Pb_{0,91}La_{0,06}Zr_{0,9}Ti_{0,1}O_3$, BB= $Pb_{0,91}La_{0,06}Zr_{0,85}Ti_{0,15}O_3$, CC= $Pb_{0,91}La_{0,06}Zr_{0,80}Ti_{0,}$).

7.2.4 Summary:

In this chapter two antiferroelectric and one ferroelectric compositions of PLZT were used as starting composition to determine the impact of alkaline ions on the properties. These acceptor ions intend to decrease the number of lattice vacancies induced by the Lanthanum.

Alkaline ions can incorporate instead of Lead in PLZT solid solutions, where the size of the ion is displayed in the variation of the cell volume. A reduction of the cell is induced by smaller ionic radii whereas a bigger ionic radius enlarges the cell. A peculiar behaviour lied in the varying preference of the occupancy of Lithium. With respect to the coordination number, Lithium fits in the position at A- or B-site. With increasing substitution with Sodium, a structural change to orthorhombic phase occurred in the composition with higher Titanium-content.

Relative permittivity at room temperature and at elevated temperature varied with the concentration of alkaline ions, but no explicit trend was detected. Nearly no temperature shift of the temperature at maximum of relative permittivity was observed with the substitution of Lead with alkaline ions. Only substitution with Sodium altered it to higher temperature.

Compositions with higher Titanium-content were close to the triple point, where two peaks in the relative permittivity curves evolved or two phase transitions – ferroelectric to antiferroelectric and antiferroelectric to paraelectric – occurred. None of the samples showed frequency dependence of the dielectric response and therefore no relaxor state could be identified.

With the substitution of Lead with alkaline ions, the saturation polarization was decreased and the switching fields were shifted to higher fields. Furthermore, a structural change could be correlated to a dielectric transition and the evolving of a double hysteresis curve.

Overall, antiferroelectric behaviour can be stabilized in PLZT by the substitution of Lead with lighter, aliovalent alkaline ions regardless of the ionic size. In the case of Sodium-substitution, a structural change and therefore antiferroelectric phase could be induced.

Again it was shown, that the amount of Lead vacancies does not show interdependence with the development of the antiferroelectric phase. In all cases the evolving of double hysteresis lopes is correlated to a structural requirement, viz the orthorhombic structure.

7.3 Isovalent doping at A-site

In this chapter the substitution of Lead by isovalent ions is exposed. Earth alkaline ions (M^{2+}) possess the same valency as Lead and vary only in mass and ionic radius. Therefore no additional Lead vacancies were created and the amount remained constant by adding 6 mol% of trivalent Lanthanum to all compositions.

$$Pb_{0,91-b}La^{\bullet}_{0,06}M^{x}_{b}V_{Pb}^{\prime\prime}{}_{0,09}(Zr_{1-x}Ti_{x})O_3$$

Therefore the impact of the radius and the mass change at the A-site could be investigated without altering the vacancy concentration in the perovskite structure.

To better understand the possible impact of the substitution with earth alkaline in PLZT on the dielectric behaviour, literature was consulted. Starting with a simple system, the well-known earth alkaline titanates $CaTiO_3$, $SrTiO_3$ and $BaTiO_3$ were compared. Considering the bonding length of Titanium to oxygen, in the order $CaTiO_3$ - $SrTiO_3$ - $BaTiO_3$ a successive increase of the distance between the Titanium and the oxygen occurs. This enlargement of the bonding length is associated to favour ferroelectricity.

Moving to a more complex system like Lead Zirconate-Lead Titanate, the influence of the earth alkaline ions on the polarization curves can be observed: In the case of Calcium and Strontium, the switching fields increase with increasing content of these earth alkaline ions, while hysteresis is suppressed[87,110,111]. Therefore antiferroelectric behaviour is stabilized, whereas with Barium the opposed happens[112]. Furthermore, a decrease of polarization with any earth alkaline ion occurs[113,114,115].

Regarding the temperature behaviour, a more diffuse phase transition is induced by introducing an additional ion at the A-site in PZT. Furthermore, by increasing the content of the earth alkaline ion the transition is shifted to lower temperature[87,111,115,116].

Interestingly, the combination of Lanthanum and Barium at A-site leads to a relaxor-like behaviour associated in Barium Zirconate-Barium Titanate with high relative permittivity and loss factor at room temperature[117].

Overall, the effects of the earth alkaline substitution in Lead Zirconate-Lead Titanate can be divided into two groups: Calcium and Strontium are claimed to be stabilizer of the antiferroelectric phase, whereas Barium is known to favour the ferroelectric phase[112,118,119].

In this study, two starting compositions of PLZT with 6 mol% Lanthanum and a Zirconium to Titanium ratio 90 to 10 and 85 to 15 were prepared. These were called in the next section AA and BB, respectively.

7.3.1 XRD Characterization:

Earth alkaline ions incorporated well in the perovskite structure (see Figure 7.3-1 and Figure 7.3-2). No secondary phases could be detected, except with the substitution with Strontium in the PLZT solid solution $Pb_{0.91}La_{0.06}Zr_{0.9}Ti_{0.1}O_3$ (AA). In that case, Zirconium dioxide precipitates could be identified in the x-ray diffraction patterns. In Figure 7.3-2 the reflection patterns next to the main peak refer to the secondary phase highlighted by rectangles.

The Rietveld refinement was carried out with the reference reflection pattern of orthorhombic structure Pba2, which obtained good fits. By increasing the Barium concentration in the PLZT system AA a structural change occurred from the orthorhombic to a rhombohedral cell. This was visible by the vanishing and shifting of reflection patterns, which was barely recognized at the substitution of 6 mol% of Lead, but with 8 mol% substitution of Lead with Barium the conversion was clearly obvious (Figure 7.3-4).

In Table 7.3-1 the charge, atomic weight and the radius of the A- and B-site ions are listed. All earth alkaline ions have the valency of two which set the number of Lead vacancies. All substituents are lighter than Lead. Calcium even possesses one fifth of the atomic weight of Lead and nearly the same ionic radius as Lanthanum. Strontium is the earth alkaline ion which comes really close to the size of Lead is only slightly smaller and owns almost the half of the weight of Lead. The weight of Barium is comparable to that of Lanthanum. But the radius of Barium exceeds all other ions in this system.

The incorporation of the smaller ions, Calcium and Strontium, led to a predictive decrease in the cell volume. Due to the bigger size of Barium the cell volume increased with further substitution of Lead. As with increasing Barium content a phase transition was induced and the lattice parameters and the angle differed. Therefore the cell volume could not be equally compared with the others in this series. An explanation for this alteration in symmetry lies in the oversized substituent which might increase the ion-ion repulsion and thus the structure was changed to the less distorted, rhombohedral structure at the substitution of 8 mol% of Lead with Barium[66]

Table 7.3-1: Comparison in charge, atomic weight and radius of the earth alkaline ions used to build the perovskite structure.

	Pb	La	Ca	Sr	Ba	Zr	Ti
Charge	+2	+3	+2	+2	+2	+4	+4
Atomic weight	207,2	138,9	40,078	87,62	137,327	91,22	47,87
Radius [XII]	1,49	1,36	1,34	1,44	1,61		
Radius [VI]						0,72	0,605

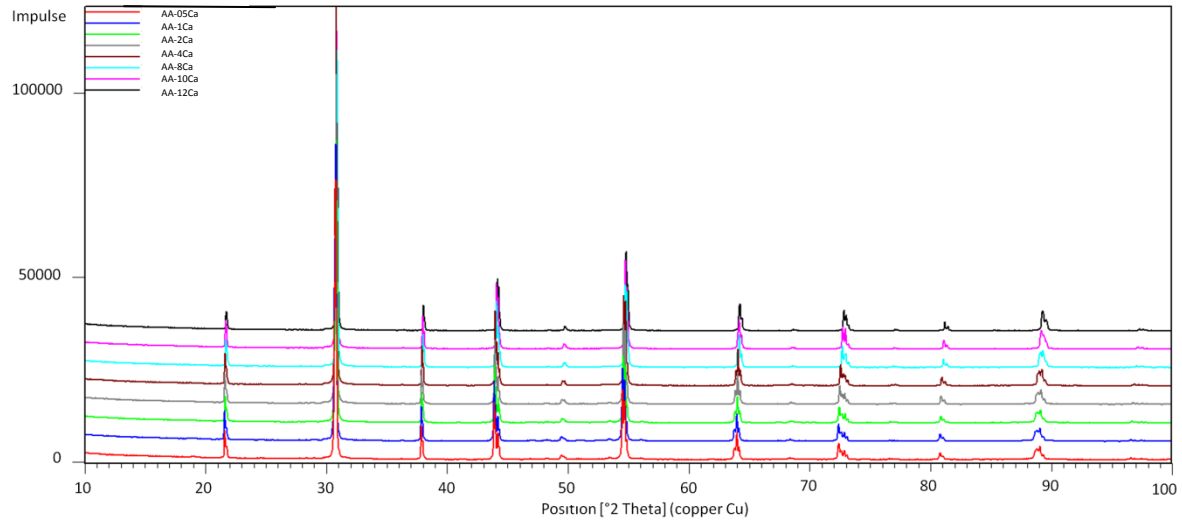

Figure 7.3-1: XRD of sintered powders of Calcium-substitution in PLZT (AA = $Pb_{0.91}La_{0.06}Zr_{0.9}Ti_{0.1}O_3$).

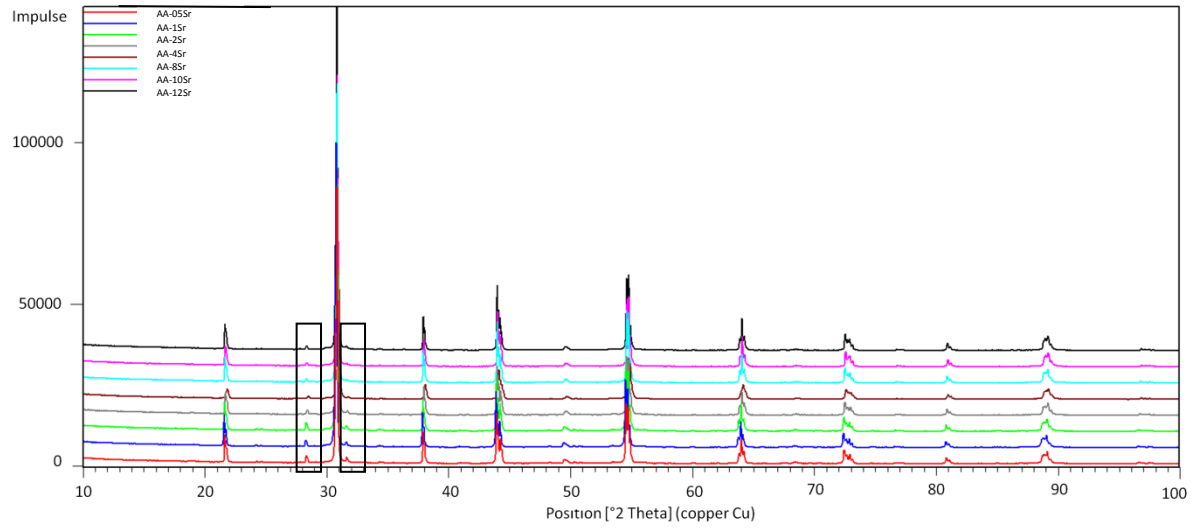

Figure 7.3-2: XRD of sintered powders of Strontium-substitution in PLZT (AA = $Pb_{0.91}La_{0.06}Zr_{0.9}Ti_{0.1}O_3$). The rectangles highlight the reflection patterns of Zirconium dioxide.

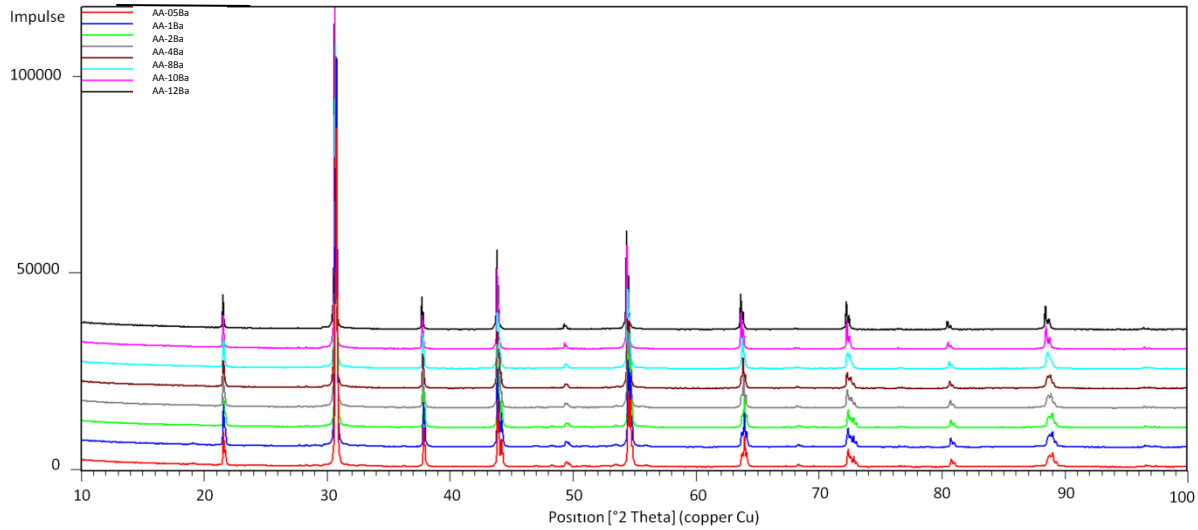

Figure 7.3-3: XRD of sintered powders of Barium-substitution in PLZT (AA = $Pb_{0.91}La_{0.06}Zr_{0.9}Ti_{0.1}O_3$).

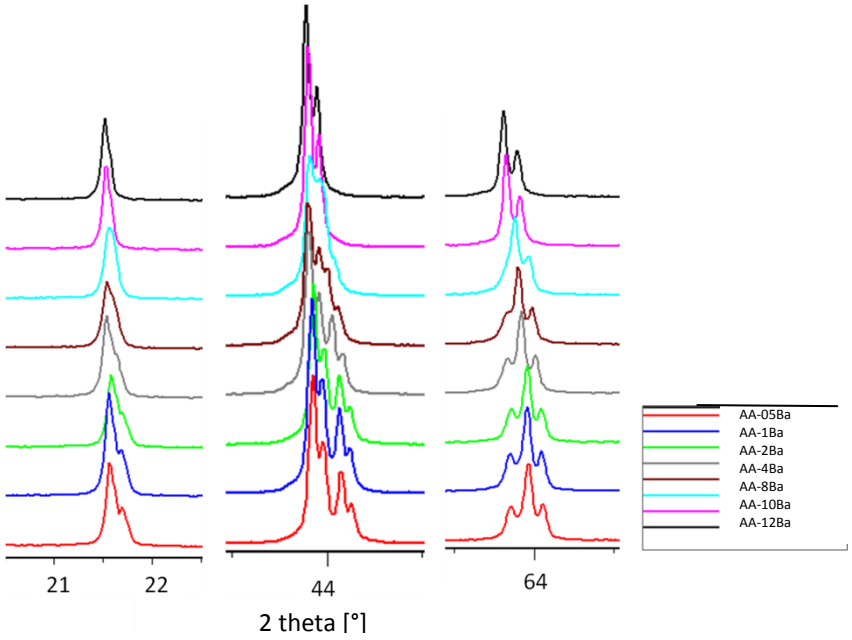

Figure 7.3-4: Detailed view of the shifting and vanishing of the reflection patterns by increasing the Barium content in the composition AA ($Pb_{0.91}La_{0.06}Zr_{0.9}Ti_{0.1}O_3$).

Theoretical density was calculated by the lattice parameters and the molar mass of the composition. With increasing substitution with Calcium and Barium the theoretical density decreased, whereas with the insertion of Strontium it seemed to increase. This might be due to the secondary phases in the samples containing Strontium which shifted the molar ratio of Zirconium to Titanium which was not considered in the calculations. All samples could achieve a density above 90% except the sample containing 6 %mol Strontium, where only 88.36% could be obtained. Overall Barium substitution led to the best densification, where nearly all ceramics possessed a relative density above 95% (Table 7.3-2 to Table 7.3-4).

Table 7.3-2: List of the cell parameters, the cell volume and the densities of Calcium-substitution in PLZT AA.

sample	c [Å]	b [Å]	a [Å]	c/a	cell volume [Å³]	theoretical density [g/cm³]	Archimedes´ density [g/cm³]	relative density [%]
AA_05Ca	8.2098	11.6903	5.8410	1.4055	560.5907	7.84	7.65	97.59
AA_1Ca	8.2084	11.6878	5.8402	1.4055	560.2943	7.83	7.59	96.96
AA_2Ca	8.2079	11.6855	5.8377	1.4060	559.9091	7.79	7.55	96.87
AA_4Ca	8.2036	11.6720	5.8328	1.4065	558.5074	7.73	7.42	95.99
AA_6Ca	8.2008	11.6594	5.8267	1.4075	557.1216	7.67	7.39	96.30
AA_8Ca	8.2001	11.6479	5.8211	1.4087	555.9952	7.61	7.14	93.89
AA_10Ca	8.1988	11.6345	5.8133	1.4103	554.5274	7.55	7.16	94.87
AA_12Ca	8.2004	11.6231	5.8090	1.4117	553.6764	7.48	6.91	92.39

Table 7.3-3: List of the cell parameters, the cell volume and the densities of Strontium-substitution in PLZT AA.

sample	c [Å]	b [Å]	a [Å]	c/a	cell volume [Å³]	theoretical density [g/cm³]	Archimedes´ density [g/cm³]	relative density [%]
AA_05Sr	8.2112	11.6903	5.8416	1.4056	560.7371	7.52	7.41	98.58
AA_1Sr	8.2100	11.6889	5.8411	1.4055	560.5515	7.83	7.59	96.83
AA_2Sr	8.2113	11.6899	5.8406	1.4059	560.6398	7.80	7.41	94.94
AA_4Sr	8.2121	11.6872	5.8391	1.4064	560.4117	7.75	7.55	97.46
AA_6Sr	8.2124	11.6867	5.8373	1.4069	560.2417	7.70	6.80	88.36
AA_8Sr	8.2102	11.6783	5.8347	1.4071	559.4340	7.65	7.17	93.76
AA_10Sr	8.2095	11.6710	5.8305	1.4080	558.6393	7.61	7.20	94.64
AA_12Sr	8.2099	11.6742	5.8322	1.4077	558.9762	7.54	7.46	98.90

Table 7.3-4: List of the cell parameters, the cell volume and the densities of Barium-substitution in PLZT AA.

sample	c [Å]	b [Å]	a [Å]	c/a	cell volume [Å³]	theoretical density [g/cm³]	Archimedes´ density [g/cm³]	relative density [%]
AA_05Ba	8.2126	11.6949	5.8418	1.4058	561.0830	7.85	7.69	98.01
AA_1Ba	8.2138	11.6945	5.8423	1.4059	561.1940	7.83	7.52	96.08
AA_2Ba	8.2188	11.6973	5.8432	1.4066	561.7551	7.81	7.61	97.37
AA_4Ba	8.2251	11.6994	5.8439	1.4075	562.3479	7.77	7.46	95.95
AA_6Ba	8.2331	11.6993	5.8450	1.4086	562.9975	7.73	7.29	94.28
AA_8Ba	8.2433	11.7071	5.8451	1.4103	564.0806	7.68	7.41	96.50
AA_10Ba	14.3308	5.8455	5.8455	2.4516	424.0743	7.63	7.26	95.17
AA_12Ba	14.3333	5.8487	5.8487	2.4507	424.6079	7.59	7.23	95.30

With a shift in the Zirconium-Titanium ratio to the Titanium-richer side (composition BB), all earth alkaline could be located at the A-site in the perovskite structure and no secondary phase was de-

tected (see Figure 7.3-5 to Figure 7.3-7). Interestingly, with increasing the Calcium content in the system to 10 mol% the reflection patterns did not only shift but some of them also vanished. Again a phase transition took place by replacing the A-site ion. This time it is a smaller ion which introduced a structural change from orthorhombic to rhombohedral structure (see Figure 7.3-8).

Consulting the Table 7.3-1, Calcium is a smaller ion than Lead and can therefore off-centre from the A-site[68]. This changes the distance between the B-site and the oxygen resulting in a higher distortion and stabilizes a more disordered structure[30],[66] with orthorhombic symmetry. Furthermore, if the ion becomes too small, a change in coordination at A-site can occur[66] which is manifested by a displacement of the A-site. This is said to additionally stabilize rhombohedral structure.

Furthermore, the bond between A-site and oxygen is less covalent in the case of Calcium compared to Lanthanum which results in a more covalent bonding between B-site and oxygen due to the inductive effect[120]. This higher covalency can induce a rectification of the oxygen octahedra and further favours a more ordered structure such as rhombohedral[67]. Additionally, the ionic interaction in the A-O bond favours the rhombohedral structure[66]. In the case of Calcium, a complex interdependence of various effects assigns the structure[66].

The substitution with Strontium - the ion which assembles the Lead in the ionic radius - did not show any impact on the type of crystal lattice. Strontium is known to stabilize the orthorhombic structure[118]. Barium, on the other hand, again changed the nature of the X-ray spectrum (see

Figure 7.3-9). The vanishing of reflections indicating transformation in a more ordered symmetry occurred at 6 mol% substitution of Lead with that earth alkaline ion.

The cell volume changed as expected by the size of the substituent. Calcium and Strontium ion minimized and Barium ion enlarged the cell.

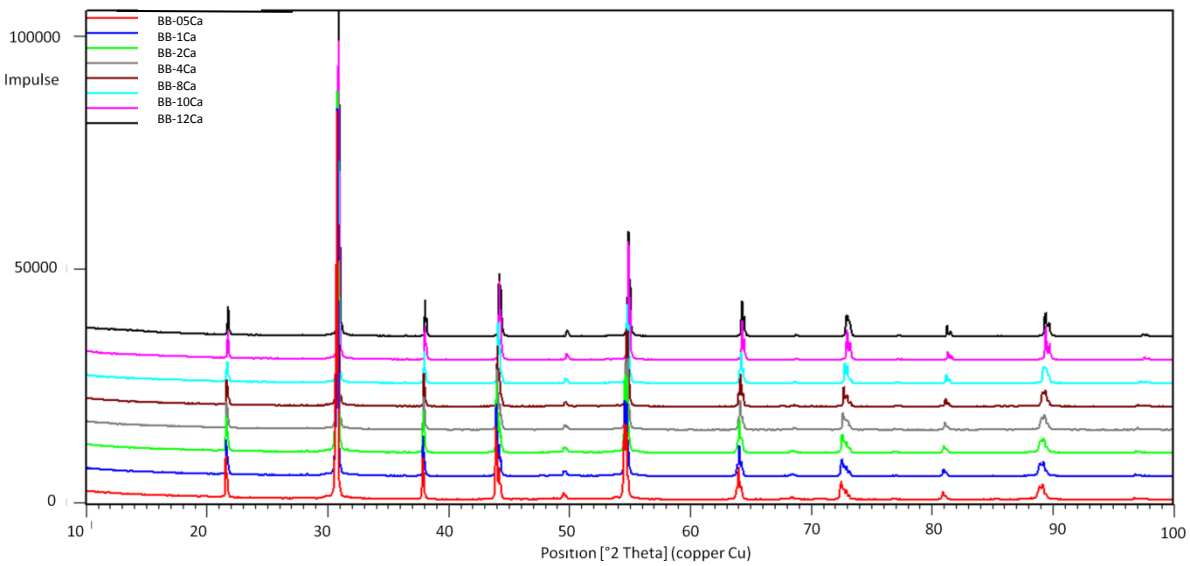

Figure 7.3-5: XRD of sintered powders of Calcium-substitution in PLZT (BB = $Pb_{0.91}La_{0.06}Zr_{0.85}Ti_{0.15}O_3$).

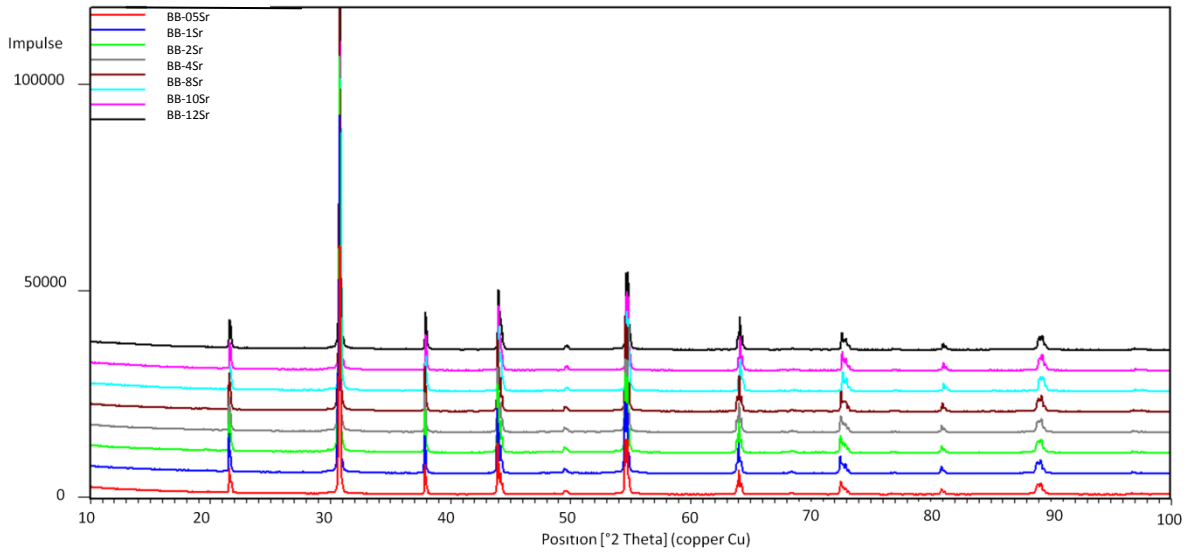

Figure 7.3-6: XRD of sintered powders of Strontium-substitution in PLZT (BB = $Pb_{0.91}La_{0.06}Zr_{0.85}Ti_{0.15}O_3$).

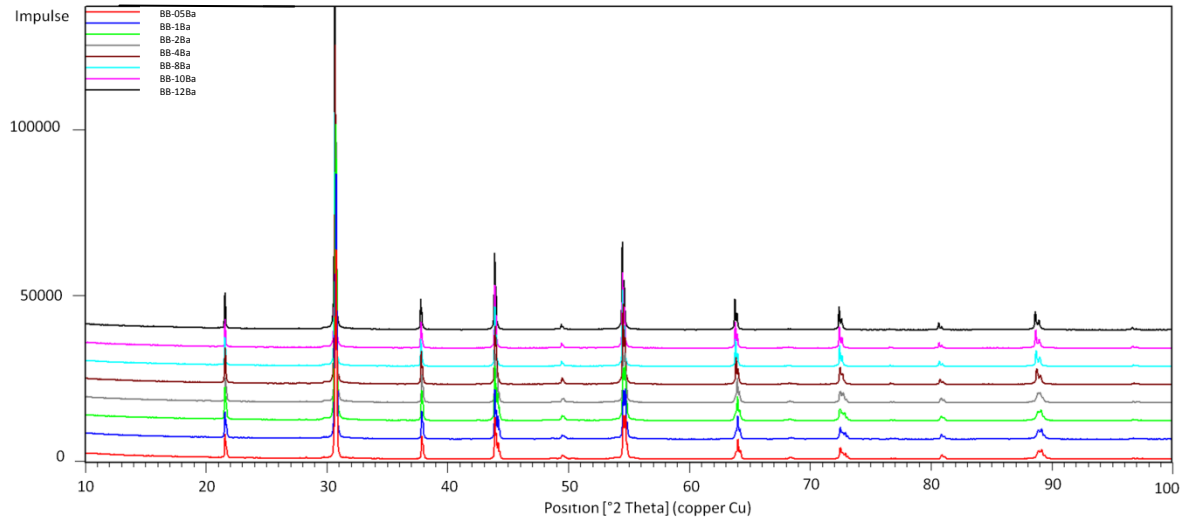

Figure 7.3-7: XRD of sintered powders of Barium-substitution in PLZT (BB = $Pb_{0.91}La_{0.06}Zr_{0.85}Ti_{0.15}O_3$).

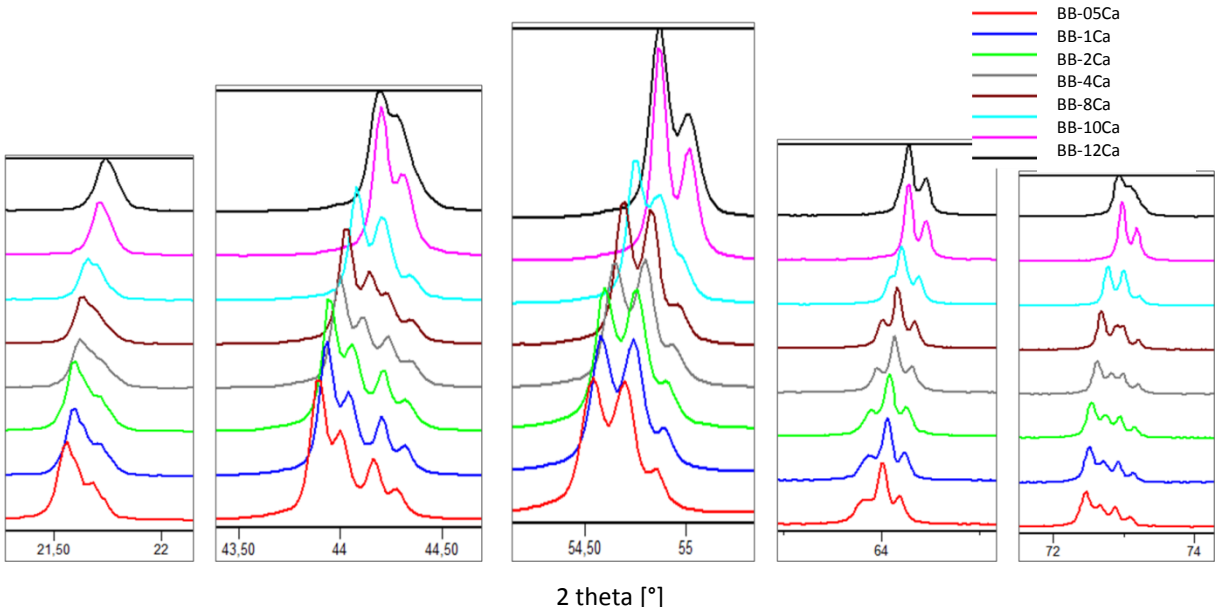

Figure 7.3-8: Detailed view of the shifting and vanishing of the reflection patterns by increasing the Calcium content in the composition BB ($Pb_{0.91}La_{0.06}Zr_{0.85}Ti_{0.15}O_3$).

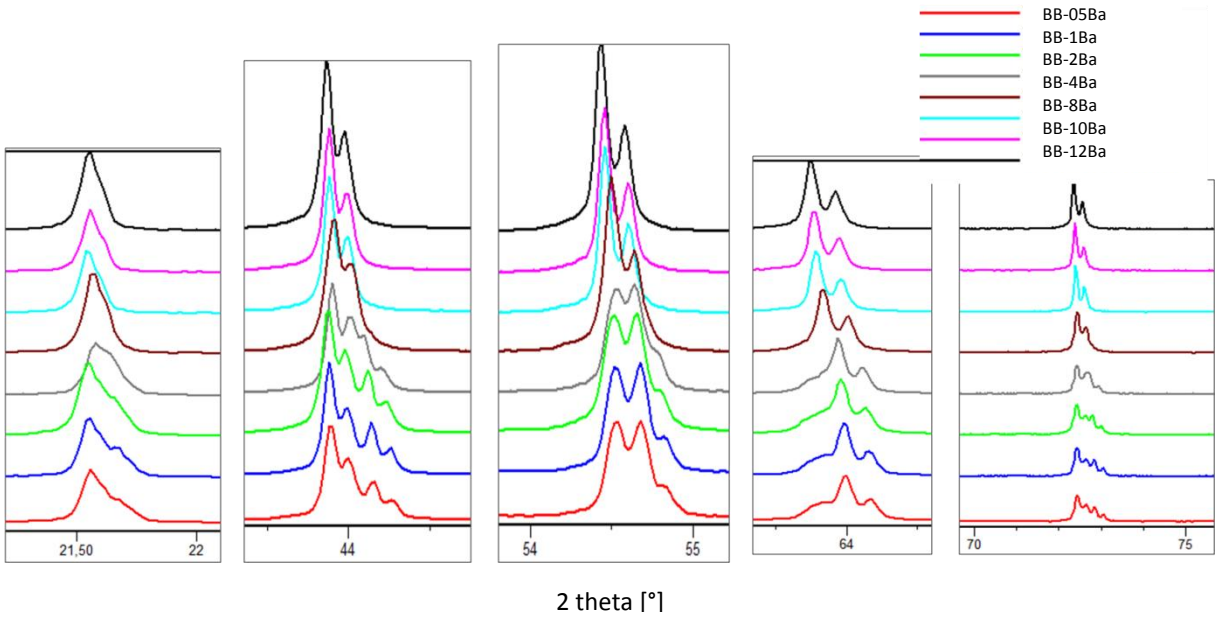

Figure 7.3-9: Detailed view of the shifting and vanishing of the reflection patterns by increasing the Barium content in the composition BB ($Pb_{0.91}La_{0.06}Zr_{0.85}Ti_{0.15}O_3$).

The value of the theoretical density decreased in all cases. All samples possessed a relative density of above 90%. By substituting Lead with Calcium and Barium the relative density declined. With Strontium, on the other hand, the highest densification was obtained. The relative densities exceeded 100% which indicates that the structural model for the calculation of the theoretical density may not be adequate. (Table 7.3-5 to Table 7.3-7).

Table 7.3-5: List of the cell parameters, the cell volume and the densities of Calcium-substitution in PLZT BB.

sample	c [Å]	b [Å]	a [Å]	c/a	cell volume [Å³]	theoretical density [g/cm³]	Archimedes´ density [g/cm³]	relative density [%]
BB_05Ca	8.1985	11.6691	5.8284	1.4066	557.5932	7.83	7.36	93.94
BB_1Ca	8.1970	11.6654	5.8274	1.4066	557.2210	7.82	7.50	95.96
BB_2Ca	8.1948	11.6592	5.8250	1.4068	556.5423	7.79	7.51	96.44
BB_4Ca	8.1921	11.6483	5.8202	1.4075	555.3861	7.72	7.28	94.22
BB_6Ca	8.1904	11.6388	5.8143	1.4087	554.2589	7.66	7.06	92.11
BB_8Ca	8.1900	11.6243	5.8075	1.4102	552.8920	7.60	7.46	98.12
BB_10Ca	14.1999	5.7948	5.7948	2.4504	412.9463	7.55	7.05	93.39
BB_12Ca	14.2126	5.7997	5.7997	2.4506	414.0085	7.45	7.10	95.24

Table 7.3-6: List of the cell parameters, the cell volume and the densities of Strontium-substitution in PLZT BB.

sample	c [Å]	b [Å]	a [Å]	c/a	cell volume [Å³]	theoretical density [g/cm³]	Archimedes´ density [g/cm³]	relative density [%]
BB_05Sr	8.2009	11.6722	5.8294	1.4068	558.0095	7.82	7.34	93.86
BB_1Sr	8.1989	11.6691	5.8293	1.4065	557.7099	7.80	7.64	97.94
BB_2Sr	8.1980	11.6653	5.8282	1.4066	557.3613	7.76	7.64	98.50
BB_4Sr	8.1970	11.6599	5.8262	1.4069	556.8510	7.67	7.54	98.40
BB_6Sr	8.1962	11.6554	5.8244	1.4072	556.3890	7.57	7.50	98.99
BB_8Sr	8.1954	11.6441	5.8171	1.4088	555.1092	7.49	7.38	98.50
BB_10Sr	8.1961	11.6480	5.8193	1.4084	555.5601	7.39	7.42	100.52
BB_12Sr	8.1957	11.6495	5.8217	1.4078	555.8307	7.28	7.44	102.20

Table 7.3-7: List of the cell parameters, the cell volume and the densities of Barium-substitution in PLZT BB.

sample	c [Å]	b [Å]	a [Å]	c/a	cell volume [Å³]	theoretical density [g/cm³]	Archimedes´ density [g/cm³]	relative density [%]
BB_05Ba	8.2027	11.6730	5.8285	1.4073	558.0830	7.83	7.65	97.66
BB_1Ba	8.2040	11.6754	5.8297	1.4073	558.3980	7.82	7.54	96.46
BB_2Ba	8.2071	11.6766	5.8293	1.4079	558.6270	7.81	7.41	94.93
BB_4Ba	8.2181	11.6800	5.8309	1.4094	559.6916	7.76	7.20	92.83
BB_6Ba	14.2887	5.8304	5.8304	2.4507	420.6467	7.71	7.46	96.77
BB_8Ba	14.2938	5.8325	5.8325	2.4507	421.1039	7.67	7.48	97.58
BB_10Ba	14.3008	5.8353	5.8353	2.4507	421.7133	7.62	7.37	96.66
BB_12Ba	14.3057	5.8373	5.8373	2.4507	422.1513	7.58	7.13	93.99

7.3.2 Microstructure:

The results of XRD show secondary phases in the samples containing Strontium. These were used to examine the microstructure in detail with SEM. In Figure 7.3-10 backscattered SEM image of the sample AA-8Sr is shown. It demonstrates the emerging of secondary phase and pores. According to the EDS-measurements, Lead Zirconate (marked with 2 and with 3) precipitated. The secondary phase could be found mostly at the contact area of the grains.

In Figure 7.3-11 a selection of channelling contrast mode SEM images are depicted. All samples contain Strontium with increasing content in the order of a to f. The microstructure shows grain sizes varying from small to big grains and exhibited an inhomogeneous grain growth. The image of the sample AA-6Sr demonstrates more pores compared to the other images and gives therefore an explanation of the low density.

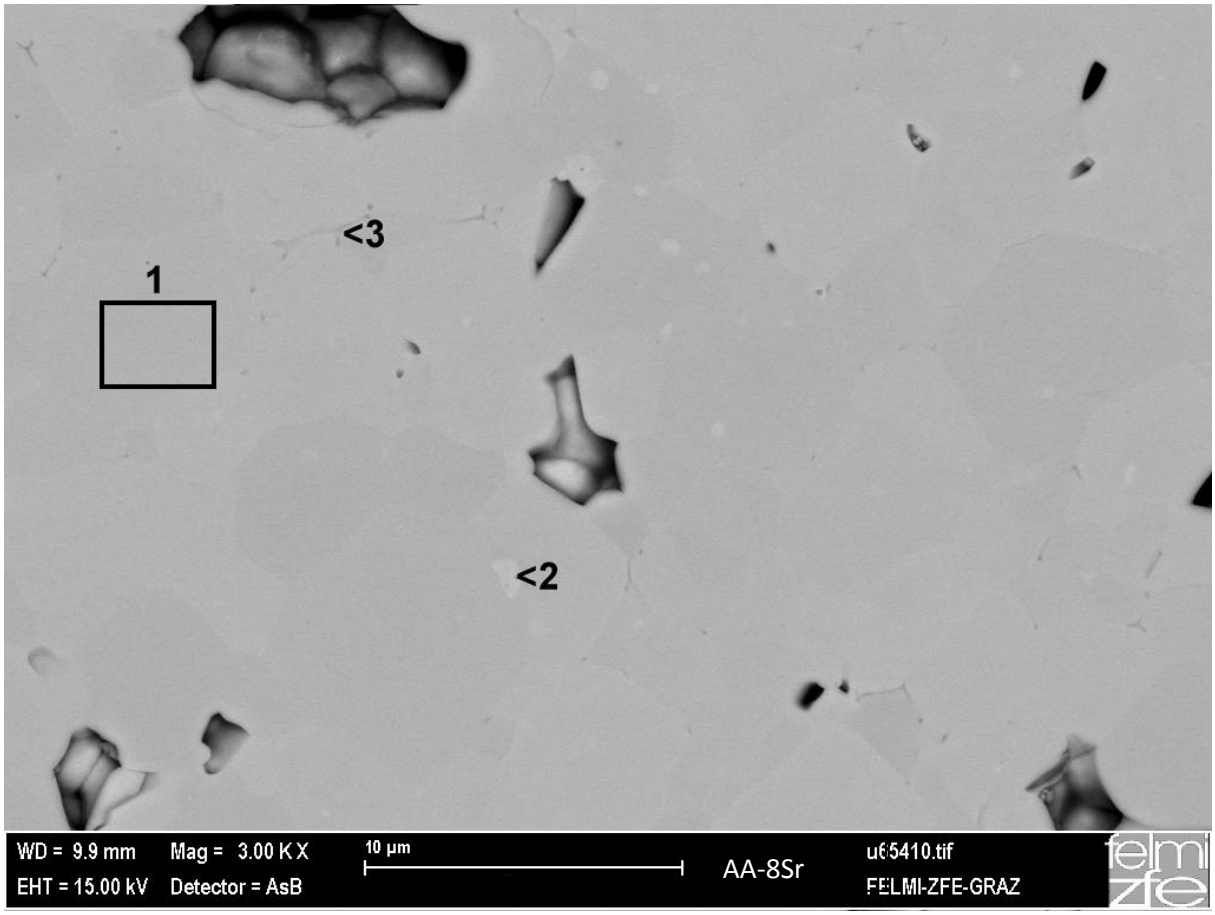

Figure 7.3-10: SEM backscattered image of AA-8Sr (2=Lead Zirconate, 3=Lead Zirconate with Titanium and Strontium).

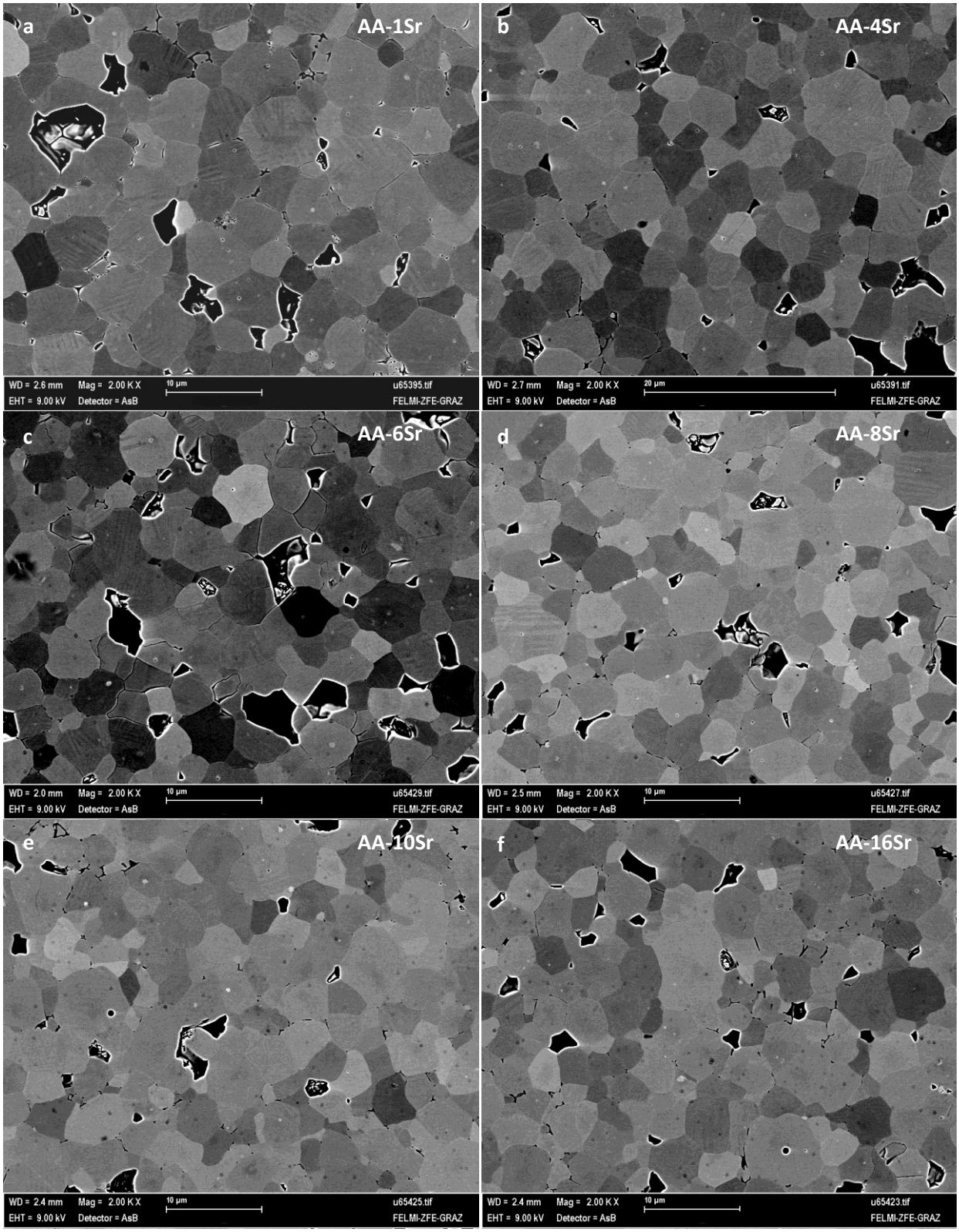

Figure 7.3-11: SEM backscattered electron images in the channelling contrast mode of various samples PLZT containing Strontium.

7.3.3 Dielectric Characterization:

Capacitance, loss factor, relative permittivity and piezoelectric constant d_{33} have been measured at room temperature (Table 7.3-8 to Table 7.3-13). In the small signal regime, substitution of Lead with Calcium decreased the capacitance from 680 pF to ~465 pF or in other words decreased relative permittivity from ~600 to ~390. The loss factor was also shifted to lower values, while the piezoelectric constant increased. At the content of 10 mol% Calcium d_{33} decupled, but the highest achievable value was only 0.30.

Likewise, the substitution of Lead with Strontium decreased capacitance and relative permittivity - but not to that extent. By substituting 12 mol% of Lead with that earth alkaline, the values dropped from 670 pF to 544 pF and from 586 to 475 in relative permittivity. Furthermore, the loss factor also decreased.

In contrast, Barium increased all parameters: The capacitance jumped from 773 pF to 3451 pF and relative permittivity from 658 to ~2720. The loss factor increased and the piezoelectric constant was almost decupled with increasing molar ratio, but the highest value was only 0.52.

Regarding the samples of composition BB on the Titanium-richer side, a similar behaviour was observed: Calcium and Strontium, both, decreased all parameters, whereas Barium increased them. The values declined gradually with increasing content of Calcium from 780 pF to 494 pF in capacitance and 1015 to 677 in relative permittivity. With the substitution of 4 mol% of Lead with Calcium the piezoelectric constant dropped from 0.48 to 0.05.

The influence of the substitution of Lead with Strontium was pretty similar: Capacitance decreased from ~825 pF to ~550 pF and relative permittivity from 1075 to ~745 pF by increasing the amount of Strontium from 1 mol% to 12 mol%. The piezoelectric constant dropped at the substitution of 6 mol% of Lead with Strontium from 0.17 to 0.07.

Barium on the other hand increased capacitance from ~800 to ~2300 pF. The piezoelectric constant increased, reached a maximum of 20.1 with 4 mol% Barium and then decreased again to around 4.

Table 7.3-8: Results of low signal dielectric measurements of Calcium-substitution in PLZT AA.

sample	capacitance [nF]	loss factor []	relative permittivity []	piezoelectric constant d33
AA_05Ca	0.6808	0.0113	604	0.03
AA_1Ca	0.7020	0.0126	605	0.02
AA_2Ca	0.6285	0.0091	531	0.02
AA_4Ca	0.5684	0.0080	480	0.04
AA_6Ca	0.5623	0.0075	471	0.03
AA_8Ca	0.5336	0.0064	445	0.03
AA_10Ca	0.5272	0.0062	439	0.30
AA_12Ca	0.4651	0.0065	388	0.30

Table 7.3-9: Results of low signal dielectric measurements of Strontium-substitution in PLZT AA.

sample	capacitance [nF]	loss factor []	relative permittivity []
AA_05Sr	0.6701	0.0121	586
AA_1Sr	0.7453	0.0100	626
AA_2Sr	0.6788	0.0088	578
AA_4Sr	0.6258	0.0089	546
AA_6Sr	0.5906	0.0067	509
AA_8Sr	0.5737	0.0053	495
AA_10Sr	0.5124	0.0046	445
AA_12Sr	0.5440	0.0056	475

Table 7.3-10: Results of low signal dielectric measurements of Barium-substitution in PLZT AA.

sample	capacitance [nF]	loss factor []	relative permittivity []	piezoelectric constant d33
AA_05Ba	0.7725	0.0068	658	0.03
AA_1Ba	0.8067	0.0072	664	0.04
AA_2Ba	0.8614	0.0084	722	0.05
AA_4Ba	1.0034	0.0098	847	0.07
AA_6Ba	1.2366	0.0111	1052	0.13
AA_8Ba	1.8338	0.0160	1565	0.52
AA_10Ba	3.2615	0.0151	2720	0.34
AA_12Ba	3.4505	0.0109	2931	0.22

Table 7.3-11: Results of low signal dielectric measurements of Calcium-substitution in PLZT BB.

sample	capacitance [nF]	loss factor []	relative permittivity []	piezoelectric constant d33
BB_05Ca	0.7796	0.0186	1015	0.46
BB_1Ca	0.7578	0.0165	986	0.37
BB_2Ca	0.6355	0.0142	823	0.24
BB_4Ca	0.5628	0.0100	743	0.05
BB_6Ca	0.5834	0.0069	775	0.04
BB_8Ca	0.5385	0.0077	742	0.04
BB_10Ca	0.4417	0.0087	583	0.03
BB_12Ca	0.4937	0.0095	677	0.03

Table 7.3-12: Results of low signal dielectric measurements of Strontium-substitution in PLZT BB.

sample	capacitance [nF]	loss factor []	relative permittivity []	piezoelectric constant d33
BB_05Sr	0.8264	0.0153	1076	0.48
BB_1Sr	0.7837	0.0149	1669	0.48
BB_2Sr	0.6817	0.0133	894	0.32
BB_4Sr	0.6889	0.0100	1337	0.17
BB_6Sr	0.6015	0.0076	788	0.07
BB_8Sr	0.5062	0.0046	693	0.01
BB_10Sr	0.5060	0.0057	695	0.05
BB_12Sr	0.5527	0.0067	745	0.05

Table 7.3-13: Results of low signal dielectric measurements of Barium-substitution in PLZT BB.

sample	capacitance [nF]	loss factor []	relative permittivity []	piezoelectric constant d33
BB_05Ba	0.7986	0.0229	1088	3.35
BB_1Ba	0.9457	0.0223	1220	4.17
BB_2Ba	1.0114	0.0250	1323	12.10
BB_4Ba	1.1340	0.0299	1502	20.10
BB_6Ba	2.0363	0.0415	2688	11.90
BB_8Ba	2.1016	0.0384	2832	5.93
BB_10Ba	2.6132	0.0207	3546	4.30
BB_12Ba	2.2923	0.0141	3073	*

Measuring the relative permittivity versus temperature revealed the phase transition temperature of the material. The increase of relative permittivity with increasing temperature completes in a maximum known as the temperature of maximum of relative permittivity T_m, which indicates a structural or at least dielectric change of the material from the polar to a non-polar state (see Figure 7.3-12a-f).

The impacts of the substitution with earth alkaline ions on the relative permittivity and on the temperature of maximum relative permittivity are graphically summarized in Table 7.3-14, Table 7.3-15, Figure 7.3-13 and Figure 7.3-14.

The substitution of Lead with earth alkaline ions altered the shape of the relative permittivity curves. With increasing substituent concentration a broadening of the peak appeared. This refers to a more diffuse phase transition. Also an alteration in the position of the peak and the height of the peak could be achieved by inserting alkaline ions.

As in Figure 7.3-12a shown, the increasing content of Calcium from 1 mol% to 12 mol% in the system AA decreased this transition temperature from 180 °C to 80 °C, whereas the same modification with Strontium only changed the temperature by 40 °C (Figure 7.3-12b). Lead substitution with Barium showed the highest impact on the temperature and shifted the transition from 180 °C to 40 °C (Figure 7.3-12c).

Similar behaviour could be observed with the substitution of Lead with these earth alkaline ions in the system BB with higher Titanium content (Figure 7.3-12c-f). The starting point of around 155 °C was decreased by incorporation of 12 mol% of Calcium to 95 °C and by substituting with 12 mol% Strontium only to 145 °C. With the same content of Barium at the A-site replacing Lead, the temperature dropped to 45 °C. A shoulder in the curve of the samples substituted with Calcium is visible. This additionally step vanished with the addition of more than 1 mol% of the substituent.

The shift in temperature obviously depends mainly on the ionic radius: Strontium ion owns nearly the same size as the Lead ion. This means, that the substitution of Lead with Strontium exerted nearly no effect on the transition temperature. Some peculiarity appeared with higher content of Strontium: An abrupt decrease in T_m occurred with 10 mol% of Strontium in the AA system and 8 mol% in the BB system. With increasing content of Strontium the transition temperature increased again.

With the substitution of Lead with Barium the structure had to cope with an ion which needs 10% more space as Lead. For this reason, the structure has to handle a lot of stress and distortion which resulted in a structural change.

Calcium on the other hand possesses only 90% of the ionic radius as Lead. Thus a substitution resulted in a shift of the phase transition to lower temperatures. The weaker effect of Calcium compared to Barium might be found in the lattice. A smaller ion might be easier to be placed in a structure than a bigger one.

In the case of the compositions BB with higher Titanium concentration the temperature shift was not that large. The reason for this might be related in the smaller ionic radius of Titanium in comparison to Zirconium.

The maximum of the relative permittivity decreased with increasing Calcium and Strontium concentration. Comparing the system AA and BB, the effect on the values was divided by two by solely increasing the Titanium content from 10 to 15 mol%. In the case of Calcium, with increasing substitution the decrease in relative permittivity from 2900 to 680 resulted in a reduction of around 75% in the system AA. On the other hand, in the BB system the same increase in substituent concentration resulted only in a reduction of relative permittivity of about 1150. Replacing Lead with Strontium in the AA system achieved a decrease in relative permittivity of about 1800 and in the BB system only about 900.

With the substitution of Lead with Barium in the PLZT systems a comparable enhancement in relative permittivity in both starting compositions was obtained. In the AA system an increase of about 1600 and in the other system of about 1400 was achieved. In the case of BB, a maximum was obtained with the substitution of 6 mol% followed by a decline to nearly the starting point of 2600 with increasing substituent content. This might be related to the structural change from orthorhombic to rhombohedral structure with this amount of Barium.

Relative permittivity is varied due to the incorporation of the earth alkaline ions. The bigger ion increases and the smaller ions decrease the values of relative permittivity. But relative permittivity might not only be influenced by the radius of the substituents. Strontium has nearly the same radius as Lead, but the exchange of them showed a similar decline in relative permittivity as with the substitution with Calcium. There might be a combination of effects: Although the size of Strontium does not deviate much of Lead, the weight is less than half of that of Lead. Then the effect of the weight might dominate over that of the ionic radius. Overall, lighter and smaller ions induce a shift in relative permittivity to lower values. In the case of Barium substitution, a lighter, but bigger ion compared to Lead increased relative permittivity.

Substitution of Lead with earth alkaline ions in the PLZT solid solutions decreased the transition temperature in all samples. Barium showed the highest decline in temperature, while Strontium showed the lowest. The reason might lie in the closeness of the radius of Strontium to that of Lead. It seems as tough, the closer the ionic radius of an isovalent ion is to that which is substituted, the lower the shift in temperature is. As the ion size deviates from Lead, the decrease in transition temperature might be affected by the mass. The higher the mass of the substituent, the higher is the shift in temperature.

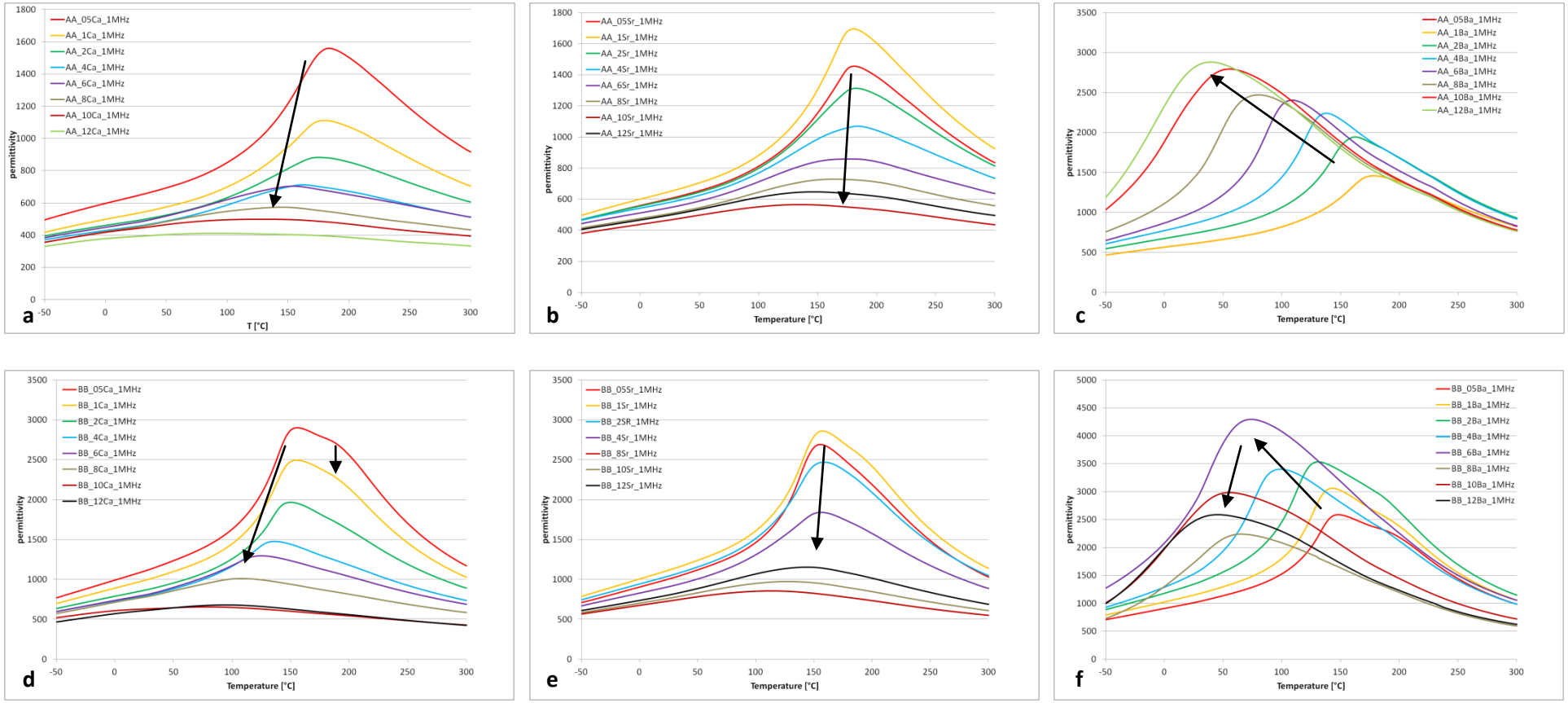

Figure 7.3-12: Relative permittivity curves versus temperature at 1 MHz (arrows indicate the maximum in relative permittivity and demonstrate the alteration with increasing concentration of substituents (AA= $Pb_{0.91}La_{0.06}Zr_{0.90}Ti_{0.1}O_3$, BB= $Pb_{.91}La_{0.06}Zr_{0.85}Ti_{0.15}O_3$).

Table 7.3-14: Results of the relative permittivity versus temperature curves of Calcium, Strontium and Barium substitution in PLZT $Pb_{0.91}La_{0.06}Zr_{0.9}Ti_{0.1}O_3$.

sample	maximum in relative per-mittivity	Temperature Tm [°C]	sample	maximum in relative permittivity	Temperature Tm [°C]	sample	maximum in relative permittivity	Temperature Tm [°C]
AA_05Ca	1560	184	AA_05Sr	1460	183	AA_05Ba	1460	180
AA_1Ca	1110	181	AA_1Sr	1690	181	AA_1Ba	1820	173
AA_2Ca	880	175	AA_2Sr	1310	184	AA_2Ba	1940	162
AA_4Ca	710	162	AA_4Sr	1070	184	AA_4Ba	2240	138
AA_6Ca	700	154	AA_6Sr	860	181	AA_6Ba	2410	113
AA_8Ca	570	145	AA_8Sr	730	176	AA_8Ba	2470	80
AA_10Ca	500	129	AA_10Sr	560	138	AA_10Ba	2790	57
AA_12Ca	410	93	AA_12Sr	650	145	AA_12Ba	2880	38

Table 7.3-15: Results of the relative permittivity versus temperature curves of Calcium, Strontium and Barium substitution in PLZT $Pb_{0.91}La_{0.06}Zr_{0.85}Ti_{0.15}O_3$.

sample	maximum in relative permittivity	Temperature Tm [°C]	sample	maximum in relative permittivity	Temperature Tm [°C]	sample	maximum in relative permittivity	Temperature Tm [°C]
BB_05Ca	2900	156	BB_05Sr	2690	156	BB_05Ba	2550	149
BB_1Ca	2490	156	BB_1Sr	2860	158	BB_1Ba	3020	144
BB_2Ca	1960	151	BB_2Sr	2470	159	BB_2Ba	3460	132
BB_4Ca	1470	138	BB_4Sr	1840	157	BB_4Ba	3310	102
BB_6Ca	1300	125	BB_6Sr	1400	155	BB_6Ba	4150	81
BB_8Ca	1010	109	BB_8Sr	860	114	BB_8Ba	2240	66
BB_10Ca	650	78	BB_10Sr	970	128	BB_10Ba	2980	56
BB_12Ca	680	95	BB_12Sr	1150	143	BB_12Ba	2590	46

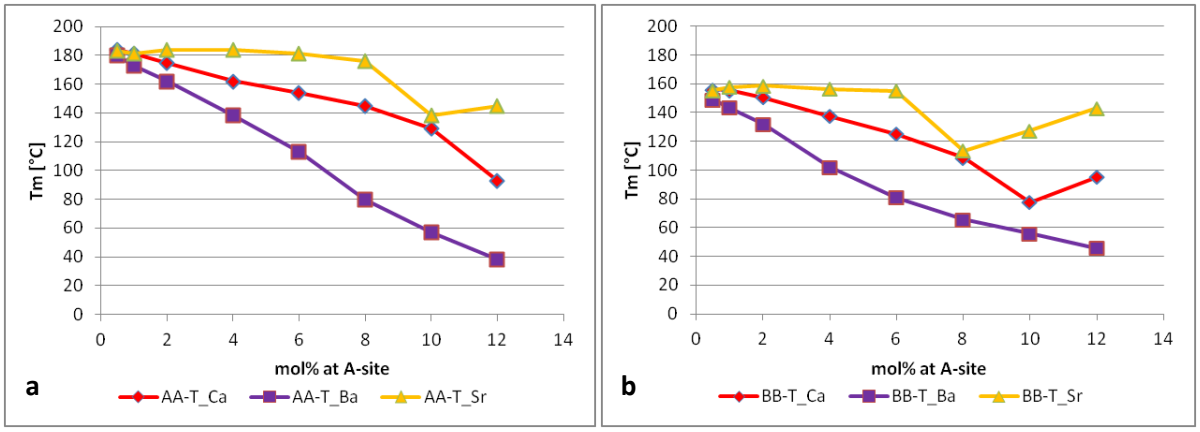

Figure 7.3-13: Influence of the earth alkaline concentration on the temperature of maximum in relative permittivity of the samples AA ($Pb_{0.91}La_{0.06}Zr_{0.9}Ti_{0.1}O_3$) and BB ($Pb_{0.91}La_{0.06}Zr_{0.85}Ti_{0.151}O_3$).

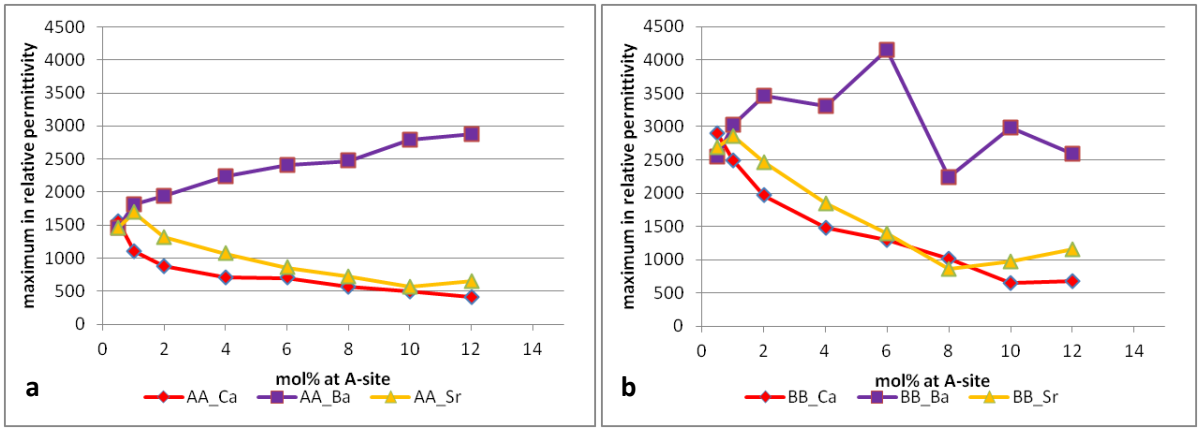

Figure 7.3-14: Influence of the earth alkaline concentration on the maximum in relative permittivity of the samples AA ($Pb_{0.91}La_{0.06}Zr_{0.9}Ti_{0.1}O_3$) and BB ($Pb_{0.91}La_{0.06}Zr_{0.85}Ti_{0.151}O_3$).

Frequency dependence of relative relative permittivity and loss factor of selected samples is shown in Figure 7.3-15. No variation of peak temperature with frequency could be detected in any sample except the sample AA with high concentration of Barium. With increasing the frequency the peak around 50 °C is shifted to higher temperature. Therefore this sample show relaxor behaviour.

In the cases of AA, where Lead is substituted with Calcium and Strontium only one peak in relative permittivity is visible. The maximum in the loss factor shows good correlation to that. None of them is moving to other temperatures by increasing the concentration of the substituents. Only an alteration in the height of the peaks is detected. By increasing the frequency the curves become broader.

With increased content of Titanium an additional step in the curves is visible. Concerning the substitution of Lead with Strontium this alteration disappeared with increasing frequency. In the case of Calcium substitution this shoulder maintained throughout all frequency changes, but overall did not shift in temperature.

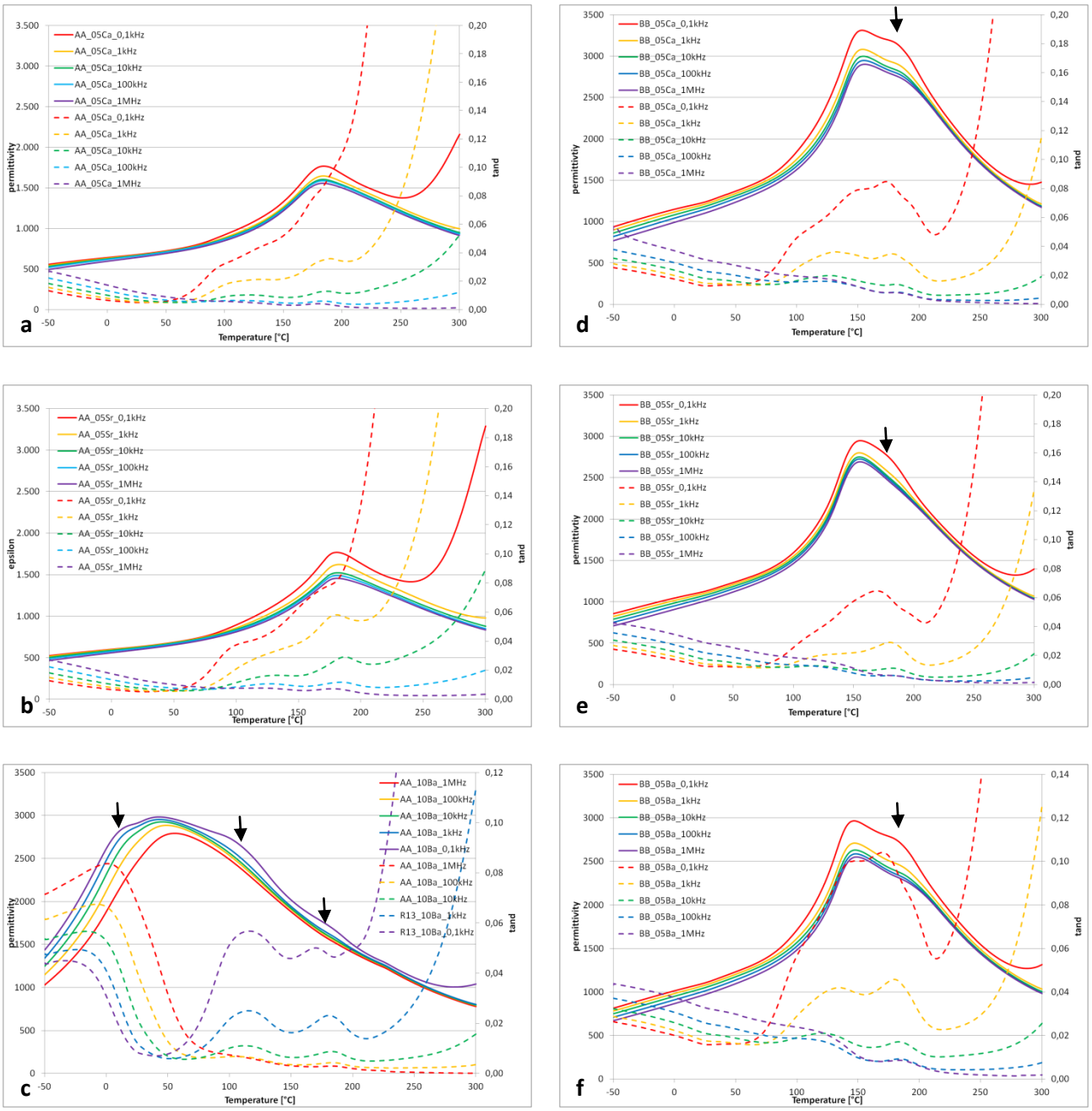

Figure 7.3-15: Frequency dependency of relative permittivity (solid line) and loss factor (dashed line) curves of selected earth alkaline substitution in PLZT (measured at 0,1 kHz, 1 kHz, 10 kHz, 100 kHz and 1 MHz). Arrows indicate anomalies in the curves (AA = $Pb_{0.91}La_{0.06}Zr_{0.9}Ti_{0.1}O_3$, BB = $Pb_{0.91}La_{0.06}Zr_{0.85}Ti_{0.15}O_3$).

In the last row Barium substituted samples are depicted which show some peculiarities: Curves recorded at low frequency show broader peaks with three shoulders. These peaks might correspond to the phase transition in Barium Titanate which emerge at low frequency (T1: rhombohedral→orthorhombic, T2: orthorhombic→tetragonal, T3: tetragonal→cubic)[121].

Overall the substitution of Lead with Barium induced a more diffuse phase transition. In the AA composition, these shoulders vanished at 100 kHz and one broad peak remained by increasing frequency to 1 MHz. In the Titanium-richer composition, these shoulders remained also at 1 MHz.

Unipolar polarization curves of AA compositions, where Lead is substituted with Calcium, Strontium and Barium, are plotted in Figure 7.3-16. All curves recorded had a slim shape. Not all samples revealed saturated curves. In some cases it was not possible to apply higher voltage due to technical limitations or due to the break down voltage of the sample itself.

Consulting Figure 7.3-16a , the influence of the increasing content of Calcium on the dielectric behaviour under field can be observed. By following the subsitution, the slope of the curves declined and the curve flattened. Only curves with low substituent concentration developed saturation in polarization. Therefore only these can be discussed concerning the change of the characteristics due to the substitution of Lead with Calcium. Substitution of Lead with Calcium induced a decrease in saturation and a shift of the switching field to higher fields.

A similar behaviour was apparent in Figure 7.3-16b with the substitution with Strontium: With increasing the molar concentration the curves approached the x-axis even in a higher degree. Again not all curves can be consulted to consider the influences of that substituent on the switching fields and saturation polarization. But for the lower concentrations a decrease in saturation and a shift to higher switching fields can be discovered for further increase of the concentration.

Barium substitution, as shown in Figure 7.3-16c, showed some peculiarity: With increasing the content of substituent a change in shape occurred. The bending of the curve altered from convex to concav. Up to the substitution of 6 mol% of Lead the curves assembled an `S´-shape. At low field polarization increased with increasing field, then the slope inclined until the curve ended in a flattening due to saturation. The curves of the samples with higher content of Barium demonstrated a higher incline at low field and leveled smoothly out at higher field. Regarding the compositions with lower molar ratios, the saturation polarization decreased as well as the switching fields by increasing the doping concentration.

The change in the shape of the hysteresis curves might correlate to the structural one. As already mentioned, with the subsitution of 8 mol% of Lead with Barium the rearrangement of the lattice resulted in a rhombohedral structure. The slope of these curves decreased with increasing concentration of Barium.

In this series, a stabilization of the antiferroelectric phase over field by substituting Lead with Calcium and Strontium can be achieved. The substitution of Barium on the other hand demonstrated the opposed behaviour. Additionally, a change in the shape of the curves due to molar concentration of that substituent was observed.

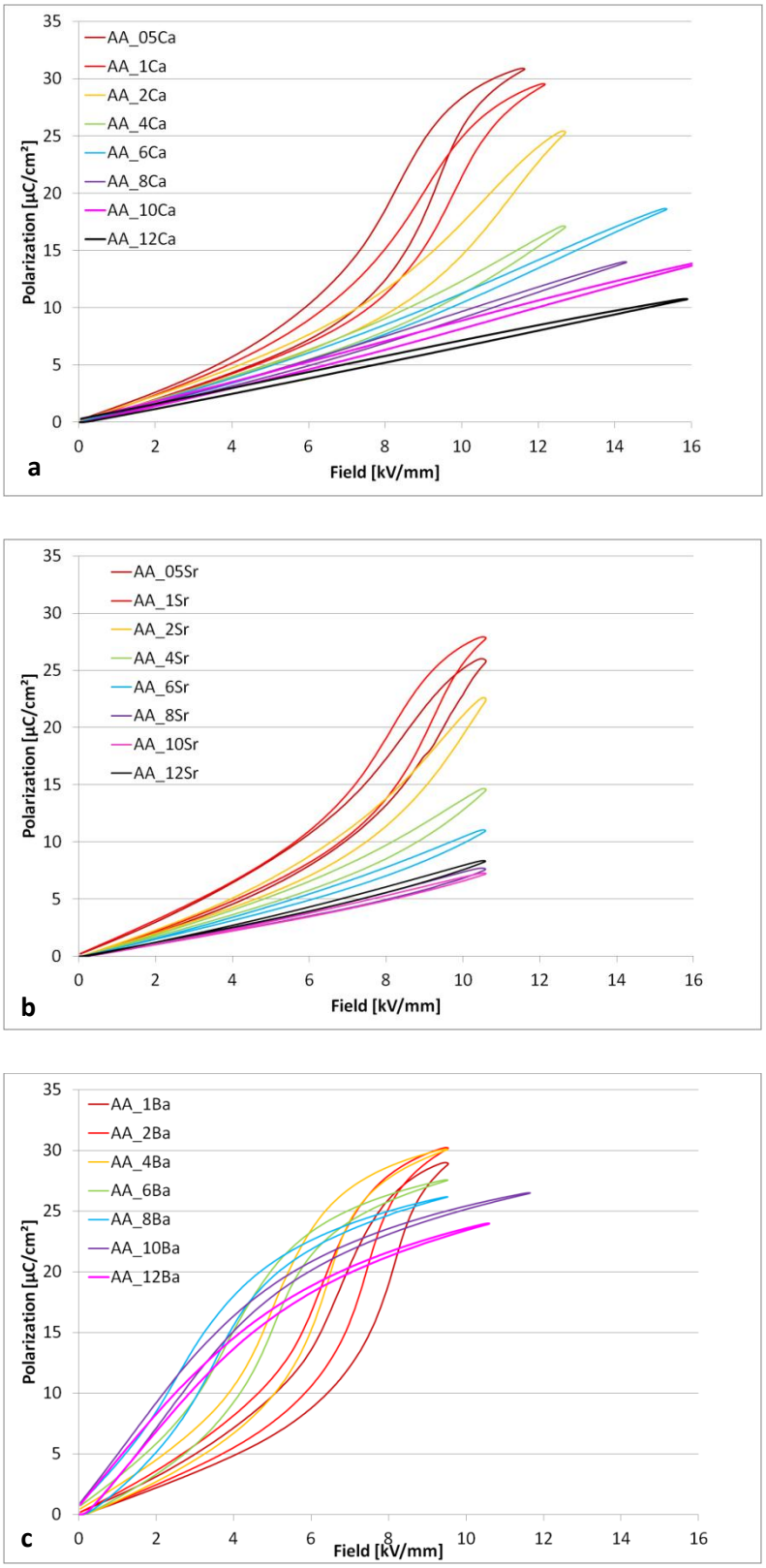

Figure 7.3-16: Unipolar polarization curves of earth alkaline substitution in PLZT AA ($Pb_{0.91}La_{0.06}Zr_{0.9}Ti_{0.1}O_3$) (a: Calcium substitution, b: Strontium-substitution, c: Barium-substitution).

The illustration of the unipolar curves of Calcium and Strontium-substitution in BB samples is depicted in Figure 7.3-17a and b. Comparing the effects of these two substituents on the hysteresis, at first glance both changed the shape of the curves in a similar way. The slope declined and approached the x-axis with further substitution of the earth alkaline ions. Moreover a decrease of the maximum value, the saturation polarization, was observed. But regarding the scale, the curves of the compositions with Calcium reached higher fields and higher values in polarization.

Combining this with the information gained of the system AA, Calcium increased the range of antiferroelectric state over field in a higher extent as Strontium did.

The polarization curves of Barium-substitution in samples are plotted in Figure 7.3-17c. In that case, the bipolar measurement was chosen due to the ferroelectric behaviour of the samples. It can easily be seen that with increasing content of substituent the shape of the curves varied. At low content of Barium the hysteresis curves showed a constriction near the origin of the axis. By further substitution of Lead with Barium the curve extended and obtained the highest coercive field. Then with higher molar ratio the curves slimmed to the smallest width and the slope flattened. At the substitution of 4 mol% of Lead with Barium the most enlarged area of the hysteresis curve of all curves was attained. Overall the maximum decreased with the content of substituent.

The structural conversion to rhombohedral structure appeared at the substitution of 6 mol% of Lead with Barium. The correlating hysteresis curve was ferroelectric with a very slim hysteresis.

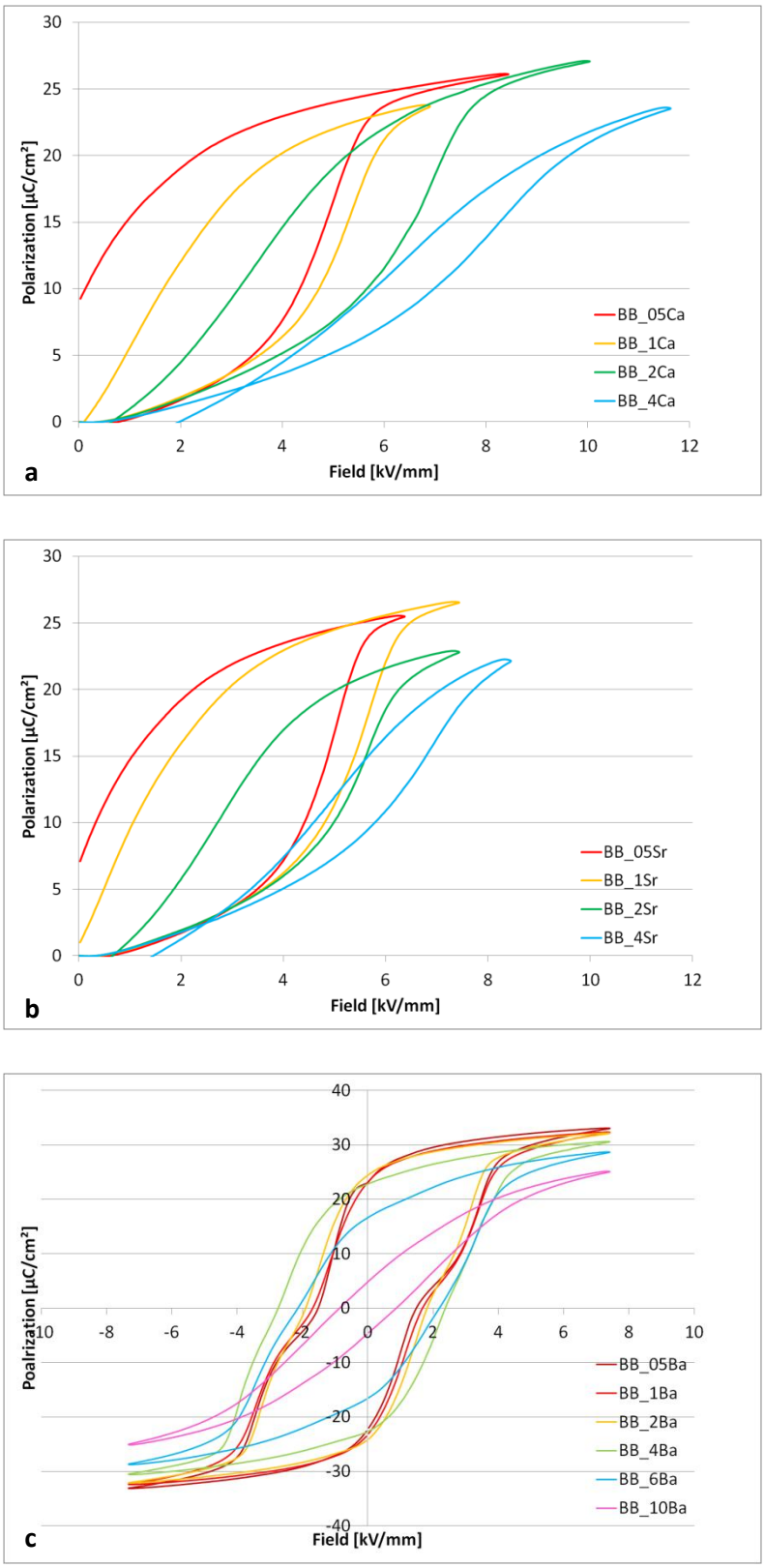

Figure 7.3-17: Unipolar polarization curves of Calcium-substitution and Strontium-substitution in PLZT BB ($Pb_{0.91}La_{0.06}Zr_{0.85}Ti_{0.15}O_3$) and bipolar polarization curves of Barium-substitution in PLZT BB ($Pb_{0.91}La_{0.06}Zr_{0.85}Ti_{0.15}O_3$).

7.3.4 Summary

Earth alkaline ions, Calcium, Strontium and Barium, which are isovalent to Lead give the opportunity to examine the difference of the substituents only considering size and weight without changing vacancy concentration. The influence of these substituents in the PLZT system on the structure and dielectric properties were examined and will now be briefly summarized:

As the diffraction pattern revealed, the incorporation of the added ions was successful. Only in the case of the substitution of Lead with Strontium in the AA system secondary phases could be observed. According to the ionic radii, the cell volume predictably decreased with the substitution of Lead with Calcium and Strontium and increased in the case of Barium. Not only the lattice parameters were affected by the substitution. The substitution of Barium induced a rhombohedral structure at concentrations lower than 10 mol%. The same happened with the substitution of Lead with Calcium in the system BB. Considering this, the orthorhombic structure is favoured by the Zirconium-richer composition.

Furthermore, the structural change depends not only on the size of the substituent but also on covalency or ionicity of the bonding of A-O and B-O. A complex intervening and influencing relationship of these effects determines the symmetry.

The dielectric response of the compositions with earth alkaline ions revealed the importance of the radius on the temperature T_m and the relative permittivity. Although it is a complex systematic which is not understood by now, the data obtained can be summarized as following: The substitution with smaller and lighter ions, like Calcium and Strontium, decreased relative permittivity and reduced the transition temperature, whereas the substitution with Barium, a lighter ion which exceeds the size of Lead, induced a decrease in peak temperature but an increase in relative permittivity.

Consulting the polarization curves, again Calcium and Strontium assembled in their impact. Saturation polarization was decreased, while the switching fields were increased by increasing the molar content of these substituents. In the case of Calcium, the effect of the structural change to rhombohedral symmetry on the polarization curves could not be examined due to low break down fields. Substitution with Barium, on the other hand, shifted the transition of antiferroelectric to ferroelectric transition to lower fields. Furthermore the phase transition due to the increasing Barium content changed the shape of the hysteresis curves.

Overall, substitution of Lead with Calcium and Strontium can be assigned to stabilize antiferroelectric state, whereas with Barium it is suppressed and a ferroelectric relaxor is formed. In the case of isovalent substituents not only relative permittivity but also the transition temperature changed according to the ionic size. Due to an interaction of various effects, a structural change to a more ordered symmetry was obtained by a bigger ion as well as with a smaller one.

7.4 B-site substitution

In this chapter the influence of a substitution on the B-site in the PLZT-system is examined. As before, the starting materials AA and BB were used and were modified according to the formula:

$$Pb_{1-1,5a-b}La_a M^x_b VPb''_{0,5a}Zr_{1-x-y}Ti_xSn_yO_3.$$

The value of Lanthanum was set to 6 mol%, therefore the compositions possessed all 3 mol% of Lead vacancies. Isovalent Tin substituted Zirconium at the B-site. The content of Titanium varied between the composition AA and BB by 5 mol%.

In literature, Tin is associated with a stabilization effect of the antiferroelectric phase in PLZT[111].

This being apparent by higher switching fields[122] and a decrease of the saturation polarization resulting in low hysteretic loss[123].

A possible explanation might lie in the fully occupied d-shell of Tin resulting in a steric hindrance of the orbitals with lower energy. In contrast, Titanium and Zirconium have no electron located in the d-shell and the accessible 3d-orbitals can hybridize with the oxygen 2p-orbitals which stabilizes the ferroelectric state[72].

In this study, the effects of a d^{10}-ion replacing a d^0-ion on the dielectric and structural properties were examined by keeping the content of Titanium constant and sequentially substituting Zirconium with Tin.

7.4.1 XRD Characterization

Consulting Table 7.4-1, Tin as a substituent of Zirconium possesses an atomic weight which is one third higher than that of Zirconium and an ionic radius which is with 0.69 Å about 5% smaller than 0.72 Å, the ionic radius of Zirconium. This gives a good explanation of the reduction in cell volume with increasing level of substitution.

As the reflection patterns in Figure 7.4-1 and Figure 7.4-2 display, the incorporation of the Tin ion at the B-site of the perovskite lattice was achieved without formation of secondary phases. Comparing the decrease of the lattice in the AA and BB system, the reduction of the volume occurred in the same extent over the compositional range.

To determine the lattice parameters and the cell volume, Rietveld refinement was performed using reference reflection patterns of a structure Pba2 as all the compositions, where Zirconium was substituted with Tin, exhibited an orthorhombic structure.

Table 7.4-1: Comparison in charge, atomic weight and radius of the alkaline ions used to build the perovskite structure.

	Pb	La	Zr	Ti	Sn
Charge	+2	+3	+4	+4	+4
Atomic weight	207.2	138.9	91.22	47.87	118.71
Radius [XII]	1.49	1.36			0.69
Radius [VI]			0.72	0.605	0.69

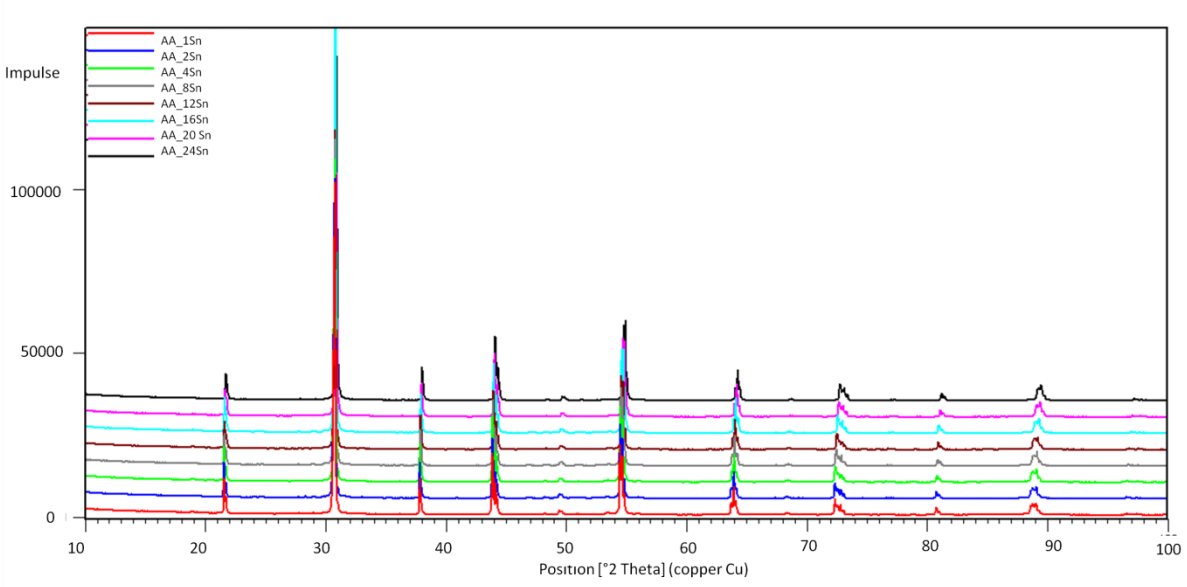

Figure 7.4-1: XRD of sintered powder of Tin-substitution in PLZT (AA = $Pb_{0.91}La_{0.06}Zr_{0.9}Ti_{0.1}O_3$).

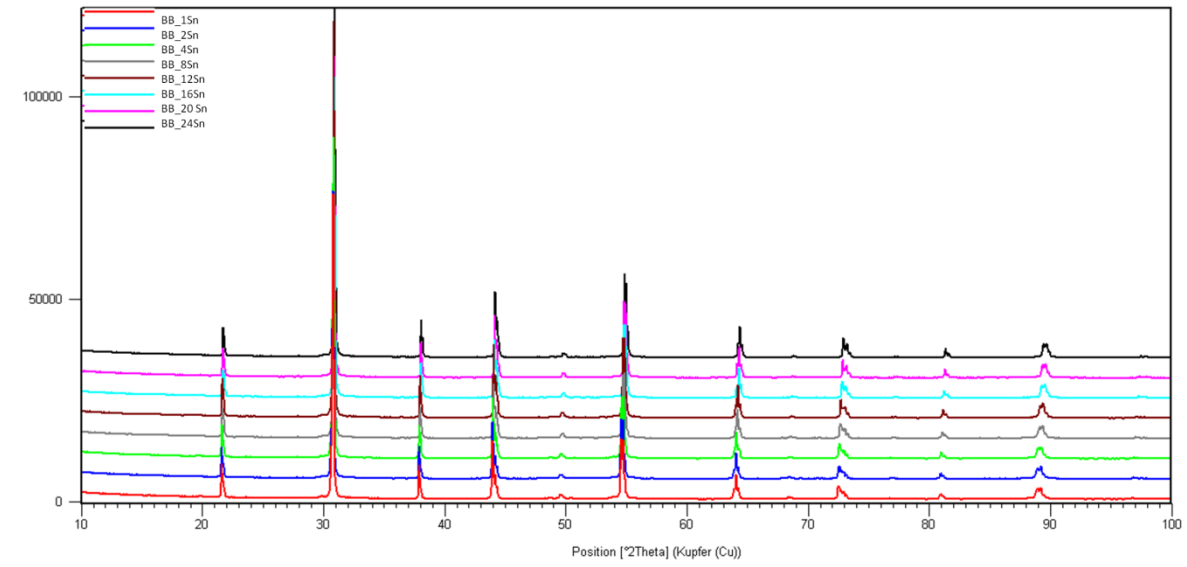

Figure 7.4-2: XRD of sintered powder of Tin-substitution in PLZT (BB = $Pb_{0.91}La_{0.06}Zr_{0.85}Ti_{0.15}O_3$).

The theoretical density decreased with substitution of Lead with Tin into the AA system from ~7.9 g/cm³ to ~7.5 g/cm³, while the Archimedes´ density increased leading to high relative densities.

Regarding the changes in the BB series, a similar decrease in theoretical density occurred by replacing Zirconium with Tin. Simultaneously, Archimedes´ density increased and relative density increased and

actually exceeded 100% (Table 7.4-2 and Table 7.4-3). That indicates that the structural model for the calculation of the theoretical density may not be adequate.

Table 7.4-2: List of the cell parameters, the cell volume and the densities of Tin-substitution in PLZT AA.

sample	c [Å]	b [Å]	a [Å]	c/a	cell volume [Å³]	theoretical density [g/cm³]	Archimedes´ density [g/cm³]	relative density [%]
AA_1Sn	8.2087	11.6908	5.8404	1.4055	560.4817	7.89	7.63	96.73
AA_2Sn	8.2067	11.6865	5.8382	1.4057	559.9351	7.88	7.70	97.80
AA_4Sn	8.2056	11.6842	5.8371	1.4058	559.6346	7.84	7.77	99.12
AA_8Sn	8.2009	11.6729	5.8318	1.4062	558.2724	7.77	7.84	100.94
AA_12Sn	8.1986	11.6681	5.8292	1.4065	557.6289	7.74	7.78	100.63
AA_16Sn	8.1917	11.6534	5.8220	1.4070	555.7768	7.63	7.88	103.29
AA_20CaSn	8.1874	11.6453	5.8177	1.4073	554.6879	7.56	7.94	105.00
AA_24CaSn	8.1835	11.6362	5.8130	1.4078	553.5386	7.49	8.01	106.99

Table 7.4-3: List of the cell parameters, the cell volume and the densities of Tin-substitution in PLZT BB.

sample	c [Å]	b [Å]	a [Å]	c/a	cell volume [Å³]	theoretical density [g/cm³]	Archimedes´ density [g/cm³]	relative density [%]
BB_1Sn	8.19887	11.6692	5.8285	1.4067	557.6324	7.83	7.62	97.37
BB_2Sn	8.19746	11.6654	5.8268	1.4069	557.1924	7.82	7.67	98.18
BB_4Sn	8.19539	11.6598	5.8247	1.4070	556.5850	7.78	7.69	98.84
BB_8Sn	8.1915	11.6499	5.8202	1.4074	555.4238	7.71	7.76	100.68
BB_12Sn	8.1857	11.6374	5.8149	1.4077	553.9276	7.64	7.81	102.15
BB_16Sn	8.18148	11.6267	5.8099	1.4082	552.6586	7.57	7.81	103.14
BB_20Sn	8.17633	11.6158	5.8049	1.4085	551.3217	7.50	7.86	104.82
BB_24Sn	8.17103	11.6051	5.7999	1.4088	549.9800	7.43	7.88	106.02

7.4.2 Dielectric Characterization

The variation of the low signal values by increasing the insertion of Tin replacing Zirconium are presented in Table 7.4-4 and Table 7.4-5. A decrease in capacitance and relative permittivity occurred with increasing level of substitution. In the AA system the values shifted from ~460 pF to 420 pF and from ~625 to ~560 in relative permittivity. The loss factor changed from 0.0081 to 0.0058 over the same compositional range. Considering the influences of the Tin-substitution in the BB composition, the values of the capacitance and the relative permittivity declined in a higher extent by the same addition of Tin. Speaking in figures, the relative permittivity decreased from ~1220 to ~1000, whereas the value of the loss factor was almost divided by two - from 0.0204 to 0.0110.

Table 7.4-4: Results of low signal dielectric measurements of Tin-substitution in PLZT AA.

sample	capacitance [nF]	loss factor []	relative permittivity []
AA_1Sn	0.4639	0.0081	626
AA_2Sn	0.4664	0.0080	623
AA_4Sn	0.4709	0.0080	627
AA_8Sn	0.4534	0.0065	605
AA_12Sn	0.4372	0.0070	578
AA_16Sn	0.4485	0.0063	595
AA_20Sn	0.4377	0.0057	566
AA_24Sn	0.4192	0.0058	560

Table 7.4-5: Results of low signal dielectric measurements of Tin-substitution in PLZT BB.

sample	capacitance [nF]	loss factor []	relative permittivity []
BB_1Sn	0.9216	0.0204	1220
BB_2Sn	0.9236	0.0207	1250
BB_4Sn	0.9028	0.0202	1239
BB_8Sn	0.8797	0.0196	1193
BB_12Sn	0.8610	0.0177	1139
BB_16Sn	0.8009	0.0169	1070
BB_20Sn	0.7831	0.0123	1055
BB_24Sn	0.7287	0.0110	1005

In Figure 7.4-3 the dielectric response versus temperature in dependence of the level of substitution for the series with Tin is presented. All curves were recorded at 1MHz. The summarized values of maximum permittivity and temperature of maximum permittivity can be found in Table 7.4-6.

Going from Figure 7.4-3a to Figure 7.4-3b, the effect of doping with Tin in the AA system and BB system can be made obvious. Replacing Zirconium with Tin, a gradually decrease of the height of the curves was visible in both cases. Furthermore the position of the peak of the curves is continuously shifted to lower values of the temperature by increasing the Tin content.

Consulting Table 7.4-6, the data extracted of the curves of samples with Tin-substitution are listed. The temperature shifts of the transition temperature over the whole compositional range were in both systems about 40 °C. In the case of the substitution with Tin in the Zirconium-richer composition AA, the temperature moved from ~180 °C to ~135 °C, whereas in the Titanium-richer composition BB a change from ~160 °C to ~120 °C occurred. Comparing this to the pure AA and BB composition, the substitution with Tin decreased the temperature of the maximum permittivity continuously from the starting point of 180 ° in the former and from 155 °C in the later case.

The same is true regarding the height of the maximum of the curves. The values of maximum permittivity decreased gradually from that of the pure compositions. In the case of AA, relative permittivity decreased from ~1480 to ~950. In the case of BB, on the other hand, the relative permittivity was divided by two by increasing the content of substituent from 1 mol% to 24 mol%.

Overall, a decrease in transition temperature and a decrease in relative permittivity is caused by substituting Zirconium with Tin.

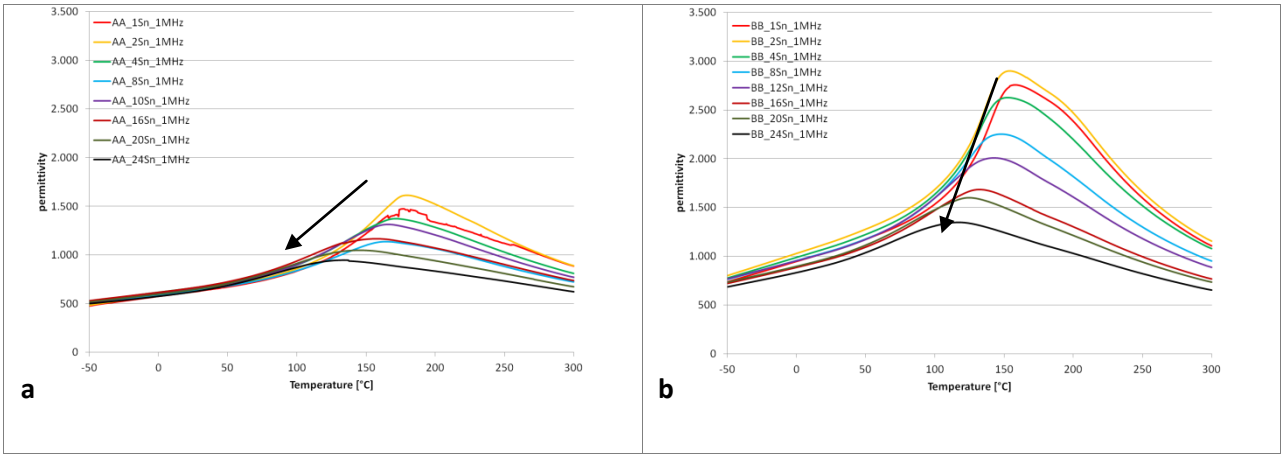

Figure 7.4-3: Results of the relative permittivity versus temperature curves of Tin- substitution in PLZT AA and BB.

Table 7.4-6: Results of the relative permittivity versus temperature curves of Tin substitution in PLZT AA and BB.

sample	maximum in relative permittivity	Temperature Tm [°C]	sample	maximum in relative permittivity	Temperature Tm [°C]
AA_1Sn	1476	177	BB_1Sn	2755	158
AA_2Sn	1614	180	BB_2Sn	2901	155
AA_4Sn	1371	173	BB_4Sn	2626	153
AA_8Sn	1137	165	BB_8Sn	2252	149
AA_12Sn	1315	166	BB_12Sn	2008	143
AA_16Sn	1168	158	BB_16Sn	1684	133
AA_20Sn	1048	146	BB_20Sn	1601	125
AA_24Sn	946	134	BB_24Sn	1348	117

In Figure 7.4-4 two selected curves of relative permittivity recorded at various frequencies are plotted. In Figure 7.4-4a, a curve out of the AA series is depicted. Only one peak in the relative permittivity curves was visible. With increasing frequency, the height of the peaks declined but did not shift in position.

At the right side in Figure 7.4-4b, the curves of sample BB-2Sn are presented.

Overall, no frequency dependence was observed in the samples containing Tin.

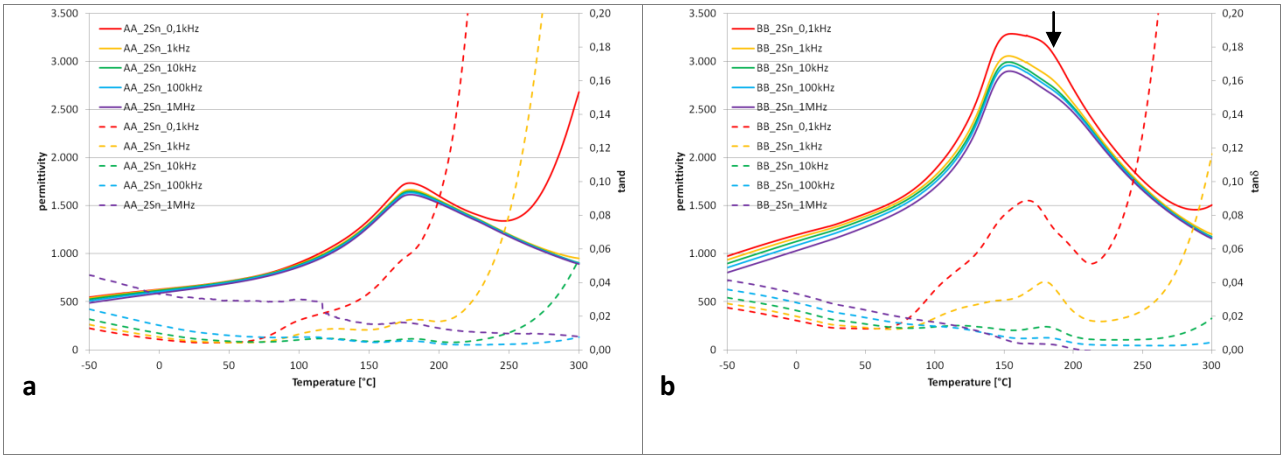

Figure 7.4-4:Frequency dependency of relative permittivity (solid line) and loss factor (dashed line) curves of selected Tin-substitution in PLZT (measured at 0,1 kHz, 1 kHz, 10 kHz, 100 kHz and 1 MHz). Anomaly is accentuated by an arrow.

Regarding the polarization curves in Figure 7.4-5a and b, no saturation in the samples with higher Zirconium-content could be reached. Therefore only the samples of the series BB can be considered discussing the influence of the substituent. With increasing Tin-content the curves slimmed, flattened and decreased in maximum. Furthermore the curves were shifted to higher switching fields with increasing ratio of substitution. This means, that substitution with Tin on B-site causes an increase in switching fields, a decrease of the saturation polarization and a reduction of the area of the hysteresis curves.

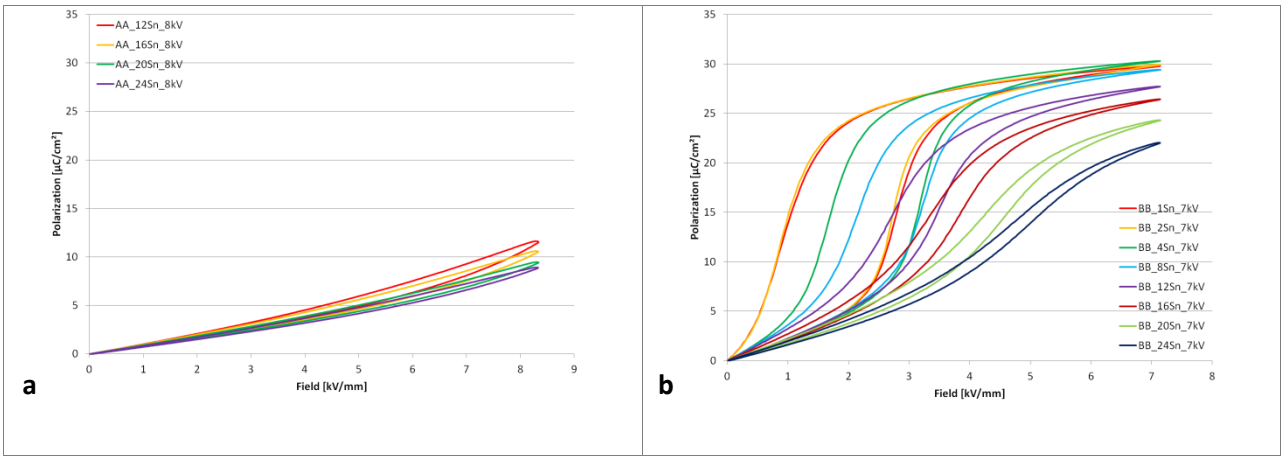

Figure 7.4-5: Unipolar Polarization curves of Tin-substitution in PLZT samples AA and BB.

7.4.3 Summary

In this chapter the effect of the substitution of Zirconium with Tin on the structural and electric properties was investigated.

All prepared compositions showed a single perovskite phase without secondary phases and possessed orthorhombic structure. The orthorhombic Lanthanum doped Lead Zirconate-Lead Titanate system is structurally more stable to substitution on B-site than on A-site.

Regarding the dielectric response, a flattening and broadening of the relative permittivity curve over temperature occurred with increasing Tin-content indicating increasingly diffuser phase transitions. Furthermore, the phase transition was shifted to lower temperature. Considering the frequency dependence, no relaxor-like behaviour could be detected.

With the substitution of Zirconium with Tin a decrease of saturation polarization, an increase of the switching fields and a reduction of the hysteretic loss occurred.

Substitution of Lead with Strontium and substitution of Zirconium with Tin in PLZT lead to a stabilization of the antiferroelectric phase. Comparing the results of the polarization measurements with those of the substitution of Lead with Strontium in PLZT, the switching fields increased, the saturation polarization decreased and the hysteresis slimmed by increasing the content of Tin but not in that extent.

This leads to the assumption that the substitution of the A-site cation reveals bigger impacts on the hysteresis curve compared with the substitution of the B-site cation.

7.5 Complex Doping

In previous chapters the substitution in PLZT was investigated by solely inserting one substituent. In this chapter combinations of two ions are examined regarding the structural and dielectric properties.

7.5.1 Isovalent substitution-pair on A-site – Barium-Calcium

In this chapter the substitution of Lead with a 1:1 ratio of Barium and Calcium in the PLZT system is presented. As shown in Table 7.5-1 the ionic radius of Calcium and Barium is 1.34 Å and 1.61 Å, respectively. This results in a mean radius of 1.48 Å of the combination, which is close to that of Lead with 1.49 Å. According to the formula

$$Pb_{0,91-b}La^{\circ}_{0,06}M^{x}_{b}V_{Pb}{}''_{0,03}(Zr_{1-x}Ti_{x})O_{3}$$

, the earth alkaline combination (M) possesses the same valency as Lead and therefore the Lead vacancies were determined by the content of Lanthanum. This value was set to 6 mol% and therefore the amount of Lead vacancies remained at the constant value of 3 mol%.

In this study, two PLZT compositions with a Zirconium to Titanium ratio 90 to 10 and 85 to 15 were prepared. These were called in the next section AA and BB, respectively.

Table 7.5-1: Comparison in charge, atomic weight and radius of the alkaline ions used to build the perovskite structure.

	Pb	La	Ca	Ba	Zr	Ti
Charge	+2	+3	+2	+2	+4	+4
Atomic weight	207.2	138.9	40.078	137.327	91.22	47.87
Radius [XII]	**1.49**	1.36	**1.34**	**1.61**		
Radius [VI]					0.72	0.605

7.5.1.1 XRD Characterization:

In Figure 7.5-1 the XRD spectra of the Barium-Calcium co-substitution in PLZT samples with the composition AA are shown. In the spectra of the sample with the lowest amount of Barium-Calcium, additional reflection pattern emerged. These referred to Zirconium dioxide indicating an A-site deficience due to Lead loss which could not be detected in the samples with higher concentration of the substituents. Solely the reflection patterns of the perovskite structure remained which proved an incorporation of the ions in the lattice.

The XRD spectra of the BB series are plotted in Figure 7.5-2. No secondary phases could be detected and the substitution can be assumed as complete. A detailed view of the reflection pattern in Figure 6.5-3 revealed a change of the shape with increasing content of substituents.

This indicates a phase transition from the orthorhombic to the rhombohedral structure. Although the ionic size of the substitution-pair averages in a radius slightly lower than that of Lead, a structural change occurred by inserting these ions in the lattice.

As discussed in a previous chapter (chapter 6.3), structural changes with substitution occur due to an interaction of various effects. In the case of a bigger ion, as Barium, the ion-ion repulsion increases and therefore a less distorted system is favoured[66]. On the other hand, a smaller ion promotes a tilting of the structure[30],[63]. At a certain point, the nature of the bondings changes with inserting a smaller substituent and encourages a less distorted structure[66],[67].

In this study, Rietveld refinement of the structure of the spectra was performed with an orthorhombic reference pattern with the symmetry Pba2 and a rhombohedral reference pattern with the symmetry R3cH. The results of the refinement for the compositions AA and BB are listed in Table 7.5-2 and Table 7.5-3.

Interestingly, the average radius of the ionic substituents could not prevail the presence of orthorhombic structure. Only in the Zirconium-richer compostion the rhombohedral structure was hindered. This indicates a complex dependency of structural influences induced by different substituents.

By substitution with Barium-Calcium the cell volume decreased. This is in good accordance to the slightly lower mean radius of the substitution-pair compared to Lead.

With the structural change in the BB series also the cell volume changed due to a different orientation and symmetry. After the conversion the cell volume reduced with further increase from 10 mol% Barium-Calcium to 12 mol% molar ratio.

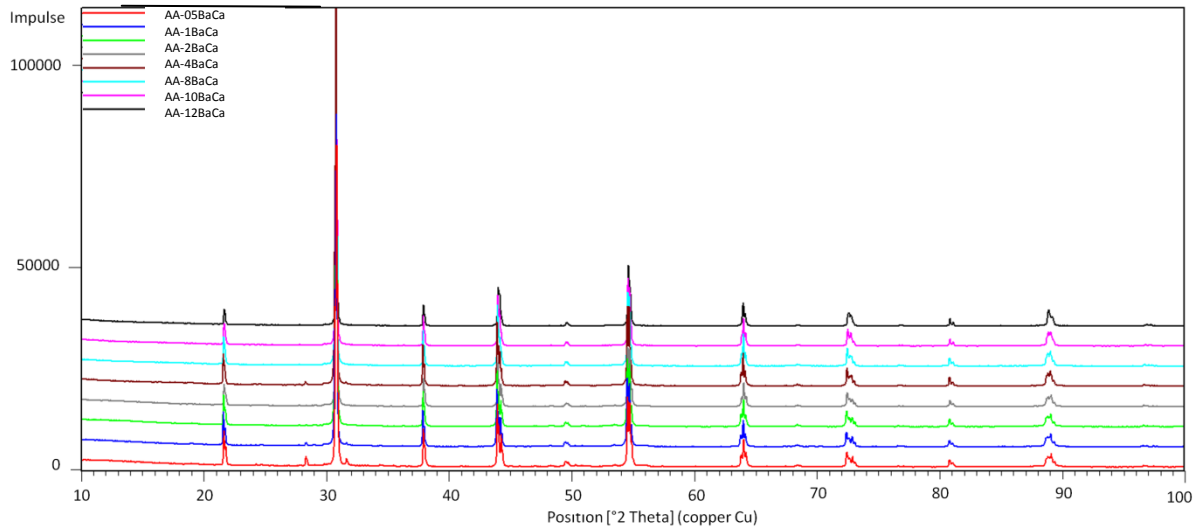

Figure 7.5-1: XRD of sintered powder of Barium-Calcium co-substitution in PLZT (AA = $Pb_{0.91}La_{0.06}Zr_{0.9}Ti_{0.1}O_3$).

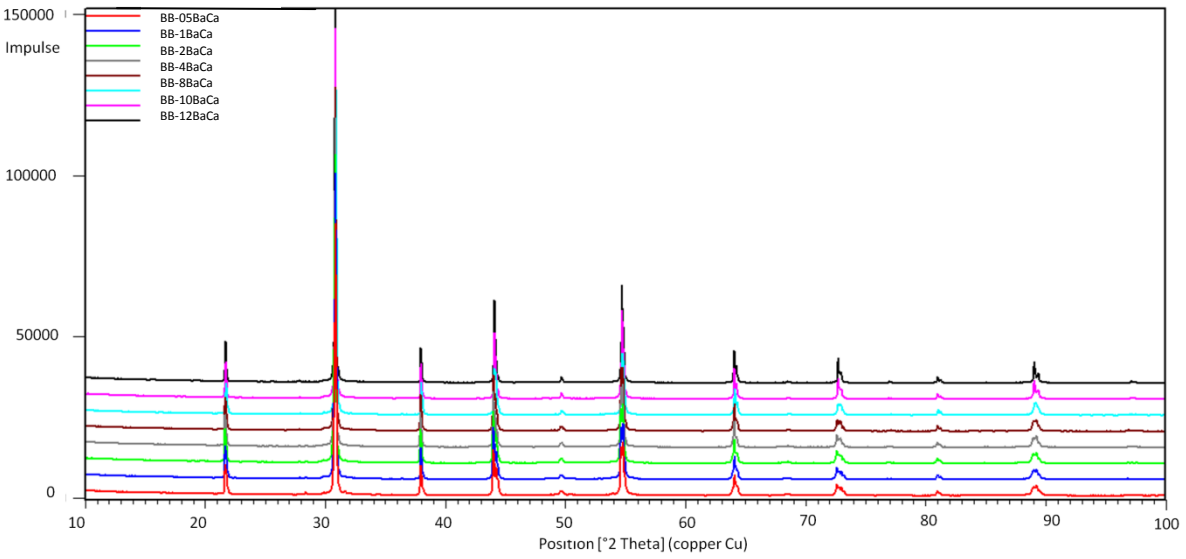

Figure 7.5-2: XRD of sintered powder of Barium-Calcium co-substitution in PLZT (BB = $Pb_{0.91}La_{0.06}Zr_{0.85}Ti_{0.15}O_3$).

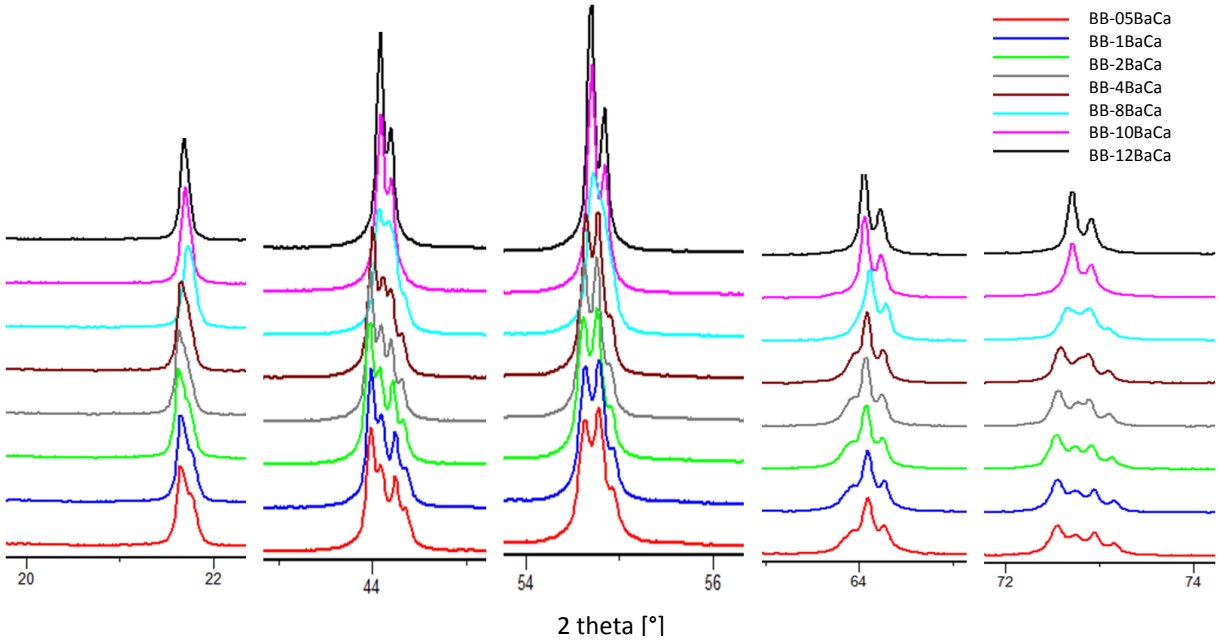

Figure 7.5-3: Detailed view of the vanishing of reflection pattern by increasing the content of Barium-Calcium substitution-pair in the composition BB ($Pb_{0.91}La_{0.06}Zr_{0.85}Ti_{0.15}O_3$).

Sintering the samples lead to a relative density of above 97% for all samples, which indicated a good densification. The relative density even increased with increasing content of the substitution-pair. This means that the samples grew more compact by the substitution of Lead with Barium and Calcium.

Theoretical density decreased in the AA system by increasing the content of substituents from 7.78 g/cm³ to 7.28 g/cm³. The values of the Archimedes density decreased with higher amount of earth alkaline ions but the relative densities increased from 97.5 to 101 % by substituting 12 mol% of Lead with Barium-Calcium. Exceeding 100% of the relative density indicates that relative density calculated from XRD data might be underestimated since no secondary phase was detected (Table 7.5-2).

Considering Table 7.5-3, a comparable effect occurred with the substitution of Lead with Barium-Calcium in the system BB. The theoretical density decreased totally from 7.83 g/cm³ to 7.33 g/cm³. This was a decline in the same amount as in the case of the series AA. The Archimedes´ density also lowered like the theoretical density but not in that extent. Therefore the relative density increased with the substitution of 12 mol% of Lead with the substitution-pair exceeding 100%. Exceeding 100% of the relative density indicates that relative density calculated from XRD data might be underestimated since no secondary phase was detected by XRD.

Table 7.5-2: List of the cell parameters, the cell volume and the densities of Barium-Calcium co- doped PLZT AA.

sample	c [Å]	b [Å]	a [Å]	c/a	cell volume [Å³]	theoretical density [g/cm³]	Archimedes´ density [g/cm³]	relative density [%]
AA_05BaCa	8.2122	11.6928	5.8413	1.4059	560.9036	7.78	7.59	97.53
AA_1BaCa	8.2121	11.6931	5.8413	1.4059	560.9138	7.76	7.64	98.43
AA_2BaCa	8.2130	11.6926	5.8410	1.4061	560.9160	7.72	7.61	98.58
AA_4BaCa	8.2151	11.6906	5.8399	1.4067	560.8636	7.63	7.56	99.02
AA_6BaCa	8.2158	11.6817	5.8360	1.4078	560.1064	7.55	7.52	99.54
AA_8BaCa	8.2192	11.6823	5.8362	1.4083	560.3867	7.46	7.50	100.56
AA_10BaCa	8.2222	11.6772	5.8333	1.4095	560.0629	7.37	7.42	100.66
AA_12BaCa	8.2320	11.6715	5.8301	1.4120	560.1507	7.28	7.36	101.01

Table 7.5-3: List of the cell parameters, the cell volume and the densities of Barium-Calcium co- doped PLZT BB.

sample	c [Å]	b [Å]	a [Å]	c/a	cell volume [Å³]	theoretical density [g/cm³]	Archimedes´ density [g/cm³]	relative density [%]
BB_05BaCa	8.2008	11.6699	5.8290	1.4069	557.8480	7.83	7.62	97.36
BB_1BaCa	8.2015	11.6701	5.8290	1.4070	557.9052	7.80	7.64	97.90
BB_2BaCa	8.2014	11.6666	5.8276	1.4073	557.6011	7.76	7.61	98.02
BB_4BaCa	8.2039	11.6626	5.8263	1.4081	557.4551	7.68	7.51	97.83
BB_6BaCa	8.2062	11.6607	5.8256	1.4086	557.4503	7.59	7.53	99.25
BB_8BaCa	8.2135	11.6566	5.8224	1.4107	557.4368	7.50	7.47	99.62
BB_10BaCa	14.2498	5.8197	5.8197	2.4486	417.9637	7.41	7.40	99.85
BB_12BaCa	14.2542	5.8169	5.8169	2.4505	417.6980	7.33	7.36	100.46

7.5.1.2 Microstructure:

SEM images revealed a nearly homogeneous composition for the samples with co-substitution (Figure 7.5-5). With increasing content of the substituents an increased appearance of precipitates could be observed. The composition of these phases, which were situated between the grain boundaries, could be identified as Lead Zirconate-Lead Titanate compounds. With further substitution additionally, Lead-Zirconate compounds appeared. In the microstructure, pores which inhibited a higher relative density could be detected.

A homogeneous grain growth was illustrated by the channelling contrast mode: Smaller grains are next to bigger grains (Figure 7.5-4).

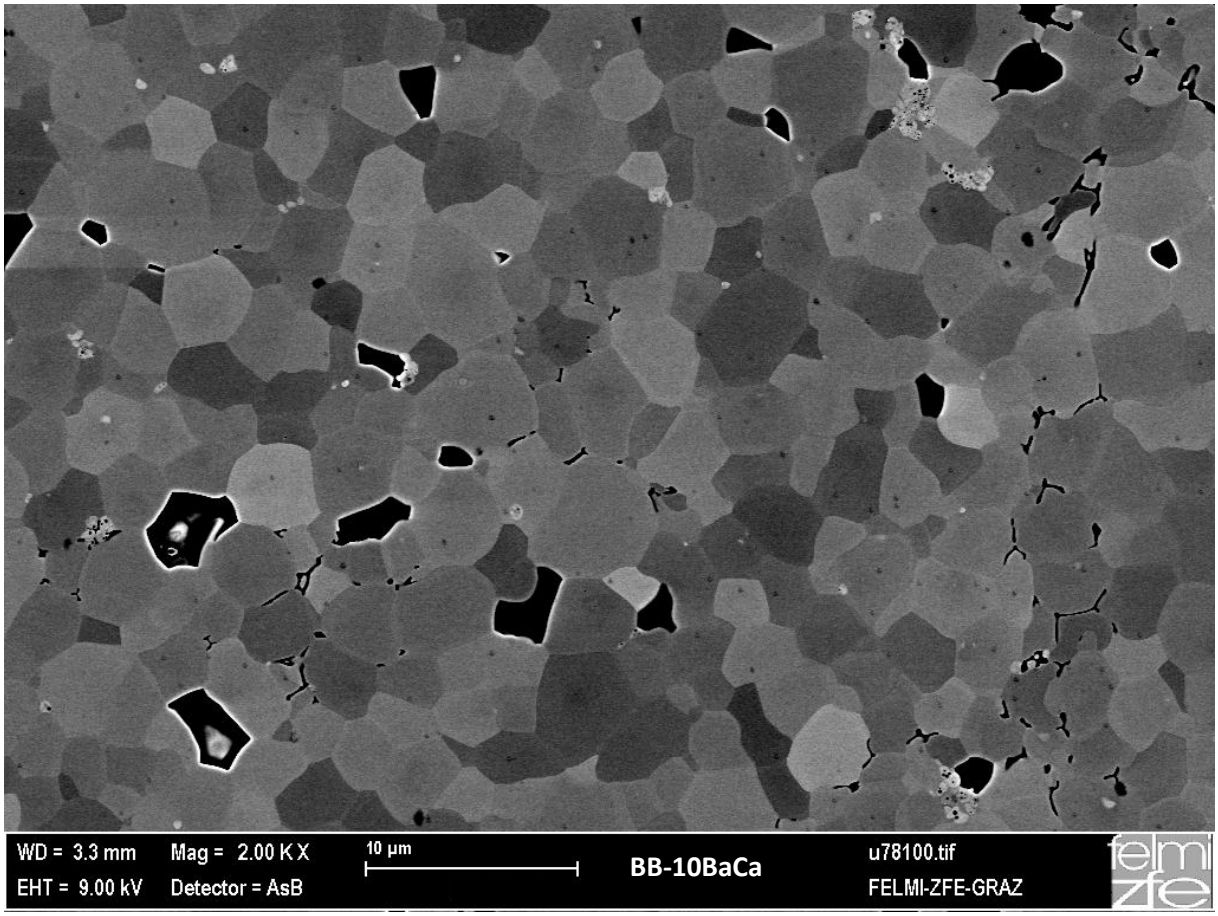

Figure 7.5-4: Backscattered SEM channelling contrast mode image of sample BB-10BaCa.

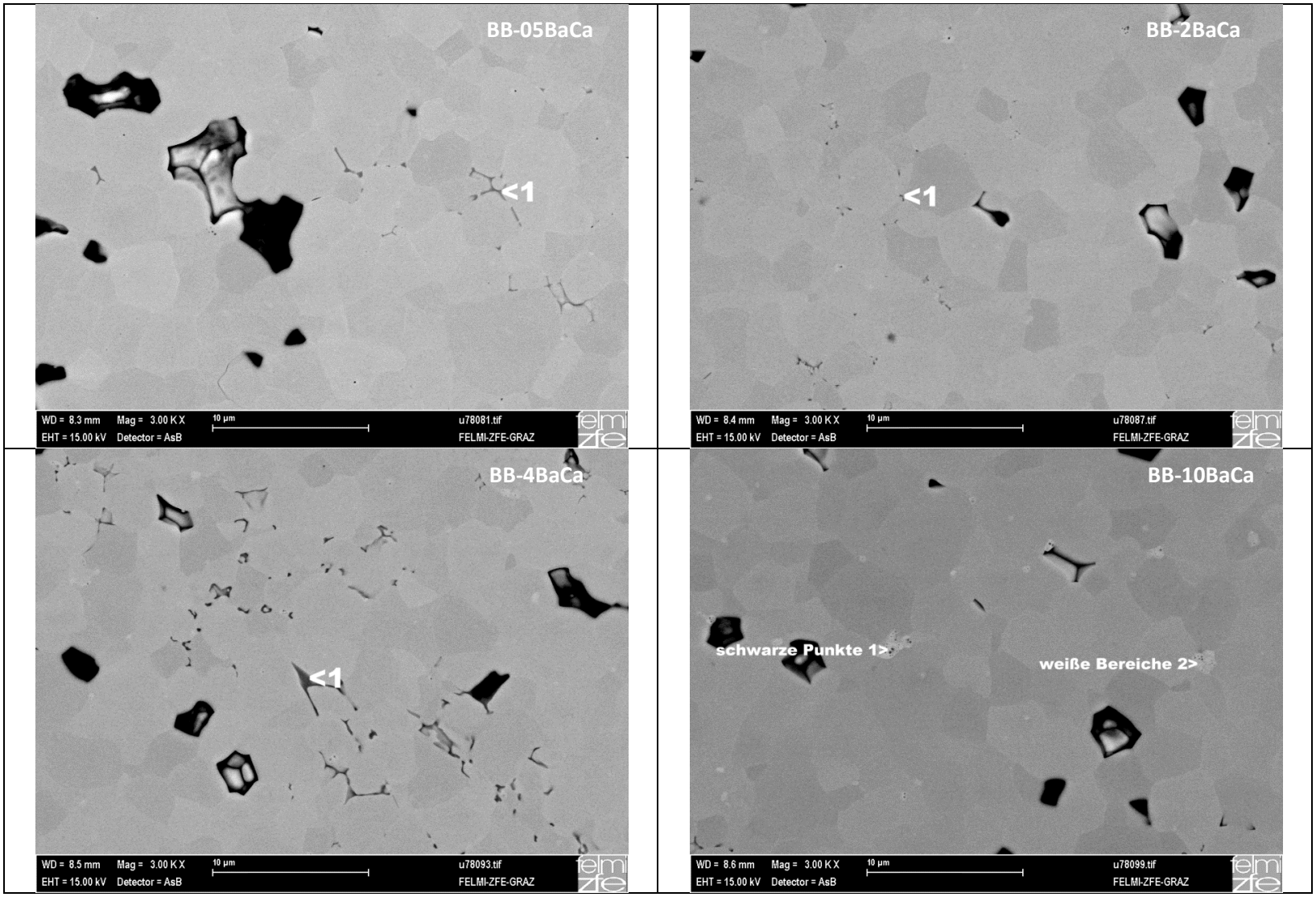

Figure 7.5-5: Backscattered SEM images of Barium-Calium co-substitution in PLZT samples BB ($Pb_{0.91}La_{0.06}Zr_{0.85}Ti_{0.15}O_3$). The compositional range varies from 0.5 mol% to 10 mol%. Secondary phases are highlighted with arrows and numbers. 1 refers to a PZT compound and 2 to a $PbZrO_3$ compound.

7.5.1.3 Dielectric Characterization

Capacitance and loss factor were measured with all samples and relative permittivity was calculated. The results can be found in Table 7.5-4 and Table 7.5-5.

In the composition AA, the co-substitution with Barium and Calcium induced a decrease in capacitance from ~455 pF to ~550 pF and in relative permittivity from ~590 to 785. Besides, the value of the loss factor lowered with increasing concentration of the substitution-pair. But two outliers were recognized. The sample AA-0.5BaCa and AA-12BaCa showed a little higher loss factors. The capacitance and the relative permittivity increased with increasing content of the substitution-pair.

In Table 7.5-5 the data of the low signal measurements of the BB compositions are listed. Capacitance and relative permittivity increased with increasing content of Barium and Calcium. The values shifted from ~870 pF to ~1130 pF capacitance and from ~1160 to 1550 relative permittivity by substituting 10 mol% of Lead with the substitution-pair. Then with further 2 mol% of substitution a drop occurred to ~1040 pF capacitance and ~1430 relative permittivity. The loss factor decreased until the molar ratio of 6 mol% of Barium-Calcium, with further increasing the content it increased again.

Table 7.5-4: Results of low signal dielectric measurements of Barium-Calcium co-substitution in PLZT AA.

sample	capacitance [nF]	loss factor []	relative permittivity []
AA_05BaCa	0.4559	0.0457	588
AA_1BaCa	0.4821	0.0159	619
AA_2BaCa	0.4832	0.0128	637
AA_4BaCa	0.4857	0.0082	644
AA_6BaCa	0.4422	0.0110	607
AA_8BaCa	0.5169	0.0046	704
AA_10BaCa	0.5434	0.0052	753
AA_12BaCa	0.5527	0.0497	785

Table 7.5-5: Results of low signal dielectric measurements of Barium-Calcium co-substitution in PLZT AA.

sample	capacitance [nF]	loss factor []	relative permittivity []
BB_05BaCa	0.8716	0.0290	1164
BB_1BaCa	0.9192	0.0236	1194
BB_2BaCa	0.9139	0.0208	1194
BB_4BaCa	0.9303	0.0189	1199
BB_6BaCa	0.9370	0.0158	1242
BB_8BaCa	1.0457	0.0171	1389
BB_10BaCa	1.1290	0.0211	1554
BB_12BaCa	1.0420	0.0452	1433

In Figure 7.5-6 and Figure 7.5-7 relative permittivity curves versus temperature of the Barium-Calcium co-substitution in PLZT samples AA and BB are plotted while the arrows indicate the decrease in the peaks with increasing concentration. Comparing both figures, the different behaviour is apparent: On the left side (Figure 7.5-6), the curves are more flat than on the right side and the peaks do not evolve as obviously as in the right figure (Figure 7.5-7). In both systems the substitution with Barium-Calcium induced a broadening of the peak resulting in a more diffuse phase transition.

In Table 7.5-6 the peak temperatures and the values of maximum in relative permittivity are presented. A continuously decrease in the system AA from ~1200 to ~980 with the substitution of 12 mol% of Lead with Barium-Calcium was detected. An exceptional behaviour in the line showed the sample AA-8BaCa which had a slightly higher relative permittivity of ~1170.

Comparing these values with those of the series BB, the drop in relative permittivity was higher and happened from ~2670 to ~1620 which was nearly five times larger than in the series AA.

A larger impact on the temperature could be obtained by the substitution of Lead with Barium-Calcium in the series AA. A shift from 207 to 90 °C arose which was nearly 40 °C larger than that from 161 to 85 °C in the case of the series BB.

Overall the substitution-pair led to a suppression of the peak. The influence of the substitution-pair on the dielectric response was higher in the case of the Titanium-richer composition (BB), but the impact of that on temperature was larger in the Zirconium-richer composition (AA).

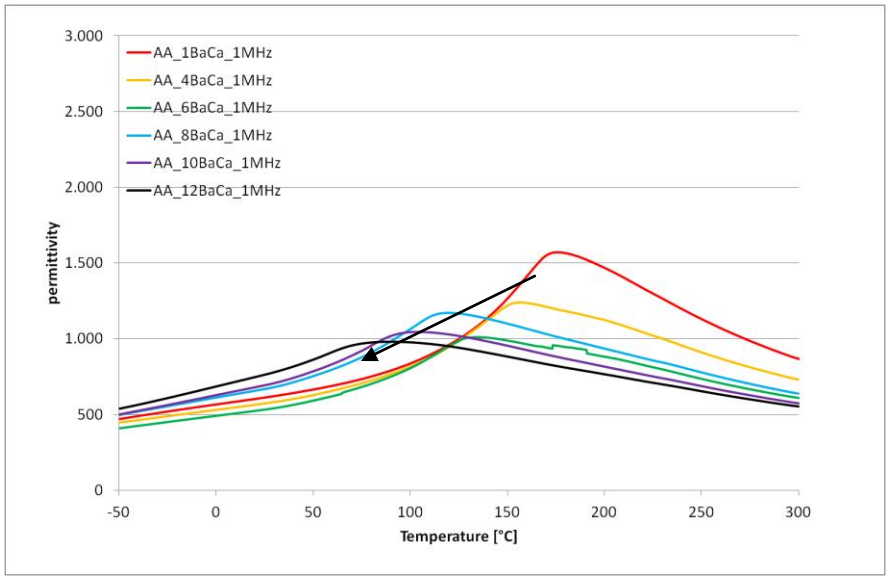

Figure 7.5-6: Relative permittivity measurements versus temperature of Barium-Calcium co-substitution in PLZT AA ($Pb_{0.91}La_{0.06}Zr_{0.9}Ti_{0.1}O_3$) at 1 MHz.

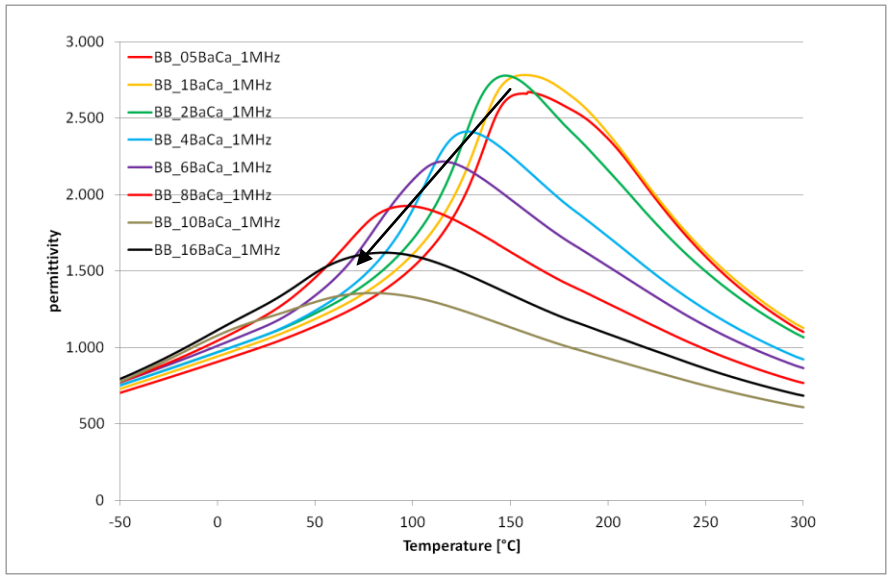

Figure 7.5-7: Relative permittivity measurements versus temperature of Barium-Calcium co-substitution in PLZT BB ($Pb_{0.91}La_{0.06}Zr_{0.85}Ti_{0.15}O_3$) at 1 MHz.

Table 7.5-6: Results of the relative permittivity versus temperature curves of Barium-Calcium co-substitution in PLZT AA and BB.

sample	maximum in relative permittivity	Temperature Tm [°C]		sample	maximum in relative permittivity	Temperature Tm [°C]
AA_05BaCa	1210	207		BB_05BaCa	2670	161
AA_1BaCa	1570	177		BB_1BaCa	2780	158
AA_2BaCa	1140	195		BB_2BaCa	2780	150
AA_4BaCa	1240	158		BB_4BaCa	2410	129
AA_6BaCa	1010	135		BB_6BaCa	2210	116
AA_8BaCa	1170	121		BB_8BaCa	1920	97
AA_10BaCa	1040	105		BB_10BaCa	1360	79
AA_12BaCa	980	90		BB_12BaCa	1620	85

Relative permittivity versus temperature curves were recorded at various frequencies to check for relaxor properties. In Figure 7.5-8a to f selected samples of relative permittivity and loss factor curves are depicted. At low concentration of Barium-Calcium substitution-pair no frequency dependence was observed for the temperature corresponding to the maximum value of the relative permittivity T_m within the investigated frequency range. Thus no evidence of relaxor-like dielectric response characteristics was observed in the series AA and BB with low content of Barium-Calcium.

The height of the peak decreased slightly with increasing frequency, but the appearance of the curve did not change. Some peculiarities occurred at 0.1 kHz: The curves of the samples BB-1BaCa, AA-4BaCa, BB-4BaCa and BB-10BaCa revealed a second peak. All additional steps appeared at higher temperature except in the case of BB-10BaCa. This composition possessed rhombohedral structure at room temperature. Regarding the graph, this temperature lies in between the two humps recorded. Furthermore the addition of 10 mol% of Barium-Calcium revealed frequency dependency. This indicates relaxor behaviour. In the case of solely adding Barium into PLZT, frequency dependency could be detected in the sample AA-10Ba. The relaxor behaviour depends on the Barium addition.

The loss factor curves showed similar peak temperatures as the relative permittivity curves.

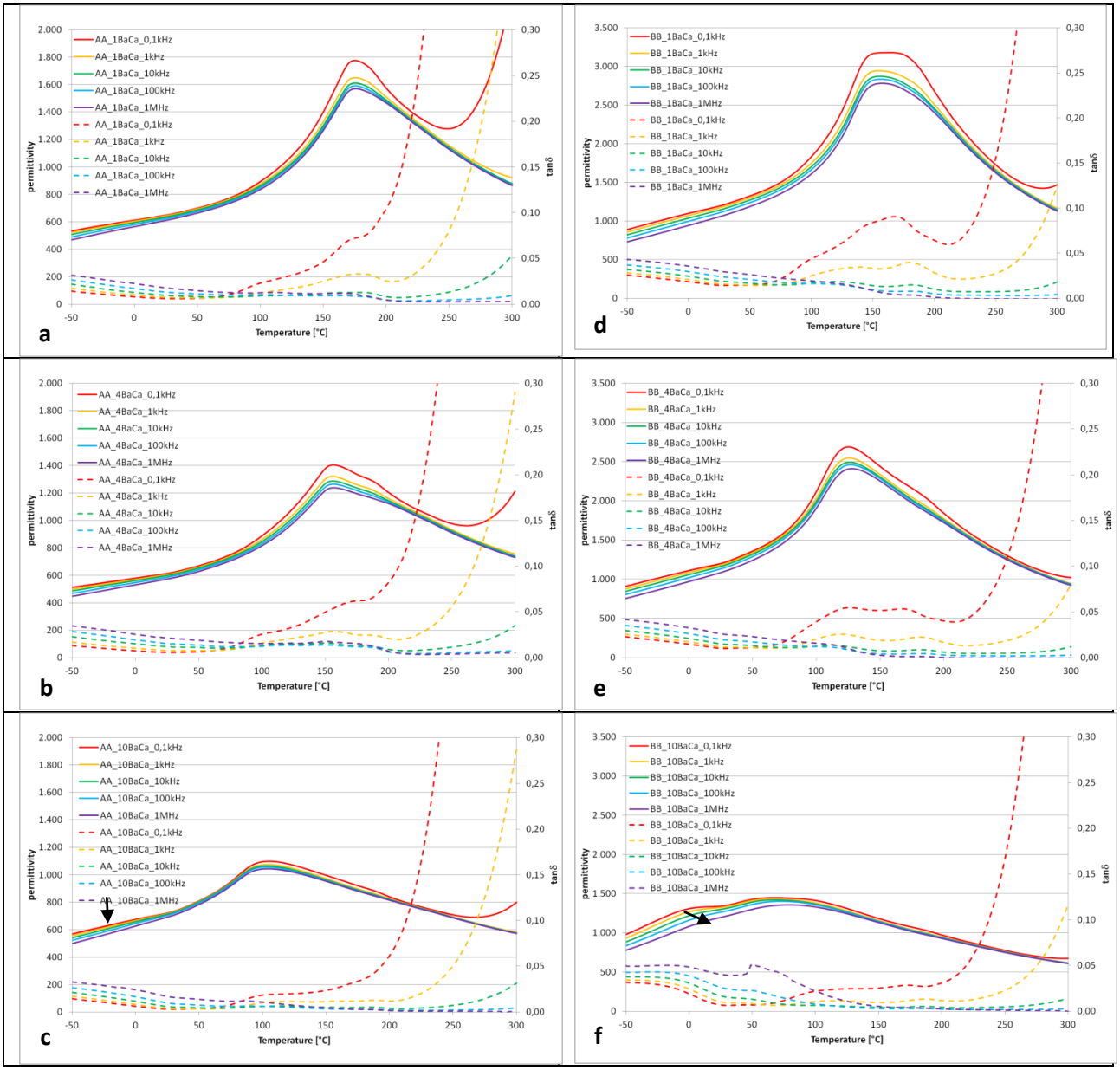

Figure 7.5-8: Frequency dependency of relative permittivity (solid line) and loss factor (dashed line) curves of selected Barium-Calcium co-substitution in PLZT AA (a-c) and BB (d-f) (measured at 0,1 kHz, 1 kHz, 10 kHz, 100 kHz and 1 MHz). Anomalies are accentuated by arrows.

Figure 7.5-9 displays the polarization curves of Barium-Calcium co-substitution in PLZT AA. None of them reached saturation and therefore the characteristics of the hysteresis curves could not be detected. The breakdown voltage was too low to gain fully evolved double-loops. A further discussion is excluded.

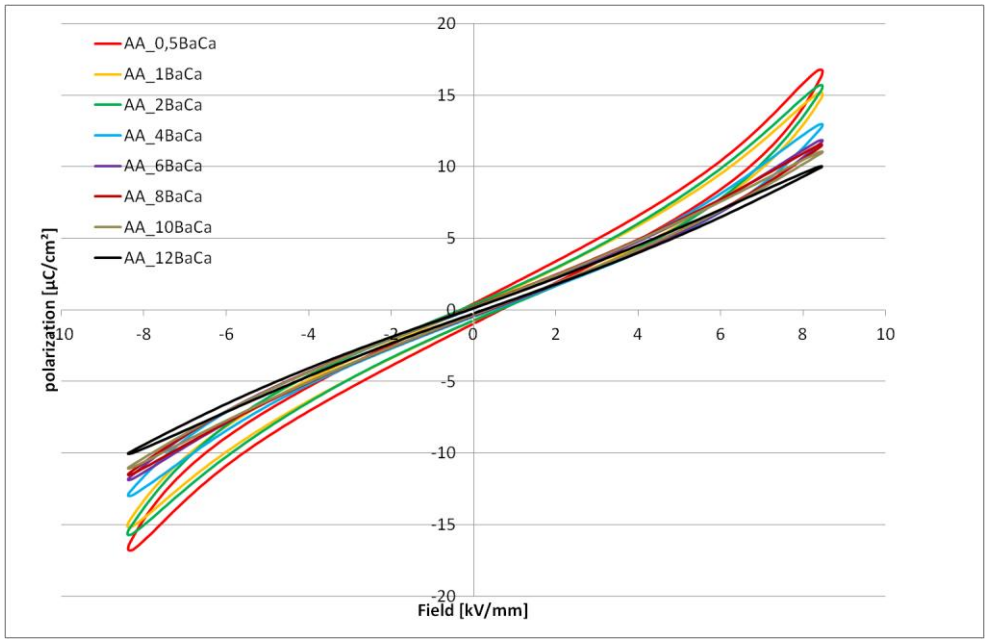

Figure 7.5-9: Polarization curves of Barium-Calcium co-substitution in PLZT AA ($Pb_{0.91}La_{0.06}Zr_{0.9}Ti_{0.1}O_3$).

Polarization curves of the system BB with co-substitution with Barium-Calcium are shown in Figure 7.5-10. The shape of the curves changed with increasing content of the substitution-pair. The largest area of the hysteresis curves could be found with the substitution of 0.5 mol% of Lead with Barium and Calcium. It seemed as tough, a combination or coexisting of various effects came into play resulting in a `triple hysteresis curve´. Following the insertion of the substitution-pair, a slimming of the curve and decreasing of the slope and of the maximum appeared. Not all curves reached saturation and therefore these cannot be considered in the following interpretation. As mentioned above the area of the hysteresis loops was reduced by co-substitution with Barium and Calcium. Hence all characteristic values of a polarization curve were lowered: The saturation polarization, the remnant polarization as well as the coercive field decreased. Solely the switching fields were enhanced.

In Figure 7.5-11, the impact on the hysteresis curves by Barium, Calcium and the combination of those are compared. With the substitution-pair of Barium and Calcium the effects seemed to be coupled: The result of this association in the PLZT system exhibits high saturation polarization like the substitution with Barium did combined with low remnant polarization like the substitution with Calcium. Furthermore, the derived curve showed an additional slimming.

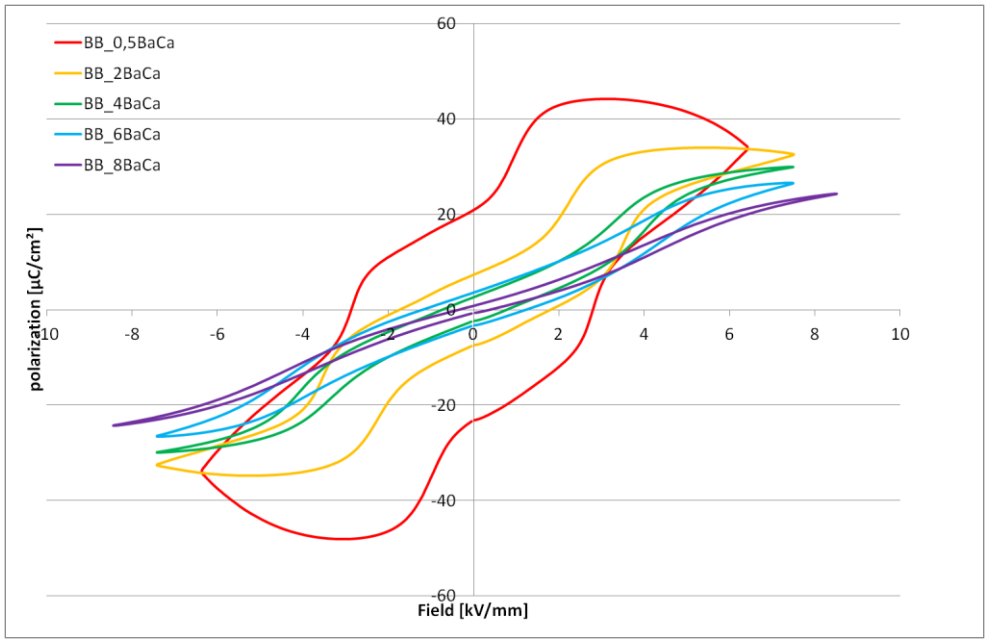

Figure 7.5-10: Polarization curves of Barium-Calcium co-substitution in PLZT BB ($Pb_{0.91}La_{0.06}Zr_{0.85}Ti_{0.15}O_3$).

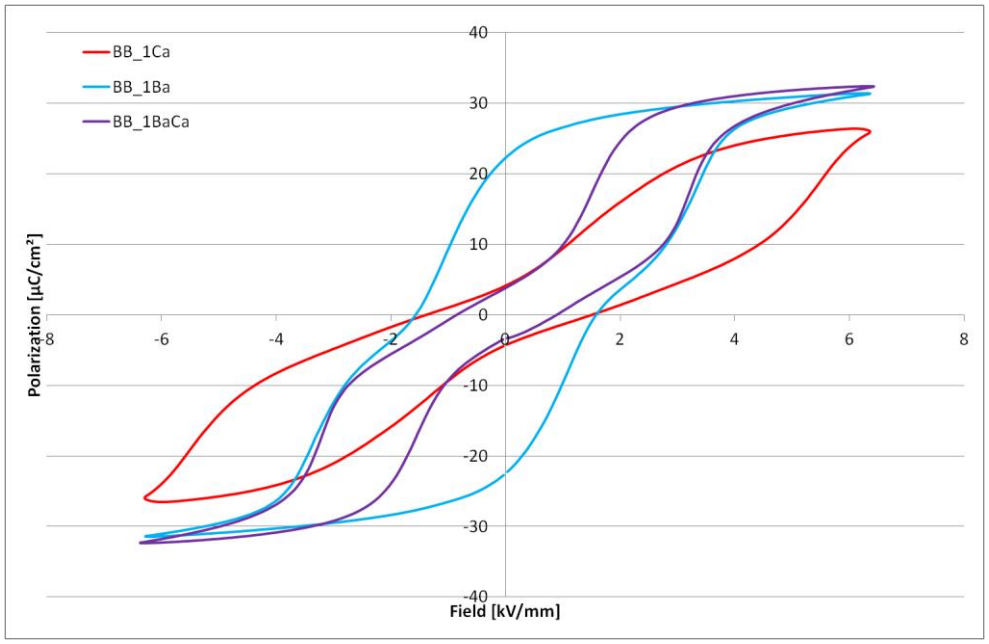

Figure 7.5-11: Comparison of polarization curves of substitution with Calcium, with Barium and Barium-Calcium co-substitution in PLZT samples BB.

7.5.1.4 Summary

In a previous chapter the separate influences of Barium and Calcium on the characteristics of the systems AA and BB were investigated, while in that section the co-substitution was examined. Now, all the gained information shall be combined.

The substitution-pair, Barium and Calcium, incorporated well in the PLZT solid solution with only small amounts of secondary phases. Due to the fact that the mean radius of the one to one combina-

tion of these ions is slightly smaller than that of Lead, a slight reduction of the cell volume was detected.

Regarding the structure of the system, all the starting compositions possessed an orthorhombic structure. Due to the substitution with Barium the ordering of the lattice changed to rhombohedral as well as with the substitution with Calcium. By inserting the substitution-pair, this rhombohedral conversion was also observed with higher concentration of the substitution pair. It can be concluded that this change was induced by both ions separately and only occurred in the Titanium-richer composition BB.

Surprisingly, not the mean ionic radii of the substitution-pair which was slightly smaller than that of Lead could determine the structure. Comparing the results to those of the substitution with Strontium (r=1.44 Å) no change to the rhombohedral structure was observed. In the case of the substitution of Lead with a bigger and a smaller ion an interaction of impacts, the structural change at higher concentration is not completely understood by now.

In the case of the dielectric response, the separate effects of the both substituents balanced and resulted in a combination of both. Considering the relative permittivity, the values of the low signal enlarged highly by the substitution with Barium while they decreased slightly with the substitution with Calcium. In sum, the combination of these two ions increased in a minor extent compared to the separate addition of Barium.

The temperature dependent measurements of the relative permittivity revealed a decrease in the transition temperature within both series. Interestingly, the deviation of the transition temperature due to the substitution of Lead depends on the ionic radius of the substituent. In the case of Calcium, a smaller ion compared to Lead, the transition temperature decreased with increasing concentration, whereas with Barium, which exceeded Lead in size, the opposed behaviour was detected. The substitution-pair which has an average radius close to that of Lead, did not induce a shift in transition temperature.

A similar behaviour could be detected regarding the deviation of the maximum of the relative permittivity by increasing the molar ratio of the substitution-pair: The high increase in the maximum of relative permittivity caused by the substitution of Lead with Barium was suppressed by the co-substitution with Calcium. As the substitution of Lead with Calcium showed a continuously decrease of the maximum of relative permittivity, the combination of Barium with Calcium as substitution-pair of Lead resulted in a slight increase of the maximum of relative permittivity.

Consulting the polarization curves, the changes due to the co-substitution of Barium and Calcium can be declared as an interaction of the effects of the single ions. A smaller ionic size at A-site increases the stability range of the antiferroelectric phase, whereas the bigger ion reduces it. The combination of a bigger and a smaller ion resulting in an ionic size slightly smaller than Lead induces an increase of the switching fields and a slimming of the hysteresis curve reducing the hysteretic losses.

Overall, it can be summarized, that structural changes caused by substitution cannot be simplified focussing only on the ionic radii of the ions used to build the perovskite structure. On the other hand the effect of two isovalent substituents on the dielectric characteristics of the material can be regarded as a counterbalance of the effects of the substitution with each ion on its own. However, the resulting major shifting of the switching fields and extraordinary slimming of the hysteretic curve could not be explained

7.5.2 Isovalent substitution-pair on A-site – Bismuth-Sodium

In the previous chapter complex isovalent substitution was done by two isovalent substituents, now a combination of two aliovalent ions, one monovalent and one trivalent ion, result in an isovalent substitution-pair. The effect of the donor-acceptor-pair Bismuth and Sodium on the properties of PLZT was investigated. These two substituents are placed at the A-site which should induce a more diffuse phase transition.

By the co-substitution Bismuth-Sodium in the molar ratio one to one, no vacancies are necessary for compensation:

$$Pb_{1-1,5a-1.5b-0.5c}La^{\circ}_{a}Bi^{\circ}_{b}\,Na'_{c}V''_{Pb\,0,5a+0.5b-0.5c}Zr_{0,9}Ti_{0,1}O_3.$$

In literature substitution of Lead with the substitution-pair Bismuth and Sodium was done in Lead Zirconate. This led to a decrease of the height of the relative permittivity curves versus temperature but nearly no shift in the transition temperature was found[97]. As in the previous chapters 6.1 and 6.2 it is shown that the substitution of Lead with Bismuth in PLZT induced a decrease of the phase transition and with Sodium a slight increase was observed, this might support the combination effect of two substituents at A-site on the dielectric response.

In other words, the combination of Bismuth and Sodium at the A-site of PLZT can be regarded as a solid solution of PZT and of Lanthanum-doped $Bi_{0.5}Na_{0.5}TiO_3$ - $(Bi_{0.5}Na_{0.5})_{(1-1.5x)}La_xTiO_3$ - abbreviated as BNLT. The starting compound $Bi_{0.5}Na_{0.5}TiO_3$ (BNT) is a well-known rhombohedral ferroelectric with relaxor-like behaviour exhibiting a broad phase transition[124].

By inserting Lanthanum into BNT an increase in symmetry occurs and with increasing the Lanthanum-content a cubic structure is stabilized. Furthermore, the phase transition occurs over a smaller temperature range compared to pure BNT[125] which is shifted to higher temperature. On the other hand, the value of the maximum relative permittivity decreases with increasing the Lanthanum concentration[126].

Incorporation of pure BNT in the structure of ferroelectric PZT generates a homogeneous structure with nearly no alteration in the lattice parameters, whereas the transition temperature decreases[127].

Comparing the effects of the incorporation of BNT and BNLT in ferroelectric PZT on the dielectric properties, both solid solutions cause a decrease of the remnant polarization and the coercive field resulting in a reduction of the hysteresis compared to pure PZT. Additionally, the phase transition becomes more diffuse by increasing the content of BNT and BNLT respectively[127],[128].

In this study, the effect of Sodium and Bismuth substitution in the antiferroelectric PLZT was examined. Again the two compositions AA with a molar ratio of Zirconium to Titanium 90 to 10 and BB with the ratio 85 to 15 both containing 6 mol% of Lanthanum were used as starting points.

7.5.2.1 XRD Characterization

Considering Table 7.5-7, the ionic radius of Bi^{3+} as well as of Na^{+} is smaller than that of Lead. Therefore a reduction in cell volume should be detected by introducing them into the system.

As shown in Figure 7.5-12 and Figure 7.5-13 the XRD spectra of the sintered samples shown next to the main reflection pattern of the perovskite phase several additional peaks. Their intensity increased enhanced with further increase of the content of substituents. Some peaks could be attributed to Zirconium dioxide. Additionally reflections of Bismuth-Titanate compounds emerged.

In $PbZr_{0.9}Ti_{0.1}O_3$, where Lead was substituted with Bismuth, all samples had rhombohedral structure, whereas this time all perovskite reflections could be refined by the Rietveld method using an orthorhombic reference of Pba2 symmetry. As mentioned above, the ionic size of both substituents is smaller than that of Lead and therefore the reduction in cell volume did not surprise. Partly the occurrence of secondary phases which shifts the composition to a higher Titanium content causes a decrease in the cell volume. A lower solubility of Bismuth in the Lead Zirconate-Lead Titanate system might be the reason for that[100].

Comparing Figure 7.5-12and Figure 7.5-13, the substitution of Lead with the substitution-pair in the AA system resulted in a higher reduction of the cell volume as in the BB system. The cell volume of the Zirconium-richer composition was influenced by the substitution in a higher extent as the Tita-

nium-richer composition. The explanation might lie in a better incorporation of Bismuth in the composition with less Zirconium and therefore less and lower reflections of secondary phases were observed.

Table 7.5-7: Comparison in charge, atomic weight and radius of the ions used to build the perovskite structure.

	Pb	La	Bi	Na	Zr	Ti
Charge	+2	+3	+3	+1	+4	+4
Atomic weight	207.2	138.9	208.98	22.99	91.22	47.87
Radius [XII]	1.49	1.36	1.45	1.39		
Radius [VI]					0.72	0.605

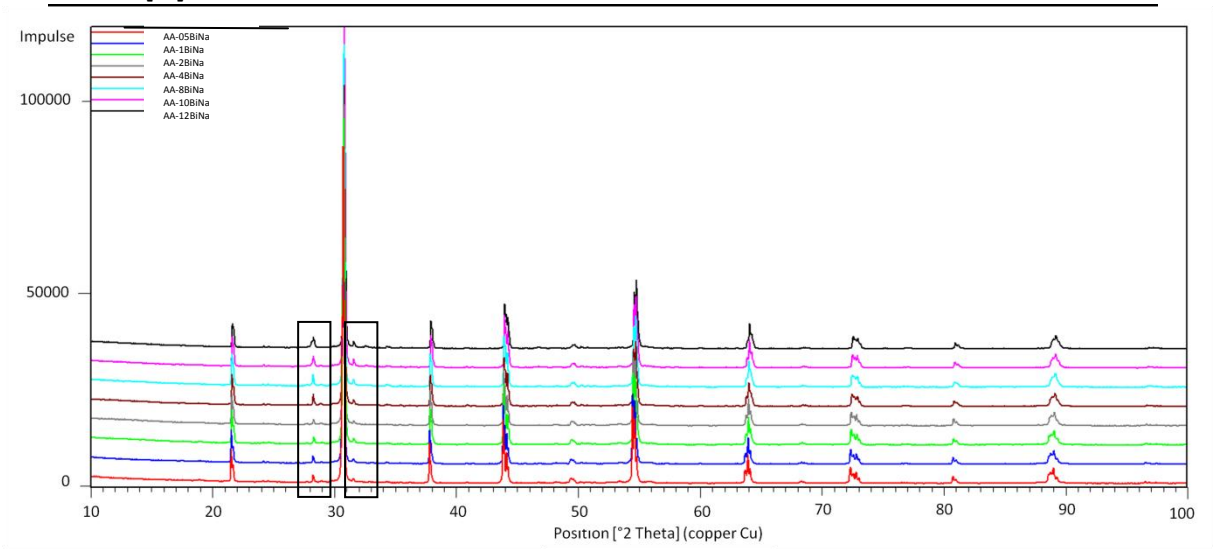

Figure 7.5-12: XRD of sintered powders of Bismuth-Sodium co-substitution in PLZT (AA = $Pb_{0.91}La_{0.06}Zr_{0.9}Ti_{0.1}O_3$). Peaks in the box indicate secondary phases of Zirconium dioxide and Bismuth-Titanate.

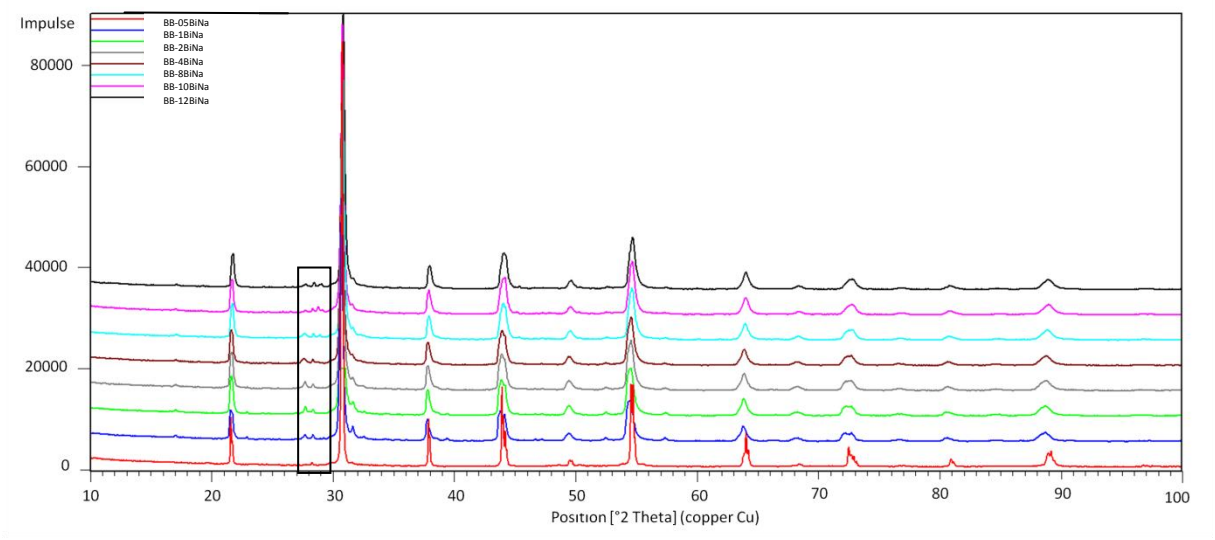

Figure 7.5-13: XRD of sintered powders of Bismuth-Sodium co-substitution in PLZT (BB = $Pb_{0.91}La_{0.06}Zr_{0.85}Ti_{0.15}O_3$). Peaks in the box indicate secondary phases of Zirconium dioxide and Bismuth-Titanate.

Concerning the substitution-pair, the effect on the theoretical densities in the system BB was slightly higher than in AA. A decrease occurred in both cases (Table 7.5-8 and Table 7.5-9).

As the theoretical density dropped in the AA system from 7.85 to 7.64 g/cm³, it decreased in the BB system from 7.84 to 7.62 g/cm³. A drop in the Archimedes´ density caused by the substitution-pair was apparent. In the case of AA it decreased by nearly 10% from 7.55 to ~7.00 g/cm³, whereas the substitution in the case of BB only shifted to ~7.30 g/cm³ from the same starting point. Thus the relative density reduced from ~96 to ~92% in the former case and did not alter in the latter one.

The highest densification of all series was achieved by the BB composition, where Lead was substituted with Bismuth and Sodium.

Table 7.5-8: List of the cell parameters, the cell volume and the densities of Bismuth-Sodium co-substitution in PLZT AA.

sample	c [Å]	b [Å]	a [Å]	c/a	cell volume [Å³]	theoretical density [g/cm³]	Archimedes´ density [g/cm³]	relative density [%]
AA_05NaBi	8.2103	11.6917	5.8412	1.4056	560.7038	7.85	7.55	96.12
AA_1NaBi	8.2117	11.6808	5.8404	1.4060	560.6834	7.84	7.57	96.61
AA_2NaBi	8.2101	11.6862	5.8379	1.4063	560.1212	7.83	7.55	96.44
AA_4NaBi	8.2085	11.6815	5.8330	1.4073	559.3081	7.79	7.56	97.00
AA_6NaBi	8.2064	11.6760	5.8294	1.4077	558.5826	7.76	7.33	94.50
AA_8NaBi	8.2064	11.6760	5.8294	1.4077	558.5626	7.72	7.18	93.07
AA_10NaBi	8.2075	11.6760	5.8313	1.4075	558.8132	7.67	6.97	90.90
AA_12NaBi	8.2051	11.6702	5.8275	1.4080	558.0196	7.64	7.00	91.67

Table 7.5-9: List of the cell parameters, the cell volume and the densities of Bismuth-Sodium co-substitution in PLZT BB.

sample	c [Å]	b [Å]	a [Å]	c/a	cell volume [Å³]	theoretical density [g/cm³]	Archimedes´ density [g/cm³]	relative density [%]
BB_05NaBi	8.19936	11.6689	5.8287	1.4067	557.6754	7.84	7.55	96.35
BB_1NaBi	8.19941	11.6680	5.8280	1.4069	557.5735	7.83	7.51	95.89
BB_2NaBi	8.19942	11.6662	5.8280	1.4069	557.4850	7.81	7.52	96.31
BB_4NaBi	8.19832	11.6623	5.8265	1.4071	557.0784	7.77	7.49	96.32
BB_6NaBi	8.19678	11.6579	5.8243	1.4073	556.5537	7.74	7.47	96.57
BB_8NaBi	8.19788	11.6573	5.8243	1.4075	556.6001	7.69	7.43	96.53
BB_10NaBi	8.19574	11.6493	5.8194	1.4084	555.6039	7.66	7.28	94.97
BB_12NaBi	8.19569	11.6507	5.8198	1.4082	555.7222	7.62	7.30	95.85

7.5.2.2 Dielectric Characterization:

Low signal values of capacitance, relative permittivity and loss factor of all samples are listed in the following tables.

Regarding the effect of Bismuth-Sodium substitution-pair on the dielectric characteristics, only small alterations took place: All parameters decreased but not in a large extent. The relative permittivity decreased from ~620 to ~465 in the case of the system AA. The loss factor fluctuated, but decreased slightly overall.

The decrease of the values in the Titanium-richer system by introducing these substituents was comparable. Relative permittivity decreased from ~980 to ~765. The loss factor behaved similar as in the case above and varied slightly with the molar ratio, but increased overall from 0.0269 to 0.0352.

Table 7.5-10: Results of low signal dielectric measurements of Bismuth-Sodium co-substitution in PLZT AA.

sample	capacitance [nF]	loss factor []	relative permittivity []
AA_05NaBi	0.6911	0.0089	619
AA_1NaBi	0.6739	0.0085	592
AA_2NaBi	0.6587	0.0178	557
AA_4NaBi	0.6520	0.0058	564
AA_6NaBi	0.6219	0.0098	539
AA_8NaBi	0.5966	0.0198	508
AA_10NaBi	0.5531	0.0140	474
AA_12NaBi	0.5296	0.0073	466

Table 7.5-11: Results of low signal dielectric measurements of Bismuth-Sodium co-substitution in PLZT BB.

sample	capacitance [nF]	loss factor []	relative permittivity []
BB_05NaBi	0.7277	0.0269	977
BB_1NaBi	0.7930	0.0252	1009
BB_2NaBi	0.7623	0.0217	964
BB_4NaBi	0.7187	0.0193	920
BB_6NaBi	0.6934	0.0134	860
BB_8NaBi	0.6756	0.0298	842
BB_10NaBi	0.5899	0.0106	737
BB_12NaBi	0.6085	0.0352	765

In Figure 7.5-14a and b the curves of relative permittivity versus temperature measured at 1 MHz are plotted for both series. Alteration in shape and height of the curves went continuously with the concentration of the substituents.

With increasing insertion of the substituents a decrease and flattening of the curves occurred. In the case of the AA system, no shift in position of the peak was apparent, while in the BB system a small deviation can be detected. Furthermore, with low content of Bismuth-Sodium in BB the shape of the curves deviated from the others. In the curves of the samples called BB-05NaBi and BB-2NaBi a shoulder at higher temperature was detected. In that case, two phase transitions emerged - the first at around 150 °C and the second at around 200 °C. The second step vanished with further increase of the content of the substitution-pair.

Consulting Table 7.5-12, the results of the relative permittivity curves of the experiments with the substitution-pair are summarized. Again the relative permittivity in the AA series was lower than in the BB series with the same modification. In the case of the AA system the values dropped from ~1670 to ~750 in relative permittivity and in the BB system from ~2070 to ~1200 in relative permittivity.

The transition temperature of the AA compositions with Bismuth-substitution did not change with the Bismuth content but stayed at around 180 °C. Compared to the pure BB composition 0.5 mol% of Bismuth increased the transition temperature of 155 °C to ~180°C. But then with proceeding substitution the values dropped to ~145 C.

Revisiting the results of the substitution solely of Bismuth or Lanthanum in PZT (chapter 6.1), a shift to lower transition temperature occurred with increasing content of substituent. Contrary, the following insertion of the substituent Sodium in PLZT (chapter 6.2) did only slightly shift the peak position of the dielectric response to higher degrees. The combination of all substituents resulted in nearly no change of the transition temperature - even at high content of the substituents.

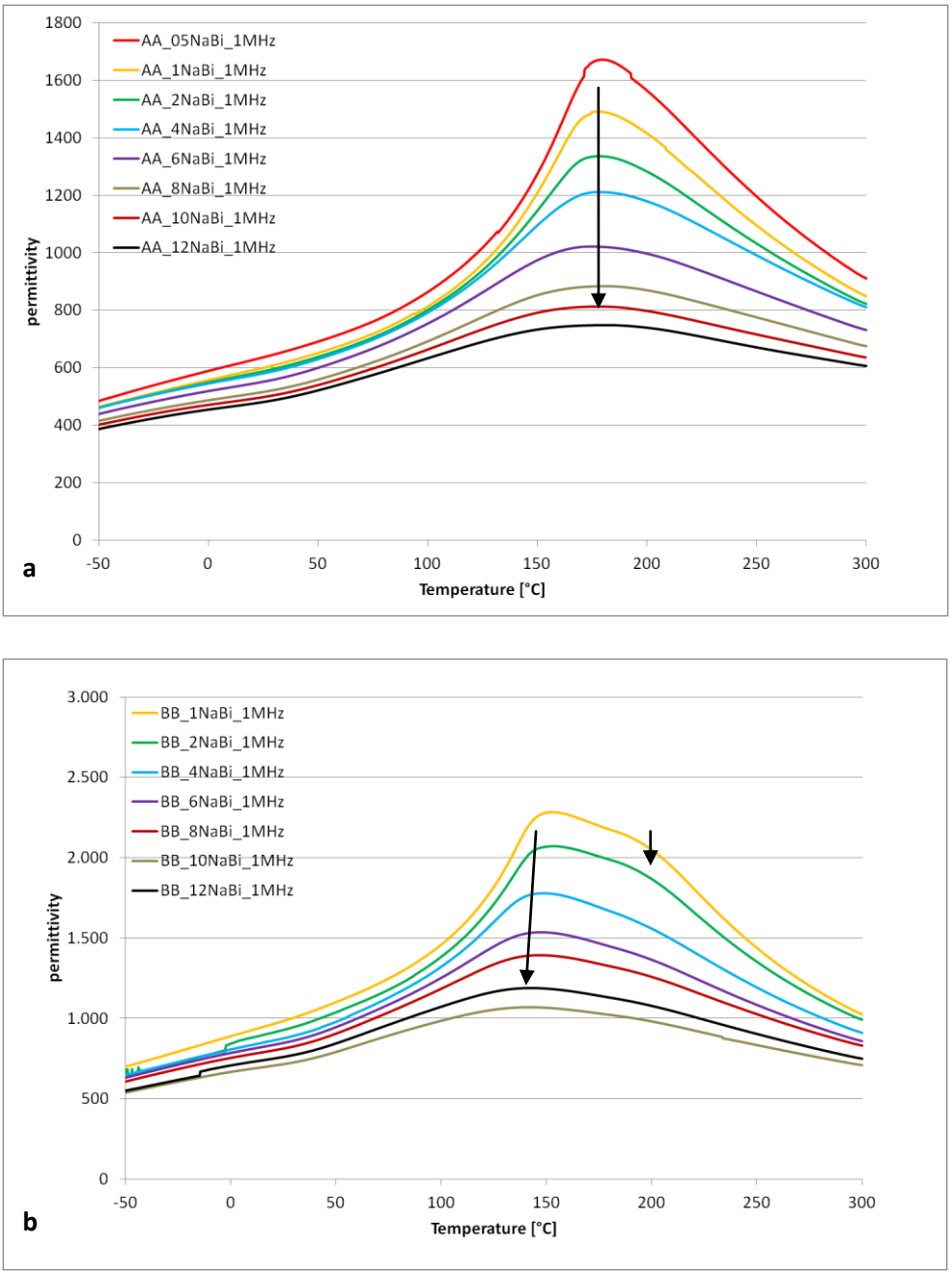

Figure 7.5-14: Relative permittivity curves versus temperature at 1 MHz (arrows indicate the maximum in relative permittivity and demonstrate the alteration with increasing concentration of substituents (AA = $Pb_{0.91}La_{0.06}Zr_{0.9}Ti_{0.1}O_3$, BB= $Pb_{0.91}La_{0.06}Zr_{0.85}Ti_{0.15}O_3$).

Table 7.5-12: Results of the relative permittivity versus temperature curves of Bismuth-Sodium co-substitution in PLZT AA and BB.

sample	maximum in relative permittivity	Temperature Tm [°C]	sample	maximum in relative permittivity	Temperature Tm [°C]
AA_05NaBi	1671	180	BB_05NaBi	2072	179
AA_1NaBi	1491	179	BB_1NaBi	2282	153
AA_2NaBi	1335	179	BB_2NaBi	2072	154
AA_4NaBi	1211	180	BB_4NaBi	1780	149
AA_6NaBi	1022	177	BB_6NaBi	1537	148
AA_8NaBi	884	181	BB_8NaBi	1392	148
AA_10NaBi	812	179	BB_10NaBi	1068	143
AA_12NaBi	747	181	BB_12NaBi	1191	143

By recording the relative permittivity curves at various frequencies, frequency dependence – if present - can be determined. In Figure 7.5-15a and b the curves of selected samples are presented. No frequency dependence could be detected in all samples. In Figure 7.5-15a the curves of the sample AA-1NaBi are depicted. As it is obvious, the loss factor curves show a peak at a temperature which is close to that of the relative permittivity curves. Also these peaks do not reveal any frequency dependence. Only the height of the curves decreases with increasing frequency.

In Figure 7.5-15b, the curves of the sample called BB-05NaBi are plotted. An additional step at higher temperature was detected. With increasing frequency the prominence of that peaks decreases but they are still recognizable. This might be due to an additional phase transition, most probably due to the closeness to the triple point which was discussed in a previous chapter. Only in the compositions with higher Titanium content BB these incidents were detected. None of these transition temperatures changed by varying the frequency, only the height of the curves decreased.

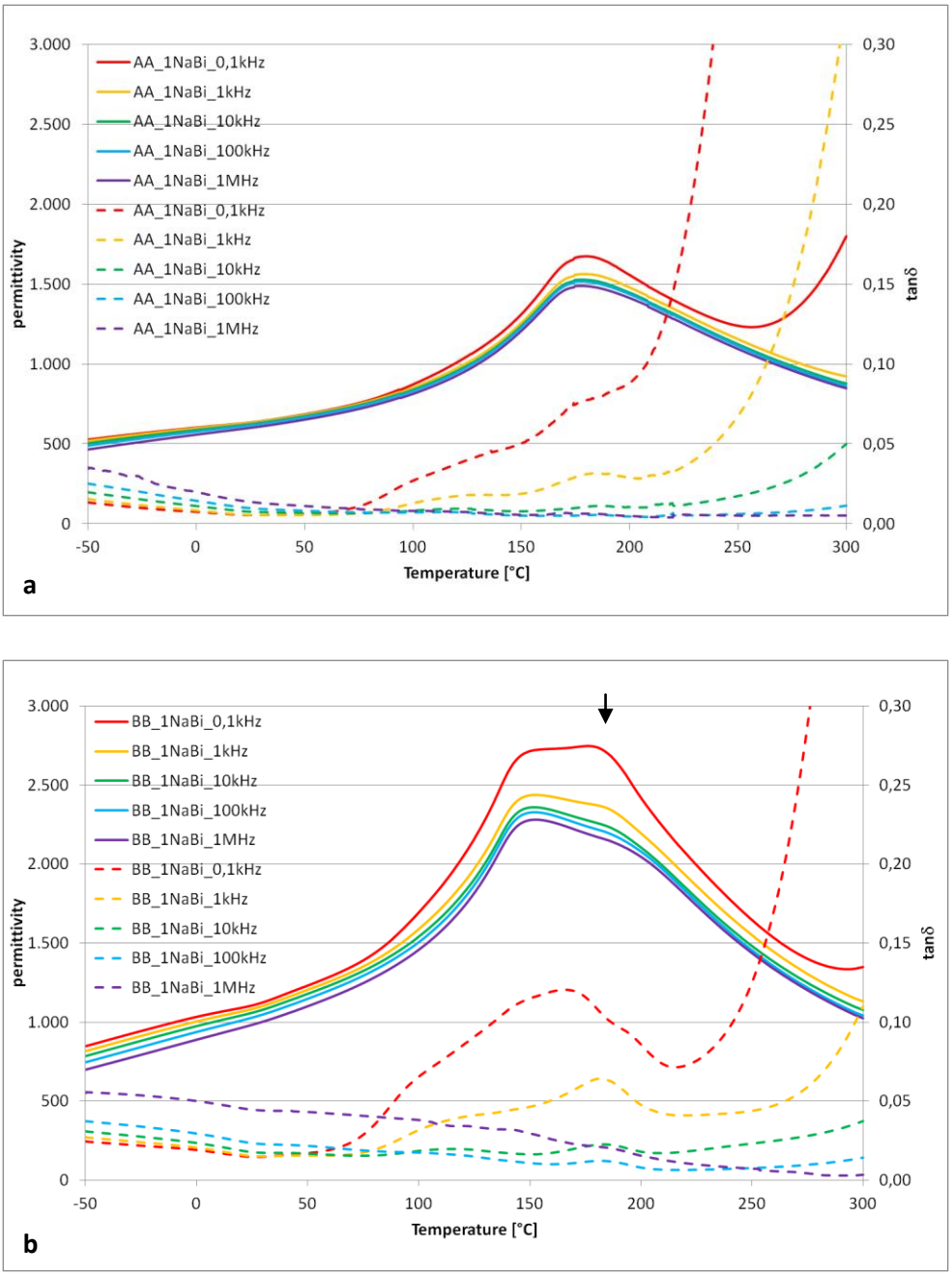

Figure 7.5-15: Frequency dependent measurements of the relative permittivity (solid line) and loss factor (dashed line) of Bismuth-Sodium co-substitution in PLZT (measured at 0,1 kHz, 1 kHz, 10 kHz, 100 kHz and 1 MHz). Anomalies are accentuated by an arrow (AA = $Pb_{0.91}La_{0.06}Zr_{0.9}Ti_{0.1}O_3$, BB= $Pb_{0.91}La_{0.06}Zr_{0.85}Ti_{0.15}O_3$).

The polarization curves of the AA compositions could not reach saturation at all and therefore they were left out in this chapter. Thus only the polarization curves of the BB system are shown.

Figure 7.5-16 presents the polarization curves of the composition BB up to 4 mol% Bismuth-Sodium. At higher concentration no saturation was obtained. The curve of sample BB-6NaBi was enlarged with a high remnant polarization and therefore a lossy behaviour occurred. Considering the low content com-

positions, the curves slimmed with increasing doping content. The switching fields were shifted to higher field and the area of the curves decreased with increasing Bismuth-Sodium substitution.

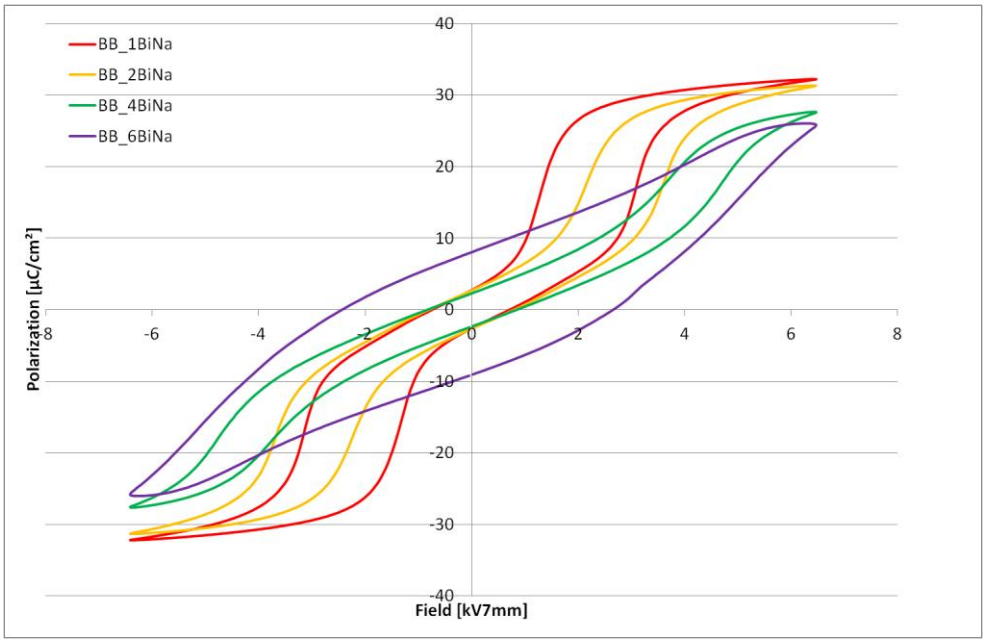

Figure 7.5-16: Polarization curves of Bismuth-Sodium co-substitution in PLZT BB ($Pb_{0.91}La_{0.06}Zr_{0.85}Ti_{0.15}O_3$).

Regarding Figure 7.5-17, the distinction of the effect of Sodium, Bismuth and a one to one combination of these substituents in PLZT samples is shown. As mentioned above, the substitution of Lead with Bismuth and Lanthanum resulted in a slim curve.

Now the effect of an additional substituent will be discussed. Comparing the shape of the curve of the sample containing Sodium and Lanthanum, the forward switching field and the saturation polarization were shifted to higher values. On the other hand, the area of the curve was enlarged due to a larger ΔE, a higher remnant polarization and higher coercive field. In the case of Bismuth-Sodium co-doping, a combination of the effects occurred: The maximum of the polarization increased, forward switching filed was shifted to higher electric fields and the shape of the curve remained slim.

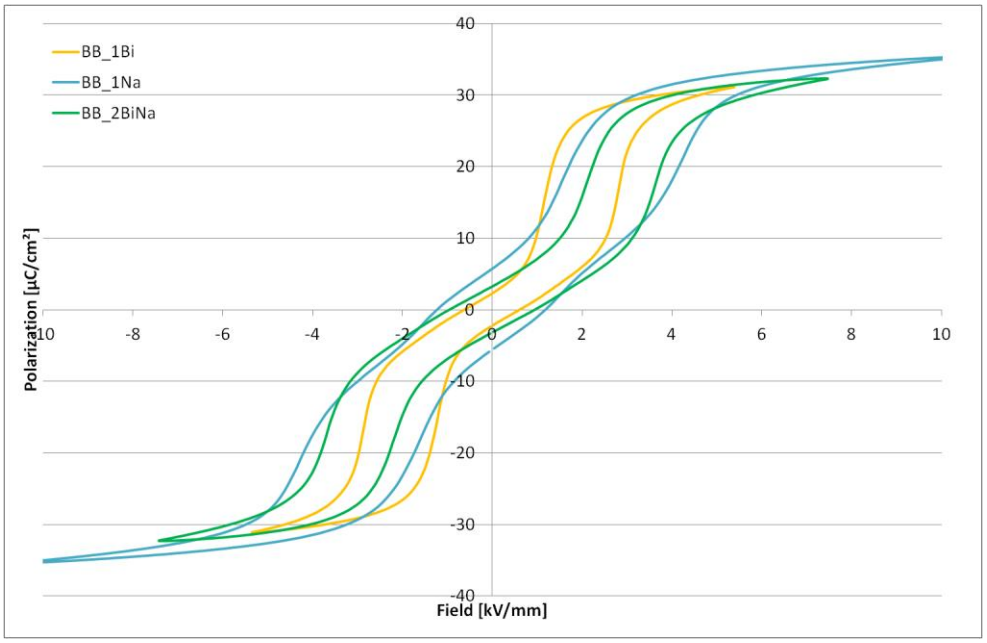

Figure 7.5-17: Comparison of the polarization curves of Bismuth- and Sodium substitution in PLZT with co-substitution of Bismuth-Sodium in PLZT $Pb_{0.91}La_{0.06}Zr_{0.85}Ti_{0.15}O_3$ (BB-1Bi contains 1 mol% Bismuth, BB-1Na 1 mol% of Sodium and BB-2BiNa 1 mol% of each substituent).

7.5.2.3 Summary

The influences of the substitution with Bismuth-Sodium substitution-pair on the properties of PLZT solid solution were examined. Regarding the incorporation of the substitution pair in PLZT, it exhibited better solubility in the structure than the substitution solely with Bismuth. Nevertheless, secondary phases were detected. As these were found in all samples in comparable amount, a comparison within the series was possible.

The dielectric parameters at room temperature decreased with increasing content of the substitution-pair. Regarding the temperature dependent measurements, the dielectric response was progressively suppressed by increasing the content of Bismuth and Sodium. In the case of the substitution of Lead with Calcium and Strontium, the relative permittivity decreased, whereas with Barium it increased. The one to one combination of Barium and Calcium at the A-site resulted in a slight decrease. This supports the assumption that a decrease in relative permittivity occurs with inserting smaller ions or even a combinations of ions with a smaller average size.

Besides, the increasing broadening of the peaks in the permittivity curves by increasing concentration of the substitution-pair Bismuth-Sodium indicates a more diffuse transition which is in good accordance to the insertion of BNT or BNLT in PZT[127],[128].

An averaging effect of the trivalent ion and the monovalent ion on the transition temperature occurred as expected. No frequency dependence could be observed in all samples.

Although the samples were not homogeneous, it can be argued that the substitution of Lead with Bismuth and Sodium results in polarization curves revealing a combination of the single effects of both substituents on the hysteresis curves. Overall, an increase of the stability of the antiferroelectric phase of PLZT under field (higher switching fields) and a reduction of the area of the hysteresis could be achieved.

In sum, PLZT is stable in the orthorhombic structure over a wide compositional range of substituents with varying size, mass and valency. The resulting properties induced by the substitution with this combination of ions can be considered as an average of all the independent effects generated by the separately inserted ions.

7.5.3 A- and B-site substitution - Calcium-Stannate and Barium-Stannate

In the previous chapters, combinations of two ions at the A-site were incorporated in the PLZT system, while now a combination of A- and B-site substitution is presented. The results will be discussed and compared to the effects of the substitution of the separately inserted ions. As before, the starting materials AA and BB were used and were modified according to the formula:

$$Pb_{1-1,5a-b}La_a M^x_b V Pb''_{0,5a} Zr_{1-x-y}Ti_xSn_yO_3.$$

The value of Lanthanum was set to 6 mol%, therefore all the prepared compositions possessed 3 mol% of Lead vacancies. At the A-site an isovalent earth alkaline substituted Lead, while the isovalent Tin substituted Zirconium at the B-site. The content of Titanium varied between the composition AA and BB by 5 mol%.

As mentioned before, Tin[111,122] and Calcium[87,111] are known to increase the stability range of the antiferroelectric phase, whereas Barium[112] shows the reverse behaviour.

Regarding the structure, the Ca^{2+} and Sn^{4+} stabilize the orthorhombic, whereas the Ba^{2+} stabilizes the rhombohedral structure. Recalling the effect of the substitution-pair Barium-Calcium at A-site on the structure, it was noticed that the orthorhombic structure is formed although one of the substituent ions tends to favour the rhombohedral structure.

In this study, two earth alkaline stannates were used - Barium-Stannate which is cubic[129] and the orthorhombic Calcium-Stannate[129,130].

As the octahedral tilting which is associated to the stabilization of the orthorhombic phase is related to the size of the A-site cation, the relation of either a bigger or a smaller ion at A-site with a smaller ion at B-site and the effect on the properties is in focus of interest[131].

7.5.3.1 XRD Characterization

To evaluate the lattice parameters and the cell volume, Rietveld refinement was performed using reference reflection patterns of an orthorhombic structure Pba2 and if required a rhombohedral structure R3cH.

Consulting Table 7.4-1, Tin as a substituent of Zirconium possesses an ionic radius which is about 5% smaller than the ionic radius of Zirconium. At the A-site, Calcium only possesses about 90% of the ionic radii of Lead, whereas Barium exceeds Lead by around 10% in ionic size. This gives a good explanation of the reduction and expansion in cell volume with increasing level of substitution.

Table 7.5-13: Comparison in charge, atomic weight and radius of the alkaline ions used to build the perovskite structure.

	Pb	La	Ca	Ba	Zr	Ti	Sn
Charge	+2	+3	+2	+2	+4	+4	+4
Atomic weight	207.2	138.9	40.078	137.327	91.22	47.87	118.71
Radius [XII]	1.49	1.36	1.34	1.61			0.69
Radius [VI]					0.72	0.605	0.69

Calcium-Stannate insertion yielded single phase perovskite phase in the system AA and BB which indicated a good incorporation (Figure 7.5-18 and Figure 7.5-19). In the detailed view of the BB system, reflections decreased and vanished with increasing content of the substituents (Figure 7.5-20). With 8 mol% Calcium-Stannate the reflections started to decrease in some extent and with 10 mol% a conversion to rhombohedral structure took place. The same behaviour was found within the sample BB-10Ca in chapter 6.3, which possessed the same amount of Calcium. Therefore, it can be assumed that A-site substitution has a bigger influence on the structure as B-site substitution.

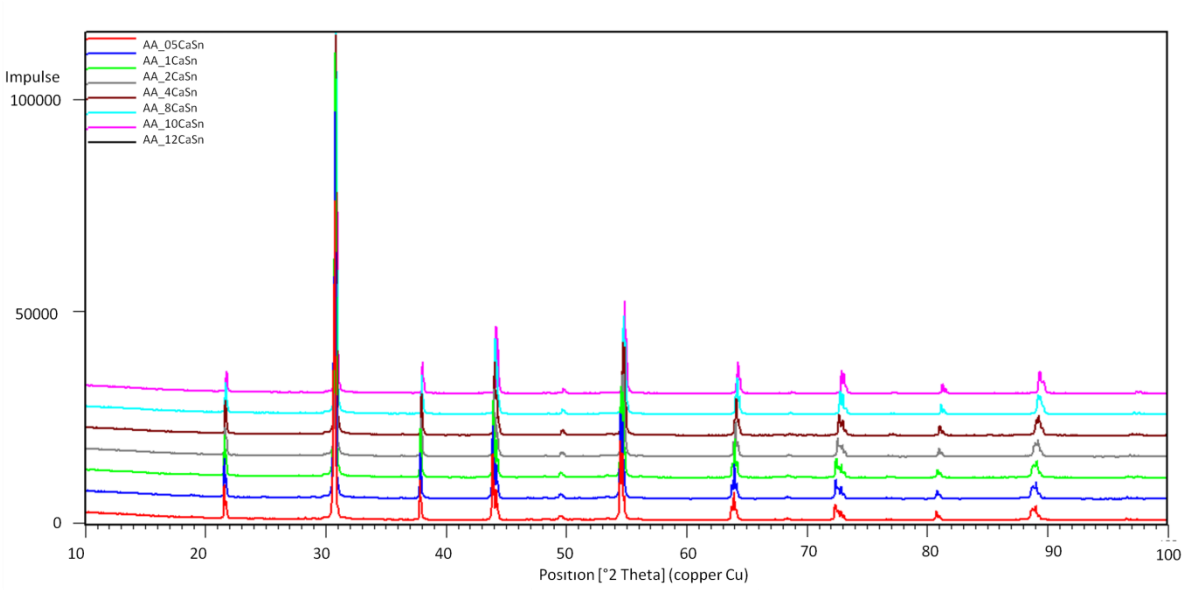

Figure 7.5-18: XRD of sintered powder of Calcium-Stannate-substitution in PLZT (AA = $Pb_{0.91}La_{0.06}Zr_{0.9}Ti_{0.1}O_3$).

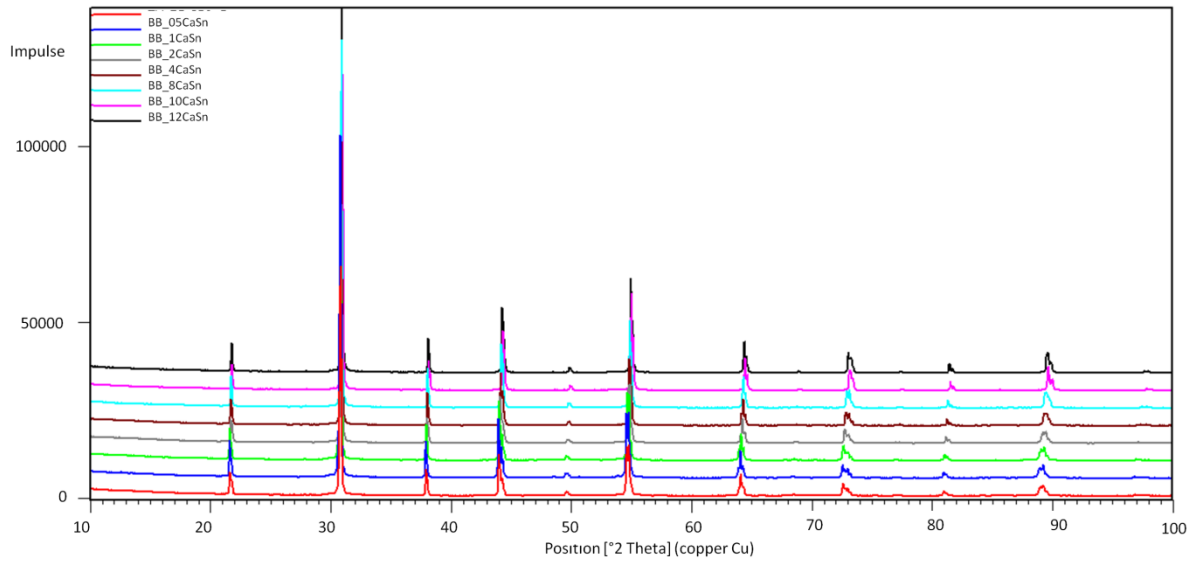

Figure 7.5-19: XRD of sintered powder of Calcium-Stannate-substitution in PLZT (BB = $Pb_{0.91}La_{0.06}Zr_{0.85}Ti_{0.15}O_3$).

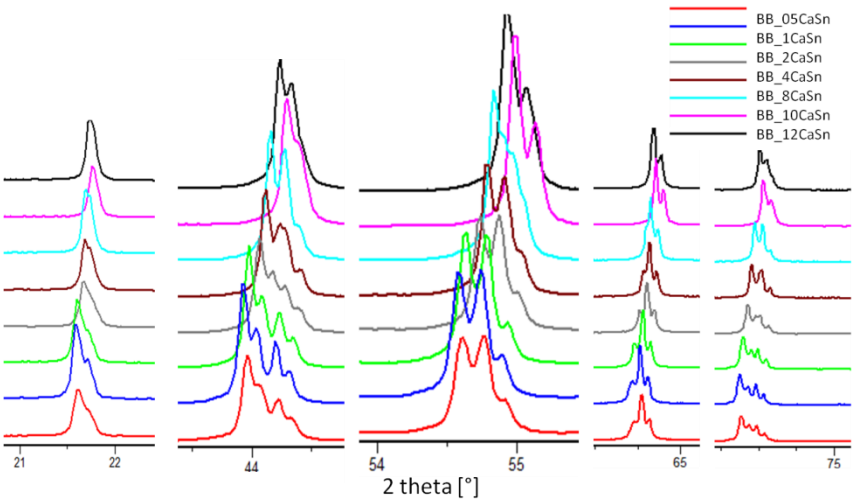

Figure 7.5-20: Detailed view of the changing of reflection pattern by increasing the content of Calcium-Stannate substitution-pair in the composition BB ($Pb_{0.91}La_{0.06}Zr_{0.85}Ti_{0.15}O_3$) due to a change from orthorhombic to rhombohedral structure.

By introducing two ions with smaller ionic radii as the ones to substitute, the cell volume decreased continuously with increasing doping-content (Table 7.5-14 and Table 7.5-15). In the case of the structural change with the substitution with 10 mol% of the substitution-pair in the BB composition, the cell volumes of the rhombohedral structure cannot be compared with the orthorhombic structure offhandedly. Besides, the theoretical densities decreased as well as the Archimedes´ density. Nevertheless the relative densities increased in both systems. Exceeding 100% of the relative density indicates that relative density calculated from XRD data might be underestimated since no secondary phase was detected.

Table 7.5-14: List of the cell parameters, the cell volume and the densities of Calcium-Stannate-substitution in PLZT AA.

sample	c [Å]	b [Å]	a [Å]	c/a	cell volume [Å³]	theoretical density [g/cm³]	Archimedes´ density [g/cm³]	relative density [%]
AA_05CaSn	8.2084	11.6881	5.8390	1.4058	560.2010	7.84	7.55	96.38
AA_1CaSn	8.2065	11.6863	5.8378	1.4058	559.8667	7.81	7.66	98.08
AA_2CaSn	8.2038	11.6791	5.8346	1.4061	559.0356	7.74	7.67	99.10
AA_4CaSn	8.2003	11.6642	5.8273	1.4072	557.3824	7.62	7.64	100.20
AA_6CaSn	8.1950	11.6458	5.8177	1.4086	555.2209	7.51	7.48	99.65
AA_8CaSn	8.1924	11.6296	5.8107	1.4099	553.6110	7.39	7.55	102.23
AA_10CaSn	8.1905	11.6126	5.8029	1.4115	551.9310	7.27	7.47	102.74

Table 7.5-15: List of the cell parameters, the cell volume and the densities of Calcium-Stannate- substitution in PLZT BB.

sample	c [Å]	b [Å]	a [Å]	c/a	cell volume [Å³]	theoretical density [g/cm³]	Archimedes´ density [g/cm³]	relative density [%]
BB_05CaSn	8.19566	11.6609	5.8251	1.4070	556.7012	7.83	7.57	96.74
BB_1CaSn	8.19688	11.6660	5.8279	1.4065	557.2970	7.79	7.55	96.91
BB_2CaSn	8.19072	11.6520	5.8220	1.4069	555.6395	7.74	7.66	99.03
BB_4CaSn	8.18828	11.6383	5.8154	1.4080	554.1957	7.61	7.56	99.22
BB_6CaSn	8.18323	11.6203	5.8072	1.4092	552.2096	7.50	7.49	99.86
BB_8CaSn	8.18161	11.6052	5.7994	1.4108	550.6478	7.38	7.53	102.05
BB_10CaSn	14.17465	5.7840	5.7840	2.4506	410.6820	7.27	7.46	102.62
BB_12CaSn	14.18747	5.7885	5.7885	2.4510	411.6848	7.11	7.48	105.15

Regarding XRD spectra in Figure 7.5-21, the incorporation of the substitution-pair Barium and Tin was performed without the formation of secondary phases. In Figure 7.5-22 a detailed view of some reflections is shown. It is obvious that with increasing the content of the substituents certain reflections decreased and eventually vanished. This indicates a phase transition from orthorhombic to rhombohedral structure at the insertion of 6 mol% of the substitution-pair. This is in good correlation with the rhombohedral conversion in samples with the same amount of Barium as singly substituent in the composition BB. Again, the dominance of the A-site variation over the B-site variation considering the structure was discovered.

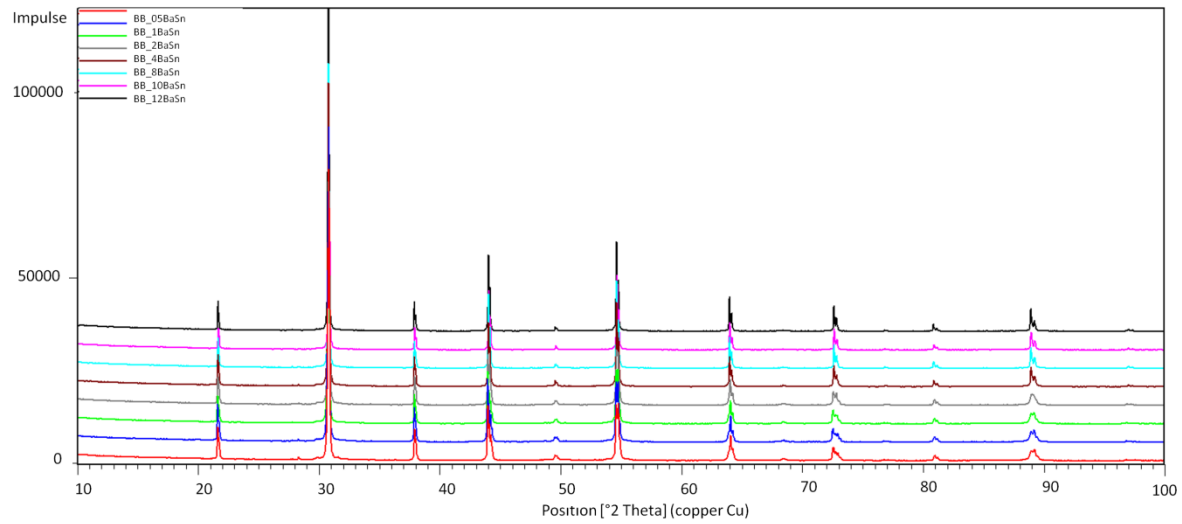

Figure 7.5-21: XRD of sintered powder of Barium-Stannate-substitution in PLZT (BB = $Pb_{0.91}La_{0.06}Zr_{0.85}Ti_{0.15}O_3$).

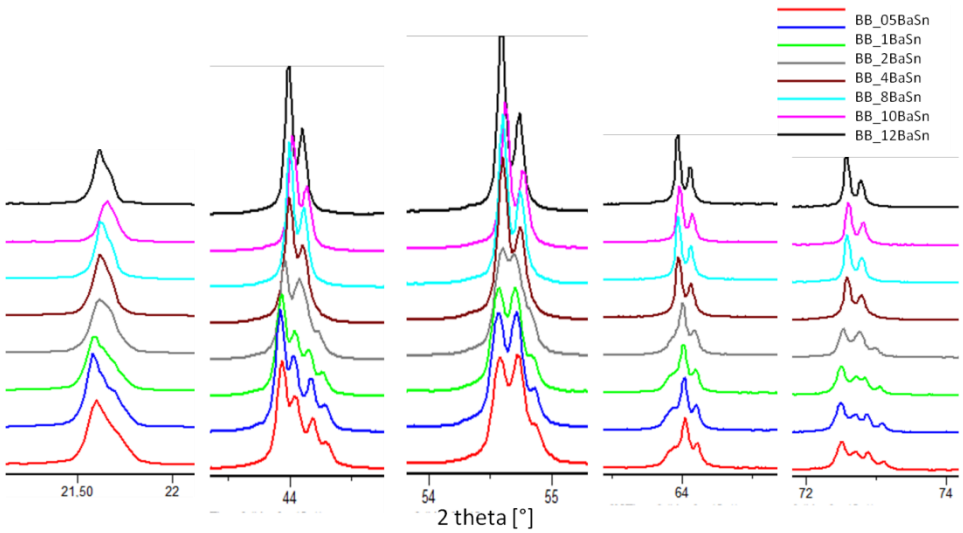

Figure 7.5-22: Detailed view of the vanishing of reflection pattern by increasing the content of Barium-Stannate-substitution in the composition BB ($Pb_{0.91}La_{0.06}Zr_{0.85}Ti_{0.15}O_3$).

The cell volume increased continuously with increasing the content of the substitution-pair due to the big ionic radius of Barium (Table 7.5-16). But the increase was not in that extent as with solely increasing addition of Barium due to the combination with Tin, which is smaller than the one it substitutes. With the transition to rhombohedral structure the lattice parameter and therefore also the cell volume changed. Theoretical density dropped with increasing content of substituents as well as the Ar-chimedes´s density. The relative density increased over the compositional range. The relative density might be underestimated as it exceeded 100% of the relative density while no secondary phase was detected.

Table 7.5-16: List of the cell parameters, the cell volume and the densities of Barium-Stannate-substitution in PLZT BB.

sample	c [Å]	b [Å]	a [Å]	c/a	cell volume [Å³]	theoretical density [g/cm³]	Archimedes´ density [g/cm³]	relative density [%]
BB_05BaSn	8,20156	11,6682	5,8279	1,4073	557,7124	7,82	7,90	101,14
BB_1BaSn	8,20207	11,6688	5,8281	1,4073	557,7980	7,78	7,63	98,05
BB_2BaSn	8,20562	11,6669	5,8272	1,4082	557,8636	7,70	7,65	99,27
BB_4BaSn	8,21418	11,6652	5,8257	1,4100	558,2169	7,56	7,60	100,57
BB_6BaSn	14,26831	5,8227	5,8227	2,4505	418,9427	7,41	7,53	101,53
BB_8BaSn	14,27073	5,8234	5,8234	2,4506	419,1042	7,27	7,55	103,84
BB_10BaSn	14,27291	5,8239	5,8239	2,4507	419,2485	7,12	7,45	104,53
BB_12BaSn	14,27082	5,8232	5,8232	2,4507	419,0855	6,98	7,53	107,79

7.5.3.2 Dielectric Characterization

The variation of the low signal values by increasing the insertion of either Calcium-Stannate or Barium-Stannate replacing Lead or Zirconium are presented in Table 7.5-17 to Table 7.5-19.

The substitution-pair Calcium and Tin in PLZT compositions led to a decrease of permittivity as well as loss factor. In the system AA a drop from ~530 to ~370 in relative permittivity occurred. In the case of the composition BB, the increasing substitution with Calcium and Tin caused a decrease from ~1060 to ~520 in relative permittivity. In both cases the loss factor dropped to one fourth by increasing the substitution-pair content from 0.5 mol% to 10 mol% and 12 mol% respectively. The values of the loss factors went below that of the single substitution by Tin and decreased from 0.0098 to 0.0021 and 0.0128 to 0.0039 in the AA and the BB system, respectively.

Table 7.5-17: Results of low signal dielectric measurements of Calcium-Stannate-substitution in PLZT AA.

sample	capacitance [nF]	loss factor [°]	relative permittivity []
AA_05CaSn	0.4078	0.0098	533.31
AA_1CaSn	0.4306	0.0193	569.12
AA_2CaSn	0.3813	0.0420	514.06
AA_4CaSn	0.3619	0.0118	497.71
AA_8CaSn	0.3170	0.0026	442.27
AA_10CaSn	0.2687	0.0021	372.28

Table 7.5-18: Results of low signal dielectric measurements of Calcium-Stannate-substitution in PLZT BB.

sample	capacitance [nF]	loss factor [°]	relative permittivity []
BB_05CaSn	0.7618	0.0128	1062.52
BB_1CaSn	0.7907	0.0125	1116.58
BB_2CaSn	0.6938	0.0076	956.44
BB_4CaSn	0.6158	0.0058	846.64
BB_6CaSn	0.5257	0.0043	696.86
BB_8CaSn	0.5072	0.0063	675.68
BB_10CaSn	0.4448	0.0040	607.39
BB_12CaSn	0.3862	0.0039	518.74

In contrast to the above described effects, relative permittivity increased with increasing content of Barium-Stannate. Over the compositional range of the substitution with Barium-Stannate, capacitance relative permittivity was multiplied by nearly 2.5. Or in other words, the relative permittivity increased from ~1040 to ~2850. Meanwhile, the loss factor decreased from 0.0295 to 0.0167.

Table 7.5-19: Results of low signal dielectric measurements of Barium-Stannate-substitution in PLZT BB.

sample	capacitance [nF]	loss factor [°]	relative permittivity []
BB_05BaSn	0.8503	0.0295	1038.84
BB_1BaSn	0.9034	0.0328	1140.41
BB_2BaSn	1.0891	0.0322	1294.01
BB_4BaSn	1.2122	0.0980	1542.64
BB_6BaSn	2.0635	0.0444	2503.60
BB_8BaSn	2.4457	0.0325	3138.95
BB_10BaSn	2.3790	0.0191	3082.68
BB_12BaSn	2.1637	0.0167	2854.12

In Figure 7.5-23 the dielectric response versus temperature of different levels of substitution for the series with Calcium-Stannate and Barium-Stannate are presented. All curves were recorded at 1MHz. The values of maximum permittivity and Temperature at maximum permittivity can be found in Table 7.5-20 and Table 7.5-21.

In Figure 7.5-23a, the impact of the substitution with Calcium-Stannate on the dielectric response is plotted. A decrease in the height of the curves in both cases can be observed even in a higher extent as with the substitution solely with Tin. The shift in position is not that evident in this figure and with higher concentration of the substitution-pair the curves did not reveal anymore a peak position due to a levelling. Due to that, only three curves could be characterized in the case of AA. Regarding these, a fluctuation of the peak temperature in the range of ~190 °C to ~160 °C and a decrease of the height of

the curves from ~1530 to 750 were apparent. In other words, by substitution with 4 mol% of Calcium-Stannate the relative permittivity was divided by two. With further increase of the concentration of the substitution-pair the decrease of relative permittivity stagnated and a flattening of the curves occurred.

In the case of the system BB (Figure 7.5-23b), a drop in relative permittivity from ~2355 to ~1370 appeared by increasing the content of Calcium-Stannate from 0.5 mol% to 4 mol%. This seemed to be a lower reduction than in the case mentioned above. The substitution with 1 mol% of Calcium-Stannate led to a higher relative permittivity of ~2570. The shift in transition temperature was from ~150 °C to ~130 °C.

Regarding the substitution with Barium-Stannate in the BB system in Figure 7.5-23c, a shift in the position of the maximum of the curve to lower temperature accompanied by an increase of the height happened with increasing level of substitution. Relative permittivity increased from ~2370 to a maximum of 3080 at 6 mol%. Higher Barium-Calcium concentration decreased relative permittivity to 2690. The transition temperature dropped from 150 °C to 16 °C by the substitution with 12 mol% of Barium-Stannate.

Combining all this, the before mentioned assumption of the effect of the ionic size (chapter 6.5.1 and 6.5.2) on the shift of relative permittivity proved to be applicable. The substituting ions, Tin and Calcium, are smaller than the ones they replace. Therefore a decline in the height of relative permittivity appeared in both systems and the association of both enhanced this effect (see the chapter 6.3 about the substitution with earth alkaline ions).

On the other hand, Barium has a bigger ionic radius as Lead and the increasing substitution increased the height of the relative permittivity curves. Having a look at the relative permittivity curves of the Barium-Stannate series, the height slightly increased by following the insertion of the substitution-pair. This might be due to the governing impact of the size of Barium. Considering the ionic radii of the substituents, Tin occupies 5% lower ionic radius as Zirconium, whereas Barium has 10% bigger ionic radius as Lead. Therefore the overall effect resulted in an increase of the relative permittivity.

a

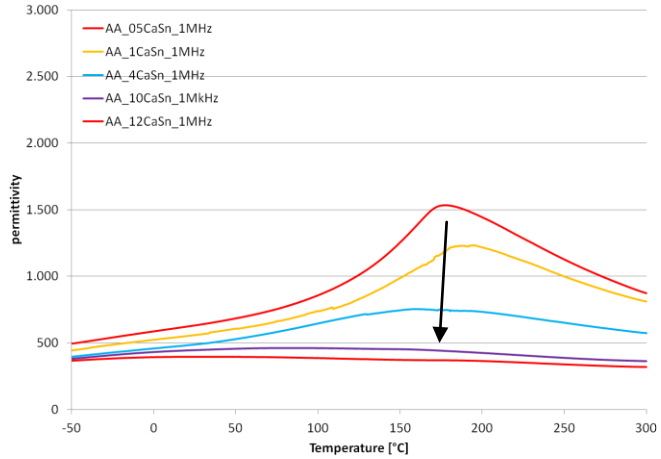

b

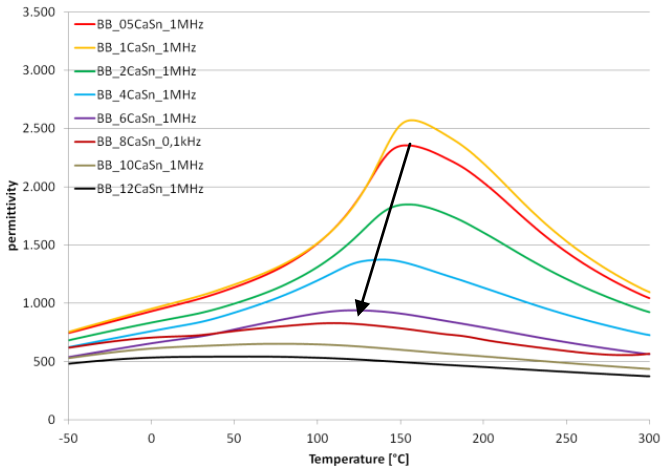

c

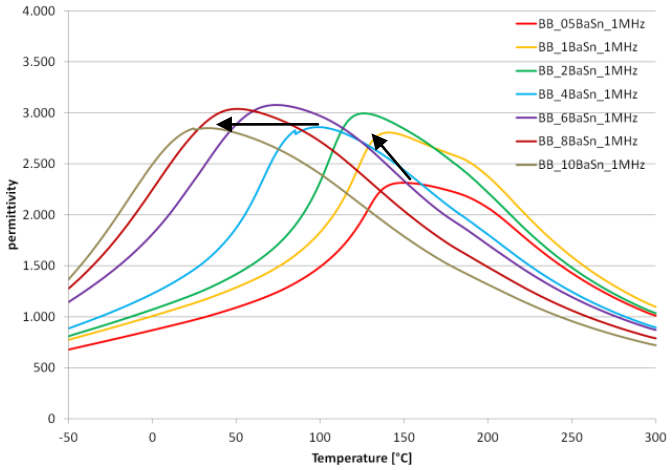

Figure 7.5-23: Relative permittivity measurements versus temperature of Calcium-Stannate and Barium-Stannate co-substitution in PLZT AA and BB at 1 MHz.

Table 7.5-20: Results of the relative permittivity versus temperature curves of Calcium-Stannate substitution in PLZT AA and BB.

sample	maximum in relative permittivity	Temperature Tm [°C]	sample	maximum in relative permittivity	Temperature Tm [°C]
AA_05CaSn	1530	175	BB_05CaSn	2355	149
AA_1CaSn	1229	188	BB_1CaSn	2572	154
AA_2CaSn			BB_2CaSn	1849	151
AA_4CaSn	751	163	BB_4CaSn	1374	130
AA_6CaSn			BB_6CaSn	942	122
AA_8CaSn			BB_8CaSn	792	104
AA_10CaSn			BB_10CaSn		
AA_12CaSn			BB_12CaSn		

Table 7.5-21: Results of the relative permittivity versus temperature curves of Bariums-Stannate substitution in PLZT BB.

sample	maximum in relative permittivity	Temperature Tm [°C]
BB_05BaSn	2317	150
BB_1BaSn	2808	141
BB_2BaSn	2995	127
BB_4BaSn	2863	99
BB_6BaSn	3079	74
BB_8BaSn	3042	51
BB_10BaSn	2851	34
BB_12BaSn	2688	16

In Figure 7.5-24 selected curves of relative permittivity curves recorded at various frequencies are plotted. In the AA series of Calcium-Stannate substitution in PLZT (Figure 7.5-24a) only one peak in the relative permittivity curves was visible which coincided with the peak in the loss factor curves. With increasing frequency, the height of the peaks declined but did not shift in position.

In the case of the BB-system in Figure 7.5-24b, at low frequency an additional step at higher temperature was recorded which could no longer be detected at 1 kHz.

In Figure 7.5-24c and d the curves of the samples BB, where 1 mol% and 10 mol% of Lead and Zirconium were substituted with Barium and Tin, are shown. With low concentration a shoulder at higher temperature emerged which decreased but did not disappear with increasing frequency. In the case of a higher content of the substitution-pair some peculiarities happened: The most prominent peak started to shift position with increasing frequency. This referred to fluctuation of nano-domains and indicated a relaxor-behaviour. Additionally two shoulders at higher temperature evolved, but they decreased with increasing the frequency. The position of the shoulders correlated to the peak positions in the loss factor curves.

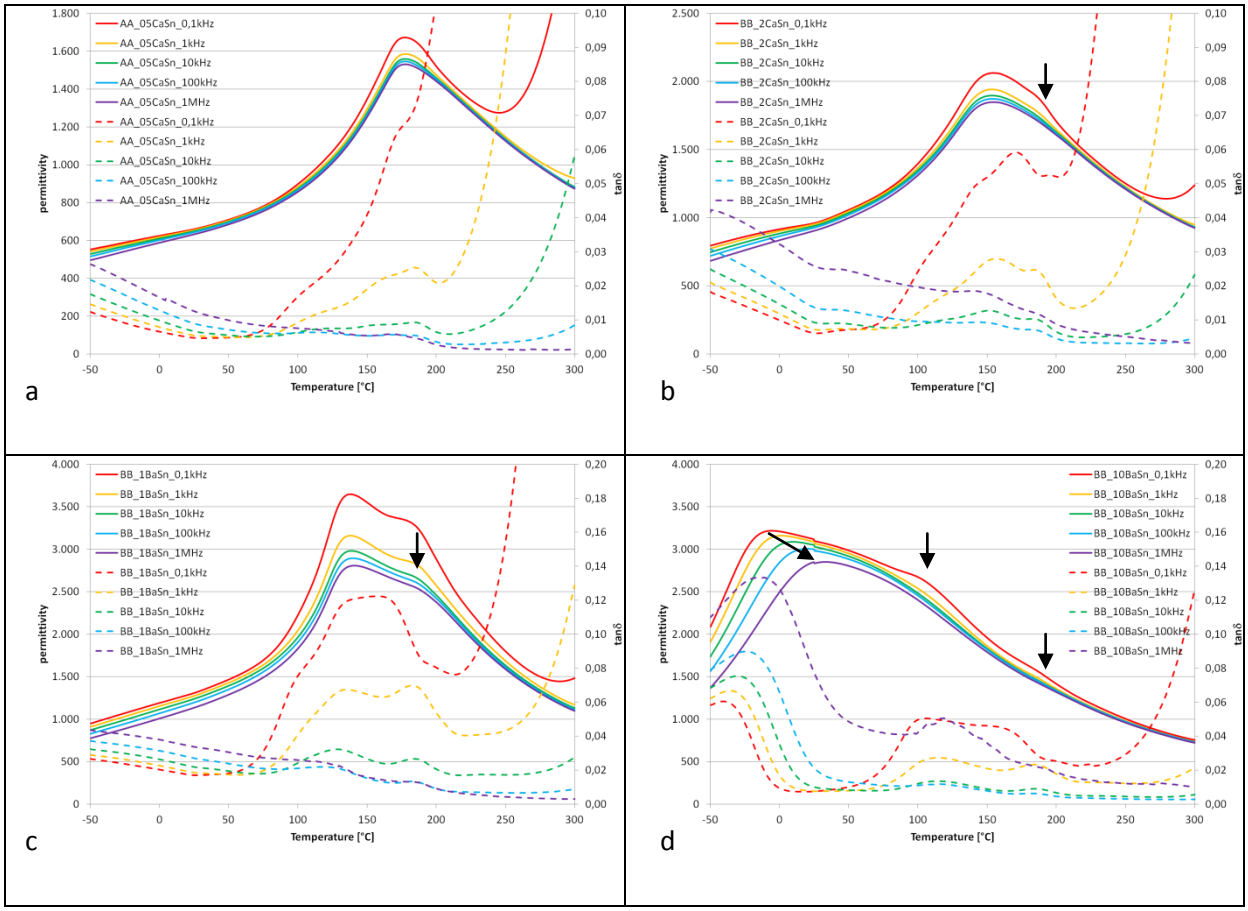

Figure 7.5-24: Frequency dependency of relative permittivity (solid line) and loss factor (dashed line) curves of selected Barium-Stannate and Calcium-Stannate substitution in PLZT (measured at 0,1 kHz, 1 kHz, 10 kHz, 100 kHz and 1 MHz). Anomalies are accentuated by arrows.

A frequency dependence could be observed in samples with high Barium-Stannate content. This resembled the behaviour of $BaZrO_3$, a relaxor material[121].

Regarding the polarization curves in Figure 7.5-25a, no saturation in the samples with higher Zirconium-content could be reached. Therefore only the samples of the series BB can be considered discussing the influence of the substituents on switching field and saturation polarization.

The effect of the substitution with Calcium-Stannate in the system BB is demonstrated in Figure 7.5-25b. Only with low contents of the substitution-pair saturation in the polarization curves was achieved. With increasing the substitution a decrease of the saturation polarization and increase of the switching fields occurred resulting in increasingly slimmer hysteresis.

In the case of the incorporation of Barium-Stannate replacing Lead and Zirconium in the system something different happened: Up to 2 mol% of the substitution-pair, the curves slimmed. The saturation polarization decreased, the backward switching field increased and the forward switching field did not alter (Figure 7.5-25c).

With further increasing the level of substitution, the curve changed to a convex shape with steep incline at low fields and a levelling out at higher fields. This fading can be shifted to higher fields with 8 mol% of Barium-Stannate (Figure 7.5-25d). A similar behaviour was observed by increasing the substitution of Lead with Barium (see the chapter 6.3 about the substitution with earth alkaline ions).

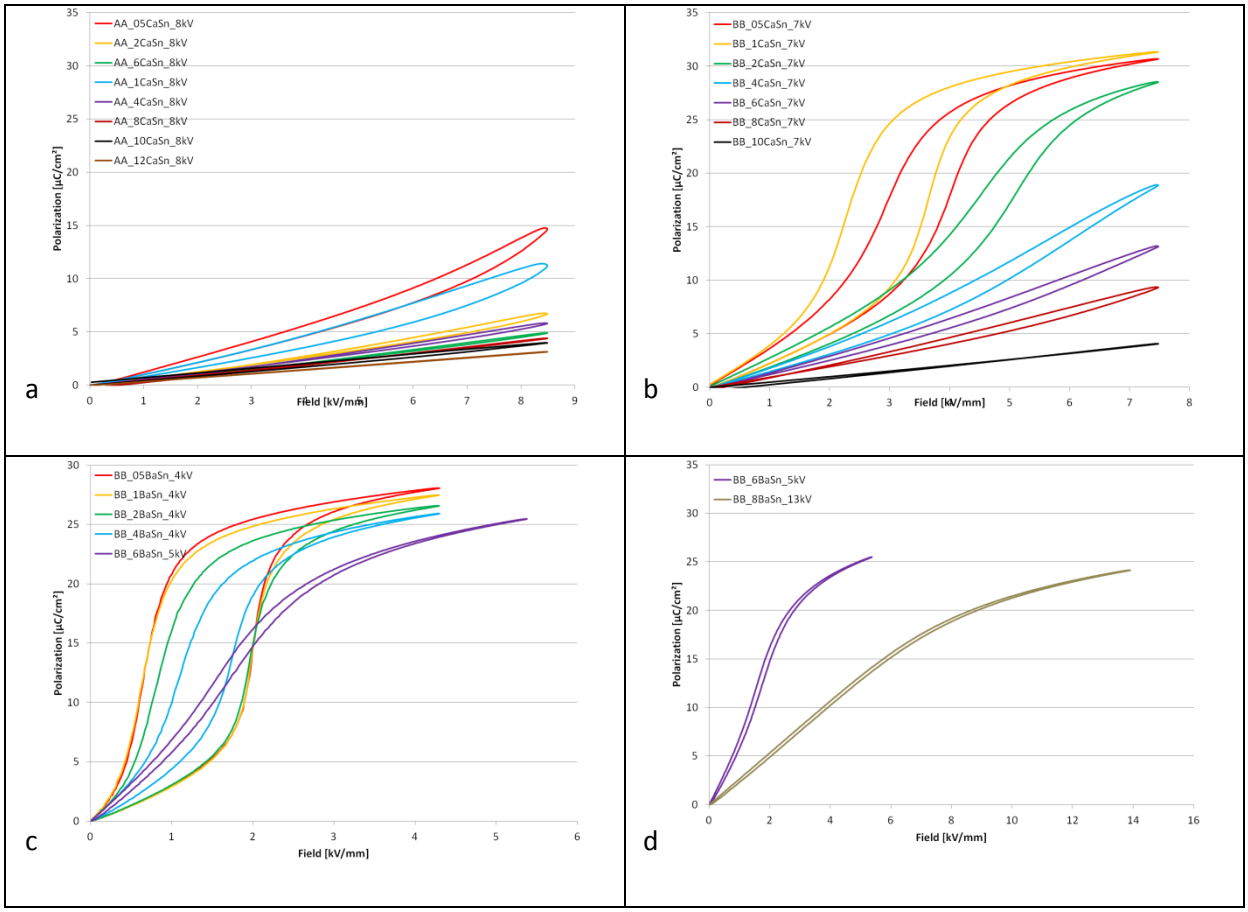

Figure 7.5-25: Unipolar Polarization curves of Calcium-Stannate and Barium-Stannate substitution in PLZT samples AA and BB.

The effects on the polarization curves in the case of the substitution-pairs can be summarized as a balancing of the individual effects of both ions. In Figure 7.5-26 the effects of each substituent on the polarization curves are compared. In the left graph, the influence of Calcium, Tin and the combination of both substituents are demonstrated. While the substitution of Zirconium with Tin showed high saturation polarization and a steep slope after switching forward and backward fields, the substitution with Calcium revealed a more flattened and slightly broader curve with low maximum. In contrast to the samples containing Tin, the curve of the sample BB-2Ca imposed higher switching fields. Co-substitution by these two ions resulted in a curve with an average saturation polarization and a position of switching which was levelled in between the before mentioned. Interestingly, the reduction of the area of the curve was almost halve of the areas of the other curves.

In the case of the combination of Barium and Tin as a substitution-pair, a remarkable change of the shape of the curve appeared. The curve of the Tin-substitution can be described by a slim-shaped,

saturated double-hysteresis loop extending over a broad range of field. On the other hand, the curve of the sample with Barium-substitution only showed a ferroelectric hysteresis loop with a coercive field of ~2kV/mm. The curve of the substitution-pair revealed a remarkably slim antiferroelectric double-hysteresis with nearly the same high saturation polarization as the Tin-substitution in the sample. A reduction of the forward switching field compared to the sample containing Tin only occurred. The backward switching field remained unchanged. This effect of Tin could be used to reduce hysteretic losses.

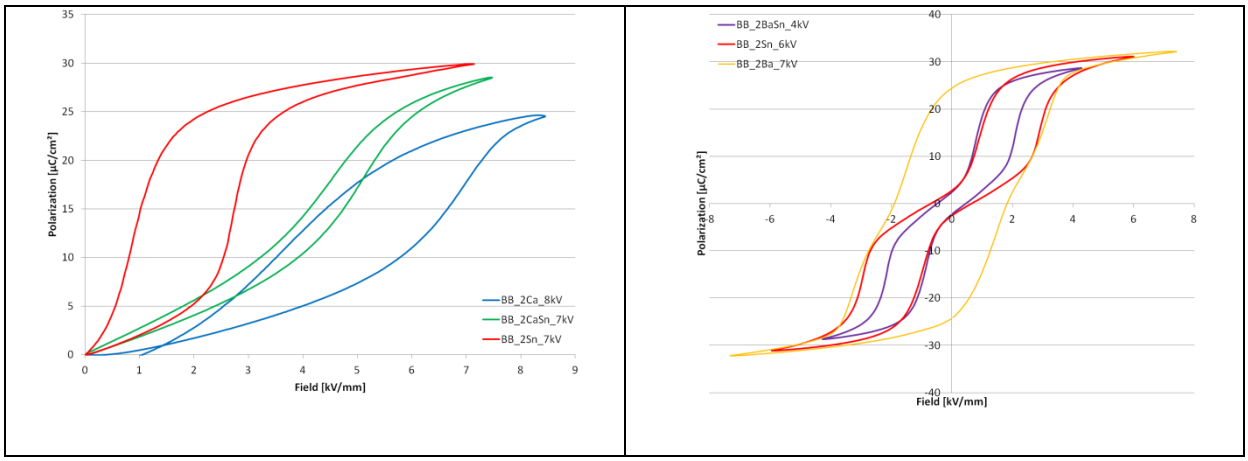

Figure 7.5-26: Comparison of the effects of the substituents Calcium, Barium and Tin and the substitution-pairs Calcium-Stannate and Barium-Stannate on the hysteresis curves.

7.5.3.3 Summary

Insertion of Tin at the B-site and of Calcium or Barium at the A-site led to a pure perovskite phase without secondary phases. At a certain concentration of the substitution-pairs the cell changed from orthorhombic to rhombohedral structure. This correlated to the same structural conversion observed in the samples with the equal concentration of the A-site substituent. Therefore it can be assumed that the structural conversion is induced by the A-site substitution.

Concerning the dielectric response of these samples, an averaging of the effects of the two substituents used in the substitution-pair occurred when both are inserted into the system. These effects correlated to the ionic size: smaller ions – no matter replacing an ion at A-site or B-site – decreased relative permittivity and vice versa. That ion, which changes the volume of the very own site in a higher extent, determines the trend of the relative permittivity change.

Regarding the effect of the substitution-pairs on the polarization curves a remarkable effect was observed. The substitution with Tin stabilized the antiferroelectric phase even in combination with Barium which substitution showed the opposed behaviour. In the case of co-substitution of Calcium and Tin an extreme slimming effect of the hysteresis curves was evident, which could not be reached with either of the substituent on its own. At higher content of the substitution-pair the shape of the

curve was not antiferroelectric anymore but approached a paraelectric shape. Further investigations are required to determine the mechanism of coinciding effects of these ions on the hysteresis curve.

Overall, not only the combination of various ions at the A-site (see chapter of complex doping at A-site) but also a co-substitution at the B-site with Tin lead to an averaging result in dielectric behaviour.

8 Summary

In this chapter a summary of the structural and dielectric properties is given.

8.1 Symmetry versus tolerance factor

It was shown, that the orthorhombic structure is crucial to display antiferroelectric behaviour and show double hysteresis curve. According to the literature, the tolerance factor is used to declare if a composition can form the perovskite structure and if it is an antiferroelectric material. Ranges of the tolerance factor for antiferroelectric and ferroelectric materials are listed[9],[51],[62] and correlations of the dielectric properties with the tolerance factor were found[56]. In this study, many substitution concepts were investigated and tried to correlate the phase stability to the tolerance factor, but that clear correlation could not be confirmed as in the cited references.

8.1.1 Substitution of Lead with trivalent ions

Substitution of Lead with Lanthanum revealed compositions with varying tolerance factor and structure. Consulting the phase diagram of PLZT[21], by increasing substitution of Lanthanum a change from rhombohedral to orthorhombic to mixed phase occurs. At low concentration, the size effect comes into play: The smaller La^{3+} cation takes an off-centre position, changes the B-O distances, distorts the lattice and thus stabilizes a more disordered structure[60],[63],[68]. At higher concentration the increased ionic interaction of the A-site cation and the oxygen due to an insertion of a trivalent ion dominates favouring a higher symmetry, such as the rhombohedral structure[66].

In Figure 8.1-1 the ratio of the lattice constant c and a are plotted against the tolerance factor. The ratio of c to a of 2.4 indicates a rhombohedral structure, whereas 1.4 refers to an orthorhombic structure. Over the whole examined range of the tolerance factor both structures – the orthorhombic and the rhombohedral structure - are stable. It can be seen that the conversion from rhombohedral to orthorhombic structure depends on the ratio of Zirconium to Titanium. Compositions with higher Titanium content possess a higher tolerance factor. The concentration of the smaller A-site cation has to be higher compared to the Zirconium-rich composition to induce a change to the orthorhombic structure.

Regarding the unit cell, Titanium displays a higher off-centring compared to the bigger Zirconium[132] . The higher the off-centring of the B-site cation, the more rigid is the unit cell. Therefore a higher concentration of a smaller ion is demanded to induce a distortion of the lattice (Figure 8.1-1).

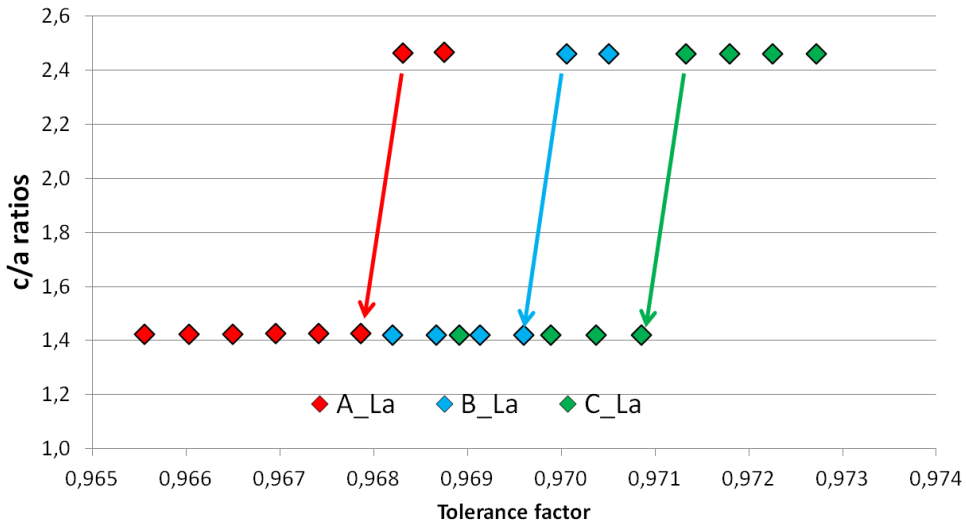

Figure 8.1-1: c/a ratio versus tolerance factor of Lanthanum substitution in PZT (A=$PbZr_{0.9}Ti_{0.1}O_3$, B $PbZr_{0.85}Ti_{0.15}O_3$ and C=$PbZr_{0.80}Ti_{0.20}O_3$); c/a~2.4 indicates a rhombohedral structure, c/a~1.4 an orthorhombic structure.

In contrast to Lanthanum, the substitution of Lead with the trivalent Bismuth could not transform the lattice into orthorhombic structure. This might be due to the solubility limit. Bismuth assembles Lead in electronic structure and weight, but the small deviation in size compared to Lanthanum could not induce a conversion. Though, Bismuth possesses a stereochemically active $6s^2$ orbital, a lone pair, which would induce off-centring, change the bonding length A-O and would distort the structure[91]. Therefore, it cannot be excluded that with higher grade of incorporation of Bismuth a change in structure could occur.

By co-substitution with either Lanthanum or Lanthanum and Sodium, the solubility of Bismuth increased, less secondary phases appeared and orthorhombic structure was stabilized (Figure 8.1-2).

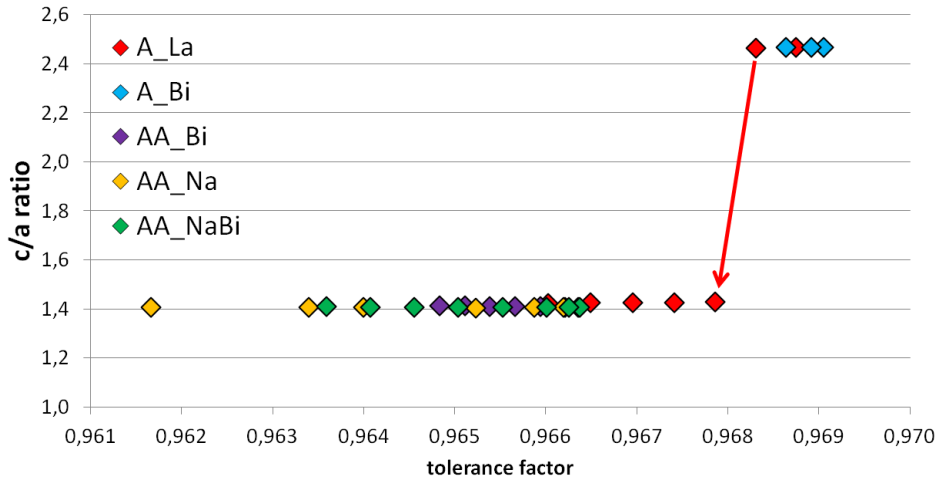

Figure 8.1-2: c/a ratio versus tolerance factor of Lanthanum, Bismuth and substitution in PZT and PLZT (A=PbZr0.9Ti0.1O3, AA=Pb0.91La0.06Zr0.9Ti0.1O3); c/a~2.4 indicates a rhombohedral structure, c/a~1.4 an orthorhombic structure

8.1.2 Substitution of Lead with monovalent ions

Consulting the structural change by the substitution of Lead with monovalent ions such as Li^+, Na^+ and K^+ no explicit trend can be detected, especially in the case of Lithium. Therefore only the results of the substitution with Sodium and Potassium are shown in Figure 8.1-3,

Sodium behaves straight forward as a smaller substituent which changes the structure by reducing the bond-length of B-O and deforming the lattice. The substitution of Lead with Sodium in the composition CC induced a phase transition at a tolerance factor around 0.97.

Potassium, on the other hand, could stabilize orthorhombic structure even at higher tolerance factors (Figure 8.1-3). There is no simple explanation for this behaviour and it contradicts the common assumptions[56]. The bigger ionic size as well as the higher ionic interaction between A-site ion and oxygen should lead to a more ordered structure, viz the rhombohedral structure[60],[63],[66],[67],[120]

To stabilize the rhombohedral structure, the Madelung energy has to be the structure determining force and outweight the covalency of A-site and oxygen. In the case of the monovalent Potassium, this might not happen, due to the lower Coloumb-interaction of the participating ions[66] and the orthorhombic structure was stabilized.

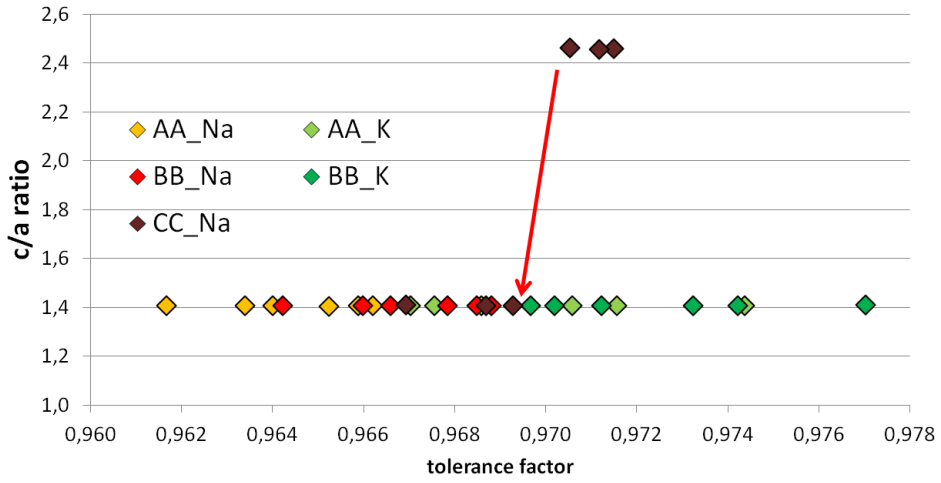

Figure 8.1-3: c/a ratio versus tolerance factor of alkaline substitution in PLZT (AA=Pb0.91La0.06Zr0.9Ti0.1O3, BB=Pb0.91La0.06Zr0.85Ti0.15O3 and CC= Pb0.91La0.06Zr0.80Ti0.20O3); c/a~2.4 indicates a rhombohedral structure, c/a~1.4 an orthorhombic structure

8.1.3 Substitution of Lead with isovalent ions

In Figure 8.1-4, the structural change due to the substitution of Lead with isovalent ions is demonstrated. The rhombohedral structure transforms to orthorhombic at a tolerance factor of around 0.971 and back again at around 0.965. Additionally, outliers at 0.968 exist.

Calcium shows a complex relationship of different effects, which determine the structure. As a smaller ion, Calcium stabilizes the orthorhombic structure similar to La^{3+} outlined in Figure 8.1-1. But at a certain value, the off-centring of the ion changes the nature of the bonds between A-site and B-site with oxygen, which promotes a rectification of the lattice and stabilizes the rhombohedral structure[60],[63],[66],[67],[120]. Strontium assembles Lead in size and is known to stabilize the orthorhombic structure[118]. The increase in the ion-ion repulsion which is caused by the substitution with a bigger ion like Barium results in a change to a more ordered structure[63],[66].

Interestingly, the combination of Barium with a smaller B-site substituent like Tin for Zirconium, which stabilizes the orthorhombic structure, showed similar behaviour. At higher concentration of Bariumstannate a structural change to rhombohedral structure occurred.

Inserting Calciumstannate into the PLZT-system also induced a change to rhombohedral structure at higher concentration. A complex interaction of both effects was observed, where the A-site substituent seems to dominate over that at the B-site.

The combination of Calcium and Barium at A-site resulted in a structural change to rhombohedral symmetry. This might be due to an interdependent stabilization effect of the rhombohedral structure caused by different reasons.

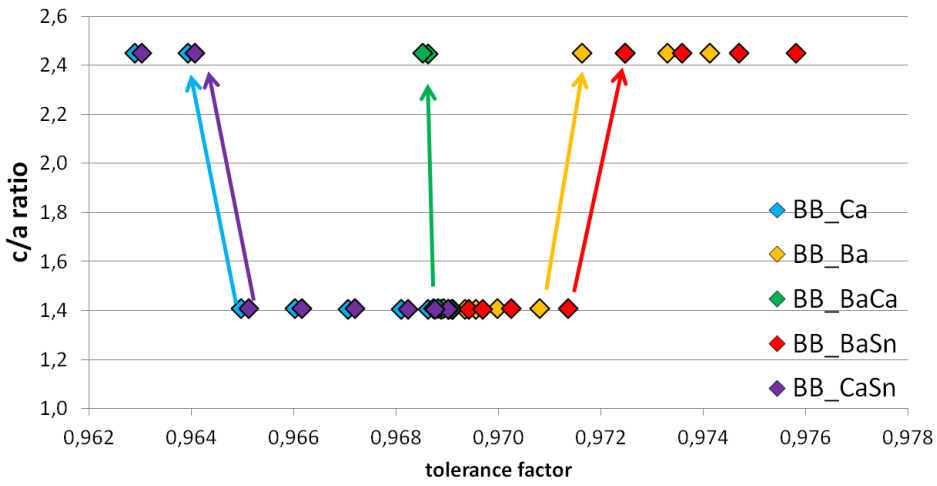

Figure 8.1-4:c/a ratio versus tolerance factor of earth alkaline and earth alkaline-stannate substitution in PLZT (BB=$Pb_{0.91}La_{0.06}Zr_{0.85}Ti_{0.15}O_3$); c/a~2.4 indicates a rhombohedral structure, c/a~1.4 an orthorhombic structure

8.2 Stabilizing the antiferroelectric phase

According to the literature A-site ions with lower electronegativity than Lead (2.33)[85] stabilize antiferroelectric behaviour. Although all A-site substituents in this study would meet this condition, not in all cases an orthorhombic phase or antiferroelectric behaviour was detected[71].

Considering the substitution of Titanium on B-site, electronegativity decreases with Zirconium, while with Tin an increase occurs. Interestingly, both B-site substituents stabilize the orthorhombic antiferroelectric phase.

No linear trend was observed regarding the change in polarizability of the substituent. In the case of Titanium-substitution, Zirconium has a higher polarizability, whereas with the substitution with Tin an ion with lower polarizability is located at B-site. All A-site substituents have lower polarizability than Lead, but not all induced antiferroelectric behaviour[81].

Considering the parameters a substituent might influence, a summary was done regarding the stability of the antiferroelectric phase. In Figure 8.2-1 to Figure 8.2-5 the parameters are summarized.

The Bismuth assembles Lead in ionic radius, atomic weight, electronegativity and polarizability (r_{Pb}=1.49Å, r_{Bi}=1.45Å ; m_{Pb}=207.02 g/mol, m_{Bi}=208.98 g/mol, electronegativity: Pb=2.33, Bi=2.02, polarizability: Pb=6.58 Å³, Bi=6.4 Å³). Regarding the valency Bismuth can be compared to Lanthanum (r_{La}=1.36Å, m_{La}=138.906 g/mol, electronegativity: 1.1, polarizability: 6.07 Å³). As Lanthanum stabilizes the antiferroelectric phase, it can be concluded that a substituent which is smaller in size, lighter and has a lower electronegativity is favourable.

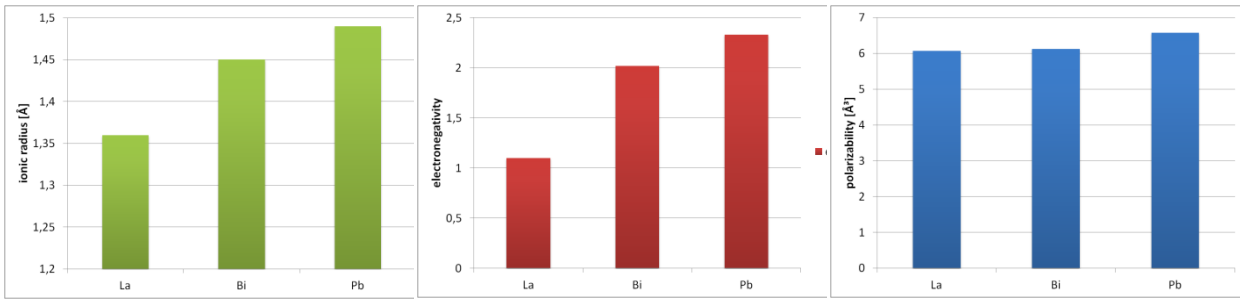

Figure 8.2-1: Comparison of ionic radius, electronegativity and polarizability the aliovalent Lanthanum and Bismuth with Lead.

In the case of isovalent substituents with Calcium, Strontium and Barium, the electronegativity is nearly halve that of Lead (Pb: 2.33, Ca:1, Sr: 0.95, Ba: 0.89). However, the ionic radius (r_{Ca}=1.34 Å, $r_{Sr=}$=1.44 Å, r_{Ba}=1.64 Å), the atomic weight (m_{Ca}= 40.078 g/mol, m_{Sr}=87.906 g/mol ,

m_{Ba}=137.327 g/mol) and the polarizability (Ca: 3.16 Å³, Sr: 4.24 Å³, Ba: 6.4 Å³) increase in the row Calcium, Strontium and Barium. As Calcium increased the stability range of the antiferroelectric phase over field in the highest extent, it can be concluded that small ionic radius, low atomic weight, low electronegativity and also low polarizability tend to stabilize the antiferroelectric phase.

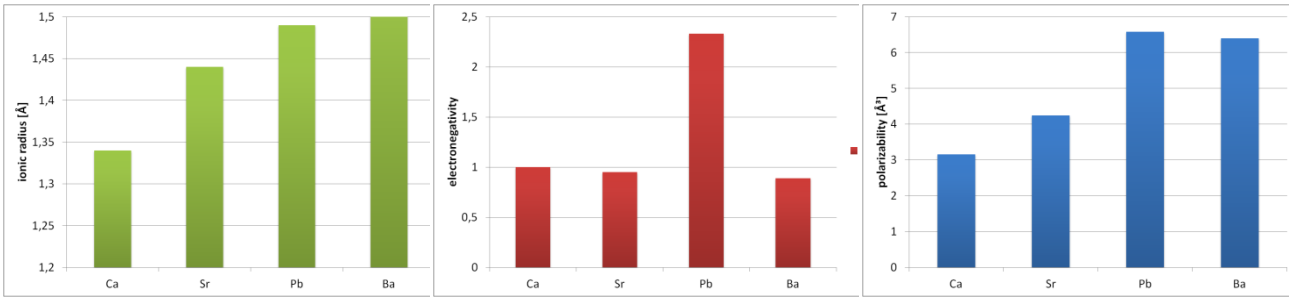

Figure 8.2-2: Comparison of electronegativity, polarizability, ionic radius and valency of the isovalent Calcium, Strontium, Lead and Barium (Calcium and Strontium stabilize the antiferroelectric phase, Barium stabilizes the ferroelectric phase).

Comparing trivalent Lanthanum, divalent Calcium and monovalent Sodium, which all stabilize the antiferroelectric phase, the ionic radii and the electronegativity are similar, whereas the polarizability decimates from 6.07 to 1.8 in that row (La: 6.07 Å³, Ca: 3.16 Å³, Na:1.8 Å³). Interestingly, the ionic size of Sodium is the highest of these three substituents (r_{La}=1.36 Å, r_{Ca}=1.34 Å, r_{Na}=1.39 Å), and possesses the lowest atomic weight (m_{La}=138.91 g/mol, m_{Ca}=40.078 g/mol, m_{Na}=22.99 g/mol). A reduction in valency combined with a reduction in atomic weight and polarizability, obviously balances a slight increase in ionic radius and the composition remains antiferroelectric.

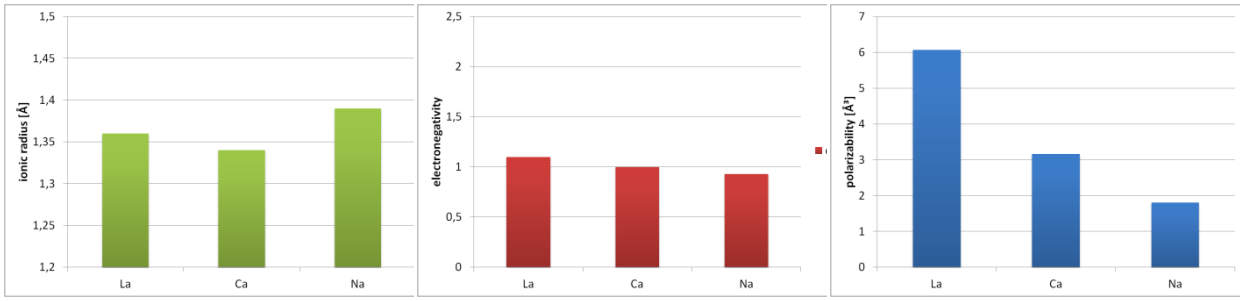

Figure 8.2-3: Comparison of electronegativity, polarizability, ionic radius and valency of trivalent Lanthanum, divalent Calcium and monovalent Sodium (all substituents stabilize the antiferroelectric phase).

In the case of the substitutents bigger than Lead, Barium and Potassium, Potassium stabilizes the antiferroelectric phase, whereas Barium favours the ferroelectric phase. Although Potassium exceeds the size of Barium (r_{Ba}=1.61 Å, r_K=1.64 Å), the lower atomic weight (m_{Ba}=137.327 g/mol, m_K=39.098 g/mol) the reduced valency and the lower polarizability (Ba: 6.4 Å³, K: 3.83 Å³) overrule the size effect on the stability of the antiferroelectric phase.

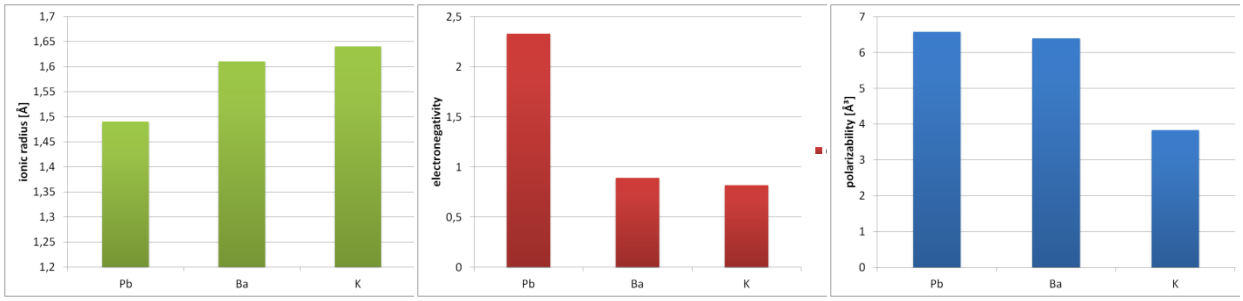

Figure 8.2-4: Comparison of electronegativity, polarizability, ionic radius and valency of Lead with isovalent Barium and aliovalent Potassium (Potassium stabilizes the antiferroelectric phase).

The substitution on B-site of Zirconium with Tin showed a stabilization of the antiferroelectric phase over field. In the starting composition PZT, Lead Zirconate is known as the antiferroelectric material and Lead Titanate as the ferroelectric material.

Comparing Titanium and Zirconium, Titanium is smaller, lighter, has smaller polarizability and higher electronegativity as Zirconium (r_{Ti}=0.605 Å, r_{Zr}=0.72 Å, m_{Ti}=47.867 g/mol, m_{Zr}=91.224 g/mol, polarizability: Ti: 2.93 Å³, Zr: 3.25 Å³, electronegativity: Ti: 1.54, Zr: 1.33). The isovalent substituent of Zirconium, Tin, assembles Zirconium in size and has the lowest polarizability and the highest electronegativity of all these three B-site cations (r_{Sn}=0.69 Å, polarizability: 2.83 Å³, electronegativity: 1.96). Tin stabilizes the antiferroelectric phase, but no linear trend can be determined out of the three parameters. Regarding the atomic weight, it increases in the row Titanium-Zirconium-Tin (m_{Ti}=47.867 g/mol, m_{Zr}=91.224 g/mol, m_{Sn}=118.71 g/mol) and might correlate to the increasing stability of the antiferroelectric phase. Though, in the study of substituting Zirconium with the isovalent Hafnium (m_{Hf}=178.49 g/mol), no confirmation of this correlation was found, i.e. the switching field remains unchanged with increasing Hafnium content[133].

The only difference of the three ions, Tin, Zirconium and Titanium, is the electronic configuration of these ions. The latter two ions are d^0-ions and the former possesses a fully occupied d^{10}-orbital. This might explain the increased stabilization effect of the antiferroelectric phase by Tin compared to Zirconium.

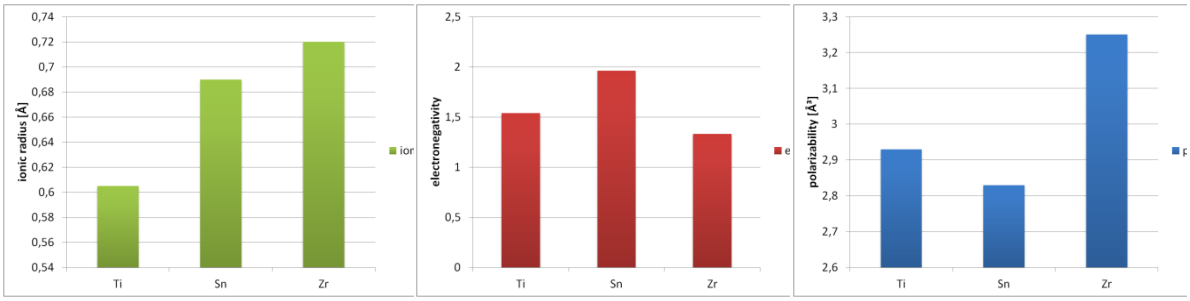

Figure 8.2-5: Comparison of electronegativity, polarizability, ionic radius and valency of Tin with Titanium and Zirconium (Titanium stabilizes the ferroelectric phase, Tin and Zirconium stabilize the antiferroelectric phase).

To sum up, small ionic radius, low atomic weight, low vacancy, low electronegativity and low polarizability of a substituent increase the stability of the antiferroelectric phase. A combination effect of ionic size, electronegativity and polarizability was found: If the ionic size of the A-cation is small and the electronegativity is low, a higher polarizability is tolerated in the antiferroelectric structure. In reverse, if the electronegativity is low as well as the polarizability of the A-cation, a bigger ionic size still forms the orthorhombic structure and shows antiferroelectric behaviour. In the case of the B-site cation, further investigations have to be done to clarify the picture and to enlighten the d^{10}-effect.

8.3 Dielectric properties versus tolerance factor

The relationship between structure and property can be demonstrated by plotting dielectric properties versus the tolerance factor. This was done before and was identified as a useful method to estimate the effect of the substituents on dielectric properties[56],[134].

8.3.1 Low signal relative permittivity:

The low signal relative permittivity was measured for all samples at room temperature. It was observed that the values for the increase with Titanium content were higher in comparison to the Zirconium-rich compositions. Furthermore, it was suggested to correlate the radius with the dielectric signal. As the samples were not only substituted at the A-site, but also at the B-site, the tolerance factor was used to follow the variation of the relative permittivity.

The effects of acceptor ions at A-site, as the alkaline ions are, only slightly changed the relative permittivity as shown in Figure 8.3-1a. With the substitution of Lead with isovalent ions a stronger correlation of relative permittivity to the tolerance factor can be observed (Figure 8.3-1b).

Overall, compositions with a higher tolerance factor demonstrated a higher value of relative permittivity.

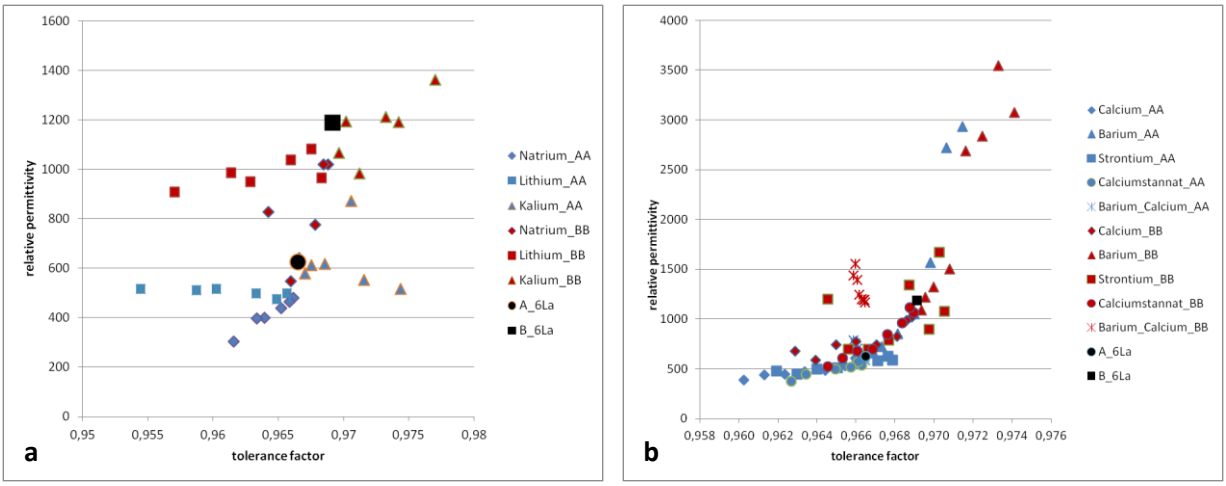

Figure 8.3-1: Low signal relative permittivity over tolerance factor for alkaline-doped and earth-alkaline doped PLZT (A=$PbZr_{0.9}Ti_{0.1}O_3$, B= $PbZr_{0.85}Ti_{0.15}O_3$, AA=$Pb_{0.91}La_{0.06}Zr_{0.9}Ti_{0.1}O_3$ and BB=$Pb_{0.91}La_{0.06}Zr_{0.85}Ti_{0.15}O_3$).

8.3.2 Relative permittivity versus temperature:

Measuring the relative permittivity as function of the temperature revealed maxima in the curve, which indicates the transition temperatures between the antiferroelectric and the paraelectric phase. The shift in height and in the position of the peak were tried to put into correlation to the substitution. Nearly all substituents reduced relative permittivity as well as the transition temperature.

In Figure 8.3-2a the maximum values of the relative permittivity was plotted over the molar ratio of the dopants. Interestingly, except of the substitution of Lead with Barium and in some extent also with Potassium all insertion of dopants led to a decrease in relative permittivity. The difference of these two ions to the other ions is the larger ionic size compared to Lead. Comparing the degree of the increase, Barium showed a higher impact on the relative permittivity than Potassium. This might be due to the higher atomic mass in the case of Barium.

In sum, the size of the substituent influences the trend of the relative permittivity.

Regarding the influence on the transition temperature T_m (temperature of maximum permittivity) in Figure 8.3-2b, the substitution of Lead decreased it nearly in all cases. The change of the transition temperature might be a more complex interaction of atomic weight and ionic radius of the substituent.

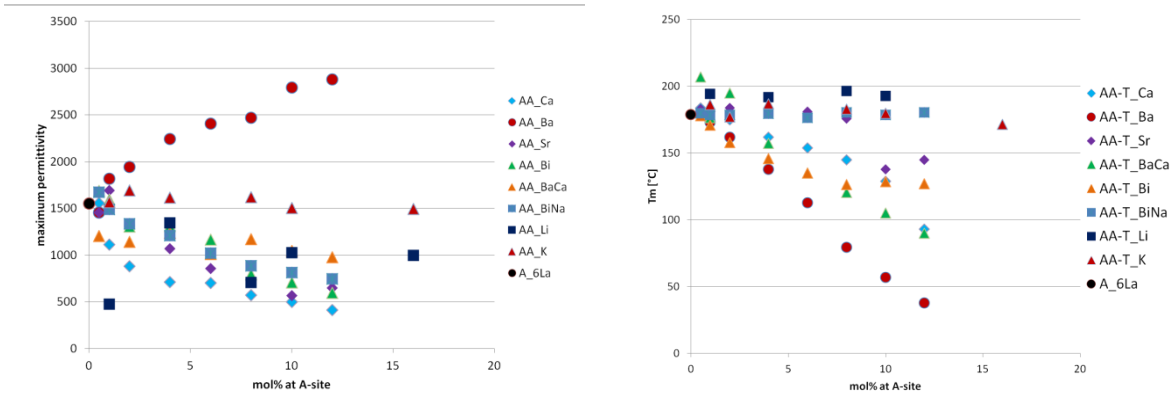

a **b**

Figure 8.3-2: Influence of the molar ratio of a dopant at the A-site on the height of relative permittivity curve and on transition temperature (A=$PbZr_{0.9}Ti_{0.1}O_3$, B= $PbZr_{0.85}Ti_{0.15}O_3$, AA=$Pb_{0.91}La_{0.06}Zr_{0.9}Ti_{0.1}O_3$).

The transition temperature of the starting compositions BB and AA cannot be exceeded by the addition of doping agents. As it is obvious from the above, every disturbance of the lattice of PZT resulted in a shift of the transition temperature to lower levels. Thereby, it was not important if the radius of the substituent is bigger (Barium), smaller (Calcium, Strontium) or nearly equal to Lead (co-substitution with Calcium and Barium). But the decrease was slightly higher in the case of Barium and Bismuth (Figure 8.3-3). This might be due to the mass. The constant level of T_m for higher nominal doping levels of Bismuth indicates the solubility limit of about 4 mol%.

In Figure 8.3-4the influence of the mean mass at the A-site on the temperature shift is presented. Mass and ionic radii are not independent from each other and therefore interfering effects are possible. It can be assumed, that an increase in mass led to an increase in transition temperature. In the case of Bismuth, the complexity of radius and weight is displayed. With increasing doping-content a decrease of the transition temperature occurred although the mass is nearly equal to that of Lead.

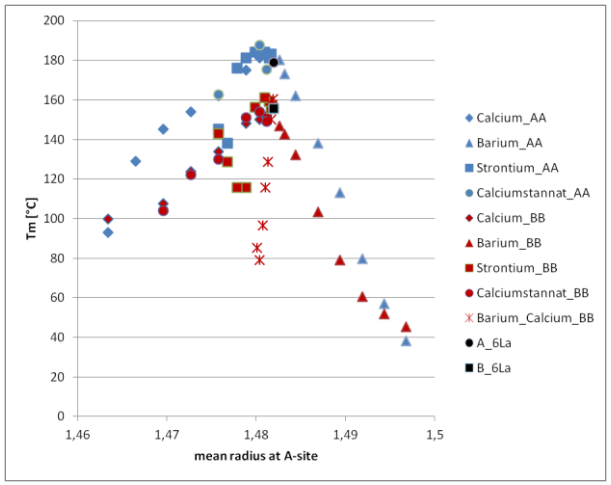

Figure 8.3-3:Correlation with the mean radius at A-site and the transition temperature Tm.

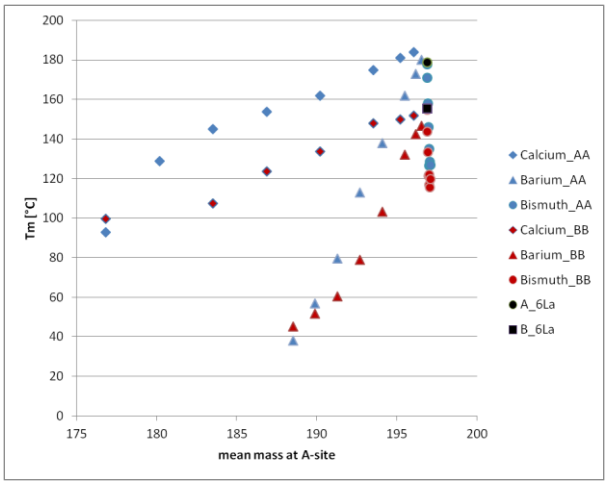

Figure 8.3-4: Correlation with the mean mass at A-site and the transition temperature Tm.

(A=$PbZr_{0.9}Ti_{0.1}O_3$, B= $PbZr_{0.85}Ti_{0.15}O_3$, AA=$Pb_{0.91}La_{0.06}Zr_{0.9}Ti_{0.1}O_3$ and BB=$Pb_{0.91}La_{0.06}Zr_{0.85}Ti_{0.15}O_3$)

Considering the substitution at A- and the B-site, the relative permittivity was plotted versus the tolerance factor. A trend to higher relative permittivity with higher tolerance factor is visible in Figure 8.3-5.

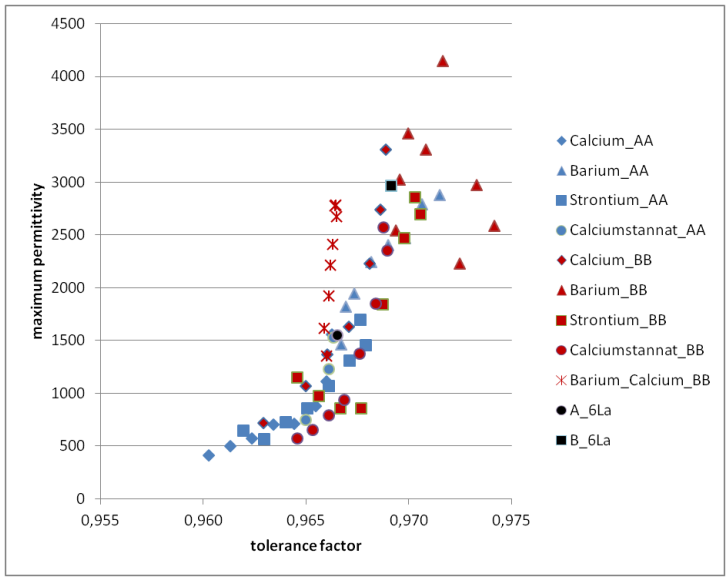

Figure 8.3-5: Correlation of relative permittivity obtained by the maxima of the dielectric response versus temperature and the tolerance factor (A=$PbZr_{0.9}Ti_{0.1}O_3$, B= $PbZr_{0.85}Ti_{0.15}O_3$, AA=$Pb_{0.91}La_{0.06}Zr_{0.9}Ti_{0.1}O_3$ and BB= $Pb_{0.91}La_{0.06}Zr_{0.85}Ti_{0.15}O_3$).

8.3.3 Polarization curves – forward switching field versus tolerance factor

Gachighi[87] has investigated the dependence of the switching fields on the tolerance factor in Lanthanum and Calcium-doped Lead Zirconate-Lead Titanate. The results can be seen in Figure 8.3-6. A linear trend is visible, where a shift to higher switching field is achieved by a lower tolerance factor.

In Figure 8.3-7a and c, the influences of the alkaline ion doping on forward switching and backward switching field are presented as function of the tolerance. A general trend was not found due to the substitution with Potassium and Lithium.

A more distinct tendency was observed in the case of the isovalent dopants (Figure 8.3-7b and d). Higher switching fields were achieved with smaller tolerance factors. In the study of Gachighi this was done by substituting Lead with Lanthanum.

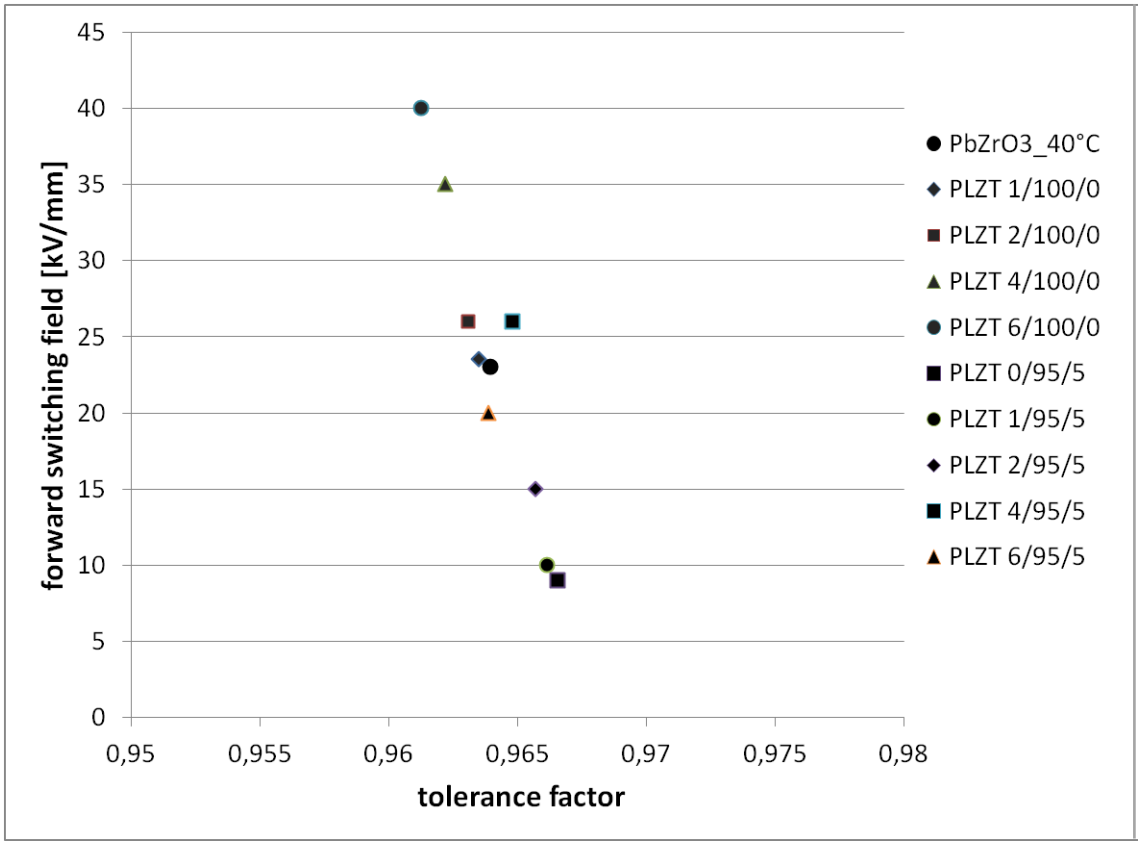

Figure 8.3-6: Correlation of the forward switching field and the tolerance factor of Lanthanum-substitution in various PZT samples ($PLa_xZr_yTi_zO_3$ is labelled as PLZT x/y/z) from Gachighi.

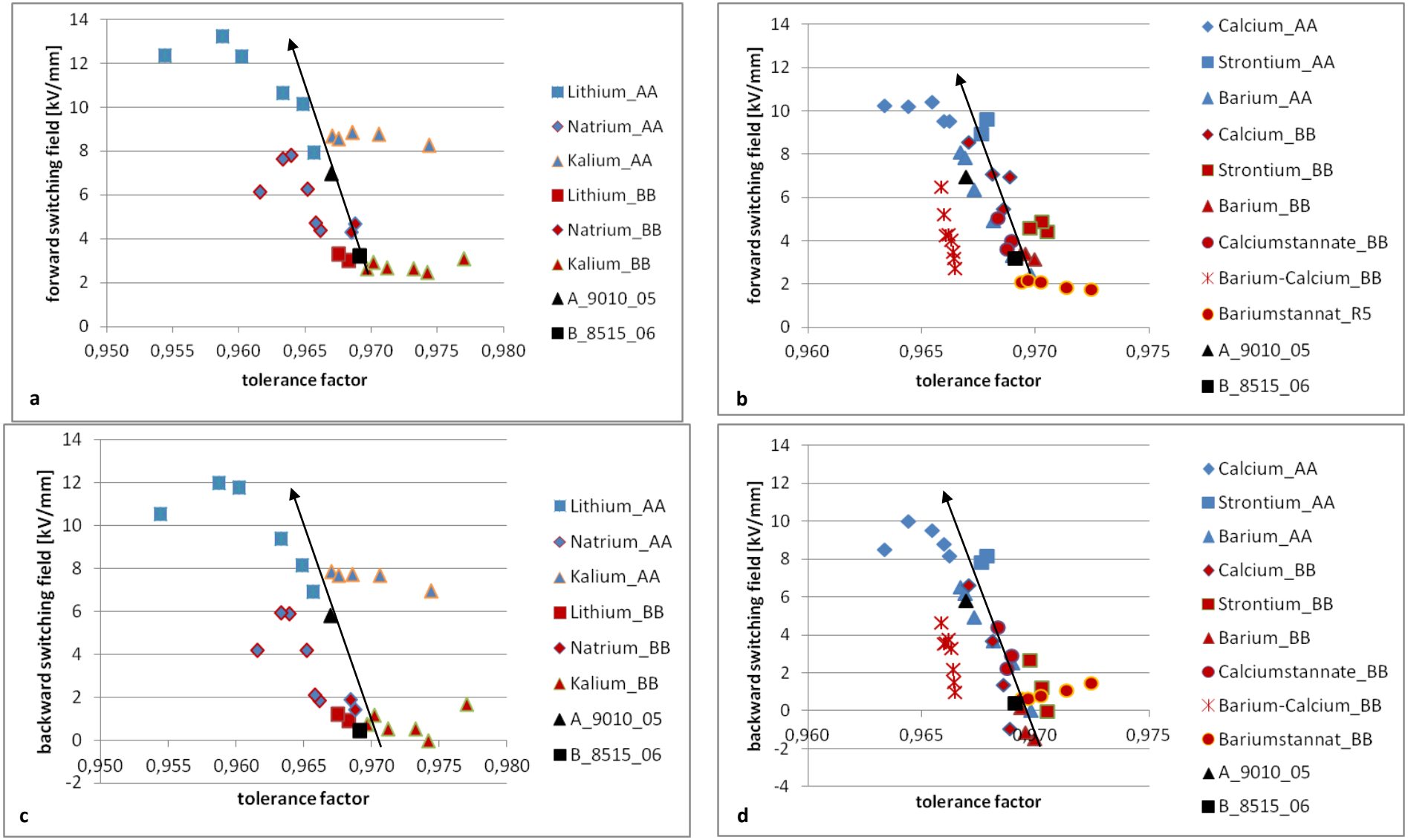

Figure 8.3-7: Correlation of the switching fields and the tolerance factor (A_90_10_06 and AA=$Pb_{0.91}La_{0.06}Zr_{0.9}Ti_{0.1}O_3$ and B_85_15_06 and BB= $Pb_{0.91}La_{0.06}Zr_{0.85}Ti_{0.15}O_3$).

8.3.4 Polarization curves – forward switching field versus average atomic weight at A-site

As the antiferroelectric to ferroelectric phase transition is claimed to be a phonon process, the effect of the atomic weight on the stability of the antiferroelectric phase was examined. By plotting the forward switching field against the average atomic weight at A-site, a lower average atomic weight seems to increase the forward switching field and thus increase the stability range of the antiferroelectric phase. But the trend is not so clear as was shown with the tolerance factor and there are some severe deviations: The substitution of Lead with a bigger monovalent Potassium did not influence the forward switching field over a broad range of average atomic weight (green dots in Figure 8.3-8 and in Figure 8.3-9). In the case of a bigger isovalent ion, Barium, the forward switching field even decreases linearly with average atomic weight (grey squares in Figure 8.3-8 and in Figure 8.3-9).

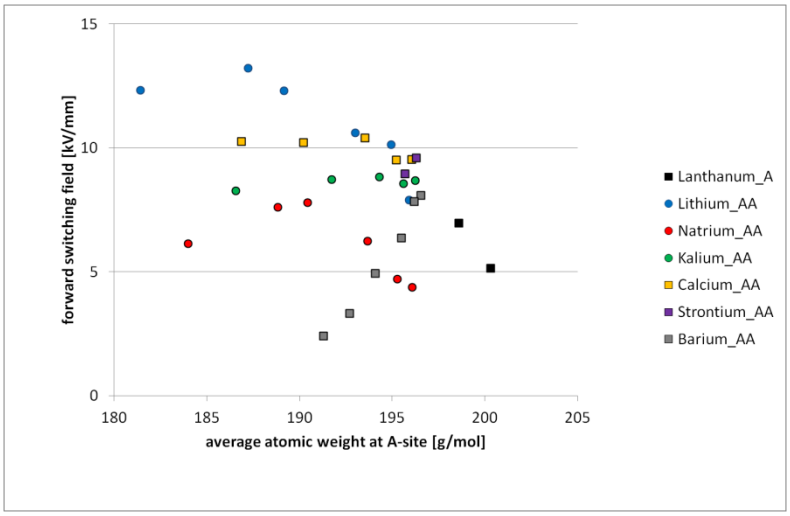

Figure 8.3-8: Forward switching field versus average atomic weight at A-site for the compositions with a molar ratio of 90 to 10 Zirconium to Titanium.

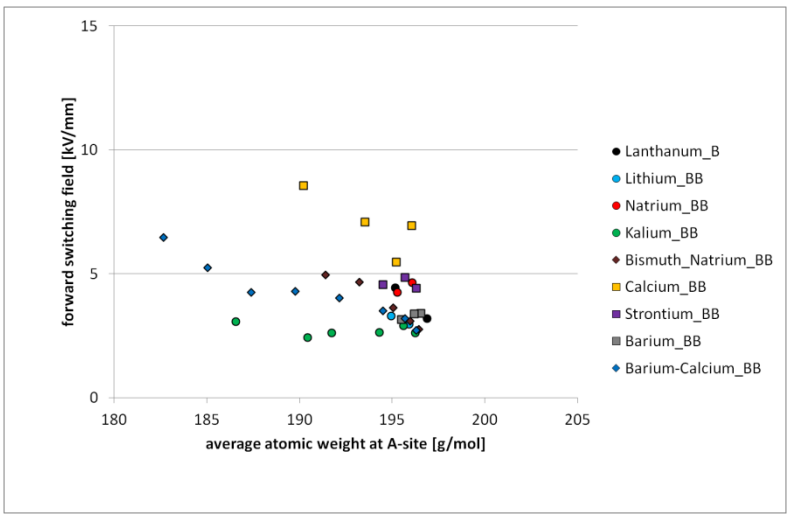

Figure 8.3-9: Forward switching field versus average atomic weight at A-site for the compositions with a molar ratio of 85 to 15 Zirconium to Titanium.

9 Conclusions

In this study the structure property relationship was confirmed for the correlation of orthorhombic structure and antiferroelectric behaviour in PLZT. Furthermore, the higher the Zirconium-content or the lower the displacement of the B-site cation, the higher is the stabilization of orthorhombic structure also with substitution on A-site.

Some parameters, which were claimed to favour the antiferroelectric phase have to be revisited:

Orthorhombic structure

Zirconium rich compositions tend to stabilize orthorhombic structure, whereas Titanium-rich compositions tend to stabilize rhombohedral structure. The orthorhombic structure can be claimed as necessary but not sufficient requirement for the formation of antiferroelectric phase. The antiferroelectric behaviour might only be detected at elevated temperature as it was in the case of 3 mol% Lanthanum substitution in $PbZr_{0,9}Ti_{0.1}O_3$, which has orthorhombic structure at room temperature but exhibits ferroelectric polarization.

Ionic size

Reduction in ionic size favours the orthorhombic antiferroelectric phase, but there are structural limitations regardless of the valency of the substituent. Inserting trivalent Bismuth in PLZT could not stabilize the orthorhombic phase due to solubility limit whereas the divalent Calcium induced a change from orthorhombic to rhombohedral structure at higher concentration. Average ionic size could not be consulted considering structural changes like it was shown with the co-substitution of Barium and Calcium. Regarding the stability of the antiferroelectric phase over field, smaller ions tend to increase the forward switching field. However, the substitution with Potassium, an ion bigger than Lead, showed antiferroelectric behaviour even at high substituent content.

Atomic weight

Lighter ions tend to stabilize the antiferroelectric phase over electric field, but this was not shown in the case of Barium (lighter than Lead, but bigger in size). Furthermore this effect cannot be completely be distinguished from the size effect.

Number of A-site vacancy

The occurrence or variation in the number of A-site vacancies did not show any effect on the stabilization of the antiferroelectric phase. In contrast to Lanthanum, the trivalent Bismuth generating the same amount of A-site vacancies could not induce orthorhombic or antiferroelectric phase. On the other hand, substitution of Lead with monovalent and divalent ions could increase the forward switching field (which indicates the stabilization of antiferroelectric phase).

Lone pair effect

Stereochemically active orbitals might induce the antiferroelectric phase, but it was not proven as requirement.

Dielectric polarizability

No consistent trend was observed regarding the change in polarizability of the substituent. It is supposed that a lower polarizability on A-site might induce antiferroelectric phase, but this was not proven generally.

Electronegativity of the ion

No linear correlation of the structure or dielectric behaviour with the electronegativity was detected. Some authors state that lowering the electronegativity promotes antiferroelectric phase, but this is a simplification. It was shown that there is a dependency of the ionic radius, the polarizability and the electronegativity regarding the stabilization of the antiferroelectric phase. If the polarizability is high, the two other parameters have to be low to keep the material antiferroelectric. In the case of low electronegativity and polarizability the antiferroelectric phase tolerates a bigger ionic radius.

d^{10}-orbital effect

The stabilization of the antiferroelectric phase over field by substituting Zirconium with Tin could not be explained by the parameters of the substituent mentioned above. The only difference of Zirconium, Titanium and Tin, which might explain this effect, lies in the electronic configuration of the ions -the fully occupied d-orbital of Tin.

Regarding the change of the structure of PLZT in the different doping systems, it was shown, that the stabilization effects of the different structures are interdependent and it is impossible to give a simple explanation. As mentioned above the orthorhombic structure is a necessary, but not sufficient condition to stabilize antiferroelectric state. Rhombohedral structure on the other hand is claimed to stabilize the ferroelectric phase.

Concerning the dielectric properties, some assumptions can be summarized as follows:

A decrease of the transition temperature occurs by any substitution of A- or B-site cation in PLZT as was shown in the summary in chapter 8.

A smaller ion either on A- or on B-site decreases relative permittivity, whereas a bigger ion increases relative permittivity. In the case of Potassium and Barium the relative permittivity increased, whereas with all other substituents the reverse effect occurred. Regarding co-substitution an averaging of both effects occurs. This was shown by the compositions containing substitution pair Bismuth-Sodium, Barium-Calcium, Bariumstannate and Calciumstannate.

A combination effect on the polarization curves occurs resulting in an exceeding behaviour of co-substitution. This was shown in the case of Bariumstannate and Calciumstannate. Both stannates induced higher switching fields and a slim hysteresis curve.

The dominance of the A-site substitution regarding the structural properties and the dielectric parameters was detected. Although Tin stabilizes the orthorhombic phase in PLZT, the insertion of Barium-Stannate and Calciumstannate in PLZT induces a change to rhombohedral structure at high concentration. This structural change also occurs with high concentration of either Barium or Calcium

The subsumed structure-property relationship in this study can be used to tailor antiferroelectric material purposefully and to broaden the potential application range.

10 References

[1] Setter, N. Piezoelectric Materials in Devices, ed. N. Setter, EPFL Swiss Federal Institute of Technology, Switzer-

[2] Moon, R. L. High Temperature Phase Equilibria in the Lead Titanate-Lead Zirconate System.Ph.D. Thesis, University of California. Berkelev. 1967; Tech. Rept. UCRL-17545, " I 85'p., May 1967.

[3]Fushimi, S. Ikeda,T. Phase Equilibrium in the System PbO-TiO2-ZrO2. Journal of The American Ceramic Society 1967; 50 (3) 129-32.

[4] Atkin, R.B. Fulrath, R.M. Point Defects and Sintering of Lead Zirconate-Titanate. *Journal of The American Ce*ramic Society 1971; 54 (5) 265-270.

[5] Ishibashi, Y. Iwata, M. Morphotrophic Phase Boundary in Solid Solution System of Perovsktie-Type Oxide Ferroelectrics. *Japanes Journal of Applied Physics* 1998; 37 L985-L987.

[6] Damjanovic, D. A morphotrophic phase boundary system based on polarization rotation and polarization extension. *Applied Physics Letter* 2010; 97 062906.

[7] Cao, W. Cross, L.E. Theoretical model for the morphotropic phase boundary in lead zirconat-lead titanate solid solution. *Physical Review B* 1993, 47, 4825.

[8] Rao, C.N.R. Rao, K.J. Phase Transitions in Solids: an approach to the study of the chemistry and physics of solids, McGraw-Hill International Book Company, United States of America, 1978.

[9] Jaffe, B. Cook, W. R. Jaffe, H. Piezoelectric Ceramics, Academic Press London, London, 1971.

[10] Vailionis, A. Boschker, H. Siemons, W. Houwman, E.P. Blank, D.H.A. Rijnders, G. Koster G. Misfit Strain Accommodation in Epitaxial O3 Perovskites: Lattice Rotations and Lattice Modulations. *Physical Review* 2011; T 83, 064101.

[11] Geller, S. Bala, V.B. Crystallographic Study of Perovskite-like Compounds. II Rare Earth Aluminates. *Acta Chrystallographica* 1956; 9, 1019-1025.

[12]Hedvall, J. A. Reaktionsfähigkeit fester Stoffe. Verlag Johann Amrosium Barth, Leipzig, 1938.

[13] Rao, C.N.R. Gopalakrishnan, J. New Directions in Solid State Chemistry, Second Edition. Cambridge University Press, Cambridge, 1997.

[14] Fleury, P.A. The effects of soft modes on the structure and properties of materials. *Annual Review of Materials Science* 1976; 6, 157-180.

[15] Buerger, M.J. Phase Transformations in Solids. edited bby R. Smoluchowski, John Wiley, New York, 1957.

[16] I. A. Kornev, L. Bellaiche, P.-E. Janolin, B. Dkhil, E. Suard, Phase Diagram of $Pb(Zr,Ti)O_3$ Solid Solutions from First Principles. *Physical Review Letters* 2006; 97, 157601.

[17] Handerek, J. Ujma, Z. Phase transitions in PZT 95/5 studied by dielectric and pyroelectric measurements: unusual properties in the vicinity of the antiferroelectric-ferroelectric phase transition. Journal *of Physics: Condensed Matter* 1995; 7 1721-1728.

[18] Zhong, W. Vanderbilt, D. Competing Structural Instabilities in Cubic Perovskites. *Physical Review Letters* 1995; 74 (13) 2587-2590.

[19] Breval, E. Wang, C. Dougherty, J. P. Gachighi, K. PLZT Phases Near Lead Zirconate: 1. Determination by X-ray. *Journal of The American Ceramic Society* 2005; 88(2)437-442.

[20] Breval, E. Wang, C. Dougherty, J. P. PLZT Phases Near Lead Zirconate: 2. Determination by Capacitance and Polarization. *Journal of The American Ceramic Society* 2006, 89(12) 3681-3688.

[21] Haertling, G.H. Lang, C.E. Hot-Pressed (Pb,La)(Zr,Ti)O3 Ferroelectric Ceramics for Electrooptic Applications. *Journal of the American Ceramic Society* 1971; 54 (1) 1-11.

[22] Berlincourt, D. Piezoelectric ceramic compositional development. *Journal of Acoustical Society of America* 1992, 91 (5) 3034-3040.

[23] I. A. Kornev, L. Bellaiche, P. Bouvier, P.-E. Janolin, B. Dkhil,J. Kreisel, Ferroelectricity of Perovskites under Pressure. *Physical Review Letters* 2005; 95, 196804.

[24] I. A. Kornev, L. Bellaiche, The nature of ferroelectricity under pressure. *Phase Transitions* 2007; 80, 385.

[25] Z. Xu, Y. Feng, S. Zheng, A. Jin, F. Wang, X. Yao, Phase transition and dielectric properties of La-doped Pb(Zr,Sn,Ti)O_3 antiferroelectric ceramics under hydrostatic pressure. *Materials Science and Engineering B* 2003; 99, 441.

[26] Christen, H.M. Specht, E.D.Silliman, S.S. and Harshavardhan, K.S. Ferroelectric and antiferroelectric coupling in superlattices of paraelectric perovskites at room temperature. *Physical Review B* 2003; 68 020101 (R).

[27] Fesenko, O.E. Kolesova, R.V. Sindeyev, Y.G. The structural phase transition in lead zircon ate in super-high electric fields. *Ferroelectrics* 1978; 20, 177-178.

[28] P. Yang, D. A. Payne, The effect of external field symmetry on the antiferroelectric-ferroelectric phase transformation. *Journal of Applied Physics* 1996; 80, 4001.

[29] Bharadwaja, S. S. N. Krupanidhi, S.B. Backward switching phenomenon from field forced ferroelectric to antiferroelectric phases in antiferroelectric PbZrO3 thin films. *Journal of Applied Physics* 2001; 89, 4541.

[30] Park, S. Pan, M. Markowski, K. Yoshikawa, S. Cross, L.E. Electric field induced phase transition of antiferroelectric Lead Lanthanum Zirconate Titanate Stannate Ceramics. *Journal of Applied Physics* 1997; 82 (4) 1798-1803.

[31] Yu, Y. Singh, R.N. Electrical properties and electric field-induced antiferroelectric-ferroelectric phase transition in Nd^{3+}-doped lead strontium zirconate titanate ceramics. *Journal of Applied Physics* 2003; 94(11) 7250-7255.

[32] Shevanov, L. Kusnetsov, M. Sternberg, A. Electric field-induced antiferroelectric-to-ferroelectric phase transition in lead zirconate titanate stannate ceramics modified with lanthanum. *Journal of Applied Physics* 1994; 76 (7) 4301-4304.

[33] Smyth, D.M. The defect chemistry of metal oxides. Oxford University Press, New York, 2000.

[34] Schaumburg, H. Werkstoffe und Bauelemente der Elektrotechnik, Bd.5, Keramik, 1994.

[35] Knudsen, J. Woodward, D.I. Reaney, I.M. Domain variance and superstructure across the antiferroelectric/ferroelectric phase boundary in $Pb_{1-1.5x}La_x(Zr_{0.9}Ti_{0.1})O_3$. *Journal of Materials Research* 2003; 18(2) 262-271.

[36] Kuscer, D. Korzekwa, J. Kosec, M, Skulski, R. A- and B-compensated PLZT x/90/10: Sintering and microcstructural analysis. *Journal of the European Ceramic Society* 2007; 27, 4499-4507.

[37] Ishchuk, V.M. Baumer, V.N. Sobolev, V.L. The influence of the coexistence of ferroelectric and antiferroelectric states on the lead lanthanum zirconate titanate crystal structure. *Journal of Physics: Condensed Matter* 2005; 17 L177-L182.

[38] Dai, X. Viehland, D. Effects of lanthanum modification on the antiferroelectric-ferroelectric stability of high zirconium-content lead zirconate titanate. *Journal of Applied Physics* 1994; 76, 3701-3709.

[39] Peláiz-Barranco, A. Guerra, J.D. García-Zaldívar, O. Calderón-Pinar, F. Araújo, E.B. Hall, D.A. Mendoza, M.E. Eiras, J.A. Effects of lanthanum modification on dielectric properties of Pb(Zr0.90Ti0.10)O3 ceramics: enhanced antiferroelectric stability. *Journal of Material Science* 2008; 43, 6087-6093.

[40] Gonnard, P. Troccaz, M. Dopant distribution between A and B sites in PZT ceramcics of type ABO_3. *Journal of Solid State Chemistry* 1978; 23, 321-326.

[41] Härdtl, K.H. Hennings, D. Distribution of A-site and B-site Vacancies in (Pb,La)(Ti,Zr)O_3 Ceramics. *Jounal of The American Ceramic Society* 1972; 55 (5) 230-231.

[42] Atkin, R.B. Fulrath, R.M. Point Defects and Sintering of Lead Zirconate-Titanate. *Journal of The American Ceramic Society* 1971; 54 (5) 265-270.

[43] Härdtl, K.H. Rau, H. PbO vapour pressure in the Pb($Ti_{1-z}Zr_z$)O_3 system. *Solid State Communications* 1969; 7, 41-45.

[44] Sun, P. Xu, C.-N. Akiyama, M. Watanabe, T. Controlled Oxygen Partial Pressure Sintering of (Pb,La)(Zr,Ti)O_3 Ceramics. *Journal of The American Ceramic Society* 1999; 82 (6) 1447-1450.

[45] Northrop, D.A. Vaporization of Lead Zirconate-Lead Titanate Materials. *Journal of The American Ceramic Society* 1967; 50 (9), 441-445.

[46] Snow, G. S. Improvements in Atmosphere Sintering of Transparent PLZT Ceramics. *Journal of The American Ceramic Society* 1973; 56 (9) 79-480.

[47] Dai, X. Xu, Z. Li, J.-F. Viehland, D. Effects of lanthanum modification on rhombohedral Pb($Zr_{1-x}Ti_x$)O_3 ceramics: Part I. Transformation from normal to relaxor ferroelectric behaviours. *Journal of Materials Research* 1996; 11 (3) 618-625.

[48] Dai, X. Xu, Z. Li, J.-F. Viehland, D. Effects of lanthanum modification on rhombohedral Pb($Zr_{1-x}Ti_x$)O_3 ceramics: Part II. Relaxor behavior versus enhanced antiferroelectric stability. *Journal of Materials Research* 1996; 11 (3) 626-638.

[49] Ishchuk, V. M. Samoylenko, Z.A. Sobolev, V.L. The kinetics of the local compositional changes at the ferroelectric-antiferroelectric interphase boundaries in lead-lanthanum titan ate-zirconate solid solutions. Journal of Physics: Condensed Matter 2006; 18, 11371-11383.

[50] Garg, A. Agrawal, D.C. Effect of rare earth (Er, Gd, Eu, Nd and La) and bismuth additives on the mechanical and piezoelectric properties of lead zirconate titanate ceramics. *Material Science and Engineering* 2001; B86, 134-143.

[51] Goldschmidt, V.M. Die Gesetze der Krystallochemie. *Die Naturwissenschaften* 1926; 12 (21) 477-485.

[52] Shannon RD. Revised effective ionic radii and systematic studies of interatomic distances in halides and chaleogenides. *Acta Crystallogrica* 1976; 32, 751.30.

[53] Goldschmidt, V.M. Skrifter Norske Videnskaps-Akad.Oslo, I: Mat.-Naturv. Kl. 2 (8), 1926.

[54] Cordero, F. Trequattrini, F. Craciun, F. Galassi, C. Octahedral tilting, monoclinic phase and the phase diagram of PZT. *Journal of Physics: Condensed Matter* 2011; 23 415901 (10p).

[55] Ghita, M. Fornari, M. Singh, D.J. Halilov, S.V. Interplay between A-site and B-site driven instabilities in perovskites. *Physical Review B* 2005; 72, 054114.

[56] Reaney, I.M. Colla, E.L. Setter, N. Dielectric and Structural Characteristics of Ba- and Sr-based Complex Perovskites as a Function of Tolerance Factor. *Japanese Journal of Applied Physics* 1994; 33, 3984-3990.

[57] Randall, C. A. Bhalla, A. S. Shrout, T. R, Cross, L. E. Classification and consequences of complex lead perovskite ferroelectrics with regard to B-site cation order. *Journal of Material Research* 1990; 5, 829-834.

[58] Howard, C. J. Stokes, H.T. Structures and phase transitions in perovskites – a group-theoretical approach. *Acta Chrystallographica Section A* 2004; A 61, 93-111

[59]Borowski, M. Perovskites – Structure, Properties and Uses. Nova Science Publisher, Inc. New York, 2010

[60] Park, H.-B. Park, C.Y. Hong, Y.-S. Kim, K. Kim, S.-J. Structural and Dielectric properties of PLZT Ceramics Modified with Lanthanide Ions. Journal of The American Ceramic Society 1999; 82(1) 94-102.

[61] Wojdel, J.C. Hermet, P. Ljungberg, M.P. Ghosez, P. Iniguez, J. First-principles model potentials for lattice-dynamical studies: general methodology and example of application to ferroic perovskite oxides. *Journal of Physics: Condensed matter* 2013; 25, 305401.

[62] Troccaz, M. Gonnard, P. Eyraud, L. Dopant distribution between A and B sites in PbZr0.95Ti0.05 ceramics of type ABO_3. *Ferroelectrics* 1978; 22, 817-820.

[63] Woodward, P.M. Octahedral Tilting in Perovskites. I Geometrical Considerations. Acta Chrystallographica 1997 B53, 32-43.

[64] Suchomel, M.R. Davies, P.K. Predicting the position of the morphotropic phase boundary in high temperature $PbTiO_3$-$Bi(B'B'')O_3$ based dielectric ceramics. *Journal of Applied Physics* 2004; 96 (8) 4405-4410.

[65] Thomas, N.W. The compositional dependence of octahedral tilting in orthorhombic and tetragonal perovskites. *Acta Crystallographica* 1996; B52, 16-31.

[66] Woodward, P.M. Octahedral Tilting in Perovskites. II Structure Stabilizing Forces. Acta Chrystallographica 1997, B53, 44-66.

[67] Taniguchi, H. Soon, H.P. Shimizu, T. Moriwake, H. Shan, Y.J. Itoh, M. Mechanism for suppression of ferroelectricity in $Cd_{1-x}Ca_xTiO_3$. Physical Review B 2011; 84, 174106.

[68] Samara, G.A. Pressure and Temperature Dependence of the Dielectric Properties and Phase Transitions of the Antiferroelectric Perovskites: $PbZrO_3$ and $PbHfO_3$. Physical Review B 1970; 1 (9) 3777-3786.

[69] Bersurker, I.B. On the origin of ferroelectricity in perovskite-type crystals. *Physics Letters* 1966; 20 (6) 589-590.

[70] Bellaiche, L. Padilla, J. Vanderbilt, D. Ferroelectric effects in PZT. cond-mat.mtrl-sci] 1998; arXiv:cond-mat/9802209.

[71] Mesquita, A. Michalowicz, A. Matelaro, V.R. Local order and electronic structure of $Pb_{1-x}La_xZr_{0.40}Ti_{0.60}O_3$ materials and its relation with ferroelectric properties. *Journal of Applied Physics* 2012; 111, 104110.

[72] Cohen, R. E. Origin of ferroelectricity in oxide ferroelectrics and the difference in ferroelectric behaviour of $BaTiO_3$ and $PbTiO_3$. *Nature* 1992; 358, 136-138.

[73] Corker, D.L. Glazer, A. M. Dec, J. Roleder, K. Whotmore, R. W. A Re-investigation of the Crystal Structure of the Perovskite $PbZrO_3$ by X-ray and Neutron Diffraction. *Acta Crystallographica* 1997; B53 135-142.

[74] Woodward, D.I. Knudsen, J. Reaney, I.M. Review of crystal and domain structures in the $PbZr_xTi_{1-x}O_3$ solid solutions. *Physical Review B* 2005; 72, 104110.

[75] Waser, R. Böttger, U. Tiedke, s. Polar Oxides: Properties, Characterization, and Imaging, Wiley-VCH Verlag GmbH &Co.KgaA, Weinheim, 2005.

[76] Berlincourt, D. Piezoelectric ceramic compositional development. *Journal of Acoustical Society of America* 1992; 91 (5) 3034-3040.

[77] Thomas, N.W. A new framework for understanding relaxor ferroelectrics. *Journal of Physics and Chemistry of Solids* 1990; 51 (12) 1419-1431.

[78] Knudsen, J. Woodward, D.I. Reaney, I.M. Domain variance and superstructure across the antiferroelectric/ferroelectric phase boundary in $Pb_{1-1.5x}La_x(Zr_{0.9}Ti_{0.1})O_3$. *Journal of Material Research* 2003; 18 (2) 262-271.

[79]Liu, H., Dkhil, B. A brief review on the model antiferroelectric $PbZrO_3$ perovskite-like material. Zeitschrift für Kristallographie Crystalline Materials 2011; 226, 163-170.

[80] Sawaguchi, E. Maniwa, H. Hoshino, S. Antiferroelectric Structure of Lead Zirconate. *Physical Review* 1951; 83, 1078.

[81] Shannon, R. D. Dielectric polarizabilities of ions in oxides and fluorides. *Journal of Applied Physics* 1993; 17 pp. 215-221.

[82] Seshadri, R. Baldinozzi, G. Felser, C. Tremel, W. Visualizing electronic structure changes across an antiferroelectric phase transition Pb2MgWO6. *Journal of Materials Chemistry* 1999; 9, 2463-2466.

[83] Watson, G. W. Parker, S.C. Origin of the Lone Pair of α-PbO from Density Functional Theory Calculations. *Journal of Physical Chemistry B* 1999; 103, 1258-1262.

[84] Heywang, W. Thomann, H. Tayloring of Piezoelectric Ceramcis. *Annual Reviews of Material Science* 1984; 14, 27-47.

[85] Allred, A.L. Electronegativity values from thermochemical data. Journal of Inorganic Nuclear Chemistry 1961; 17 pp. 215-221.

[86] Higuchi, T. Tsukamoto, T. Hattori, T. Honda, Y. Electronic Structure of $(Pb,La)(Zr,Ti)O_3$ Thin Film Probed by Soft-X-ray Spectroscopy. *Japanese Journal of Applied Physics*. 2005; 44 (9B) 6923-6926.

[87] K. W. Gachighi, *Electrical Energy Storage in Antiferroelectri-Ferroelectric Phase Switching. Chemically Modified Lead Zirconate Ceramics,* The Pennsylvania State University: Doctoral Thesis, 1997.

[88]Yang, P, Payne, D.A. The Effect of External Field Symmetry on the Antiferroelectric-Ferroelectric Phase Transformation. *Journal of Applied Physics* 1996; 80,4001-5.

[89] Moulson, A.J. Herbert, J.M. Electroceramics. 2003

[90] Burn, I., & Smith, D. M. Energy Storage in Ceramic. *Journal of Materials Science* 1972;*7*(3) 339-343.

[91] Seshadri, R. Hill, N.A. Visualizing the Role of Bi 6s „Lone Pairs“ in the Off-Center Distortion in Ferromagnetic BiMnO3. *Chemistry of Materials* 2001; 13, 2892-2899.

[92] Ishchuk, V.M. Baumer, V.N. Sobolev, V.L. The influence of the coexistence of ferroelectric and antiferroelectric states on the lead lanthanum zircon ate titan ate crystal structure. *Journal of Physics: Condensed Matter* 2005; 17 L177-L182.

[93] Viehland, D. Dai, X.H. Li.J.F. Xu, Z. Effects of quenched disorder on La-modified lead zirconate titanate: Long- and short-range ordered structurally incommensurate phases, and glassy polar clusters. *Journal of Applied Physics* 1998; 84, 458.

[94] Hiremath, B.V. Kingon, A.I. Biggers, J.V. Reaction Sequence in the Formation of Lead Zirconate-Lead Titanate Solid Solution: Role of Raw Materials. *Journal of The American Ceramic Society* 1983; 66(11) 790-793.

[95] Lee, Y.-J. Yen, F.-S. Phase-formation mechanism for hydrothermally synthesizing lanthanum-modified lead zirconate titanate powders. *Journal of Crystal Growth* 1997; 178, 335-344.

[96] Mohiddon, A. Yadav, K.L. Reaction kinetics of PLZT formation and its effect on structural and dielectric properties. *Advances in Applied Ceramics* 2008; 107(6) 354-359.

97 Buhrer, C.F. Some Properties of Bismuth Perovskites. *The Journal of Chemical Physics* 1962; 36 (3) 798-803.

[98] Khalyavin, D.D. Salak, A.N. Vyshatko, N.P. Lopes, A.B. Olekhnovich, N.M. Pushkarev, A.V. Maroz, I. Radyush, Y.V. Crystal Structure of Metastable Perovskite $Bi(Mg_{1/2}Ti_{1/2})O_3$: Bi-Based Structural Analogue of Antiferroelectric $PbZrO_3$. *Chemistry of Materials* 2006; 18, 5104-5110.

[99] Choudhary, R.N.P. Mal, J. Phase transition in Bi-modified PLZT ferroelectrics. *Materials Letters* 54 (2002) 175–180.

[100] Raia, R.Sharma, S. Structural and dielectric properties of (La, Bi) modified PZT ceramics. *Solid State Communications* 129 (2004) 305–309.

[101] Dutta, S. Choudhary, R.N.P. Sinha, P.K. Ferroelectric phase transition in Bi-doped PLZT ceramics. *Materials Science and Engineering* B98 (2003) 74-80.

[102] Ujma, Z. Handerek, J. Peculiarities of the pyroelectric effect and of the dielectric properties in Bi-doped $Pb(Zr_{0.95}Ti_{0.05})O_3$ ceramics. *Journal of the European Ceramic Society* 23 (2003) 203‑212.

[103] Rukmini, H.R. Choudhary, R.N.P. Prabhakara, D.L. Effect of sintering temperature on Na-modified PLZT ceramics. *Materials Chemistry and Physics* 2000; 64, 171-178.

[104] Shannigrahi, S.R. Choudhary, R.N.P. Acharya, H.N. Microstructure and electrical characterisations of K-modified PLZT. *Journal of Materials Science* 2000; 25, 1737-1742.

[105] Rukmini, H.R. Choudhary, R.N.P. Rao, V.V. Effect of doping pairs (La, Na) on structural and electrical properties of PZT ceramics. *Materials Chemistry and Physics* 1998; 55, 108-114.

[106] Shannigrahi, S. Choudhary, R.N.P. Acharya, H.N. Sinha, T.P. Phase transition in sol-gel-derived Na-modified PLZT ceramics. *Journal of Physics D: Applied Physics* 1999; 32, 1539-1547.

[107] Rukmini, H.R. Choudhary, R.N.P. Rao, V.V. Structural and electrical properties of sol-gel prepared (La,Ll) modified PZT ceramics. *Materials Letters* 1998; 37, 268-275.

[108] Yadav, K.L. Choudhary, R.N.P. Structural and dielectric properties of PLLZT ceramics. Journal *of Materials Science Letters* 1993; 12, 1722-1725.

[109] Ishchuk, V.M. Matveev, S.V. Two-phase (ferroelectric and antiferroelectric) nuclei and diffuse phase transition in the vicinity of the ferroelectric-antiferroelectric-paraelectric triple point. *Applied Physics Letter* 2001; 79(18) 2949-2951.

[110] Bersurker, I.B. On the ferroelectricity in perovskite-type crystals. *Physics Letters* 1966; 20(6) 589-590.

[111] Yu, Y. Singh, R.N. Effect of composition and temperature on field-induced properties in the lead strontium zirconate titanate system. *Journal of Applied Physics* 2000; 88, 7249.

[112] Pokharel, B.P. Pandey, D. Effect of Ba2 substitution on the stability of the antiferroelectric and ferroelectric phase in $(Pb_{1-x}Ba_x)ZrO_3$. *Physical Review B* 2002; 65, 214108.

[113] Cerqueira, M. Nasar, R.S. Longo, E. Piezoelectric behaviour of PZT doped with calcium: a combined experimentyl and theoretical study. *Journal of Materials Science* 1997; 32, 2381-2386.

[114] Dutta, I. Singh, R. N. Effect of electrical fatigue on the electromechanical behaviour and microstructure of strontium modified lead zirconate titanate ceramics. *Materials Science and Engineering B* 2010; 166, 50-60.

[115] Zhang, N. Xu, Z. Feng, Y. Yao, X. Dielectric and relaxor ferroelectric properties of Ba-doped $Pb(Zr,Ti)O_3$ ceramics. *Journal of Electroceramics* 2008, 21; 609-612.

[116] Robert, S. Dielectric Properties of Lead Zirconate and Barium-Lead Zirconate. *Journal of The American Ceramic Society* 1950; 33 (2) 63-66.

[117] Ostos, C. Mestres, L. Martínez-Sarrión, M.L. García, J.E. Albereda, A. Perez, R. Synthesis and characterization of A-site deficient rare-earth doped $BaZr_xTi_{1-x}O_3$ perovskite-type compounds. *Solid State Sciences* 2009; 11, 1016-1022.

[118] Pan, M.-J. Markowski, K.A. Park, S.-E. Yoshikawa, S. Cross, L.E. Antiferroelectric-to-Ferroelectric Phase Switching PLSnZT Ceramics-I. Structure, Compositional Modification and Electrical Properties. Applications of Ferroelectrics 1996; ISAF ´96., *Proceeding of the Tenth IEEE International Symposium on Application of* Ferroelectrics, Volume 1, 267-270.

[119] Kim, S.-H. Ha, J. Hwang, C.S. Kingon, A. Ca- and Sr-doped (Pb1-xLax)(ZryTi1-y)1-x/4O3 thin films for low-voltage operations. *Thin Solid Films* 2001; 394, 131-135.

[120] Whangbo, M.-H. Koo, H.-J. Effect of Metal-Oxygen Covalent Bonding on the Competition between Jahn-Teller Distortion and Charge Disproportionation in the Perovskites of High-Spin d4 Metal Ions LaMnO3 and CaFeO3. Inorganic Chemistry 2002; 41, 1920-1929.

[121] Ravez, J. Broustera, C. Simon, A. Lead-free ferroelectric relaxor ceramics in the $BaTiO_3$-$BaZrO_3$-$CaTiO_3$ system. *Journal of Materials Chemistry* 1999; 9, 1609-1613.

[122] Xu, B. Ye, Y. wang, Q.-M. Pai, N.G. Cross, L.E. Effect of compositional variations on electrical properties in phase switching $(Pb,La)(Zr,Ti,Sn)O_3$ thin and thick films. *Journal of Materials Science* 2000; 35, 6027-6033.

[123] Zheng, Q. Yang, T. Wei, K. Wang, J. Yao, X. Effect of Sn:Ti variations on electric field induced AFE-FE phase transition in PLZST antiferroelectric ceramics. *Ceramics International* 2012; 38S, S9-S12.

[124] Smolensky, G. A. Isupov, V. A. Agranovskaya, A. I. Krainic, N. N. New ferroelectrics with complex compounds. IV. Fizika Tverdogo Tela 1960; 2, 2982-2985.

[125] Herabut, A. Safari, A. Processing and Electromechanical Properties of $(Bi_{0.5}Na_{0.5})_{(1-1.5x)}La_xTiO_3$ Ceramics. Journal of The American Ceramic Society 1997; 80(11) 2954-2958.

[126] Barick, B.K. Choudhary, R.N.P. Pradhan, D.K. Phase transition and electrical properties of lanthanum-modified sodium bismuth titanate. *Materials Chemistry and Physics* 2012; 132, 1007-1014.

[127] Jaita, P. Watcharapasorn, A. Jiansirisomboon, S. Effects BNT compound incorporated on structure and electrical properties of PZT ceramic. *Current Applied Physics* 2011; 11, S77-S81.

[128] Jaita, P. Watcharapasorn, A. Jiansirisomboon, S. A role of BNLT compound addition on structure and properties of PZT ceramics. *Solid State Sciences* 2010; 12, 1608-1614.

[129] Megaw, H.D. Crystal structure of double oxides of the perovskite type. *The Proceedings of the Physical Society* 1946; 58 (2) 326, 133-152.

[130]Vegas, A. Vallet-Regi, M. Gonzalez-Calbet, J. M. Alario-Franco, M. A. The $ASnO_3$ (A=Ca,Sr) perovskites. *Acta Crystallographica* 1989; B 42, 167–72.

[131] Sim, H. Cheong, S.W. Kim, B.G. Octahedral tilting-induced ferroelectricity in $ASnO_3/A´SnO_3$ superlattices (A,A´= Ca, Sr, and Ba). Physical Review B 2013; 88, 014101.

[132] Abrahams, S.C. Kurtz, S.K. Jameson, P.B. Atomic Displacement Relationship to Curie Temperature and Spontaneous Polarization in Displacive Ferroelectrics. *Physical Review* 1968; 172(2); 551-553.

[133] Yasmin C. Bürkl. Isovalent B-site doping of Lead-Lanthanum-Zirconate-Titanate with Hafnium, University of Technology Graz: Diploma thesis, 2014.

[134] I.M. Ubic, R. Dielectric and structural characteristics of perovskites and related materials as a function of tolerance factor. *Ferroelectrics* 1999; 228 (1) 23-38.

11 Figure caption

12 Table caption

13 Equation caption